ENGINEERING OF BIOBASED INDUSTRIAL PRODUCTS FROM RENEWABLE (AGRICULTURAL) RESOURCES

By

Sayli Devdas Bote

A DISSERTATION

Submitted to
Michigan State University
in partial fulfillment of the requirements
for the degree of

Chemical Engineering – Doctor of Philosophy

2019

ABSTRACT

ENGINEERING OF BIOBASED INDUSTRIAL PRODUCTS FROM RENEWABLE (AGRICULTURAL) RESOURCES

By

Sayli Devdas Bote

Replacing petro/fossil carbon by biobased renewable carbon derived from agricultural feedstocks offers the value proposition of (1) reduced carbon footprint, (2) supporting rural agrarian economy and improved food security, and (3) creation of "wealth" in the rural agriculture through manufacturing value-added industrial products. Our work reports on the synthesis of novel, scalable, and economically viable biobased polyols derived from soybean. Polyols find commercial use in the manufacture of polyurethane (PU) products, particularly flexible and rigid PU foams. Drop-in replacements of the currently used polyols with biobased polyols suffer from inferior performance properties with increasing biobased polyol content, high production cost, and incompatibility with petroleum-based polyols. The thesis also reports on the synthesis of novel polyols from meso-lactide and the production of value-added products therefrom. Meso-lactide is a co-product in the manufacture of polylactide (PLA). Polylactide (PLA) is the world's foremost completely biobased and fully compostable polymer with a production capacity of 140 kt/year by NatureWorks in Blair, NE and a 75 kt/year by Total Corbion PLA in Rayong, Thailand.

The first section focuses on facile reaction chemistries to produce biobased polyols from a protein-carbohydrate residue derived from soybean meal or soymeal. The components of the soymeal were characterized to optimize processing options. The soymeal component was converted to polyols using transamidation chemistry, followed by a ring-opening reaction with carbonates. The process is cost effective with zero waste generated during the synthesis.

In the second section, new biobased building blocks were synthesized from meso-lactide by

reacting it with primary amines and alcohols. The ring-opening reaction of meso-lactide with an amino-alcohol produced diols containing amide and ester linkages in the backbone. These new biobased building blocks can be used to manufacture biobased polyesters and polyurethanes. Reacting meso-lactide with long-chain alcohols produces a diol containing ester and ether linkages with lower viscosity and hydroxyl value. This diol was further reacted with biobased dimer acid using polycondensation chemistry. A series of polyester-ether polyols with low viscosity and hydroxyl value (40 - 90 mg of KOH/g) were obtained which are suitable for applications in flexible PUF and coatings. The renewable carbon content of these polyols was 50 - 70% which can be increased to 100%.

The third section focuses on evaluating the performance properties of PUF synthesized from biobased polyols. The biobased rigid PUF containing 20 - 50% of soymeal and lactide polyols were characterized for application as insulation materials in building and construction. The flexible PUF containing 10 - 50% of biobased polyol content were evaluated for automotive applications such as engine cover, car seat, and headrest.

In the last section, reactive extrusion processing of lactide-dimer acid polyols with PLA was studied. The reactive blending of polyols with PLA increased the crystallinity of PLA by ~ 60 - 75% and decreased the glass transition temperature by ~18°C. The elongation at break increased to 120%, and the impact strength was increased by 300%. The melt crystallization kinetics showed a reduction in the total crystallization time with increasing polyol content in PLA.

To conclude the entire work, a series of cost-effective, scalable, diverse applications-oriented, and most importantly biobased, polyols were synthesized using inexpensive bioresources that have a potential for commercialization.

Copyright by
SAYLI DEVDAS BOTE
2019

Dedicated to my parents and grandparents for their support and love across the ocean

ACKNOWLEDGMENTS

I would like to sincerely express my gratitude towards my advisor Dr. Ramani Narayan for his patient guidance and encouragement during my graduate studies. He is very knowledgeable, kind, and a thought-provoking advisor. He provided a valuable contribution to my academic studies, research, and professional career. He gave me the freedom to explore new materials, always promoted independent research, and provided the necessary feedback. After working with him I feel more confident, motivated, and independent as a researcher.

I would also like to thank my other committee members Dr. Martin Hawley, Dr. Rafael Auras, Dr. Christopher Saffron, and Dr. Alper Kiziltas for their valuable contribution to my work. I would especially like to thank Dr. Auras and his students who were always there to help me in using their instruments. The life cycle assessment course with Dr. Saffron was challenging but his feedback and guidance were very helpful in understanding the learning objectives of LCA.

I am very grateful to our collaborators and my supervisors at Ford Motor Company, Dr. Debbie Mielewski and Dr. Alper Kiziltas who supported our work and provided the required facility to conduct experiments. During my internship at Ford, I got an exposure to various biobased materials being used by Ford in their vehicles. Dr. Kiziltas provided an industrial perspective on my research work which helped me in developing more suitable products for automotive applications. Working with him and the entire Sustainable Biomaterials and Plastic Research Group at Ford was very helpful in deciding my future career path.

I would like to thank Abby Vanderberg at Center for Advanced Microscopy who helped me in sample preparation and obtaining 3-D microscopy images of foams. Making foams was interesting but looking at its 3-D images was even more exciting! I would sincerely like to thank all the members of the Composite Materials and Structures Center who were readily available to help

when it was needed. Special thanks to Brian Rook who quickly responded to all queries and taught me helpful techniques and troubleshooting for different instruments. Also, I would like to thank Dr. Dan Holmes at the Department of Chemistry who helped me in analyzing NMR spectra. I also owe a thank you to Aaron Walworth, Sonal Karkhanis, Pooja Mayekar, and Gauri Awalgaonkar at School of Packaging who trained me on different instruments and provided assistance during initial testing of materials.

I am very grateful to all the members of Biobased Materials Research Group (BMRG) including Dr. Daniel Graiver, Dr. Ken Farminer, Dr. Chetan Tambe, Dr. Sudhanwa Dewasthale, Dr. Jeff Schneider, and Hugh MacDowell who helped me in learning and understanding our group's work. A special thanks goes to Dr. Chetan Tambe because of whom I joined the group. I would also like to thank Preetam for being there when additional help was required, and for being the designated BMRG driver. I owe a big thank you to our undergrads - Sara Kolar, Ian Scheper, Nathan Arnold, Clayton Threatt, Ariel Rose, and Melissa Joslyn who were passionate about their research and constantly provided feedback for any improvements needed. Their contribution to my work is huge and it would have taken longer to complete these studies without their help. I would like to thank Apoorva Kulkarni, Manas Nigam, and Moh Alhaj for being there when additional assistance was needed.

My initial days at MSU would have been more difficult without these people – Oishi Sanyal, Chetan Tambe, and Tridip Das who provided everything I needed. I really appreciate my friends who are always there for me - Shreya, Kirti, Ali, Amol, Karthik (Baba), Dhruv (Brody), Abhishek, Vivek, Mayank, Shivam, and Arjun.

I would like to thank another family away from home - Preetam (Ramu Kaka), Aritra (A.C.), Kanchan (K.C.), Sabyasachi (Saby Baby), and Saptarshi (Sap Da) with whom I enjoyed camping,

biking, cooking, outings, swimming - pretty much everything. A big hug to the new member of my life, Poopy (cutest cat in the world and my love) who was there all the time mingling around me and sleeping on my chair. His love and affection definitely helped a lot to pass through difficult times. Thank you Kshitija for making Poopy a part of my life. I owe a big thank you to my best friend Apoorva for her best wishes and being on my side whenever needed it the most.

At last, I would like to thank my mom and dad who supported me through each step of my life. Their constant motivation and love helped me in pursuing a lot of things. A big hug to my brother Aniket and my grandmother who were there for me all the time. I would also like to thank my cousins Aparna, Rohit, and Amol who are my constant supporters. I am very grateful to Savita mami, Anand mama, Manisha mami, Pramod mama, Kaki, and Bhau for spoiling me with good food. It is very difficult to stay away from such a loving family, but their love and support helped me succeed through this phase of life.

TABLE OF CONTENTS

LIST OF TABLES ..... **xiii**

LIST OF FIGURES ..... **xv**

KEY TO ABBREVIATIONS ..... **xxi**

1 INTRODUCTION **1**
1.1 VALUE PROPOSITION OF BIOBASED PRODUCTS 1
1.2 SOYBEAN 2
1.2.1 SOYBEAN MEAL OR SOYMEAL 3
1.2.2 SOYBEAN OIL 7
1.3 POLYLACTIDE FROM CORN 9
1.4 POLYURETHANE FOAMS 10
1.5 BIOBASED POLYOLS 13
1.5.1 Transesterification 13
1.5.2 Epoxidation 14
1.5.3 Ozonolysis 15
1.5.4 Hydroformylation 15
1.5.5 Commercially available biobased polyols 16
1.6 SYNTHESIS OF BIOBASED POLYOLS FOR POLYURETHANE FOAMS AND POLYESTERS 16

2 POLYOLS DERIVED FROM PROTEIN-CARBOHYDRATE BIOMASS (SOYMEAL) RESIDUE: COMPOSITION ANALYSIS, SYNTHESIS, AND CHARACTERIZATION **19**
2.1 INTRODUCTION 19
2.2 EXPERIMENTAL 22
2.2.1 Materials and chemicals 22
2.2.2 Composition analysis of soymeal 22
2.2.2.1 Separation of soluble carbohydrates 22
2.2.2.2 Characterization of soluble carbohydrates and soymeal 22
2.2.2.3 Polyol synthesis from soymeal 23
2.2.2.4 Synthesis of amine derivatives using transamidation process 23
2.2.2.5 Synthesis of soymeal-based polyol 23
2.2.2.6 Characterization of amine derivatives and polyols 24
2.3 RESULT AND DISCUSSION 24
2.3.1 Composition analysis of soymeal 24
2.3.1.1 Separation of soluble carbohydrates 24
2.3.1.2 Thermogravimetric analysis and deconvolution of DTG graphs 25
2.3.1.3 Fourier Transform Infrared Spectroscopy (FTIR) 28
2.3.1.4 Protein, moisture, and ash content analysis 31
2.3.2 Polyol synthesis from soymeal 33
2.3.2.1 Polyol synthesis and characterization 34
2.3.2.2 Synthesis of amine derivatives using transamidation process 35

2.3.2.3 Synthesis of soymeal-based polyols 37
2.3.2.4 Fourier Transform Infrared Spectroscopy (FTIR) 39
2.3.2.5 Nuclear Magnetic Resonance (NMR) Spectroscopy 40
2.3.2.6 Thermogravimetric Analysis 41
2.4 CONCLUSION 42
2.5 ACKNOWLEDGMENTS 43

3 SYNTHESIS OF BIOBASED BUILDING BLOCKS FROM LACTIDE AND SOYBEAN OIL FOR APPLICATIONS IN POLYURETHANES AND POLYESTERS... 44
3.1 INTRODUCTION 44
3.2 EXPERIMENTAL 46
3.2.1 Materials and chemicals 46
3.2.2 Synthesis of diols by ring opening of meso-lactide using amines 46
3.2.3 Synthesis of diols by ring opening of meso-lactide using hydroxyl group 46
3.2.4 Synthesis of low hydroxyl value polyols using polycondensation chemistry 47
3.2.5 Characterization of lactide polyols 48
3.3 RESULTS AND DISCUSSION 49
3.3.1 Synthesis of diols by ring opening of meso-lactide using amines 49
3.3.2 Synthesis of diols by ring opening of meso-lactide using hydroxyl group 50
3.3.3 Synthesis of low hydroxyl value polyols using a polycondensation chemistry 52
3.3.4 Fourier Transform Infrared Spectroscopy (FTIR) 55
3.3.5 Nuclear Magnetic Resonance (NMR) Spectroscopy 57
3.3.6 Thermogravimetric analysis (TGA) 60
3.4 CONCLUSION 63

4 RIGID POLYURETHANE FOAMS DERIVED FROM SOYMEAL AND LACTIDE POLYOLS 65
4.1 INTRODUCTION 65
4.2 EXPERIMENTAL 67
4.2.1 Materials and chemicals 67
4.2.2 Polyol synthesis 67
4.2.2.1 Synthesis of soymeal-based polyol 67
4.2.2.2 Synthesis of lactide polyol 67
4.2.3 Free rise study of polyurethane foams 68
4.2.4 Box foam and its characterization 68
4.3 RESULT AND DISCUSSION 70
4.3.1 Free rise study of PUF 70
4.3.2 Thermogravimetric analysis of PUF 73
4.3.3 Density, compressive strength, and thermal conductivity of PUF 74
4.3.4 Scanning Electron Microscopy (SEM) images of PUF 75
4.3.5 Aging and water absorption tests of PUF 77
4.3.6 Comparison of biobased and petroleum-based rigid PUF 81
4.4 CONCLUSION 83
4.5 ACKNOWLEDGMENTS 83

5 BIOBASED FLEXIBLE POLYURETHANE FOAMS FOR AUTOMOTIVE APPLICATIONS 84
5.1 INTRODUCTION 84
5.2 EXPERIMENTAL 86
5.2.1 Materials and chemicals 86
5.2.2 Free rise study of PUF 87
5.2.3 Box foam and its characterization 88
5.3 RESULT AND DISCUSSION 90
5.3.1 Free rise study of PUF 91
5.3.2 Thermogravimetric analysis of PUF 93
5.3.3 Density of PUF 95
5.3.4 Scanning Electron Microscopy (SEM) images of PUF 96
5.3.5 Wet compression set of PUF 98
5.3.6 Tensile properties of PUF 99
5.3.7 Tear resistance of PUF 102
5.3.8 Compressive properties of PUF 103
5.3.9 Miscibility study and comparison of different biobased PUF 106
5.4 CONCLUSION 108
5.5 ACKNOWLEDGMENTS 109

6 PLASTICIZATION OF POLYLACTIDE WITH BIOBASED POLYOLS VIA REACTIVE BLENDING 110
6.1 INTRODUCTION 110
6.2 EXPERIMENTAL 112
6.2.1 Materials and chemicals 112
6.2.2 Synthesis via Reactive extrusion 113
6.2.3 Characterization of modified PLA 113
6.2.4 Effect of lower concentrations of polyols on performance properties of PLA 118
6.3 RESULTS AND DISCUSSION 118
6.3.1 Transesterification chemistry 118
6.3.2 Soxhlet extraction 120
6.3.3 Gel Permeation Chromatography (GPC) 120
6.3.4 Thermal properties of modified PLA resins 121
6.3.5 Mechanical properties of modified PLA resins 126
6.3.6 Scanning Electron Microscopy (SEM) images 131
6.3.7 Dynamic Mechanical Analysis (DMA) 133
6.3.8 Melt crystallization kinetics 136
6.3.9 Effect of lower concentrations of polyols on performance properties of PLA 141
6.3.9.1 Gel Permeation Chromatography (GPC) 141
6.3.9.2 Thermal properties 142
6.3.9.3 Mechanical properties 144
6.3.9.4 Scanning Electron Microscopy (SEM) images 148
6.3.9.5 Dynamic Mechanical Analysis (DMA) 149
6.4 CONCLUSION 151

7 SUMMARY AND FUTURE WORK 154

APPENDIX **160**

BIBLIOGRAPHY **163**

LIST OF TABLES

Table 1-1: Composition of components of NSP [15] 7

Table 2-1: Composition of ethanol washed soymeal and soluble carbohydrates 27

Table 2-2: Calculating conversion factor for protein content present in the soymeal from amino acid content 32

Table 2-3: Composition of soymeal 33

Table 2-4: Characterization of different amine derivatives and soymeal polyols 39

Table 3-1: Characteristics of diols synthesized from lactide 51

Table 3-2: Characteristic of dimer acid-based polyols 54

Table 4-1: Formulations of soymeal and lactide polyols with Jeffol-SG-360 71

Table 4-2: Thermal degradation analysis of polyurethane foams 74

Table 4-3: Properties of polyurethane rigid foams 75

Table 4-4: Comparison of biobased and petroleum-based rigid PUF 82

Table 5-1: Physical properties of polyols 87

Table 5-2: Formulation used for flexible polyurethane foams 88

Table 5-3: Characteristic time (top of the cup, string gel time, rise time) for all free rise profiles 92

Table 5-4: Temperatures for 5%, 10%, and 50% mass loss, and residual weight of PUF 94

Table 5-5: Cell size of biobased PUF 98

Table 5-6: Comparison of different biobased PUF containing 30% biobased polyol with petroleum-based PUF 108

Table 6-1: Properties of biobased polyols 112

Table 6-2: Molecular weight distribution of neat PLA, extruded PLA, and modified PLA resins 121

Table 6-3: Thermal transition and crystallinity of modified PLA resins - non-annealed 123

Table 6-4: Thermal transitions and crystallinity of modified PLA test bars - non-annealed 125

Table 6-5: Thermal transitions and crystallinity of modified PLA test bars - annealed..... 126

Table 6-6: Isothermal melt crystallization half times and Avrami constants for modified PLA 140

Table 6-7: Molecular weight distribution of neat PLA, and modified PLA containing 1% and 5% of polyols 142

Table 6-8: Thermal transition and crystallinity of modified PLA test bars containing 1% and 5% of polyols 143

Table 6-9: Thermal transition and crystallinity of modified PLA test bars containing 1% and 5% of polyols - Annealed..... 144

LIST OF FIGURES

Figure 1-1: Bioplastic Feedstock Alliance (BFA) [2] 1

Figure 1-2: Typical composition of soybean [12] 3

Figure 1-3: Composition of soymeal after extracting soybean oil 4

Figure 1-4: Protein structure 4

Figure 1-5: Amino acids present in soymeal [14] 5

Figure 1-6: Types and amount of various carbohydrates present in soymeal 6

Figure 1-7: Fatty acids composition in soybean oil [16] 8

Figure 1-8: Structures of dimer acids [19] 9

Figure 1-9: Stereoisomers of lactide 10

Figure 1-10: Various sources of lactide 10

Figure 1-11: Global polyurethane market, 2014-2020 [28] 11

Figure 1-12: Reaction of diisocyanate with polyol 11

Figure 1-13: Reaction of diisocyanate with water 12

Figure 1-14: Scanning Electron Microscopy images of closed cell (left) and open cell (right) polyurethane foam 12

Figure 1-15: Transesterification of triglyceride with glycerol [36] 14

Figure 1-16: Epoxidation of soybean oil followed by ring opening [37] 14

Figure 1-17: Ozonolysis of monoglyceride to synthesize polyols via different routes [39] 15

Figure 1-18: Hydroformylation of monoglyceride [11] 16

Figure 2-1: (a) TGA and DTG of soymeal (b) Deconvolution of DTG graph of soymeal (c) TGA and DTG of ethanol washed soymeal (EWS) (d) Deconvolution of DTG graph of ethanol washed soymeal (EWS) 29

Figure 2-2: (a) TGA and DTG of soluble carbohydrates (SC) (b) Deconvolution of DTG graph of soluble carbohydrates (SC) (c) FTIR of soymeal (d) FTIR of soluble carbohydrates 30

Figure 2-3: Different routes used for synthesis of polyols from soymeal (1) Hydrolysis [6, 59] (2) Activation [55] (3) Transamidation [58] 34

Figure 2-4: Transamidation of proteins with ethanolamine 35

Figure 2-5: Change in the percentage of insoluble soymeal present in amine derivatives with time during the transamidation reaction 36

Figure 2-6: Kinetics of transamidation reaction 37

Figure 2-7: Ring opening of propylene carbonate with amines of hydroxylamine derivative 38

Figure 2-8: Overall pathway for soymeal polyol synthesis 38

Figure 2-9: FTIR spectra of soymeal, amine derivative, and soymeal polyol 40

Figure 2-10: ^{13}C NMR spectrum of ethanolamine and propylene carbonate reaction 41

Figure 2-11: TGA graphs of soymeal, amine derivative, and soymeal polyol 42

Figure 3-1: Set-up for polycondensation reaction 47

Figure 3-2: Reaction of meso-lactide with ethanolamine in molar ratio 1:1 49

Figure 3-3: Reaction of meso-lactide with ethanolamine in molar ratio 1:2 50

Figure 3-4: Reaction of meso-lactide with PEG-400 in molar ratio 1:1 51

Figure 3-5: Reaction of dimer acid with MLPEG-7-202 in molar ratio 1:2 and 1:1 53

Figure 3-6: Reaction of dimer acid with PEG-400 in molar ratio 1:2 and 1:1 54

Figure 3-7: FTIR spectra of meso-lactide, MLE-529, and MLE-818 55

Figure 3-8: FTIR spectra of dimer acid, PEG-400, MLPEG-7-202, DAMLPEG-7-94, and DAPEG-33 56

Figure 3-9: ^{13}C NMR spectrum of MLE-818 57

Figure 3-10: ^{1}H NMR spectrum of MLE-818 58

Figure 3-11: ^{13}C NMR spectrum of MLE-529 59

Figure 3-12: ^{13}C NMR spectrum of MLPEG-7-202 60

Figure 3-13: Thermogravimetric analysis of meso-lactide, PEG-400, MLE-529, MLE-818, MLPEG-7-202, and MLPEG-3-186 61

Figure 3-14: Derivative thermogravimetric graphs of meso-lactide, PEG-400, MLE-529, MLE-818, MLPEG-7-202, and MLPEG-3-186 61

Figure 3-15: Thermogravimetric analysis of dimer acid, PEG-400, DAMLPEG-7-94, DAMLPEG-

7-47, DAMLPEG-3-80, DAPEG-94, and DAPEG-33 62

Figure 3-16: Derivative thermogravimetric graphs of dimer acid, PEG-400, DAMLPEG-7-94, DAMLPEG-7-47, DAMLPEG-3-80, DAPEG-94, and DAPEG-33 62

Figure 4-1: Free rise profiles of JPF (0% SP), SPF 20% (20% SP), SPF 50% (50% SP), SPF 80% (80% SP), and SPF 100% (100% SP)..... 72

Figure 4-2: Free rise profiles of JPF (0% LP), LPF 20% (20% LP), LPF 50% (50% LP), LPF 80% (80% LP), and LPF 100% (100% LP) 72

Figure 4-3: TGA graphs of Jeffol-SG-360, soymeal polyol, lactide polyol, JPF, SPF (20%, 50%), and LPF (20%, 50%)..... 73

Figure 4-4: SEM images of (a) JPF 2 (b) SPF 20% (c) SPF 50% foams parallel to the rise direction; SEM images of (d) JPF 2 (e) SPF 20% (f) SPF 50% foams perpendicular to the rise direction (rise direction is shown with an arrow for a, b, c; rise direction is perpendicular to the plane of paper for d, e, f) 76

Figure 4-5: SEM images of (a) JPF 1 (b) LPF 20% (c) LPF 50% foams parallel to the rise direction; SEM images of (d) JPF 1 (e) LPF 20% (f) LPF 50% of foams perpendicular to the rise direction (rise direction is shown with an arrow for a, b, c; rise direction is perpendicular to the plane of paper for d, e, f)..... 77

Figure 4-6: Density of control foams (JPF 1, JPF 2), soymeal polyol foams (SPF 20, SPF 50), and lactide polyol foams (LPF 20, LPF 50) 78

Figure 4-7: Mass loss (%) of PUF over 3 weeks at 25°C 79

Figure 4-8: Mass loss (%) of PUF over 3 weeks at 70°C 79

Figure 4-9: Dimensional stability of PUF over 3 weeks at 25°C 80

Figure 4-10: Dimensional stability of PUF over 3 weeks at 70°C 80

Figure 4-11: Water absorption test of PUF at room temperature 81

Figure 4-12: Miscibility study of lactide polyol (left, Day 0 and Week 2) and soymeal polyol (right, Day 0 and Week 2) with Jeffol-SG-360 82

Figure 5-1: Effect of change in concentration of different catalysts on flexible foams 90

Figure 5-2: Effect of unopened cells on flexible foams..... 91

Figure 5-3: TGA graphs of flexible PUF containing 20% of biobased polyol..... 93

Figure 5-4: TGA graphs of flexible PUF containing 40% of biobased polyol..... 94

Figure 5-5: Densities of flexible polyurethane foams..... 95

Figure 5-6: SEM images of (a) 0% (b) 20% (c) 40% of DAMLPEG-7-94, (d) 0% (e) 20% (f) 40% of Agrol Prime A-56 96

Figure 5-7: SEM images of (a) 0% (b) 20% (c) 40% of DAPEG-38, (d) 0% (e) 20% (f) 40% of DAMLPEG-7-47 97

Figure 5-8: SEM images of (a) 0% (b) 20% of DAPEG-94, (c) 0% (d) 20% of DAMLPEG-3-80 97

Figure 5-9: Wet compression set values of biobased PUF 99

Figure 5-10: Tensile strength at maximum load of biobased PUF 100

Figure 5-11: Young's modulus of biobased PUF 101

Figure 5-12: Elongation at maximum load of biobased PUF 102

Figure 5-13: Tear resistance of biobased PUF 102

Figure 5-14: Compression modulus of biobased PUF 103

Figure 5-15: Compressive strength at 25% strain of biobased PUF 104

Figure 5-16: Compressive strength at 50% strain of biobased PUF 104

Figure 5-17: Compressive strength at 65% strain of biobased PUF 105

Figure 5-18: Sag factor 50%/25% of biobased PUF 106

Figure 5-19: Sag factor 65%/25% of biobased PUF 106

Figure 5-20: Miscibility study of biobased polyols (a) DAMLPEG-7-94, (b) DAMLPEG-3-80, (c) DAMLPEG-7-47, (d) DAPEG-94, (e) DAPEG-38, (f) Agrol Prime A-56, with Voranol 4701 107

Figure 6-1: Screw configuration of twin-screw extruder from feed-die 113

Figure 6-2: Structures of different polyols used in transesterification reaction 119

Figure 6-3: Transesterification reaction between PLA and DAPEG-94 120

Figure 6-4: Thermogravimetric (TGA) graphs of modified PLA resins 122

Figure 6-5: Derivative thermogravimetric (DTG) graphs of modified PLA resins 122

Figure 6-6: DSC thermograms of modified PLA test bars – non-annealed 124

Figure 6-7: DSC thermograms of modified PLA test bars – annealed 126

Figure 6-8: Stress-strain graph of modified PLA containing 10% of polyols 127

Figure 6-9: Stress-strain graph of modified PLA containing 15% of polyols 127

Figure 6-10: Tensile moduli of modified PLA resins 128

Figure 6-11: Tensile stress at yield of modified PLA resins 129

Figure 6-12: Tensile strain at break of modified PLA resins 129

Figure 6-13: Notched Izod impact strength of modified PLA resins 130

Figure 6-14: SEM images of tensile fractured surfaces of (a) Neat 3001D (a') Neat 3001D_A (b) 10% MLE (b') 10% MLE_A (c) 10% DAPEG (c') 10% DAPEG_A (d) 10% DAMLPEG (d') 10% DAMLPEG_A 131

Figure 6-15: SEM images of tensile fractured surfaces of (a) Neat 3001D (a') Neat 3001D_A (b) 15% MLE (b') 15% MLE_A (c) 15% DAPEG (c') 15% DAPEG_A (d) 15% DAMLPEG (d') 15% DAMLPEG_A 132

Figure 6-16: SEM images of impact fractured surfaces of (a) Neat 3001D (a') Neat 3001D_A (b) 10% MLE (b') 10% MLE_A (c) 10% DAPEG (c') 10% DAPEG_A (d) 10% DAMLPEG (d') 10% DAMLPEG_A 133

Figure 6-17: SEM images of impact fractured surfaces of (a) Neat 3001D (a') Neat 3001D_A (b) 15% MLE (b') 15% MLE_A (c) 15% DAPEG (c') 15% DAPEG_A (d) 15% DAMLPEG (d') 15% DAMLPEG_A 133

Figure 6-18: Storage modulus of modified PLA injection molded samples 134

Figure 6-19: Loss modulus of modified PLA injection molded samples 135

Figure 6-20: Tan δ curves of modified PLA injection molded samples 135

Figure 6-21: DSC graphs of isothermal melt crystallization of modified PLA samples at different isothermal temperatures 137

Figure 6-22: Change in fractional crystallinity of modified PLA samples with time at different isothermal temperatures 138

Figure 6-23: Avrami double-log plots for the melt crystallization kinetics of samples at different isothermal temperatures 139

Figure 6-24: TGA graphs of modified PLA test bars containing 1% and 5% of polyols 142

Figure 6-25: DSC thermograms of modified PLA test bars containing 1% and 5% of polyols. 143

Figure 6-26: DSC thermograms of modified PLA test bars containing 1% and 5% of polyols – Annealed 144

Figure 6-27: Stress-strain curves of modified PLA containing 1% and 5% of polyols 145

Figure 6-28: Modulus of modified PLA samples containing 1% and 5% of polyols..... 145

Figure 6-29: Tensile stress at yield of modified PLA containing 1% and 5% of polyol..... 146

Figure 6-30: Tensile strain at break of modified PLA samples containing 1% and 5% of polyols 147

Figure 6-31: Notched Izod impact strength of modified PLA samples containing 1% and 5% of polyols..... 147

Figure 6-32: SEM images of tensile fractured surfaces of (a) Neat 3001D (a') Neat 3001D_A (b) 10% DAMLPEG-5% (b') 10% DAMLPEG-5%_A (c) 10% DAPEG-5% (c') 10% DAPEG-5%_A 148

Figure 6-33: SEM images of impact fractured surfaces of (a) Neat 3001D (a') Neat 3001D_A (b) 10% DAMLPEG-5% (b') 10% DAMLPEG-5%_A (c) 10% DAPEG-5% (c') 10% DAPEG-5%_A 149

Figure 6-34: Storage modulus of modified PLA injection molded samples containing 1% and 5% of polyols 150

Figure 6-35: Loss modulus of modified PLA injection molded samples containing 1% and 5% of polyols..... 150

Figure 6-36: Tan δ of modified PLA injection molded samples containing 1% and 5% of polyols 151

Figure A.1: 3D image of rigid closed cell polyurethane foam 161

Figure A.2: 3D image of flexible open cell polyurethane foam 162

KEY TO ABBREVIATIONS

PUF – Polyurethane Foams

PLA – Polylactide

SC – Soluble Carbohydrates

EWS – Ethanol Washed Soymeal

SP – Soymeal Polyol

SPF – Soymeal Polyol Foam

LP – Lactide Polyol

LPF – Lactide Polyol Foam

JPF – Jeffol Polyol Foam (Control)

DA – Dimer acid

ML – Meso-lactide

PEG – Polyethylene glycol

SEM – Scanning Electron Microscopy

TGA – Thermogravimetric Analysis

DTG – Derivative Thermogravimetry

DSC – Differential Scanning Calorimetry

NMR – Nuclear Magnetic Resonance Spectroscopy

FTIR – Fourier Transform Infrared Spectroscopy

1 INTRODUCTION

1.1 VALUE PROPOSITION OF BIOBASED PRODUCTS

The term biobased products is defined as "commercial or industrial products that are composed in whole, or in significant part, of biological products or renewable domestic agricultural materials or forestry materials"[1]. These products can be adhesives, solvents, plastic, paint, packaging material, or construction materials. In recent years, there has been considerable interest in the manufacture of biobased products using plant-biomass feedstock e.g. Ford Motor Company's biobased polyurethanes, Coco-Cola's bio-polyethylene terephthalate, NatureWorks's Ingeo bioplastics, Braskem's polyethylene. This drive towards the use of bioresources is mainly to control emissions of greenhouse gases and to decrease dependency on petroleum feedstock. There are similar products derived from petroleum resources, however, petroleum resources are non-renewable. In future, they may not be adequate for synthesis of all the necessary products. Whereas biobased feedstocks are renewable, abundant, and most importantly they are usually less expensive. The use of biobased resources in products provide a value proposition of reduced carbon footprint and managed end-of-life. Also, it increases the demand for domestic feedstock and economic development in rural agriculture [1]. The Bioplastic Feedstock Alliance (BFA) is a group of companies which support the development of products from biobased resources. Many companies such as The Coco-Cola Company, Ford Motor Company, PepsiCo (Figure 1-1) are part of BFA and support the use of biobased resources in their products.



Figure 1-1: Bioplastic Feedstock Alliance (BFA) [2]

With an increase in the awareness about the environment, many companies are working diligently

towards reducing their carbon footprint. Some companies are using available bioresources such as castor oil, cashew nutshell liquid, soybean oil as a starting material for synthesis of new biobased building blocks. Corn is the most widely produced feed grain and soybean is the dominant oilseed amongst other oilseeds produced in the United States [3]. These crops are renewable and can be used for the synthesis of biobased materials. Biorefineries such as soybean refinery, corn refinery etc. produce a main product and some co-products. For example, soybean refinery produces soybean oil as a main product and soymeal as a co-product [4]. Corn refinery produces ethanol as a main product with many other co-products such as starch, corn oil, distiller's dried grains with solubles (DDGS) etc [5]. These products from biorefineries can be used for the synthesis of biobased products which can partially or fully replace the existing petroleum products. The use of agricultural and biorefinery products creates wealth in rural agriculture through value-added industrial products. Thus, our work is focused on the use of products obtained from soybean and corn refineries for the synthesis of new biobased building blocks which can be used as a starting material for polyurethane synthesis [6, 7] and for various other applications.

1.2 SOYBEAN

Soybean is the most widely produced oilseed in the United States amongst other oilseeds e.g. cottonseed, sunflower seed, canola, rapeseed, and peanuts, accounting for almost 90% of U.S. oilseed production [8]. Soybeans are used in wide variety of foods for humans and animals. The typical composition of soybean is shown in Figure 1-2. The soybean contains 38% proteins, 30% carbohydrates, 18% oil, and 14% moisture, ash and hull. The oil is extracted from soybean as shown in Figure 1-3 and the remaining residue is called as soymeal or soybean meal. As oil is the main product of soybean processing which is comprised of only 20% of soybean, the remaining residue i.e. soymeal is produced in larger quantities. The soymeal is used in the animal feed and

in human nutrition and its use is not high as compared to its production [6, 9]. Also, a very small percentage (less than 1%) of soymeal is being utilized for industrial products like adhesives [6]. Hence, there is a necessity to look for new industrial uses of soymeal [6, 9]. Also, the cost of soymeal is almost half of the cost of soybean oil [6]. The soybean oil is mainly used in the production of bio-diesel [10], food, and biobased industrial products [11]. The composition of soymeal and soybean oil is discussed in the next section.

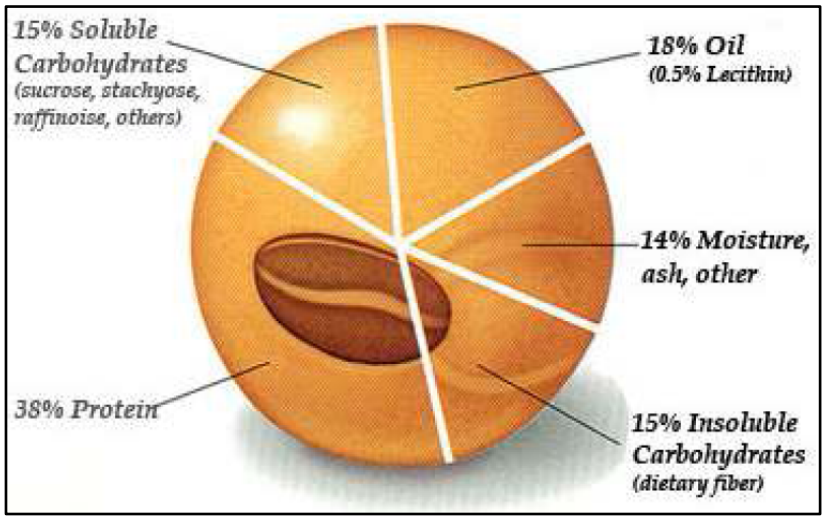


Figure 1-2: Typical composition of soybean [12]

1.2.1 SOYBEAN MEAL OR SOYMEAL

The soybean meal or soymeal is the remaining residue after extraction of soybean oil from soybean as shown in Figure 1-3. This protein-carbohydrate residue contains 46% proteins, 36% carbohydrates, and 18% moisture, ash and hull. As the protein content in the soymeal is higher than distiller's dried grains with solubles (DDGS) obtained from corn, soymeal is most commonly used as an animal feed. The use of soymeal in industrial products along with animal feed will be economically beneficial to biorefineries as well as to the rural agriculture. It should be noted that the amount of proteins, carbohydrates, moisture, and minerals changes with the change in location of soybean production and with time [13]. Thus, for the industrial use of soymeal it is important

to determine its composition and effect of each component on the performance properties of the final product.

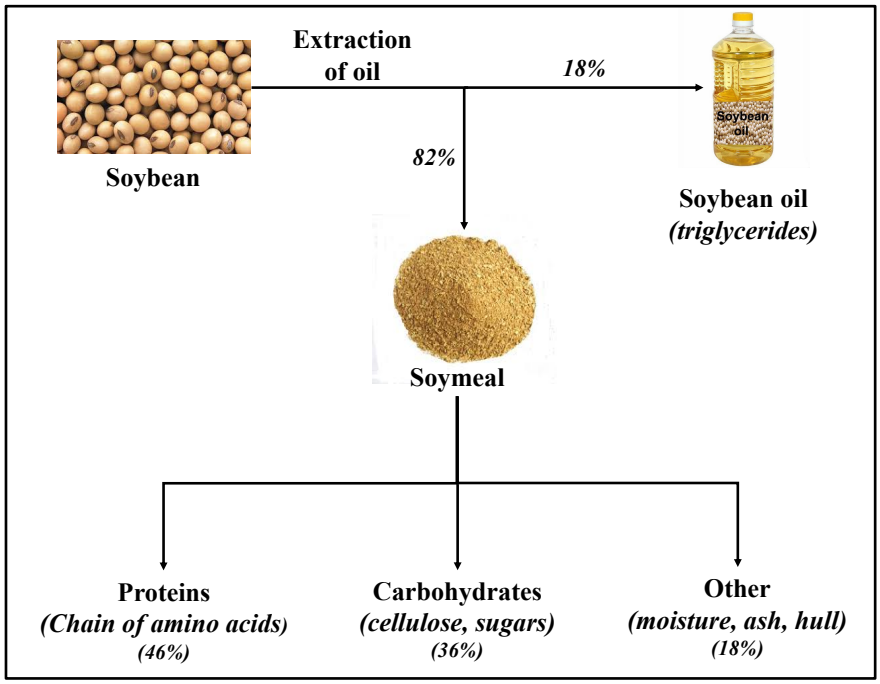


Figure 1-3: Composition of soymeal after extracting soybean oil

Proteins are chains of amino acids as shown in Figure 1-4, where R represents different substituents on the amino acid backbone. Carboxylic group of an amino acid reacts with an amino group of another amino acid forming amide linkage also known as “peptide linkage”. The structure and composition of amino acids [14] present in the soymeal are shown in Figure 1-5. The amino acid contains aromatic as well as aliphatic groups. The composition of amino acids present in soymeal varies and it is determined by complete hydrolysis of soymeal to amino acids [6].

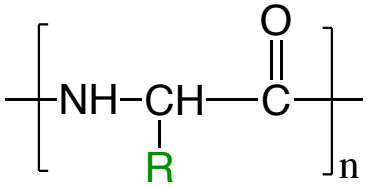


Figure 1-4: Protein structure

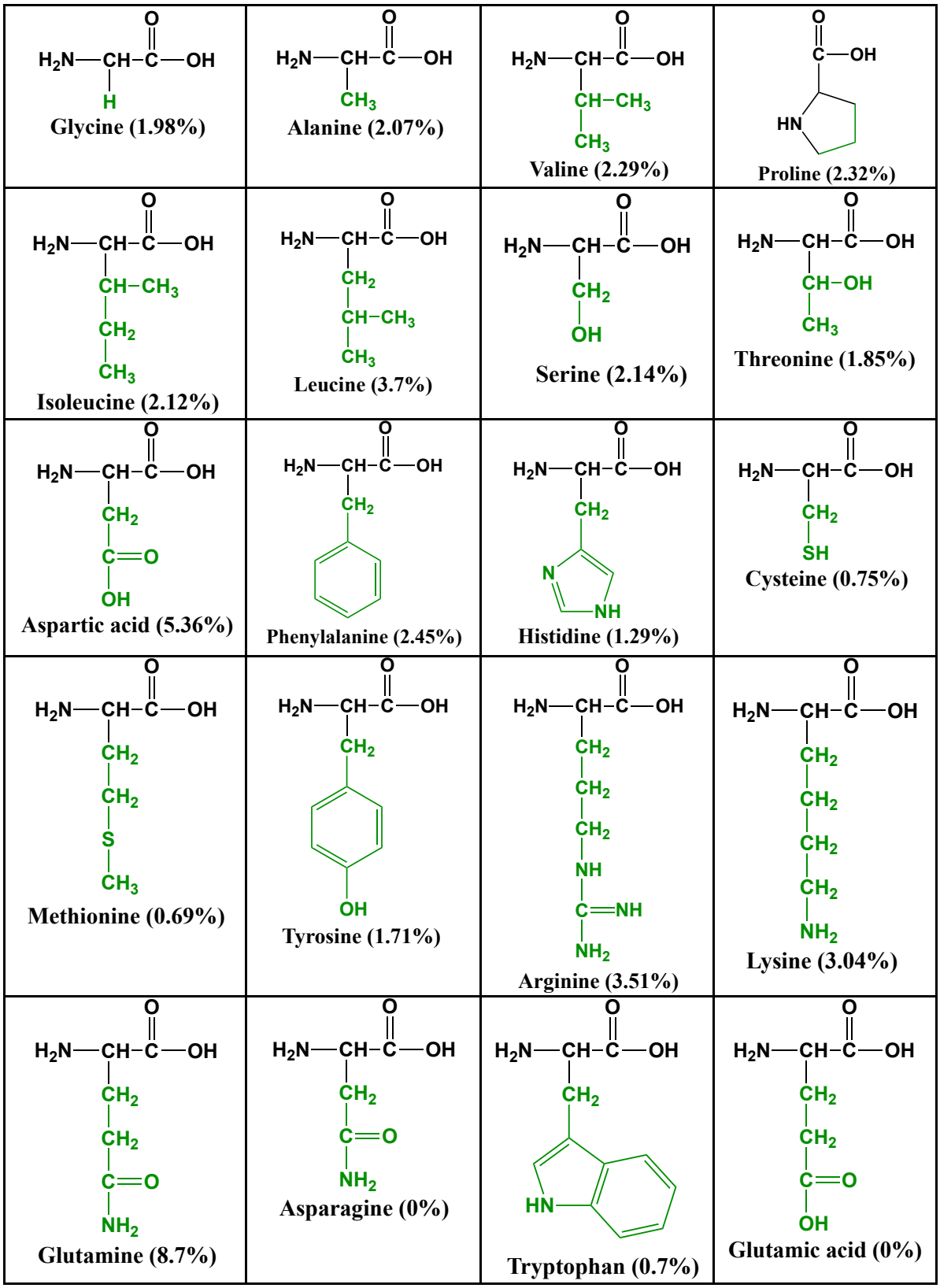


Figure 1-5: Amino acids present in soymeal [14]

The carbohydrates present in soymeal consist of free sugars (mono-, di-, and oligosaccharide), non-starch polysaccharides (NSP), and starch. The composition of each component may vary in different soymeal samples. The carbohydrates present in soymeal approximately contains 10% free sugars, 20 - 30% NSP, and less than 1% starch as shown in Figure 1-6 [15].

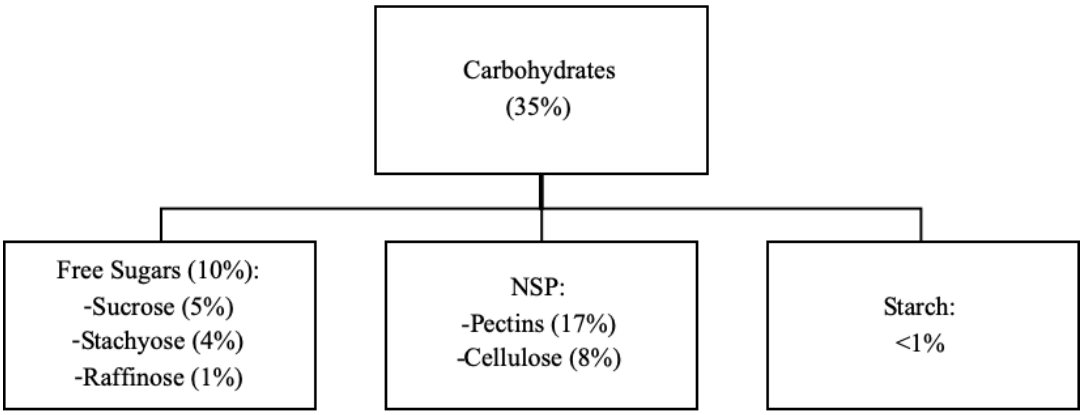


Figure 1-6: Types and amount of various carbohydrates present in soymeal

Free sugars present in soymeal are sucrose, stachyose, and raffinose. The main pectin polymer present in soymeal is rhamnogalacturonans, apart from that arabinogalactan I and xylogalacturonan pectins are also present [15]. Non-starch polysaccharides (NSP) present in soymeal are rhamnose, fucose, arabinose, xylose, mannose, galactose, glucose, uronic acids, and cellulose. Their composition is given in Table 1-1.

Table 1-1: Composition of components of NSP [15]

Components of NSP	Composition (% w/w)
Rhamnose	0.42
Fucose	0.26
Arabinose	2.08
Xylose	1.51
Mannose	1.08
Galactose	3.33
Glucose	4.91
Uronic Acid	3.41
Cellulose	8.00
Total	**25**

1.2.2 SOYBEAN OIL

Soybean oil has a triglyceride structure containing saturated and unsaturated fatty acids as shown in Figure 1-7. The saturated fatty acids present in the soybean oil are palmitic acid (16:0) and stearic acid (18:0). The unsaturated fatty acids present in the soybean oil are oleic acid (18:1), linoleic acid (18:2), and linolenic acid (18:3) [16]. The fatty acids derived from soybean oil, castor oil, and other vegetable oils are being used as building blocks for the synthesis of new raw materials. As fatty acids have one functional group (carboxylic group), it can't be used directly in the synthesis of polymers via polycondensation. The double bonds present in the unsaturated fatty acids can undergo Diels-Alder reaction producing dimer acids [17, 18]. The probable structures of dimer acids are shown in Figure 1-8. The dimerization of a conjugated linoleic acid with another linoleic acid by a Diels-Alder reaction produces a cyclohexane adduct [11]. The oleic acid can also be dimerized by using a clay catalyst through protonation of the double bond which attacks the double bond present on another molecule [11].

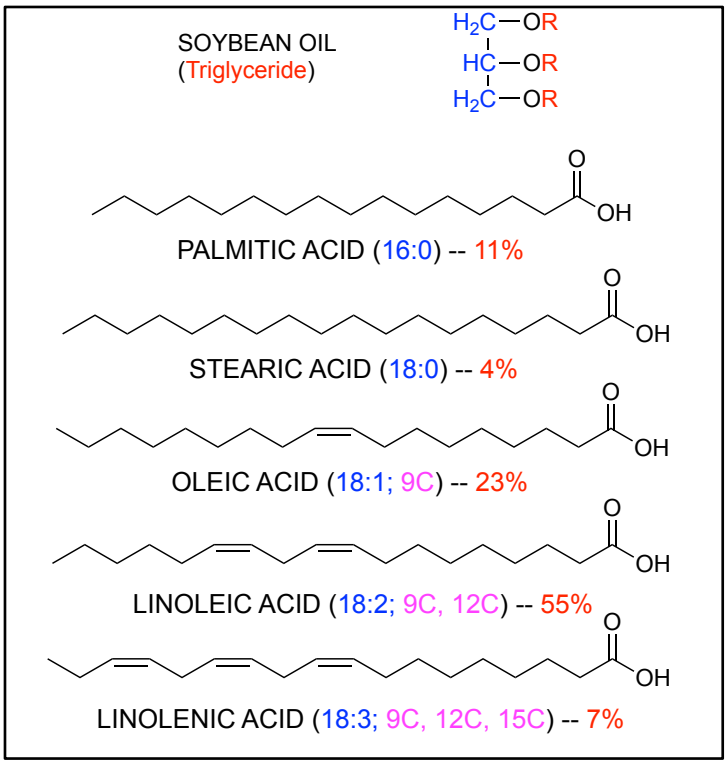


Figure 1-7: Fatty acids composition in soybean oil [16]

The two acid functionalities present in dimer acid makes it a suitable candidate for polyester or polyamide synthesis via polycondensation reaction. Different grades of dimer acids are commercially available in the market and supplied by companies like Croda and Oleon. As dimer acids contain thirty-six carbon atoms and long carbon chain, its incorporation in the polymer will increase renewable carbon content as well as the flexibility of the polymer.

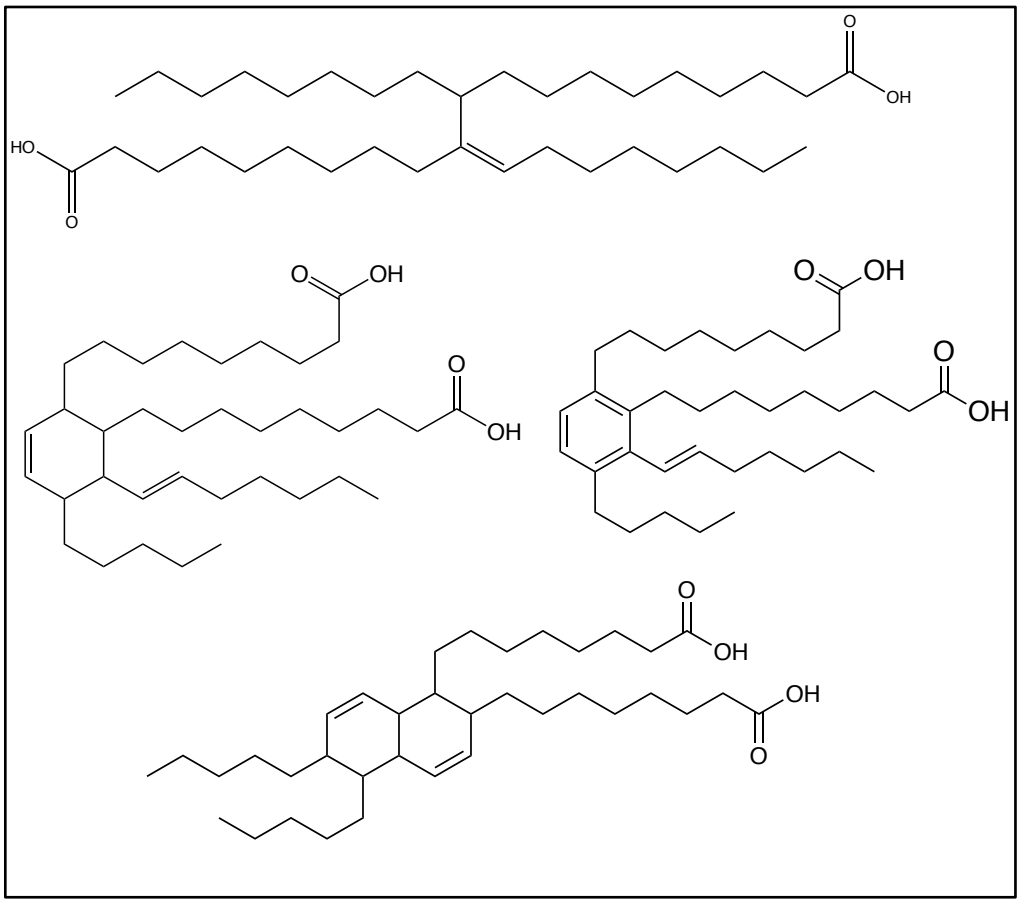


Figure 1-8: Structures of dimer acids [19]

1.3 POLYLACTIDE FROM CORN

Commercially, lactic acid is obtained by bacterial fermentation of corn starch using organisms called lactobacilli [20] which produces, predominantly L-lactic acid. Lactic acid is polymerized to form oligomers of polylactide (PLA) which are depolymerized to produce lactide [21]. Due to the presence of asymmetric carbon atom, there are three different stereoisomers of lactide i.e. L-lactide, D-lactide, and meso-lactide [22] as shown in Figure 1-9. PLA is synthesized from ring-opening polymerization of lactide which is produced from lactic acid. PLA is a slowly crystalizing polymer [22]. During the synthesis, if the meso-lactide content goes above 7-8% then PLA becomes completely amorphous [21, 23]. Thus, excess of meso-lactide is continuously removed during the synthesis of PLA as shown in Figure 1-10.

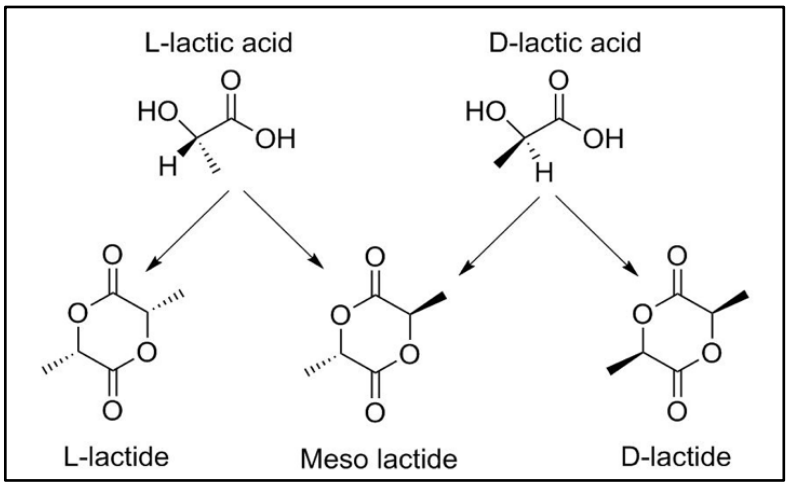


Figure 1-9: Stereoisomers of lactide

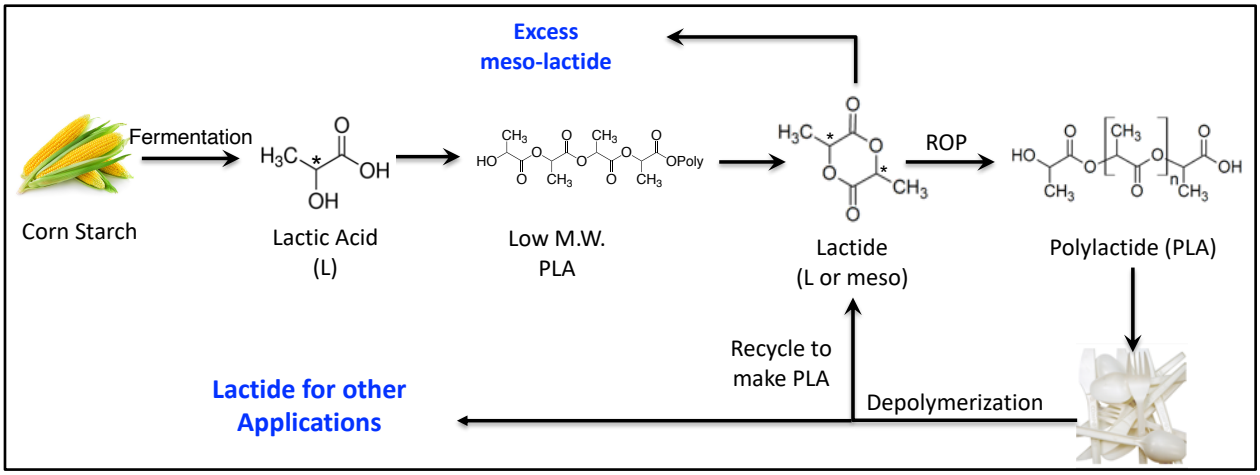


Figure 1-10: Various sources of lactide

A large quantity of PLA is being produced all over the world, and NatureWorks is the largest producer with the capacity of producing 140 kt/year [23]. PLA products can be easily depolymerized back to lactide [24] to form lactide. Thus, meso-lactide separated during PLA synthesis and recycled lactide can be used for the synthesis of new building blocks for applications in polyurethanes and polyester.

1.4 POLYURETHANE FOAMS

Polyurethanes are the most versatile polymers having a variety of applications in foams, coatings, adhesives, sealants, and elastomers. Polyurethane foams (PUF) are widely used and are preferred

over other foams (e.g. expanded polystyrene (EPS), extruded polystyrene (XPS) and polyethylene foam) due to their good thermal insulation properties, easy installation, and relatively low cost [25, 26]. They have various applications in building & construction, electronics, automotive, packaging materials, and cushioning industries. The demand for polyurethane is continuously growing as shown in Figure 1-11. Polyurethane foam is a major sector of polyurethanes [27]. Polyurethanes are synthesized using two major components i.e. polyols and isocyanates. Polyols are polymeric materials containing hydroxyl groups. Isocyanates are chemical building blocks containing isocyanate groups.

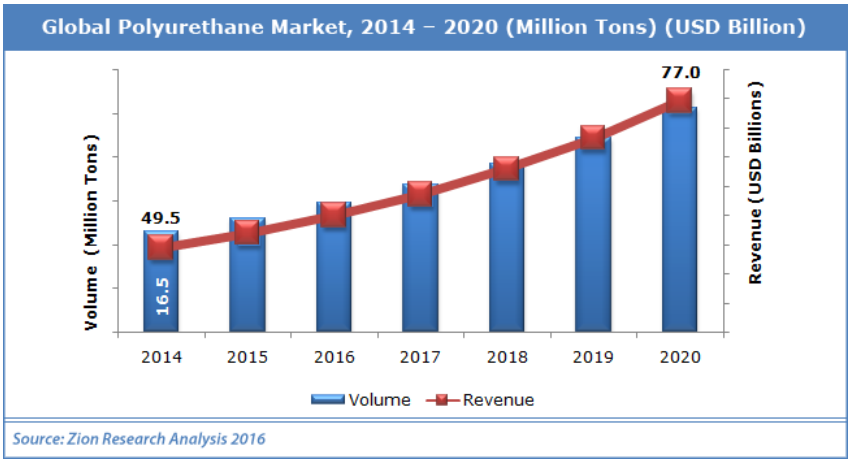


Figure 1-11: Global polyurethane market, 2014-2020 [28]

Hydroxyl groups of polyols react with isocyanate groups of isocyanates forming urethane linkages as shown in Figure 1-12. This reaction is also called as "gelling reaction" [29].

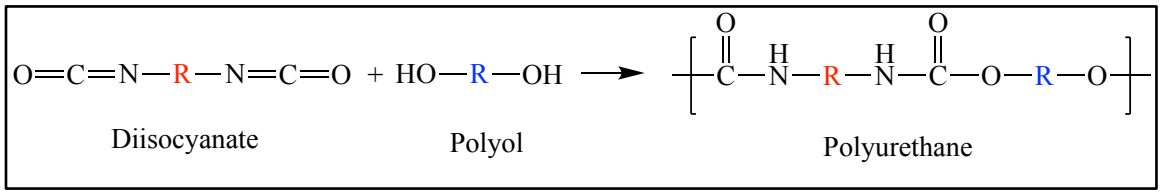


Figure 1-12: Reaction of diisocyanate with polyol

In a polyurethane, the urethane linkages act as a hard segment whereas carbon chain present on the polyol side act as a soft segment. Presence of long carbon chain in polyol increases the

molecular weight of polyol which decreases its hydroxyl value. As hydroxyl value increases, the number of urethane linkages formed in polyurethane also increases which makes polyurethane hard and brittle. Polyurethane produced from a low hydroxyl value polyol has fewer urethane linkages which make it soft and elastic. In polyurethane foam synthesis, another reaction occurs between isocyanate and water giving carbon dioxide gas. This reaction is shown in Figure 1-13 and called as "blowing reaction" [29].

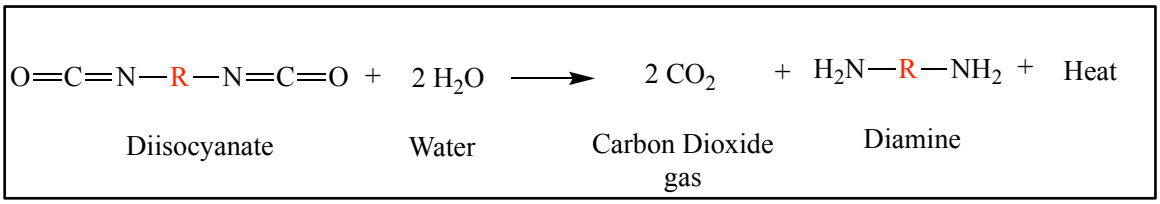


Figure 1-13: Reaction of diisocyanate with water

Two different types of polyurethane foams exist i.e. rigid polyurethane foams and flexible polyurethane foams. Polyols with high hydroxyl value give rigid polyurethane foams and low hydroxyl value give flexible polyurethane foams. Foams can have an open cell or closed cell structure as shown in Figure 1-14 depending on their applications.

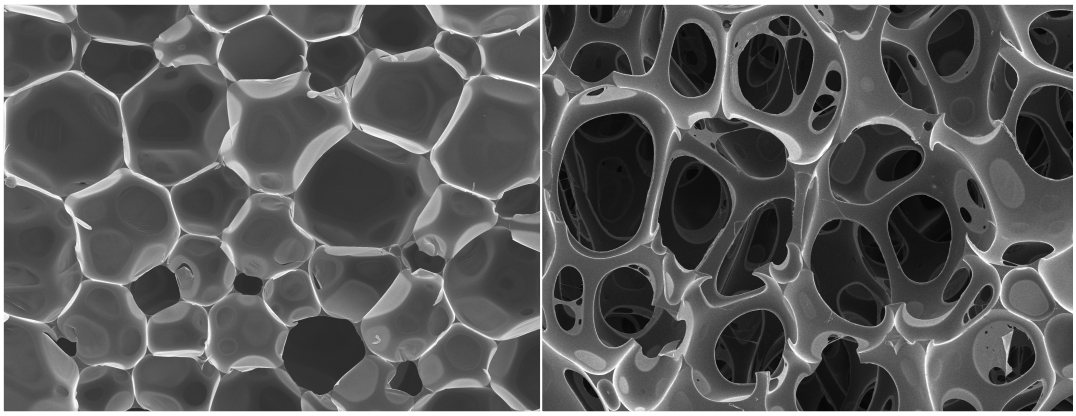


Figure 1-14: Scanning Electron Microscopy images of closed cell (left) and open cell (right) polyurethane foam

Closed-cell foams do not allow permeation of gases or heat as they have closed air pockets. Thus, closed-cell foams act as an insulator [30]. Open-cell foams have open air pockets which allow

permeation of air through them and hence they are used in cushioning applications [30]. Conventionally, polyurethane foams were synthesized from petroleum polyols i.e. polyether polyols obtained by ring-opening polymerization of propylene oxide or ethylene oxide on a multifunctional initiator like ethylene glycol or glycerol. The isocyanates used for polyurethane foams are methylene diphenyl diisocyanate (MDI) and toluene diisocyanate (TDI). MDI has two benzene rings whereas TDI has one benzene ring. The presence of two isocyanate groups on the same benzene ring makes TDI very reactive. MDI exists in a polymeric form called as polymeric MDI which is commonly used for polyurethane foams [31, 32]. In recent years, biobased polyols were introduced in the market and there is ongoing research for the development of polyols from various raw materials i.e. castor oil, cashew nutshell liquid [33, 34].

1.5 BIOBASED POLYOLS

Most of the biobased polyols are derived from plant oils. Soybean oil was most commonly used. Different routes such as transesterification, epoxidation, ozonolysis, and hydroformylation were used for polyol synthesis from plant oils [11]. Plant oils are triglycerides having two reactive sites one is the double bond and the other side is the ester group.

1.5.1 Transesterification

In transesterification chemistry, the reaction of ester groups is involved. Transesterification of triglycerides with multifunctional alcohol groups like glycerol in the presence of strong acid or inorganic bases as catalyst gives polyols [35] as shown in Figure 1-15. Soybean oil monoglyceride (SOMG) polyol was also prepared from soybean oil and glycerol in the presence of calcium hydroxide as a catalyst [36].

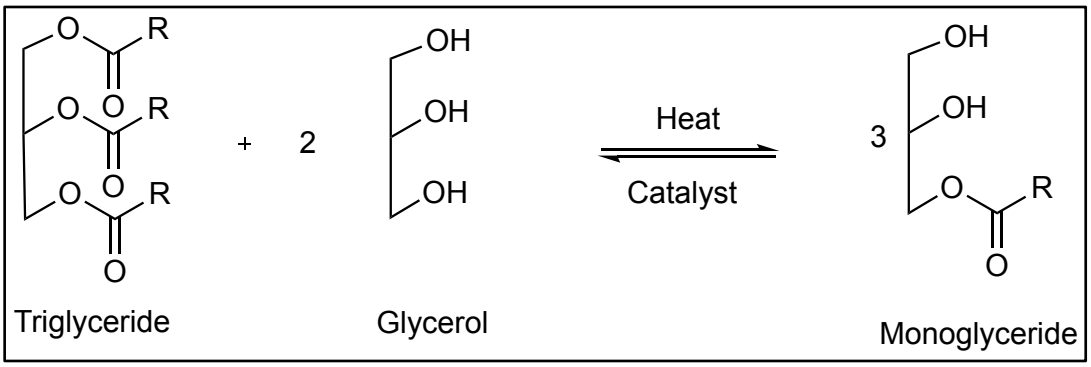


Figure 1-15: Transesterification of triglyceride with glycerol [36]

1.5.2 Epoxidation

This route is most commonly used for commercial synthesis of biobased polyols from plant oils. In the epoxidation route, the reaction of the carbon-carbon double bond is involved. Triglycerides having carbon-carbon double bond were converted into epoxides in presence of hydrogen peroxide and acids [36]. These epoxy rings can be opened by alcohol or acid giving secondary hydroxyl group as shown in Figure 1-16. These polyols are less reactive as hydroxyl group is secondary.

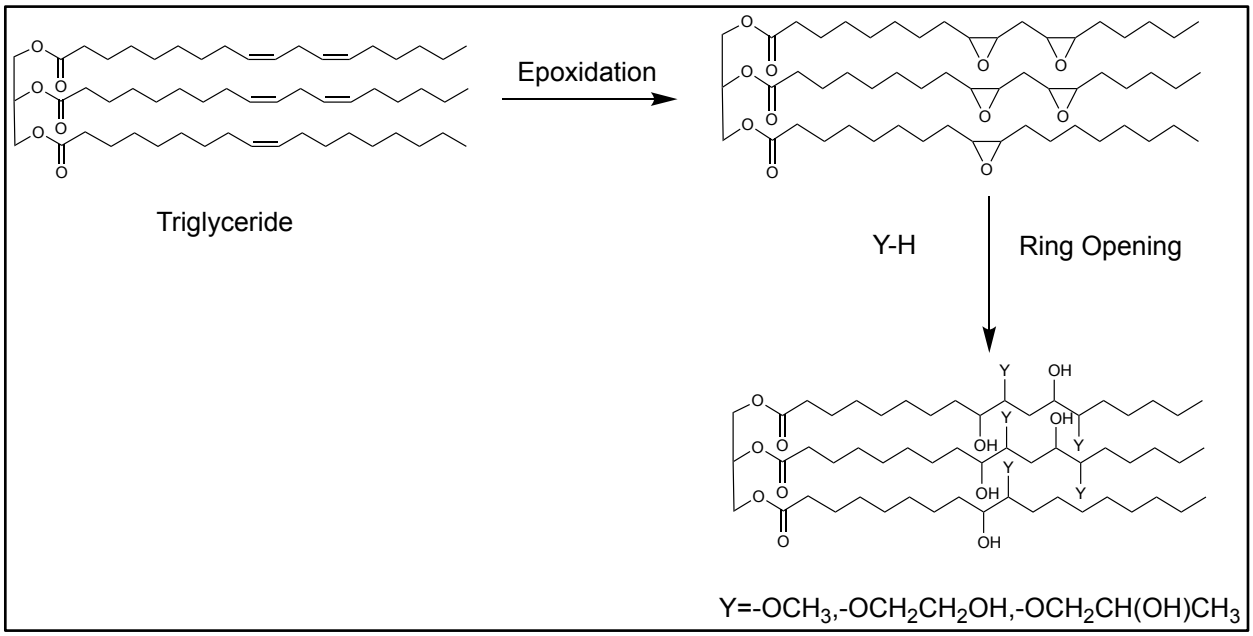


Figure 1-16: Epoxidation of soybean oil followed by ring opening [37]

1.5.3 **Ozonolysis**

Ozonolysis is another method used for the synthesis of polyols. Ozone can be used to oxidize the double bond in the triglycerides and then those compounds can be reduced to alcohols using reducing agents like $NaBH_4$ [38]. Ozonolysis of soybean oil or monoglyceride with an excess of ethylene glycol in the presence of alkaline catalyst like NaOH produced a mixture of polyols [38] as shown in Figure 1-17.

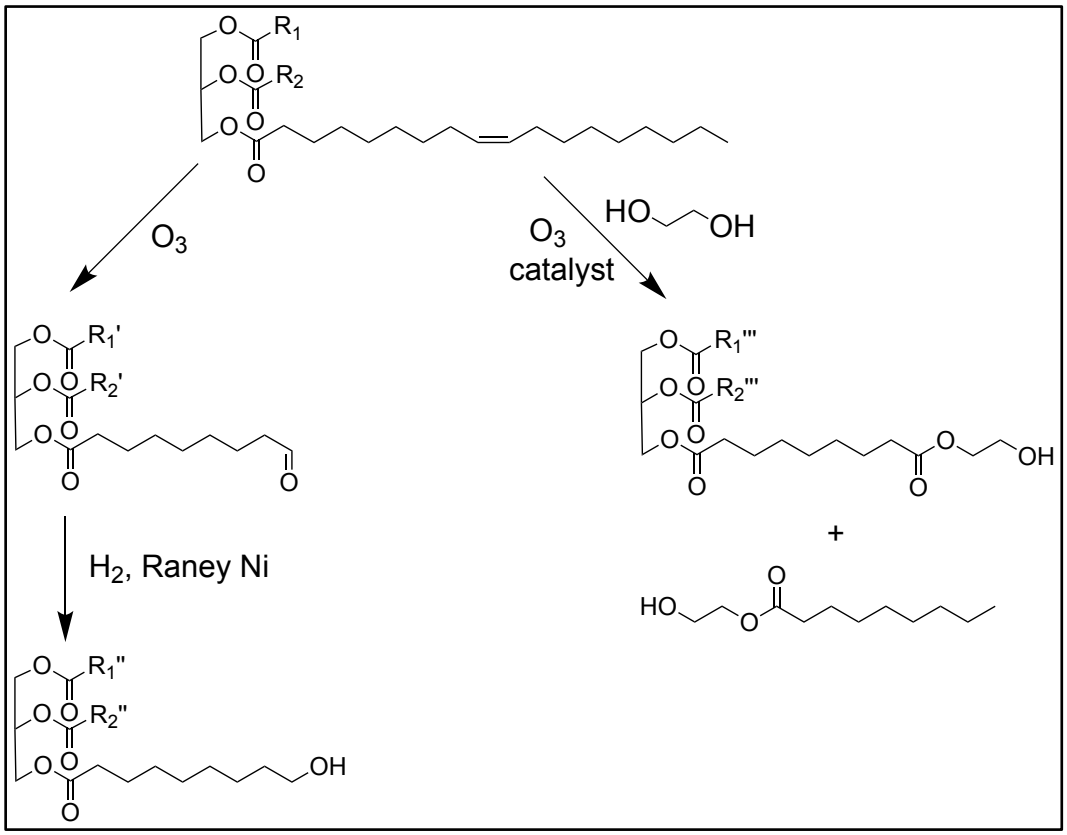


Figure 1-17: Ozonolysis of monoglyceride to synthesize polyols via different routes [39]

1.5.4 **Hydroformylation**

Hydroformylation involves the reaction of a double bond of triglycerides with carbon monoxide and hydrogen in the presence of rhodium or cobalt catalysts to yield aldehydes as shown in Figure 1-18. Then these aldehydes are hydrogenated to polyols using Raney nickel as a catalyst [35] [40]. As rhodium catalyst is very expensive, total recovery of catalyst is required for this process to be

economical [40]. The cobalt catalyst is not expensive, but it gives a lower yield which adds to separation costs. Also, for the hydrogenation step, Raney nickel catalyst is required. This process requires various catalysts which will increase the production cost of polyols.

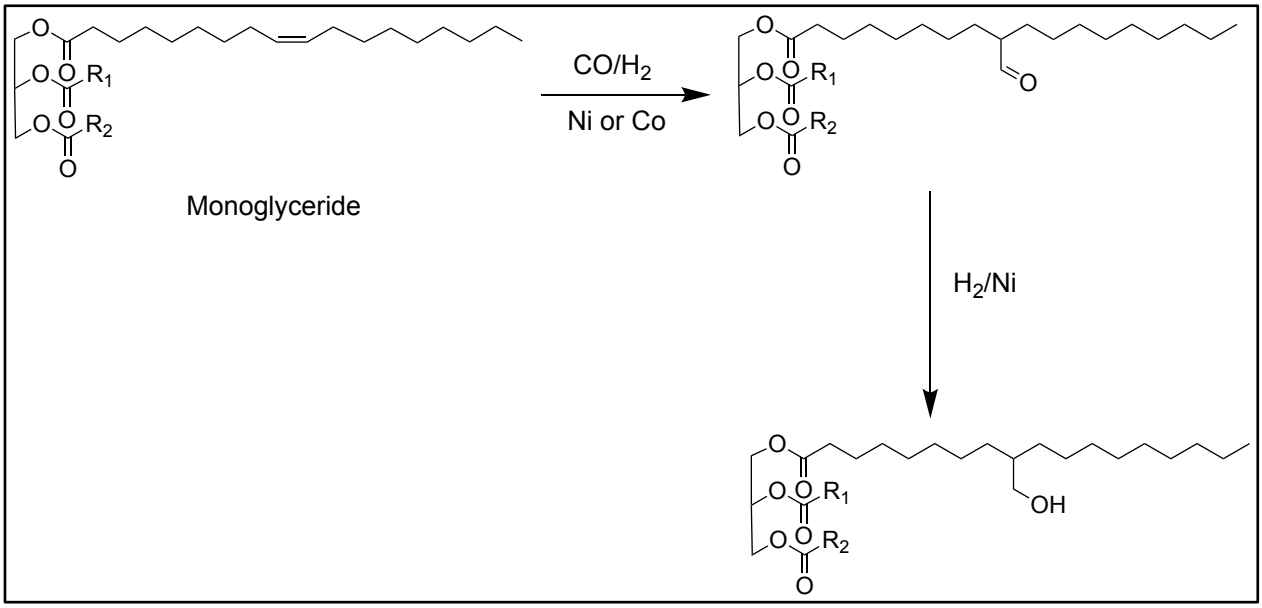


Figure 1-18: Hydroformylation of monoglyceride [11]

1.5.5 Commercially available biobased polyols

CERENOL™ is a polyol produced from glucose fermentation by DuPont. Most of the biobased polyols are synthesized from the epoxidation of vegetable oils. For example, JEFFADD™ B650 by Huntsman, AGROL® by Biobased Technologies (now Cargill), BIOH® by Cargill, SOVERMOL® by BASF (COGNIS), and RADIA ® by Oleon, etc. The Dow Chemical Company started production of biobased Renuva™ from soybean oil. However, its production stopped as several steps involved in the process increased the cost of polyol.

1.6 SYNTHESIS OF BIOBASED POLYOLS FOR POLYURETHANE FOAMS AND POLYESTERS

Although there are different biobased polyols available in the market, most of them are derived from soybean oil. In this work, biobased polyols were synthesized from protein-biomass residue

i.e. soymeal, and lactide. These polyols were synthesized by using simple chemistries and one-pot synthesis process. The polyols with higher hydroxyl value were used in rigid polyurethane foams and polyols with lower hydroxyl value were used in flexible polyurethane foams. The properties of polyurethane foams produced were compared with the properties of existing petroleum products. Some of the biobased polyols were used as a plasticizer for polylactide (PLA). The detailed description of each chapter is given below.

In chapter 2, the use of a novel method to determine the composition of soymeal will be discussed. It will also cover the use of a two-step, single-pot reaction to transform a low-cost protein-carbohydrate residue into a new and usable biobased polyol. Using this process, the whole soymeal can be converted to polyols without the need to separate or purify the soymeal constituents. This will provide a considerable cost advantage and make these soymeal polyols the lowest cost biobased polyols on the market.

In chapter 3, the synthesis of new biobased building blocks from meso-lactide will be discussed. The new monomers will be synthesized by ring-opening of meso-lactide with primary amines and alcohols. The ring-opening of meso-lactide with amino-alcohol will give low molecular weight diols which can be used in polyester synthesis (e.g. PET) or polyurethanes. The ring-opening of meso-lactide with long-chain alcohols (e.g. PEG) will give a diol. The diol will be reacted with dimer acid using polycondensation chemistry to synthesize low hydroxyl value polyols for application in flexible polyurethane foams.

In chapter 4, the use of new biobased polyols synthesized from soymeal and lactide in rigid polyurethane foams (PUF) for its application as an insulation material will be covered. The mechanical properties, thermal properties, and morphology of biobased PUF will be compared with the PUF made from commercial petroleum-based polyols. The thermal conductivity, aging

study, and water absorption study will be performed on biobased PUF for its application in building and construction material.

In chapter 5, the synthesis of flexible polyurethane foams from a series of biobased polyols produced from dimer acids will be discussed. As flexible polyurethane foams have application in automotive and cushioning, the properties of produced flexible PUF will be tested accordingly. The effect of different catalysts and optimization of catalyst concentration for biobased PUF will also be discussed. The mechanical properties, thermal properties, and morphology of biobased PUF will be compared with the PUF made from commercial petroleum-based polyol and commercial biobased polyol.

In the last chapter, biobased polyols derived from lactide and dimer acids will be used as a plasticizer for PLA. The transesterification reaction of polyols with PLA will be done via reactive extrusion (REX). The thermal properties of modified PLA such as glass transition temperature, crystallization temperature, and crystallinity will be studied. The effect of reactive blending of PLA and polyol on mechanical properties such as tensile strength, elongation at break, and impact strength will be evaluated.

2 POLYOLS DERIVED FROM PROTEIN-CARBOHYDRATE BIOMASS (SOYMEAL) RESIDUE: COMPOSITION ANALYSIS, SYNTHESIS, AND CHARACTERIZATION

2.1 INTRODUCTION

Polyurethanes are the most versatile polymers having a variety of applications in foams, coatings, adhesives, sealants, and elastomers. Polyurethane foams are used in a variety of applications and their demand is continuously growing. Polyol and isocyanate are the two major components used in polyurethane synthesis. Conventionally, petroleum feedstocks were used to make polyols and isocyanates, but in recent years, bio-based feedstocks are being used in combination with petroleum feedstocks. Recently, many companies are incorporating renewable biomass carbon in their products (e.g. Ford Motor Company's polyurethanes, NatureWorks's Ingeo polymers) in order to reduce product's carbon footprint and environmental impacts. Literature reports the synthesis of polyols and PUF using different biomass resources such as cardanol (obtained from cashew nutshell liquid) [41, 42], α-amino-ε-caprolactam (obtained from L-lysine) [43], cellulose [44], and algae oil [45]. However, most of these commercially available biobased polyols are derived either from plant oils e.g. soybean oil [11] or from saccharides e.g. sucrose. Various routes are used to produce polyols from a plant oil including transesterification [46], epoxidation [47], ozonolysis [38], hydroformylation [11]. The epoxidation route is most commonly used in industry for the synthesis of polyols from plant oil [11]. However, this route gives secondary hydroxyl groups which are less reactive towards isocyanates than the primary hydroxyl groups [38]. Plant oils include canola oil, castor oil, rapeseed oil, and soybean oil, with soybean oil being the most used for polyol synthesis [36, 38, 48, 49]. As soybean crop is 55% of the total world's production of oilseeds [50], the soybean oil is commonly used in food, in synthesis of polyols, in production

of biodiesel [10, 51, 52], and in other industrial products. The co-product of soybean oil i.e. soymeal is primarily used in animal feed and human nutrition [9, 53], and a small amount is used by the chemical industry [7]. Protein-rich sources like soy protein concentrate (SPC - 70% proteins) and soy protein isolate (SPI - 90% proteins) are being used in bioplastic production [51, 54] but they are expensive compared to soymeal. There are other protein-rich byproducts available like Jatropha meal (a byproduct of biodiesel production), distiller's dried grains with solubles (DDGS, a byproduct of ethanol production from starch) but protein content in soymeal is more. Thus, protein-rich soymeal is being used in research as a biobased material in the synthesis of additives, adhesives, and composites [55] [56]. As soymeal is inexpensive [7] and is a co-product, its new industrial uses will be economically favorable for biofuel industries [6, 9]. Hence, it can be used in various biobased materials like polyols and polyurethane foams to improve mechanical and thermal properties, and to increase their bio-renewable content. Commercialization of products made from biobased feedstocks will also contribute to reduced carbon footprint and create more value for agriculture.

The properties of a material depend on the chemical activity which depends on the composition of material [57]. For example, soymeal is used as fillers in composites where moisture content becomes critical [51]. It is also used in the synthesis of polyols from protein residues where protein content becomes critical [58, 59]. Hence, the properties of materials made from soymeal will depend on the composition of components of soymeal i.e. proteins, carbohydrates, moisture, and minerals. Though the average composition of components of soymeal is known it may vary due to different processing conditions and species [51]. Also, change in the composition of soymeal will affect the final properties of products produced from it. Hence, it is important to know the composition of soymeal being used in the research.

Different analytical methods have been used to determine the composition of crude protein, fat, ash, and moisture present in biomass [54, 60] which are time-consuming. Recently, Near Infrared Reflectance (NIR) spectroscopy is being used for the analysis of crude protein, fat, carbohydrates, and crude fibers but it requires large high-quality data and initial blank spectrum which limits its application [57]. Thermogravimetric analysis (TGA) was performed in an inert atmosphere to study pyrolysis behavior and composition of lignocellulosic biomass [57, 61]. TGA has been used to determine the composition of hemicellulose and cellulose present in wood and fern which was successfully correlated with experimentally obtained composition [57]. The composition of different components of material can be obtained using TGA if decomposition temperatures of components present in the material are different. The individual composition of small components like amino acids of proteins, free sugars of carbohydrates cannot be determined using TGA.

In this study, deconvolution of derivative thermogravimetric (DTG) graph obtained from TGA will be used to find the overall composition of proteins, ash, moisture, and carbohydrates. Soluble carbohydrates will be separated using ethanol extraction and percentages of soluble and insoluble carbohydrates will be obtained by deconvolution of their DTG graphs. After obtaining the composition of soymeal, a two-step, a single-pot reaction will be used to transform a low-cost protein-carbohydrate residue from a soybean refinery to new and usable biobased polyol. Using our process, we can successfully transform the whole soymeal to polyols without the need to separate or purify the soymeal constituents [58]. This provides a considerable cost advantage and makes these soymeal polyols the lowest cost biobased polyols on the market. This soymeal polyol can be used in rigid biobased PUF.

2.2 EXPERIMENTAL

2.2.1 Materials and chemicals

The soymeal used in these experiments was received from Zeeland Farm Services, Inc. (Michigan, USA) with a particle size of 18F (mesh size). Propylene carbonate (99%) was purchased from Sigma-Aldrich (Wisconsin, USA). Ethanolamine or monoethanolamine (MEA) (99%) was purchased from Fisher Scientific (Pennsylvania, USA).

2.2.2 Composition analysis of soymeal

The composition of soymeal used for the synthesis of polyol was determined using simple analytical techniques. This involves the separation of soluble carbohydrates from soymeal and using a deconvolution method to determine the composition of individual components.

2.2.2.1 Separation of soluble carbohydrates

Soluble carbohydrates were separated from soymeal using 50% (v/v) ethanol-water mixture. In a round bottom flask, 8 grams of soymeal and 100 ml of ethanol (50% v/v) solution was taken and stirred at room temperature (20°C) for 20 hours. Following that, the insoluble part of soymeal was separated by using a simple filtration method. The insoluble residue was called as ethanol washed soymeal (EWS) and it was dried in an oven. Water and ethanol from filtrate were removed and the residue obtained was called as soluble carbohydrates (SC).

2.2.2.2 Characterization of soluble carbohydrates and soymeal

Thermogravimetric measurements were conducted under nitrogen flow using a thermogravimetric analyzer, TGA Q50 (TA Instruments, Delaware, USA). In this analysis, a sample (10 - 15 mg) was taken in an aluminum pan and heated to 600°C with a heating rate of 10°C /min. The weight loss (%) of a sample as a function of temperature (°C) was obtained from this analysis. The derivative thermogravimetric graphs (DTG) (%/ºC) were used to identify the degradation temperatures.

Attenuated Total Reflection-Fourier Transform Infrared Spectroscopy (ATR-FTIR) spectra were acquired on a FTIR (Shimadzu Co., Tokyo, Japan, IRAffinity-1) equipped with a single reflection ATR system (PIKE Technologies, Wisconsin, USA, MIRacle ATR). ATR-FTIR used with resolution 4 cm^{-1}, Happ-Genzel apodization function and 64 scans were conducted on the powdered sample. The output from FTIR was recorded as transmittance (%) as a function of wavenumber (cm^{-1}). The nitrogen content of soymeal was determined using a CHN analyzer (PerkinElmer, Massachusetts, USA). Ash content of soymeal was determined by running TGA in air atmosphere. The moisture content in soymeal was determined by the MX-50 moisture analyzer (A&D Weighing, California, USA).

2.2.2.3 Polyol synthesis from soymeal

After analyzing the composition, soymeal was directly used without any purification for the synthesis of polyols. This is a two-step and one-pot synthesis process.

2.2.2.4 Synthesis of amine derivatives using transamidation process

The soymeal and ethanolamine (1:2, 1:3 and 1:5 mass ratios used) were reacted in a round-bottom flask and nitrogen gas was purged initially for 15 - 20 minutes. The reaction was conducted for 2 hours at a temperature of 100 - 105ºC. The intermediate products obtained were referred to as amine derivatives which were characterized for amine value, TGA, and FTIR.

2.2.2.5 Synthesis of soymeal-based polyol

Amine derivatives were reacted with 10% molar excess of propylene carbonate at a temperature of 70 - 75ºC for 2 hours to produce the soymeal-based polyol called as soymeal polyol. A mole of amino groups reacts with a mole of propylene carbonate. The soymeal polyols were characterized for hydroxyl value, amine value, viscosity, specific gravity, TGA, FTIR, and percent insolubles.

2.2.2.6 Characterization of amine derivatives and polyols

The hydroxyl value of the polyol was determined by ASTM E1899-16 and the amine value was determined by ASTM D2073-92. All titrations were performed using 857 Titrando (Metrohm, Florida, USA) auto-titrator. The viscosity of the soymeal polyol was measured at room temperature using a Brookfield viscometer-LVDV-E model (AMETEK Brookfield, Massachusetts, USA).

The amount of insoluble matter present in the amine derivatives was determined for a kinetic study of the transamidation reaction. A small amount of the amine derivatives was dissolved in water followed by filtering out the liquid and finally drying the residue in an oven for 24 hours. A similar method was used to determine the percentage of insoluble matter present in the soymeal polyol.

The ^{13}Carbon-nuclear magnetic resonance (^{13}C NMR) spectrum was recorded on a 500 MHz NMR spectrometer (Varian Inc., USA, Unity Plus 500 MHz) using deuterated dimethyl sulfoxide (DMSO-d_6) as a solvent having tetramethylsilane as an internal standard. The spectrum was recorded at ambient temperature (22°C), relaxation delay 25 s, number of scans 256, and inverse gated decoupling (decoupling only during acquisition).

2.3 RESULT AND DISCUSSION

2.3.1 Composition analysis of soymeal

As discussed earlier, the composition of soymeal may vary depending on species or location. Also, the composition of proteins and carbohydrates is different for different biomass residue such as DDGS, jatropha meal etc. Thus, it was important to determine composition of soymeal being used for polyol synthesis.

2.3.1.1 Separation of soluble carbohydrates

The carbohydrates present in the soymeal consist of 10% of free sugars (mono-, di-, and oligosaccharide), 20 - 30% of non-starch polysaccharides (NSP), and 1 % of starch [15]. Free

sugars present in the soymeal i.e. sucrose, stachyose, and raffinose are soluble in water as well as in ethanol solution [62-64]. Non-starch polysaccharides (NSP) consists of pectins and cellulose [15]. Pectins are mainly composed of rhamnose, fucose, arabinose, xylose, mannose, galactose, glucose, and uronic acids. They are partially soluble in water and can be precipitated in 66 - 80% ethanol [15]. Cellulose and starch are insoluble in water. The soluble carbohydrates which consist of free sugars and some NSP can be separated from soymeal by 50 - 70% aqueous alcohol solution [15]. Free sugars can be easily extracted in water but it is also a good solvent for some proteins [62, 63]. Therefore, the alcohol-water solution was used for extraction instead of using just water. Incomplete extraction of soluble sugars was observed with an increase in the strength of alcohol from 50% to 90% [62-64]. Also, the effect of 50% (v/v) of ethanol or methanol was same on the extraction of soluble carbohydrates from soymeal, and the effect of temperature was also negligible [63]. Considering these, the separation of soluble carbohydrates was carried out at an ambient temperature and using 50% (v/v) ethanol-water solution. The experimental results of separation of soluble carbohydrates are given in Table 2-1. The ethanol washed soymeal (EWS) contains proteins, insoluble carbohydrates, and minerals. Whereas soluble carbohydrates (SC) contains some soluble proteins and residual moisture along with soluble carbohydrates.

2.3.1.2 Thermogravimetric analysis and deconvolution of DTG graphs

The DTG graph of soymeal gave three major degradation peaks 91°C, 226°C, and 296°C as shown in Figure 2-1(a). In previous literature, three degradation stages were observed in TGA of soymeal [51, 56] and other biomass like corn stover, DDGS, and rice straw [51, 54]. Stage I (25°C - 140°C) was due to the residual moisture in soymeal [56]. Stage II (150°C - 300°C) could be due to the degradation of soy proteins [56], cleavage of peptide bonds with dissociation of some bonds [54] or degradation of hemicellulose, starch, polysaccharide, proteins [51]. The stage III (250°C -

400°C) was due to the degradation of proteins in soymeal [54, 56]. Also, degradation of stable metal traces and minerals was observed after stage III at around ~500°C [51].

The DTG graphs of ethanol washed soymeal (EWS) and soluble carbohydrates (SC) are shown in Figure 2-1(c) and Figure 2-2 (a), respectively. In DTG graph of EWS, the degradation peak around ~220°C disappeared which was observed in DTG graph of soymeal. But it was observed in DTG graph of soluble carbohydrates. Thus, we can say that stage II (150°C - 300°C) of degradation of soymeal was due to the degradation of soluble oligosaccharide and soluble NSP present in the soymeal. Initial separation of soluble carbohydrates from soymeal was useful in understanding the degradation behavior of components of soluble carbohydrates (SC) as well as ethanol washed soymeal (EWS). But to confirm the result obtained, the degradation temperatures of soluble carbohydrates which were reported in previous literature were studied.

The sucrose, raffinose, and stachyose are low molecular weight oligosaccharides [63] which means they will degrade before the degradation of high molecular weight polysaccharides and proteins. The degradation temperature of sucrose and raffinose is 215°C [65], and DTG graph of arabinose, xylose and mannose showed that the degradation of these NSP occurs around 200°C, 250°C, 360°C and 500°C [66]. Thus, it can be confirmed that the peak at 220ºC was due to degradation of free sugars (sucrose, stachyose, raffinose) and soluble part of NSPs (arabinose, xylose, fucose, glucose, rhamnose, galactose) [65].

In DTG graph of EWS, four degradation stages 150°C - 270°C, 250°C - 350°C, 300°C - 450°C, and 450°C - 525°C were observed. Cellulose degrades around 245ºC [65], starch degrades around 350°C [67], and some NSPs degrade over range of temperatures i.e. 250°C, 350°C, 500ºC [66]. Thus, there was a possibility of the presence of two more degradation peaks around 250°C and 370°C for the remaining insoluble carbohydrates which might have been merged with the peak at

293°C. The peak at 496°C is mostly due to insoluble carbohydrates [66] and other components like minerals, metal traces.

Deconvolution of DTG graph of EWS was done to get individual compositions of components present. Thermogravimetric analysis was previously used as a tool for determination of the composition of lignin and cellulose present in biomass like wood, fern [57, 61]. Lignin and cellulose were separated from biomass experimentally and the compositions obtained by deconvolution of DTG of biomass was in good agreement with that of experimental compositions [57, 61]. Thus, deconvolution was used to find the composition of soymeal, and Fityk software was used for deconvolution [68]. The deconvoluted graph of EWS is shown in Figure 2-1 (d) and composition of proteins and insoluble carbohydrates is given in Table 2-1 as a percent of the total weight of EWS. These percentages were obtained from calculating the area under each peak and then dividing each area by the sum of all areas. Similarly, deconvolution of DTG graph of SC was done as shown in Figure 2-2 (b) to get the composition of soluble carbohydrates and proteins.

Table 2-1: Composition of ethanol washed soymeal and soluble carbohydrates

Weight of EWS or SC (g)	**Peak**	**Component**	**Percentage (%)**	**Weight (g)**
Ethanol washed soymeal (5.576 ± 0.021)	293°C	Proteins	66	3.680
	244°C	Insoluble Carbohydrates	10	1.394
	379°C		15	
	496°C	Other	9	0.502
Total			100	5.576
Soluble carbohydrates (1.961 ± 0.050)	126°C	Moisture	14	0.275
	210°C	Soluble Carbohydrates	32	1.471
	249°C		28	
	413°C		15	
	296°C	Proteins	11	0.215
Total			100	1.961

2.3.1.3 Fourier Transform Infrared Spectroscopy (FTIR)

The ATR-FTIR spectra of soymeal and soluble carbohydrates are given in Figure 2-2 (c) and (d) respectively. The peak at 3200 cm^{-1} was attributed to OH stretch of water and carbohydrates [51, 54]. The small peaks at 2900 cm^{-1} were expected due to C-H stretch [69]. The peaks at 1635 cm^{-1} and 1533 cm^{-1} present in FTIR of soymeal were attributed to C=O and N-H bonds of amide linkages [56]. Amide linkages are characteristic of proteins which are a major component in soymeal. The peaks around ~1500 cm^{-1} - 1400 cm^{-1} present in FTIR of soluble carbohydrates were attributed to N-H or CH_2 wag [69]. The peaks at 1394 cm^{-1}, 1234 cm^{-1}, and 1028 cm^{-1} were expected due to C-N and C-O bonds [69].

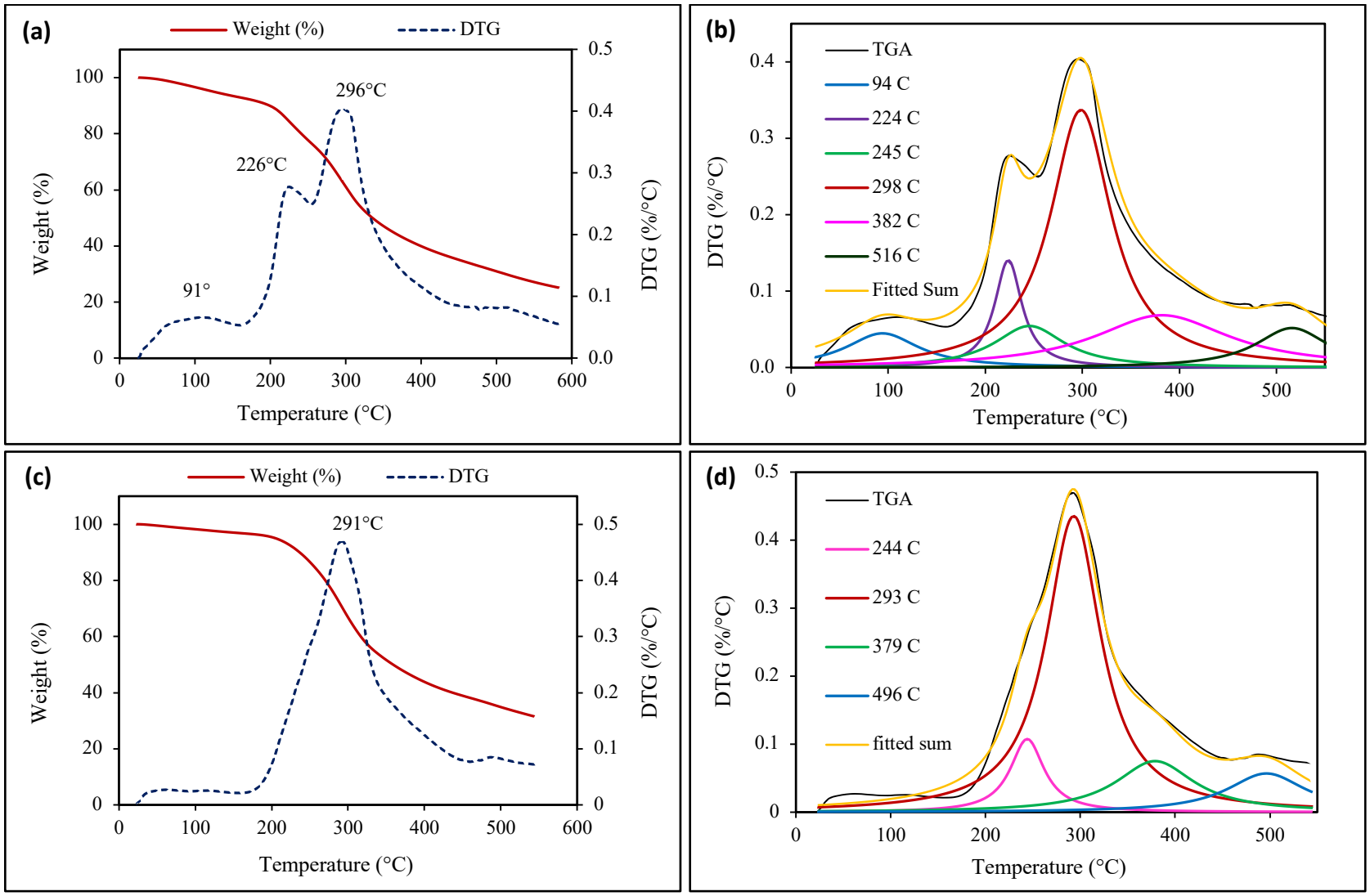


Figure 2-1: (a) TGA and DTG of soymeal (b) Deconvolution of DTG graph of soymeal (c) TGA and DTG of ethanol washed soymeal (EWS) (d) Deconvolution of DTG graph of ethanol washed soymeal (EWS)

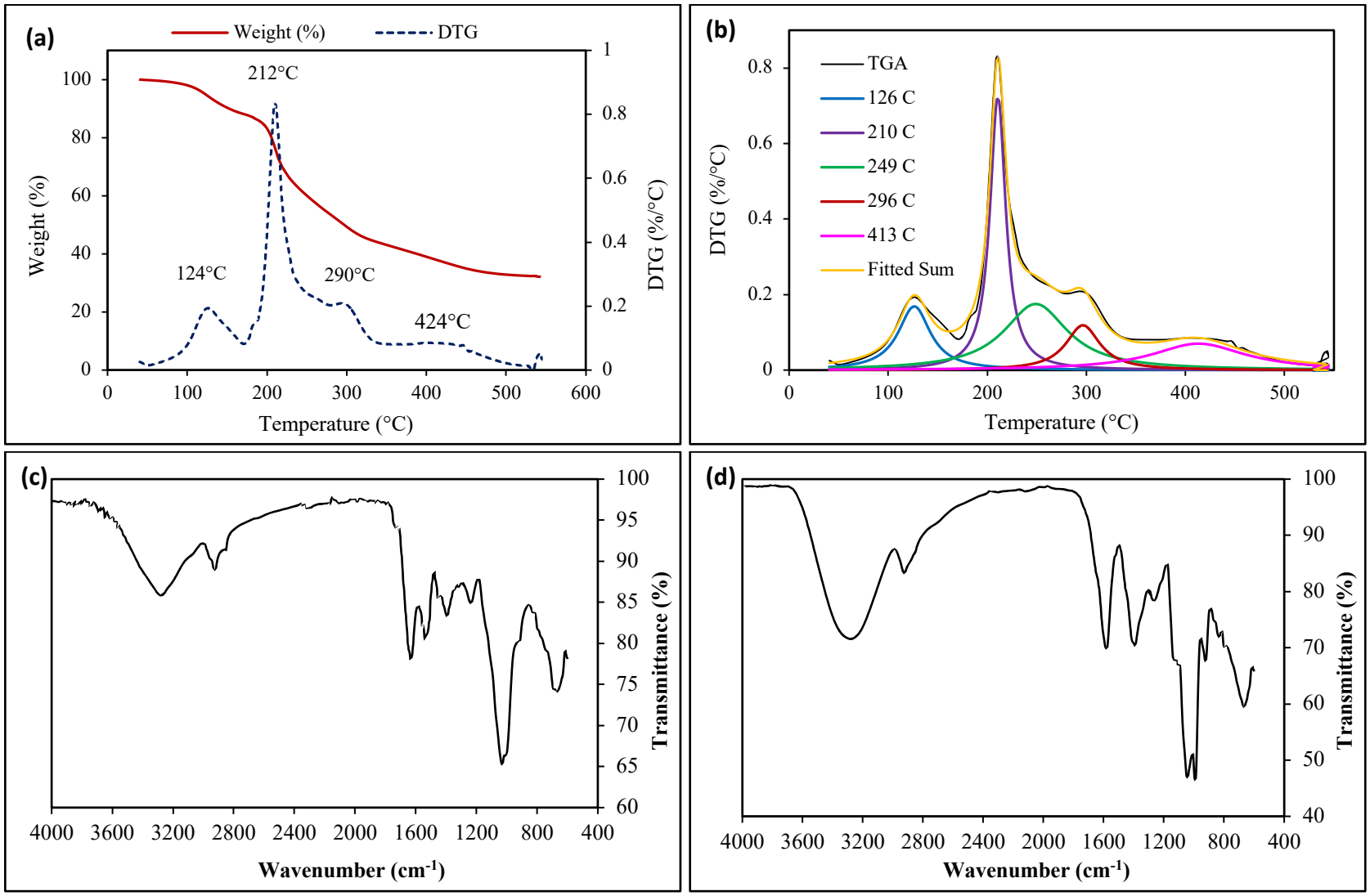


Figure 2-2: (a) TGA and DTG of soluble carbohydrates (SC) (b) Deconvolution of DTG graph of soluble carbohydrates (SC) (c) FTIR of soymeal (d) FTIR of soluble carbohydrates

2.3.1.4 Protein, moisture, and ash content analysis

The crude protein content of foodstuff can be determined by multiplying conversion factor to the nitrogen content of foodstuff [70]. Jones found that the nitrogen content in total proteins of a variety of foodstuff varies from 13% to 19% [70]. Since then it was assumed that the average nitrogen content of foodstuff is 16% of total proteins, thereby multiplying 6.25 to nitrogen content to get the crude protein content [71]. Morr used the Factor method and the Kjeldahl method for calculating nitrogen content present in soymeal [72]. The conversion factor was calculated by dividing total amino acid content by nitrogen content [72]. Later, Morr corrected Factor method by using residue weights of amino acids instead of molecular weights, and the conversion factor for soymeal was calculated as 5.6 - 5.7 [14]. Recently some studies showed that the conversion factor for a variety of foodstuff varies from 5.2 to 5.9 [71, 73] and hence suggested to use 5.6 as conversion factor instead of using 6.25 [71]. As the conversion factor obtained by Factor method was in good agreement with that obtained by Kjeldahl method [14], the Factor method was used for determining conversion factor for a given composition of amino acids in soymeal. The composition (% w/w) of amino acids present in soymeal is given in Table 2-2. This composition is of soymeal which is harvested in the USA and was used to calculate the conversion factor [50]. The amino acids present in soymeal are in the form of peptide linkages. As peptide linkages are formed by condensation of amine and acid groups of amino acids with the removal of water, the molecular weight of amino acids in peptide linkages will be less than its actual molecular weight. Thus, residue weight of amino acids was obtained by subtracting the molecular weight of water from the molecular weight of amino acids and these residue weights of amino acid were then used for calculating total protein content [14] and nitrogen content.

Table 2-2: Calculating conversion factor for protein content present in the soymeal from amino acid content

Compound	Composition (% w/w)	Composition (residue) (% w/w)	Molecular Weight (g/mol)	Residue Molecular Weight (g/mol)	Nitrogen Content (% w/w)
alanine	2.07	1.652	89.09	71.09	0.325
arginine	3.51	3.147	174.2	156.2	1.128
asparagine	0	0	132.12	114.12	0
aspartic acid	5.36	4.635	133.1	115.1	0.564
cystine	0.75	0.694	240.3	222.3	0.087
glutamine	8.7	7.628	146.15	128.15	1.667
glutamic acid	0	0	147.13	129.13	0
glycine	1.98	1.505	75.07	57.07	0.369
histidine	1.29	1.14	155.16	137.16	0.349
isoleucine	2.12	1.829	131.17	113.17	0.226
leucine	3.7	3.192	131.17	113.17	0.395
lysine	3.04	2.666	146.19	128.19	0.582
methionine	0.69	0.607	149.21	131.21	0.065
phenylalanine	2.45	2.183	165.19	147.19	0.208
proline	2.32	1.957	115.13	97.13	0.282
serine	2.14	1.773	105.09	87.09	0.285
threonine	1.85	1.57	119.12	101.12	0.217
tryptophan	0.7	0.638	204.23	186.23	0.096
tyrosine	1.71	1.54	181.19	163.19	0.132
valine	2.29	1.938	117.15	99.15	0.274
Taurine	0.05	0.043	125.15	107.15	0.006
Hydroproline	0.05	0.043	131.13	113.13	0.005
Lanthionine	0.01	0.009	208.24	190.24	0.001
Hydroxylysine	0.02	0.018	162.19	144.19	0.003
Ornithine	0.03	0.026	132.16	114.16	0.006
Total	**46.83**	**40.433**			**7.272**

The composition based on residue weight was calculated by dividing actual composition (% w/w) by the actual molecular weight of amino acids and then multiplying it by residual weight of amino acids as given in Table 2-2. The total composition of amino acids based on the residue molecular weight was divided by nitrogen content to obtain conversion factor which was found as 5.56.

The analytically determined nitrogen content of soymeal was 8.23 % (determined by CHN analyzer) and hence protein content of soymeal was 45.76%. Ash content is obtained by running TGA above 500°C in an oxygen environment. The percentage of ash present in soymeal on the wet basis was 6.41% (determined using TGA). The moisture content in soymeal was 6.5% (determined using moisture content analyzer). The final composition of soymeal is given in Table 2-3. The composition of soymeal was also obtained by deconvolution of DTG of soymeal as shown in Figure 2-1(b) and it is given in Table 2-3.

Table 2-3: Composition of soymeal

Components	**Composition obtained by separation of soluble carbohydrates & analytical methods (%)**	**Composition obtained by deconvolution of DTG graph of soymeal (%)**
Moisture	6.50 $\pm$ 0.19	~7
Proteins	45.76 $\pm$ 0.44	~46
Soluble Carbohydrates	18.36 $\pm$ 0.47	~36
Insoluble Carbohydrates	17.40 $\pm$ 0.07	
Ash	6.41 $\pm$ 0.73	6.41
Other (minerals)	5.73 $\pm$ 2.06	~5
Total	**100**	**100**

2.3.2 Polyol synthesis from soymeal

The soymeal which was used for polyol synthesis contains 46 - 47% proteins, 35 - 36% carbohydrates, 6 - 7% moisture, and 11 - 12% ash and minerals. For polyol synthesis, soymeal was

used directly without removing any of the components.

2.3.2.1 Polyol synthesis and characterization

Polyols from soymeal have been reported by us and others as shown in Figure 2-3. In the first route (hydrolysis), soymeal was hydrolyzed to a mixture of amino acids which were further converted to a polyol [6, 59]. In the second route (activation), alkali treatment method was used to modify soymeal which was directly used in PUF synthesis [55].

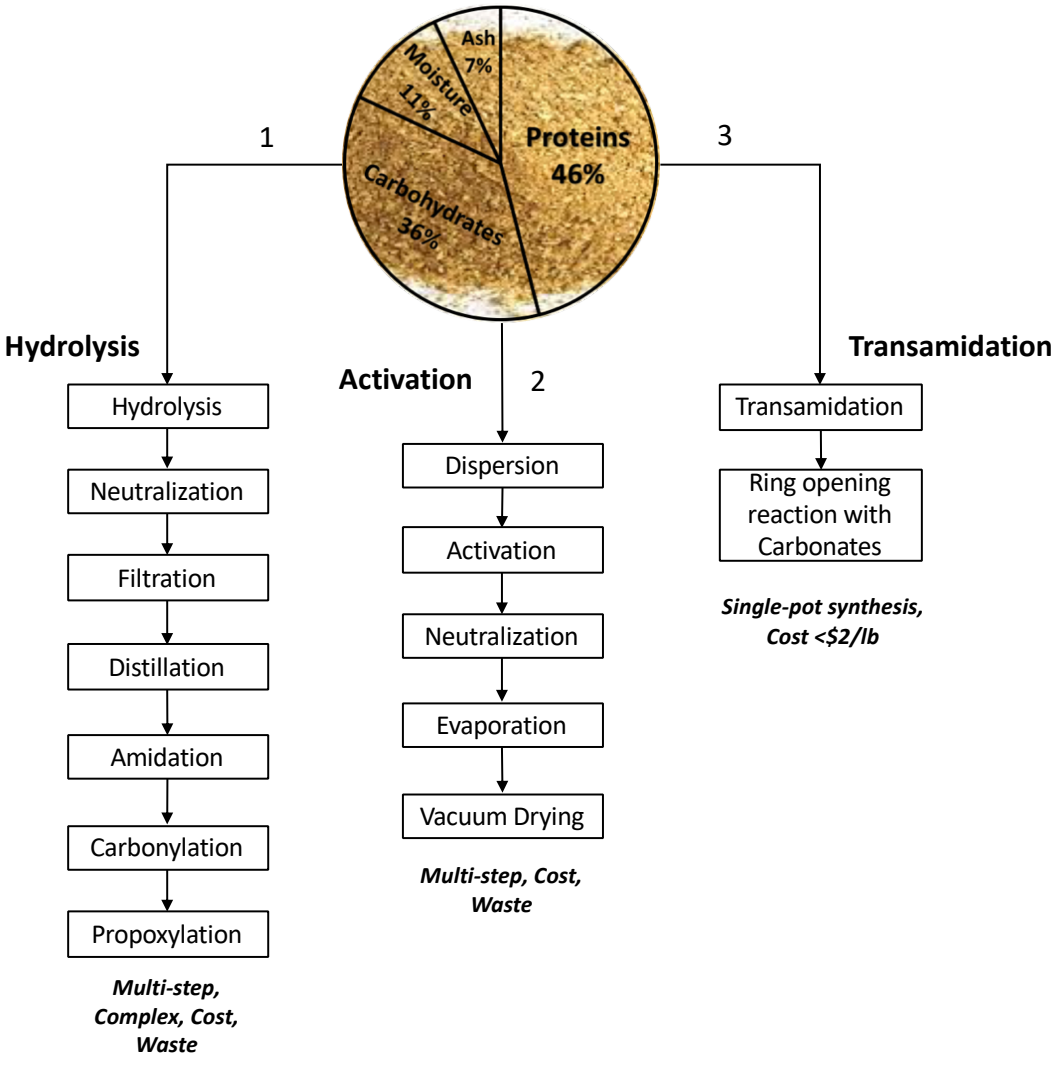


Figure 2-3: Different routes used for synthesis of polyols from soymeal (1) Hydrolysis [6, 59] (2) Activation [55] (3) Transamidation [58]

However, the number of steps involved, and resultant product properties made these approaches commercially not viable (see Figure 2-3). The transamidation chemistry approach (third route) eliminated many steps and reagent usage. It allowed us to synthesize the polyols in two steps and one-pot chemistry approach. In transamidation route, soymeal was converted to amine derivatives which were further converted to a soymeal polyol. The detailed procedure used for the synthesis of amine derivatives and the soymeal polyol is described in the next sections.

2.3.2.2 Synthesis of amine derivatives using transamidation process

The protein-carbohydrate residue i.e. soymeal was used directly without removing carbohydrates or other components. The transamidation reaction between proteins of soymeal and amine of ethanolamine (MEA) is shown in Figure 2-4. Attack of the amino group on the carbonyl carbon gives the hydroxylamine derivative (product A, Figure 2-4). There was also a possibility of the hydroxyl group of ethanolamine reacting with acid groups of proteins, and giving diamine derivative (product B, Figure 2-4).

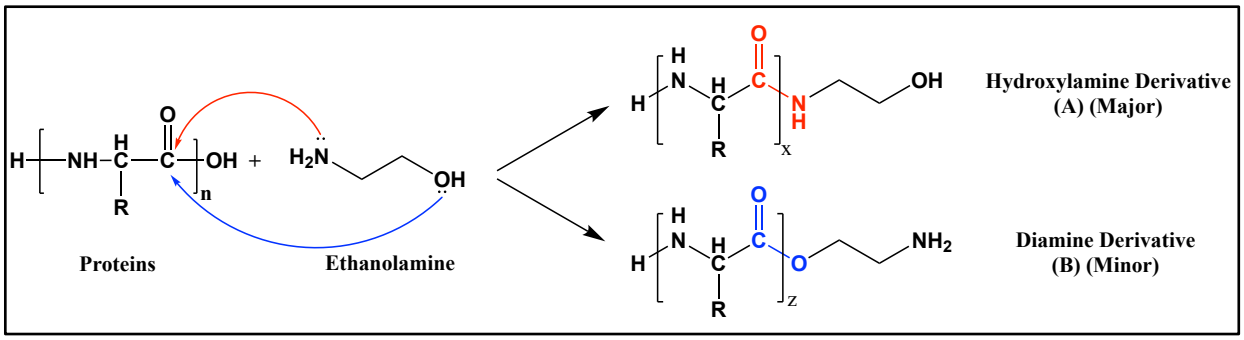


Figure 2-4: Transamidation of proteins with ethanolamine

When the soymeal was reacted with pure ethylene glycol at a temperature of 100 - 105ºC (mass ratio 1:3), it was found that the unreacted or insoluble soymeal was more than 90%. Also, when soymeal was reacted with pure ethylene diamine, the insoluble soymeal was less than 12%. This concludes that the amine group is more reactive than the alcohol group towards soymeal. Thus,

the amine derivatives obtained from the reaction of soymeal and ethanolamine contain hydroxylamine derivatives (A) as a major product along with diamine derivative as a minor product. When soymeal was reacted with ethanolamine, the percentage of insoluble soymeal decreased with time as shown in Figure 2-5, as the reaction products were soluble in the liquid phase. Thus, the amount of insoluble soymeal present at any time will be equal to the amount of unreacted soymeal. It was assumed that the reaction was homogeneous and the density of reaction mixture remains the same throughout the reaction. The concentration of soymeal was obtained in g/l and it was used to find the kinetics of the soymeal-ethanolamine reaction. The first-order rate equation $\left[ln\left(\frac{C_A}{C_{Ao}}\right) = -(0.0428\ s^{-1}) \cdot t\right]$ gave the best fit as shown in Figure 2-6.

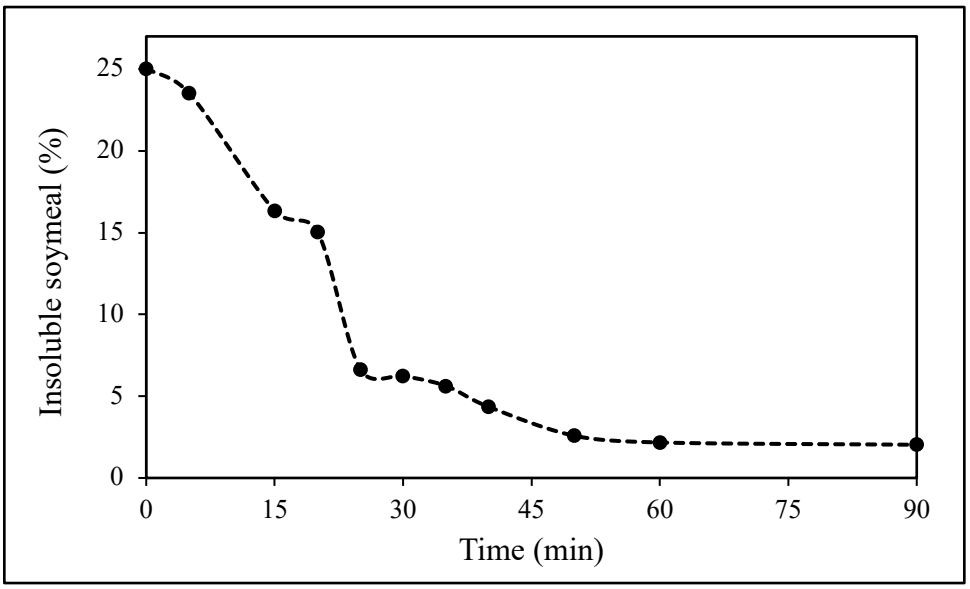


Figure 2-5: Change in the percentage of insoluble soymeal present in amine derivatives with time during the transamidation reaction

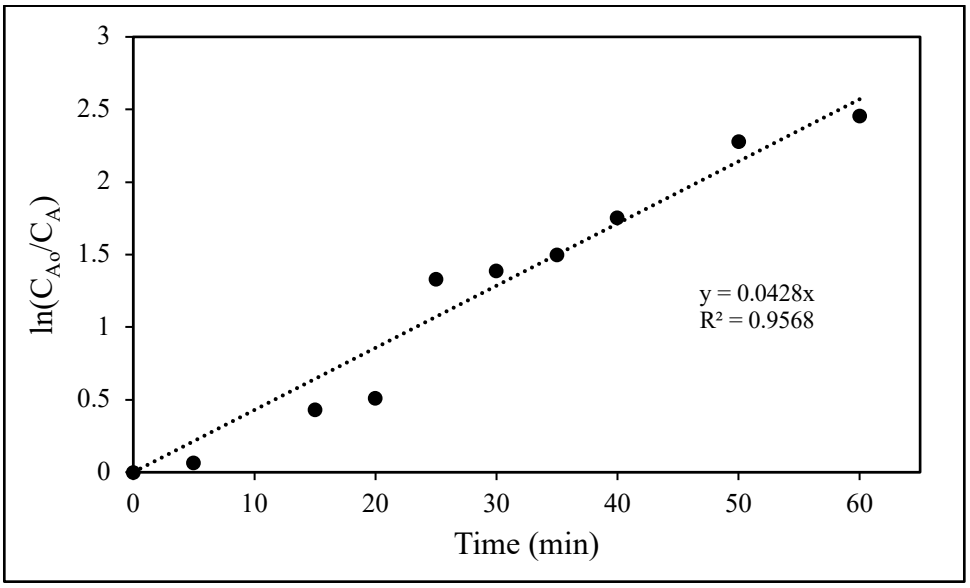


Figure 2-6: Kinetics of transamidation reaction

2.3.2.3 Synthesis of soymeal-based polyols

The amino end-group of amine derivatives (hydroxylamine and diamine derivative) can be converted to hydroxyl end group by reacting it with ethylene carbonate (EC) or propylene carbonate (PC). We discovered that using PC, which is a liquid at room temperature instead of EC, provided a solution with much reduced viscosity – an essential requirement for manufacturing foams [74]. Viscous polyols hinder uniform mixing which is a primary requirement to obtain a good foam. Also, the cost of PC (0.5 - 1.0 $/kg) is considerably lower than EC (1.1 - 1.5 $/kg) [75].

The reaction of amine derivatives with propylene carbonate was carried out at 70 - 75°C to avoid the formation of substituted ureas [76]. The reaction of hydroxylamine derivative (A) with PC is shown in Figure 2-7. The amino group can break any one of the two ester linkages of PC giving products containing 1º or 2º hydroxyl group (Figure 2-7). Diamine derivative also reacts in a similar pathway. The NMR spectroscopy was used to quantify 1º and 2º hydroxyl group content. The ring-opening reaction of PC with amine derivative was instantaneous, as the amine value of

amine derivatives decreased drastically during the reaction. The overall soymeal polyol synthesis pathway is shown in Figure 2-8.

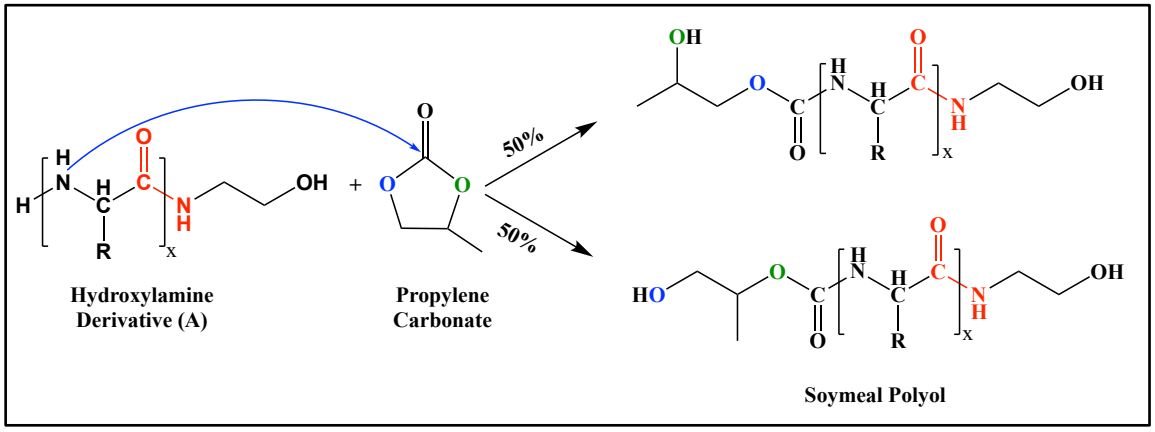


Figure 2-7: Ring opening of propylene carbonate with amines of hydroxylamine derivative

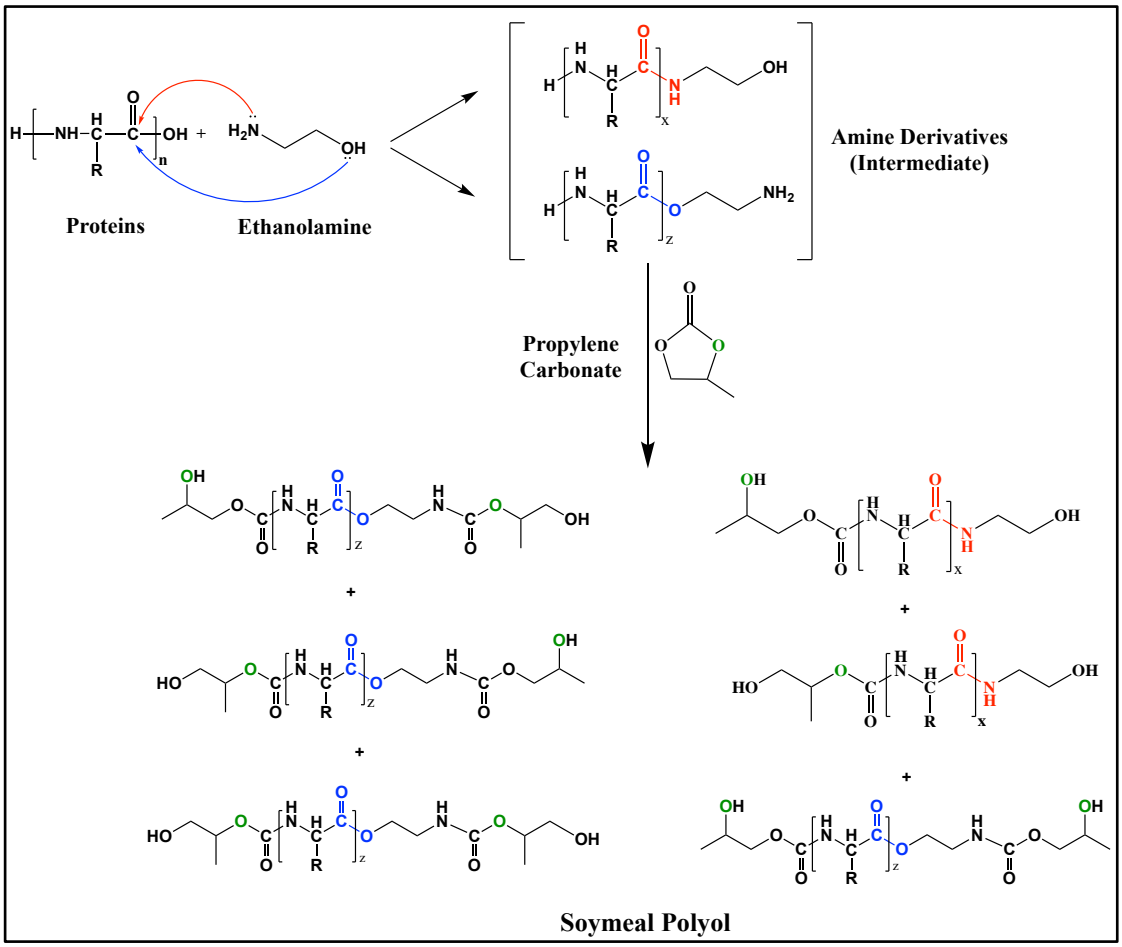


Figure 2-8: Overall pathway for soymeal polyol synthesis

Different mass ratios 1:2, 1:3, and 1:5 of soymeal to ethanolamine (MEA) were used. The intermediate product amine derivatives (AD) and the corresponding soymeal polyol (SP) were characterized and results are shown in Table 2-4. The SP 1:2 polyol was very viscous compared to the SP 1:3 and SP 1:5 polyols. The SP 1:3 polyol was chosen to make PUF due to the higher biobased content and lower cost as compared to the SP 1:5. The soymeal polyol also contains carbohydrates and other components of soymeal as they were not separated from the soymeal. The hydroxyl value of these polyols was around 500 - 600 mg of KOH/g which can be reduced by using long-chain amino-alcohol.

Table 2-4: Characterization of different amine derivatives and soymeal polyols

	Amine Value (mg of KOH/g)	**Hydroxyl Value (mg of KOH/g)**	**Specific Gravity**	**Viscosity @ 25°C Pa·s**	**Insolubles (%)**
AD 1:2	563 ± 11	-	-	-	-
AD 1:3	772 ± 8	-	-	-	-
AD 1:5	716 ± 15	-	-	-	-
SP 1:2	10 ± 1	613 ± 10	1.15	230	< 4
SP 1:3	6 ± 2	568 ± 10	1.18	37	< 2
SP 1:5	5 ± 1	647 ± 15	1.15	28	< 1
MEA + PC	3 ± 1	709 ± 12	1.20	5	-

2.3.2.4 Fourier Transform Infrared Spectroscopy (FTIR)

The ATR-FTIR spectra of soymeal, amine derivative, and soymeal polyol are given in Figure 2-9. The peak at 3200 cm^{-1} present in the spectrum of soymeal was attributed to the OH stretch [77], which was also present in the spectra of amine derivative and soymeal polyol. The additional peaks around 3300 cm^{-1} present in the spectrum of amine derivatives were attributed to the N-H stretch of 1° and 2° amines [69]. The C-H stretch was observed around 2900 cm^{-1} in the spectra of all compounds. The small peak around 1750 cm^{-1} present in the spectrum of soymeal polyol was

expected due to the C=O group of esters [69, 78, 79] or urethane linkages. The peaks around 1690 cm^{-1} and 1530 cm^{-1} present in the spectrum of soymeal polyol were attributed to the C=O and N-H groups of amide linkages [69].

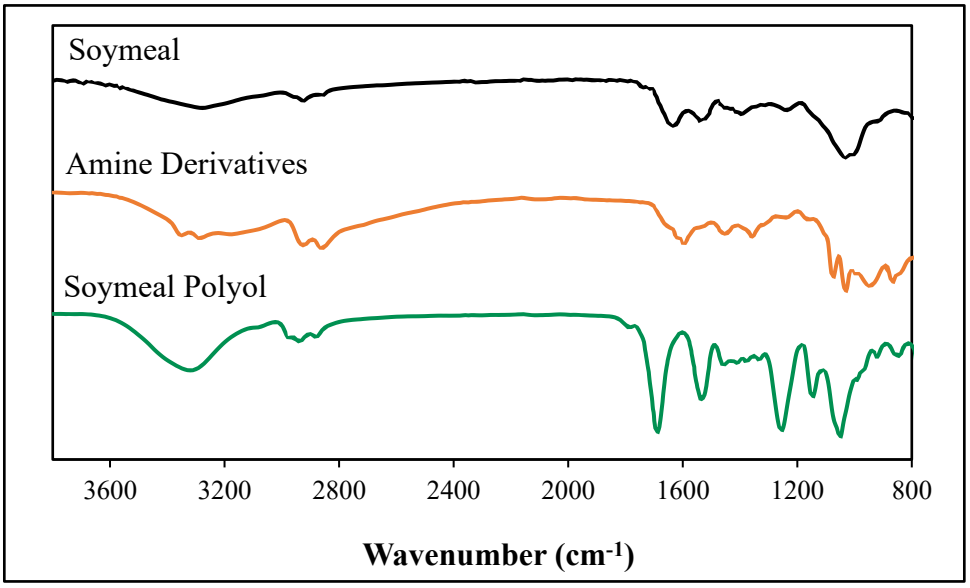


Figure 2-9: FTIR spectra of soymeal, amine derivative, and soymeal polyol

2.3.2.5 Nuclear Magnetic Resonance (NMR) Spectroscopy

The ratio of a secondary alcohol (2º) to primary alcohol (1º) produced from a ring-opening reaction of cyclic carbonates with different primary amines, has been determined previously [76, 80]. Baizer et al. used an infrared spectroscopy technique to obtain the ratio as 65:35 [81]. Steblyanko et al. found the ratio as 82:18 using a ^{1}H NMR spectroscopy [82]. This ratio was also obtained by a ^{13}C NMR spectroscopy [83, 84]. In this study, the ratio was determined using the ^{13}C NMR spectroscopy, as reactivity of polyol towards isocyanate depends on the relative concentration of 2º to 1º alcohol [84, 85]. The ring-opening of propylene carbonate (PC) with ethanolamine was used as a model reaction and the ^{13}C NMR spectrum of the obtained products (a and b) is given in Figure 2-10. All peaks present in the ^{13}C NMR spectrum are assigned to the carbon atoms present in both products as shown in Figure 2-10.

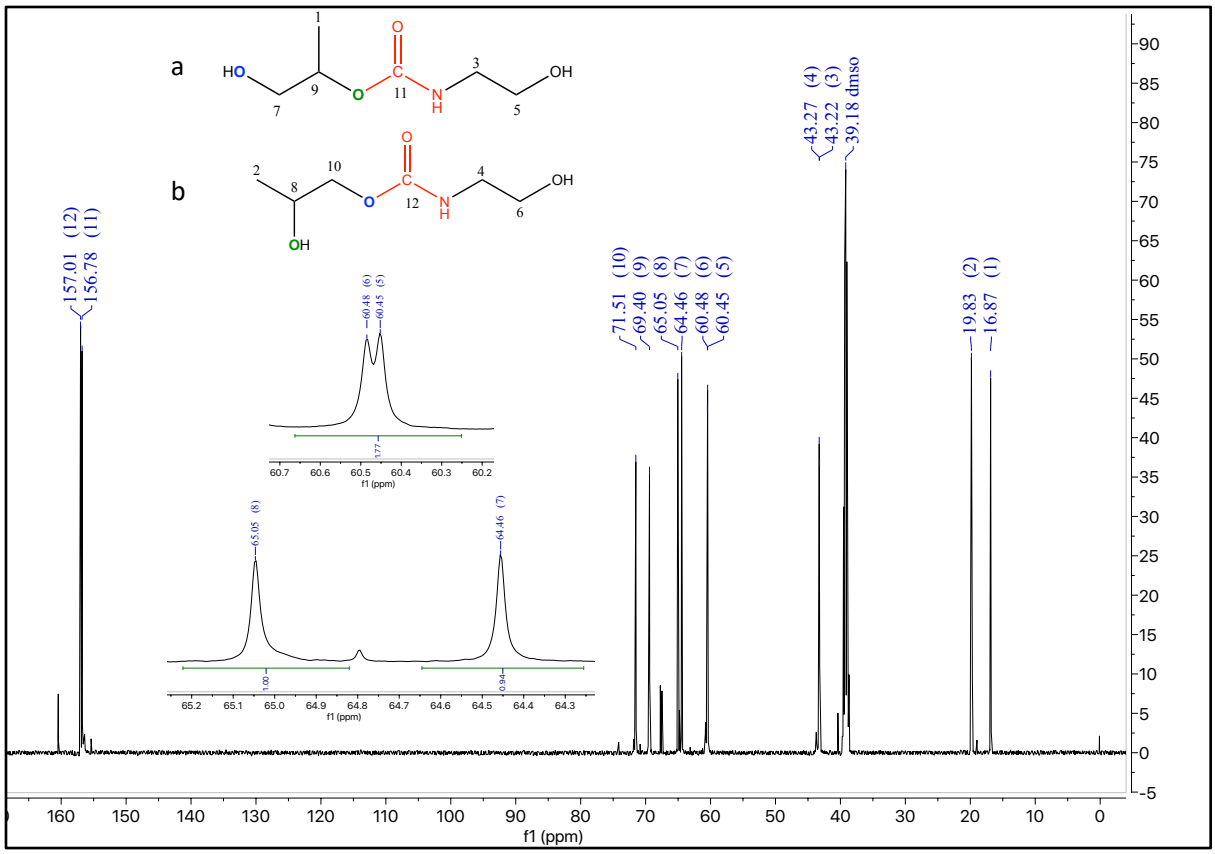


Figure 2-10: ^{13}C NMR spectrum of ethanolamine and propylene carbonate reaction

The peaks at 60.45 ppm (5) and 60.48 ppm (6) correspond to the primary hydroxyl carbon from ethanolamine [83, 84], whereas the peak at 65.05 ppm (8) corresponds to the secondary hydroxyl carbon [84]. The peak at 64.46 ppm (7) also corresponds to the primary hydroxyl carbon. These peaks were integrated to calculate the ratio of secondary to primary hydroxyl groups and this was found to be 27 : 73. Thus, it was confirmed that the soymeal polyol contains more primary hydroxyl group than secondary hydroxyl groups. Also, using this ratio, the product distribution of a : b was found as approximately 50 : 50.

2.3.2.6 Thermogravimetric Analysis

The thermogravimetric analysis (TGA) graphs of soymeal, amine derivatives, and soymeal polyol are shown in Figure 2-11. In the TGA graph of amine derivatives, the degradation stage I (50°C - 150°C) was due to ethanolamine and water, the degradation stage II (150°C - 250°C) and stage III

(250°C - 350°C) were due to the low and high molecular weight amine derivatives respectively. Whereas in the TGA graph of the soymeal polyol, the two degradation stages, i.e. stage I (75°C - 175°C) and stage II (175°C - 275°C) could be due to the polyols with different molecular weights.

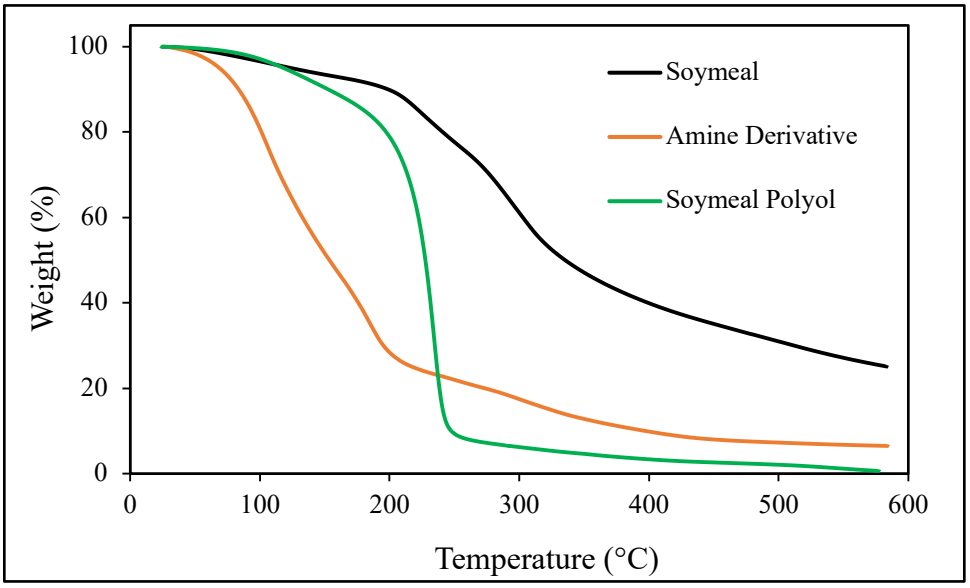


Figure 2-11: TGA graphs of soymeal, amine derivative, and soymeal polyol

2.4 CONCLUSION

This study mainly focuses on the engineering of greener, value-added, and cost-effective polyol synthesis from an inexpensive agriculture residue. In the first part, the composition of biomass was determined using simple analytical methods combined with the deconvolution of DTG graphs of soluble carbohydrates and ethanol washed soymeal. This combined technique can be applied to any other protein-carbohydrate residues to determine the composition of components. After obtaining the composition of soymeal, the biobased polyol was synthesized by adopting a two-step process: transamidation followed by ring-opening reaction with carbonates. In the transamidation step, the soymeal was converted to amine derivatives containing a majority of hydroxylamine. In the subsequent ring-opening step, amine derivatives were converted to the soymeal polyol which was majorly comprised of primary hydroxyl groups. The insoluble soymeal

content in the soymeal polyol was less than 2% which confirmed that most of the constituents of soymeal were taking part in the reaction. Also, it was found that the primary amino groups were more reactive towards soymeal and carbonyl compounds than alcohol groups. The soymeal polyol contained amide linkages as well as urethane linkages which are less prone to degradation by hydrolysis or UV-radiation. The commercially available polyols contain ether or ester linkages. The hydroxyl value of polyol is 550 mg of KOH/g which makes it suitable for application in rigid polyurethane foams. This hydroxyl value depends on the chain length of amino-alcohol used. Thus, polyols with lower hydroxyl value can also be synthesized using long-chain amino-alcohol or diamines like hexamethylene diamine (HMDA). The biobased HMDA is commercially available. The use of simple chemistry i.e. the one-pot synthesis method, and easily available inexpensive raw materials could significantly reduce the cost of the soymeal polyol (material cost ~ 0.6 - 0.7 $/lb) and make its commercial production viable.

2.5 ACKNOWLEDGMENTS

The authors thank Zeeland Farm Services, Inc. for providing the soymeal sample.

3 SYNTHESIS OF BIOBASED BUILDING BLOCKS FROM LACTIDE AND SOYBEAN OIL FOR APPLICATIONS IN POLYURETHANES AND POLYESTERS

3.1 INTRODUCTION

The use of plastic in day-to-day life has tremendously increased in the past few years [86], most of which goes to landfills after its use. The growing concern about the plastic waste debris on land and in oceans has emphasized the area of biobased polymers and chemical recycling of polymers. In recent years, biobased building blocks such as ethylene glycol, 1,3-propanediol, 1,4-butanediol, succinic acid, adipic acid, sebacic acid, etc. [87] have been successfully used in the commercial synthesis of polymers. Some of the petrochemical-based polymers have been replaced with partially biobased polymers e.g. polyesters such as bio-polyethylene terephthalate (PET), polybutylene terephthalate (PBT), and polyamides such as polyamide 6,10 (PA 6,10). Polylactide (PLA), polyamide 6, 6 (PA 6, 6), and polyamide 10, 10 (PA 10, 10) are some of the examples of 100% biobased polymers which are commercially available.

There is a predominant increase in the literature on products derived from cashew nutshell liquid (CNSL) [88], castor oil [89], soybean oil [11], lignin [90], etc. Epoxy resins and polyols derived by chemical modification of cardanol are commercially available products supplied by Cardolite [88]. Cardanol is obtained by thermal treatment CNSL followed by distillation [91]. Sebacic acid and diamines derived from castor oil are used in the synthesis of biobased polyamides and polyesters by Arkema. Polyols obtained from soybean oil via various routes i.e. epoxidation, hydroformylation, ozonolysis are used in polyurethanes [11]. Fatty acids obtained from soybean oil are dimerized by Diels-Alder reaction to synthesize dimer acids [17, 18]. Dimer acids are interesting biobased building blocks containing long carbon chain and thirty-six carbon atoms. The

two acid functionalities present in dimer acids make them a suitable candidate for polyester or polyamide synthesis via polycondensation reaction [92] and long-chain increases the renewable carbon content as well as the flexibility in the final polymer.

PLA is a commercially available biobased and biodegradable polymer which is synthesized from ring-opening polymerization of lactide. Lactide is produced from lactic acid. Commercially, lactic acid is obtained by bacterial fermentation of corn starch using organisms called lactobacilli which produces predominantly L-lactic acid [20]. Lactic acid is polymerized to form oligomers of PLA which are depolymerized to produce lactide [21]. Lactide has three different forms i.e. L-lactide (two L-lactic acid molecules), D-lactide (two D-lactic acid molecules), and meso-lactide (an L-lactic acid and a D-Lactic acid molecule). During the synthesis of PLA, meso-lactide is continuously removed as it affects the properties of PLA beyond a certain percentage [23]. This meso-lactide can be used as a raw material for the synthesis of new biobased building blocks.

Recently, polyols derived from polylactide were used in the synthesis of polyurethanes [93]. PLA polyols were synthesized by polymerization of lactic acid with diol e.g. 1,4-butanediol [93], polyethylene glycol [94] or ethylene glycol [95]. PLA polyols were also synthesized by reacting PLA with glycerol or sucrose at high temperature where PLA oligomers with hydroxyl end-groups were formed [96]. Reaction products of natural oil derived polyol and lactide were used in biobased coatings [97, 98]. Ring-opening polymerization of lactide was done using various organocatalysts [99, 100]. Ring-opening of lactide can also be done using primary amines where it forms amide linkage after ring-opening [100, 101]. The previous literature is mainly focused on ring-opening polymerization of lactide.

In our work, new biobased building blocks will be synthesized from meso-lactide, which is a side product in PLA synthesis. The new monomers will be synthesized by ring-opening of meso-lactide

with primary amines and alcohols. The ring-opening of meso-lactide with amino-alcohol will give low molecular weight diols which can be used in polyester synthesis (e.g. PET) or polyurethanes. The ring-opening of meso-lactide with long-chain alcohols (e.g. PEG) will give a diol with moderate molecular weight. This diol will be reacted with dimer acid using polycondensation chemistry to synthesize low hydroxyl value polyols for application in flexible polyurethane foams.

3.2 EXPERIMENTAL

3.2.1 Materials and chemicals

Meso-lactides Vercet^{TM} M700 (>99.5%) and M3002 (>96%) were received from NatureWorks LLC (Minnesota, USA). Dimer acid Radiacid 0955 was purchased from Oleon (Ertvelde, Belgium). Monoethanolamine (ethanolamine), polyethylene glycol (PEG-400), and titanium butoxide ($Ti(OBu)_4$) were purchased from Sigma-Aldrich (Wisconsin, USA). All other chemicals used were purchased from Fisher-Scientific or Sigma-Aldrich.

3.2.2 Synthesis of diols by ring opening of meso-lactide using amines

The reaction of meso-lactide (M700) and ethanolamine was carried out in a 2 L three-neck glass round bottom flask with a nitrogen purge. The reaction of lactide with amines is an exothermic reaction. Therefore, the reaction was carried out at 10 - 20°C in a water bath and the temperature of the water was controlled using ice. After 30 minutes, the temperature of the final product was increased to 100 - 110°C to ensure completion of the reaction. Meso-lactide and ethanolamine were reacted in 1:1 and 1:2 molar ratios. The subsequent products obtained were labelled as MLE-529 and MLE-818, respectively. The diols were characterized for acid value, amine value, hydroxyl value, FTIR, NMR, and TGA.

3.2.3 Synthesis of diols by ring opening of meso-lactide using hydroxyl group

One mole of meso-lactide (M700) was reacted with one mole of PEG-400 in a 2 L three-neck glass

round bottom flask at 80 - 100°C with 15 - 20 minutes of a nitrogen purge. The temperature was increased to 160 - 170°C after 2 hours. The reaction was carried out for 3 hours and the product was labelled as MLPEG-7-202. Similarly, meso-lactide M3002 was reacted with PEG-400 and the product was labelled as MLPEG-3-186.

3.2.4 Synthesis of low hydroxyl value polyols using polycondensation chemistry

Dimer acid (Radiacid 0955, MW = 575 g/mol, f = 2.02) was reacted with different diols MLPEG-7-202, MLPEG-3-186, and PEG-400 in presence of titanium butoxide a catalyst at 120 - 130ºC for 3 - 4 hours. The reaction was carried out in a 2-L three-neck glass round bottom flask. The temperature was raised to 200 - 220 ºC and the vacuum was applied to remove water formed during the condensation reaction. The set-up used for the polycondensation reaction is shown in Figure 3-1. The diol was used in 10% excess and the reaction was continued until the acid value decreased below 2 - 3 mg of KOH/g. Dimer acid was reacted with diols in 1:2 and 1:1 molar ratio.

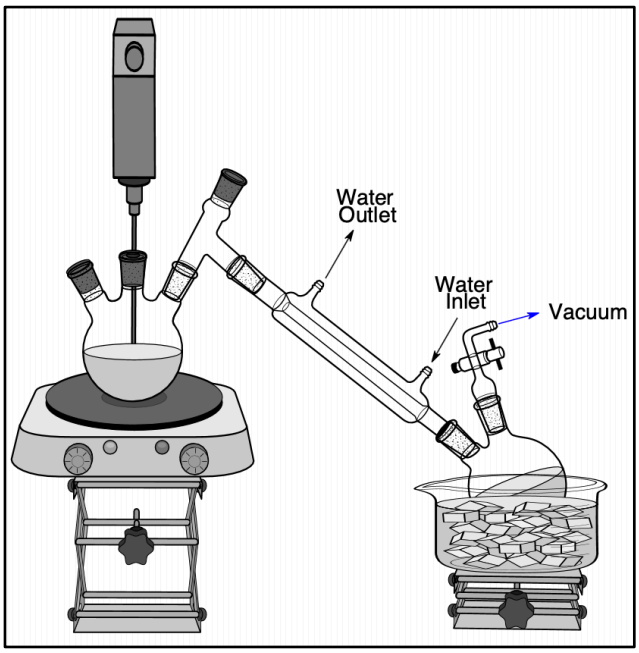


Figure 3-1: Set-up for polycondensation reaction

3.2.5 Characterization of lactide polyols

The hydroxyl value of polyols was determined by ASTM D4274-16 and the amine value was determined by ASTM D2073-92. The acid value was determined by dissolving a sample in 2-propanol and titrating it against sodium hydroxide (NaOH) solution. All titrations were performed using an 857 Titrando (Metrohm, Florida, USA) auto-titrator. The viscosity of all samples was measured at room temperature using a Brookfield viscometer-LVDV-E model (AMETEK Brookfield, Massachusetts, USA).

The ^{13}C and ^{1}H nuclear magnetic resonance (NMR) spectra were recorded on a 500 MHz NMR spectrometer (Varian Inc., USA, Unity Plus 500MHz) using deuterated dimethyl sulfoxide (DMSO-d_6) as a solvent having tetramethylsilane as an internal standard. The ^{13}C spectrum were recorded at ambient temperature (22°C), relaxation delay 1 s, and the number of scans 256. The ^{1}H spectrum were recorded at ambient temperature (22°C), relaxation delay 1 s, and the number of scans 8.

The Attenuated Total Reflection-Fourier Transform Infrared (ATR-FTIR) spectra were acquired on a FT-IR (Shimadzu Co., Tokyo, Japan, IRAffinity-1) equipped with a single reflection ATR system (PIKE Technologies, Wisconsin, USA, MIRacle ATR). ATR-FTIR was used with resolution 4 cm^{-1}, Happ-Genzel apodization function and 64 scans were conducted on the sample. Thermogravimetric measurements were conducted under nitrogen flow using a thermogravimetric analyzer, TGA Q50 (TA Instruments, Delaware, USA). In this analysis, a sample (10 - 15 mg) was taken in an aluminum pan and heated to 600°C with a heating rate of 10°C /min. The weight loss (%) of a sample as a function of temperature (°C) was obtained from this analysis. The derivative thermogravimetric graphs (DTG) (%/ºC) were used to identify the degradation temperatures.

3.3 RESULTS AND DISCUSSION

3.3.1 Synthesis of diols by ring opening of meso-lactide using amines

Amino groups were very reactive towards meso-lactide even at room temperature. Since the reaction was exothermic, it was carried out in a water bath and its temperature was maintained by adding ice. The amino group of ethanolamine attacks the carbonyl carbon of lactide forming a diol as shown in Figure 3-2. The amino group breaks the ester linkage present in lactide forming a new amide linkage. When meso-lactide and ethanolamine were reacted in a molar ratio 1:1, only one ester linkage was converted to the amide linkage as shown in Figure 3-2 (major product). However, there was also a possibility of breaking both the ester linkages of lactide forming a minor product as shown in Figure 3-2. Alba et al. have used this approach to remove unreacted lactide from PLA samples [101].

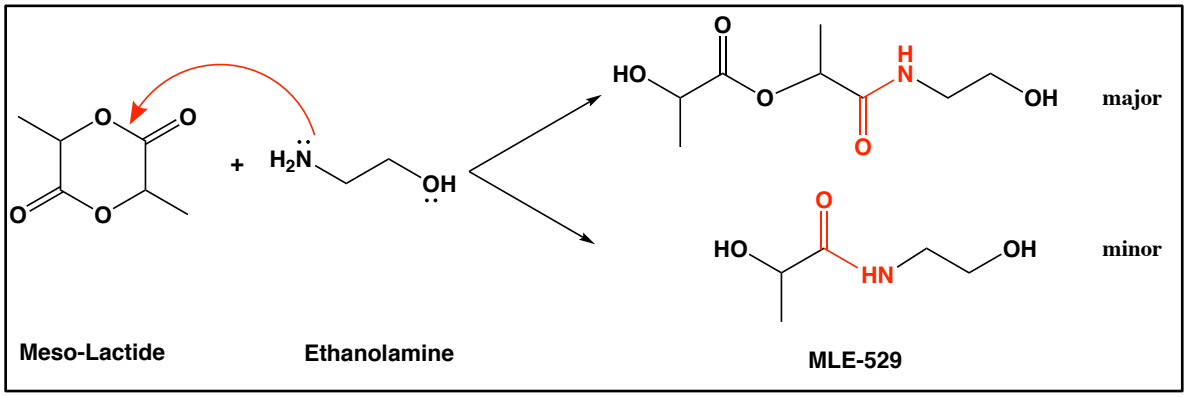


Figure 3-2: Reaction of meso-lactide with ethanolamine in molar ratio 1:1

When meso-lactide and ethanolamine were reacted in a molar ratio 1:2, both of the ester linkages of lactide were converted to amide linkages as shown in Figure 3-3. The theoretical hydroxyl value of a polyol can be calculated by Equation 3-1.

Equation 3-1:

$$\text{Theoretical hydroxyl value (OH \#)} = \frac{Functionality\ x\ 56100}{Molecular\ weight}$$

The theoretical molecular weight of MLE-529 (major product) and MLE-818 is 205 g/mol and 133 g/mol, respectively. Thus, the theoretical hydroxyl value of MLE-529 and MLE-818 is 547 mg of KOH/g and 843 mg of KOH/g, respectively. The theoretical values were in good agreement with the experimental hydroxyl values which confirms the predicted reaction chemistry. As MLE-529 has some acid content (Table 3-1) there was a possibility of formation of lactic acid during the reaction. MLE-529 has high hydroxyl value and viscosity as reported in Table 3-1. Thus, it was used directly in polyurethane rigid foams for heat insulation applications. The product MLE-818 is a perfect diol and its structure was confirmed by NMR and FTIR study. The MLE-818 product is pure (>99%) and can be used as a biobased diol in a polyester synthesis e.g. PET.

MLE-818 product was reacted with dimer acid in order to reduce its hydroxyl value for flexible polyurethane foam applications. But the viscosity of final polyol was very high which was affecting the properties of flexible polyurethane foams. The higher viscosity could be the result of amide linkages. Thus, the chemistry was changed in order to reduce viscosity along with the hydroxyl value which is discussed in the next section.

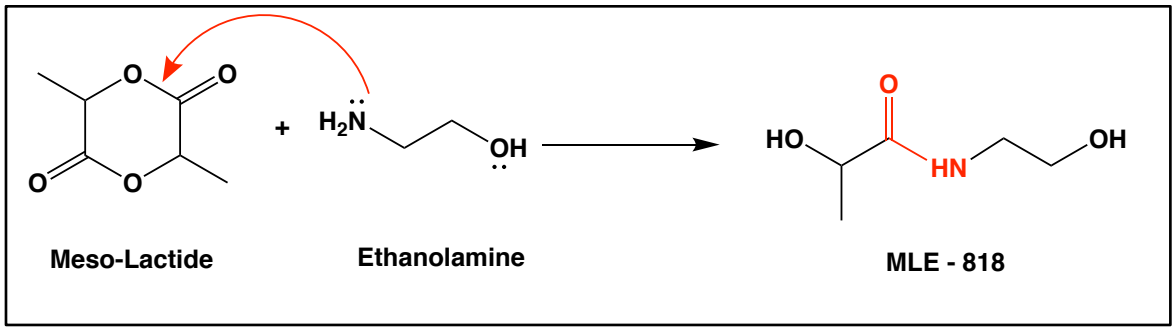


Figure 3-3: Reaction of meso-lactide with ethanolamine in molar ratio 1:2

3.3.2 Synthesis of diols by ring opening of meso-lactide using hydroxyl group

Lactide can be ring-opened by amine or hydroxyl groups. As a product with low viscosity and hydroxyl value was desired, polyethylene glycol with molecular weight 400 g/mol (PEG-400) was used as a reactant. However, the hydroxyl group was less reactive compared to the amino group

towards meso-lactide. Thus, the reaction of meso-lactide and PEG-400 in a molar ratio 1:1 was carried out at a higher temperature. The hydroxyl group of PEG-400 breaks ester bond of lactide and forms a new ester bond as shown in Figure 3-4. There is also a possibility of breaking the second ester linkage and formation of a minor product.

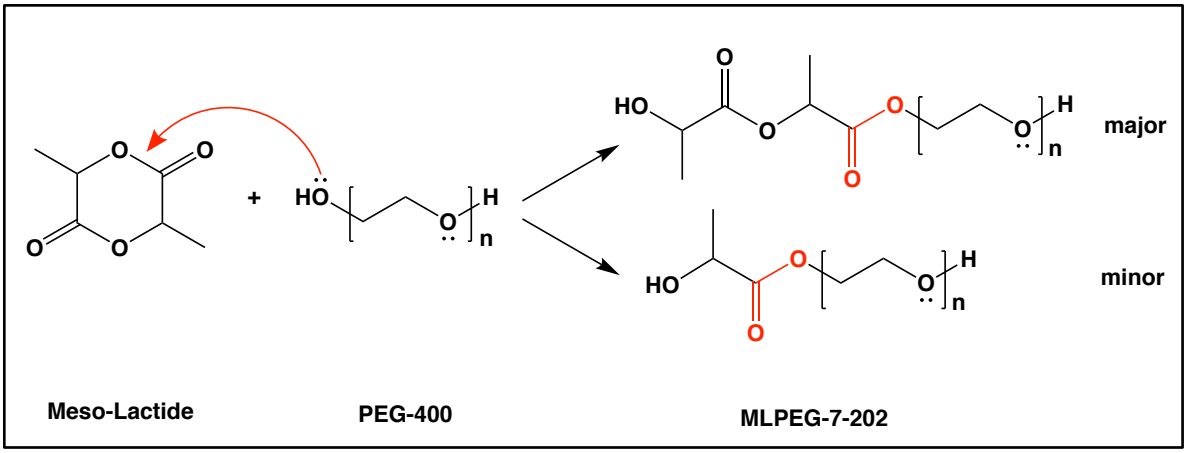


Figure 3-4: Reaction of meso-lactide with PEG-400 in molar ratio 1:1

The diol synthesized from meso-lactide M700 and M3002 were labelled as MLPEG-7-202 and MLPEG-3-186 respectively. Both products have low hydroxyl value as well as viscosity. Also, both the products have an acid value as reported in Table 3-1 which indicates the formation of lactic acid during the synthesis of MLPEG product.

Table 3-1: Characteristics of diols synthesized from lactide

Compound	**Hydroxyl Value (mg of KOH/g)**	**Amine Value (mg of KOH/g)**	**Acid Value (mg of KOH/g)**	**MW* (g/mol)**	**Viscosity @ 25°C (cPs)**
Ethanolamine	918.5*	918.5*	-	61	19
PEG – 400	280.5*	-	-	400	120
MLE-529 (1:1)	529 ± 4 (547)	1.77 ± 0.6	5.8 ± 1.2	212	30000
MLE-818 (1:2)	818 ± 1 (843)	10 ± 5	-	137	2100
MLPEG-7-202 (1:1)	202 ± 2 (206)	-	2 ± 0	555	326
MLPEG-3-186 (1:1)	186 ± 3 (206)	-	3 ± 0	603	300

*values calculated based on Equation 3-1

3.3.3 Synthesis of low hydroxyl value polyols using a polycondensation chemistry

Biobased diols described in the previous section have hydroxyl value greater than 200 mg of KOH/g. The polyols used in flexible polyurethane foams require hydroxyl value less than 100 mg of KOH/g. The hydroxyl value is directly proportional to the manufacturing price of foam and its stiffness. As hydroxyl value increases, it increases the amount of isocyanate required to make foam which increases its overall cost. Also, the number of urethane linkages increases which makes foam stiffer or rigid. In order to reduce the hydroxyl value, biobased diols can be reacted with a diacid forming a polyester polyol. Dimer acid derived from soybean oil contains thirty-six carbon atoms which increases the renewable carbon content and molecular weight of a final polyol. The long carbon chain present in the dimer acid could increase the flexible nature of a foam produced from dimer acid-based polyol. Thus, dimer acid was reacted with MLPEG-7-202 in molar ratios 1:2 and 1:1 as shown in Figure 3-5. Initially, the reaction was carried at a lower temperature until low molecular weight oligomers were formed. After a certain time when water vapor started condensing on the inner wall of the flask the temperature was increased (usually after 3 hours) and the vacuum was applied to remove water. The samples were collected in regular intervals of time for the acid value measurements. The reaction was stopped after the acid value reached 2 - 3 mg of KOH/g. The reaction of dimer acid with a diol in a molar ratio 1:2 had an excess of diol which terminated the polymerization reaction. The product obtained had hydroxyl value 94 mg of KOH/g and labelled as DAMLPEG-7-94. The reaction of dimer acid with a diol in the molar ratio 1:1 led to a polymerization reaction between dimer acid and diol. The product was labelled as DAMLPEG-7-47 and it had higher molecular weight and viscosity compared to DAMLPEG-7-94. Similarly, dimer acid was reacted with PEG-400 in a molar ratio 1:2 and 1:1 as shown in Figure 3-6. The 1:2 molar ratio of dimer acid to PEG-400 formed a product with the hydroxyl value 94

mg of KOH/g and it was labelled as DAPEG-94. The 1:1 molar ratio of dimer acid to PEG-400 formed a product labelled as DAPEG-33 with much lower hydroxyl value and higher viscosity as reported in Table 3-2.

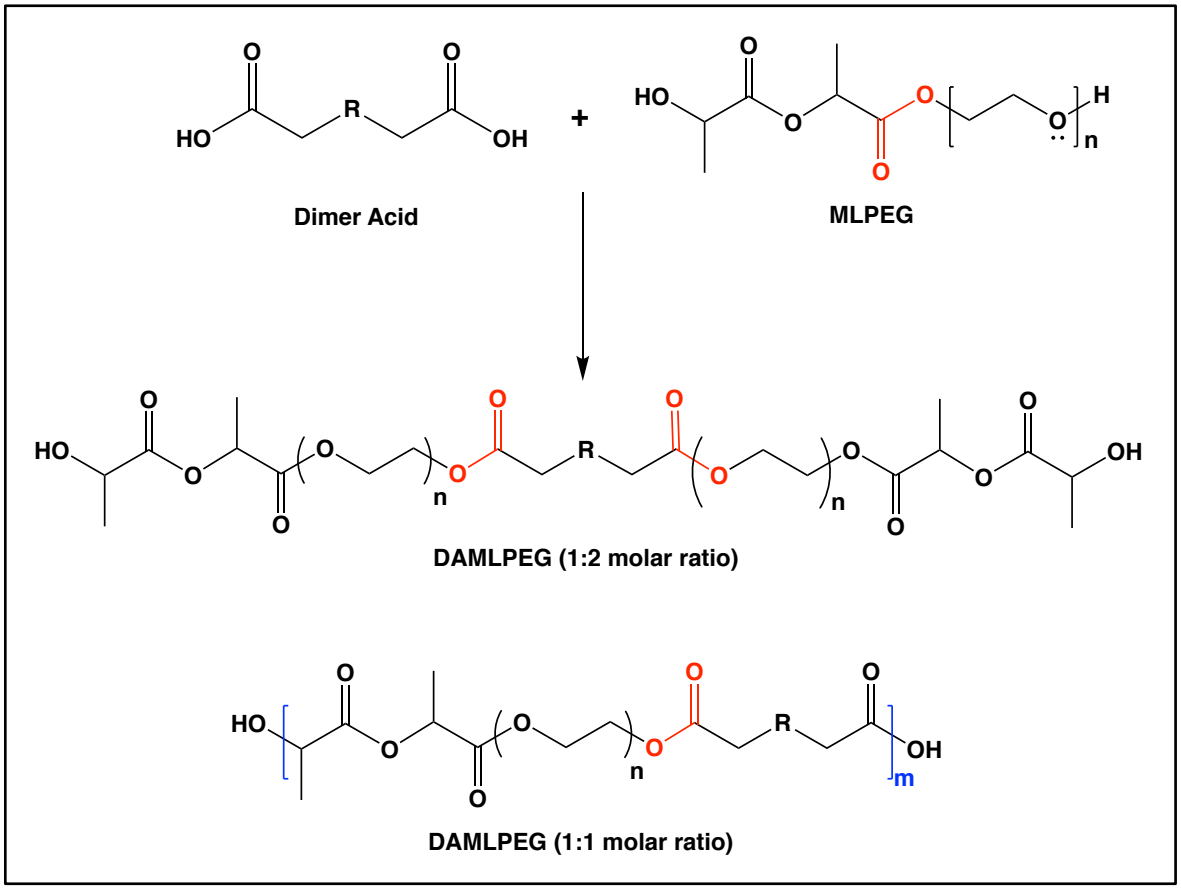


Figure 3-5: Reaction of dimer acid with MLPEG-7-202 in molar ratio 1:2 and 1:1

The DAMLPEG-3-80 polyol was synthesized by reacting dimer acid with MLPEG-3-186 in the molar ratio 1:2. It can be seen in Table 3-2 that as hydroxyl value of polyol decreases, the viscosity and molecular weight increases. Different molar ratios produced polyols with different hydroxyl values and viscosities. Depending on the application, a polyol can be chosen from a series of newly synthesized biobased polyols derived from dimer acid. The renewable carbon content is 50 - 70% which can be increased to 100% by using biobased PEG-400 [102].

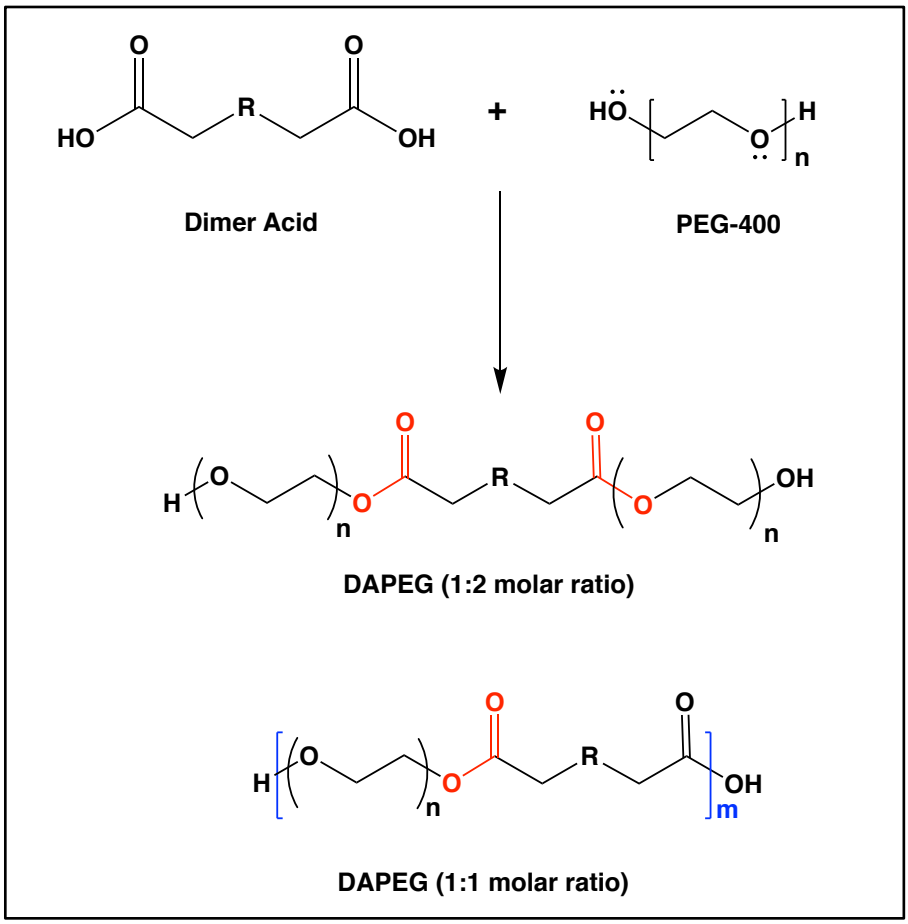


Figure 3-6: Reaction of dimer acid with PEG-400 in molar ratio 1:2 and 1:1

Table 3-2: Characteristic of dimer acid-based polyols

Compound	Hydroxyl Value (mg of KOH/g)	Acid Value (mg of KOH/g)	MW (g/mol)	Viscosity @ 25°C (cPs)	Renewable Content (%)
Dimer Acid (Radiacid 0955)	-	188 ± 3	575	4950	100
DAMLPEG-7-94 (1:2)	94 ± 9	1 ± 0	1194*	2980	57
DAMLPEG-7-47 (1:1)	47 ± 4	3 ± 0	2387*	5850	70
DAPEG-94 (1:2)	94 ± 5	< 1.5 ± 0	1194*	1022	50
DAPEG-33 (1:1)	33 ± 3	< 1 ± 0	3400*	7130	67
DAMLPEG-3-80 (1:2)	80 ± 5	2 ± 0	1400*	1968	57

*Calculated assuming functionality of polyol is 2

3.3.4 Fourier Transform Infrared Spectroscopy (FTIR)

The ATR-FTIR spectra of meso-lactide, MLE-529, and MLE-818 are shown in Figure 3-7. Meso-lactide has two ester linkages. The peaks around 1750 cm^{-1} and 1200 cm^{-1} present in the FTIR of meso-lactide were attributed to C=O and C-O of ester linkages [69]. The peaks around 1639 cm^{-1} and 1530 cm^{-1} present in the FTIR of MLE-529 were attributed to C=O and N-H of amide linkages [69]. The intensity of the peak around 1750 cm^{-1} present in the FTIR of MLE-529 was reduced. Thus, it can be confirmed that MLE-529 contains one ester and one amide linkage. Also, the peak at 3300 cm^{-1} present in FTIR of MLE-529 corresponds to OH groups [69]. Similarly, the peaks around 1639 cm^{-1} and 1530 cm^{-1} present in the FTIR of MLE-818 were attributed to C=O and N-H of amide linkages. No peak was observed around 1750 cm^{-1} in FTIR of MLE-818. Thus, it can be confirmed that MLE-818 contains only amide linkages. Also, the intensity of the peak at 3300 cm^{-1} present in FTIR of MLE-818 is more than that of MLE-529 which is due to the higher hydroxyl value of MLE-818. These FTIR spectra confirmed the reaction chemistry shown in Figure 3-2 and Figure 3-3.

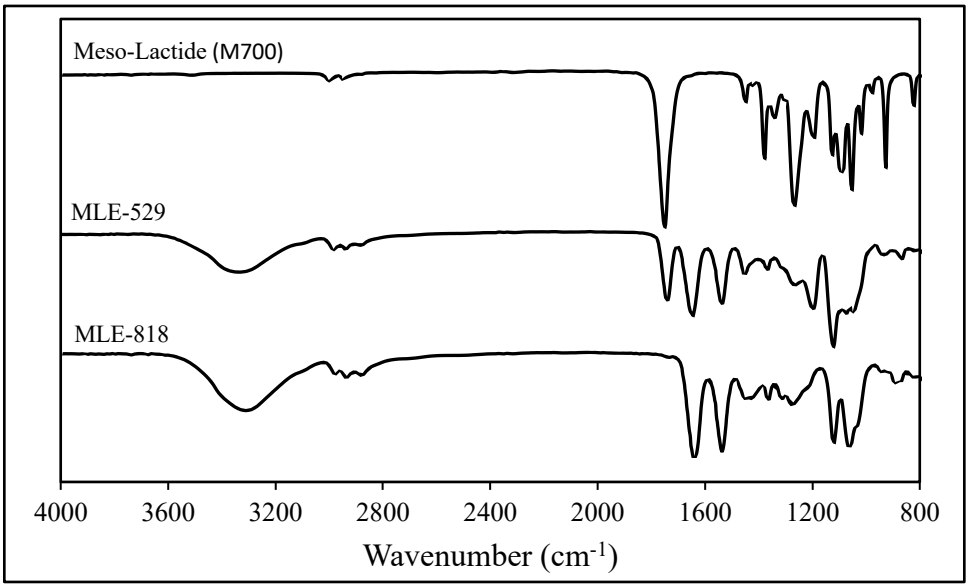


Figure 3-7: FTIR spectra of meso-lactide, MLE-529, and MLE-818

The ATR-FTIR spectra of dimer acid, PEG-400, MLPEG-7-202, DAMLPEG-7-94, and DAPEG-33 are shown in Figure 3-8. The O-H and C-H stretch was observed around 2900 cm^{-1} in FTIR of dimer acid [69]. The peak around 2950 cm^{-1} present in FTIR of all other compounds was attributed to C-H stretching [69]. In FTIR of dimer acid, the C=O stretch, O-H bend, and C-O stretch of carboxylic acid groups were observed around 1700 cm^{-1}, 1420 cm^{-1}, and 1290 cm^{-1} respectively. Also, the peak at 3300 cm^{-1} present in the FTIR of PEG-400, MLPEG-7-202, DAMLPEG-7-94, and DAPEG-33 was attributed to OH groups. The intensity of this peak is reducing as shown in Figure 3-8 which is due to the decrease in the hydroxyl value of polyols. As MLPEG-7-202, DAMLPEG-7-94, and DAPEG-33 has ester linkages, the peaks around 1750 cm^{-1} and 1250 cm^{-1} were attributed to C=O and C-O of ester linkages. The peaks around 1420 cm^{-1} and 1080 cm^{-1} were attributed to OH bend and C-O-C linkages present in PEG-400, MLPEG-7-202, DAMLPEG-7-94, and DAPEG-33 [69].

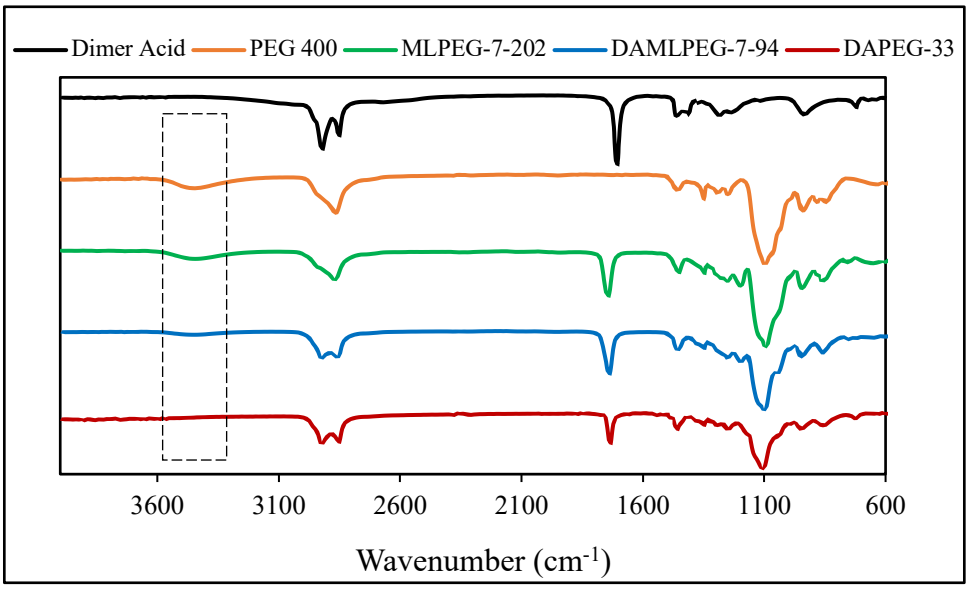


Figure 3-8: FTIR spectra of dimer acid, PEG-400, MLPEG-7-202, DAMLPEG-7-94, and DAPEG-33

3.3.5 Nuclear Magnetic Resonance (NMR) Spectroscopy

^{13}C and ^{1}H NMR spectra were used to confirm predicted structures of diols. ^{13}C NMR spectrum of MLE-818 is shown in Figure 3-9. The peak at 60 ppm (3) corresponds to the primary hydroxyl carbon of MLE-818 [83, 84] whereas peak at 67.48 ppm (4) corresponds to secondary hydroxyl carbon [84]. The peak at 21.48 ppm (1) corresponds to methyl carbon (CH_3) whereas peak at 41.38 ppm (2) corresponds to methylene carbon (CH_2) present in MLE-818. The peak at 174.76 ppm (5) corresponds to carbonyl carbon (C=O).

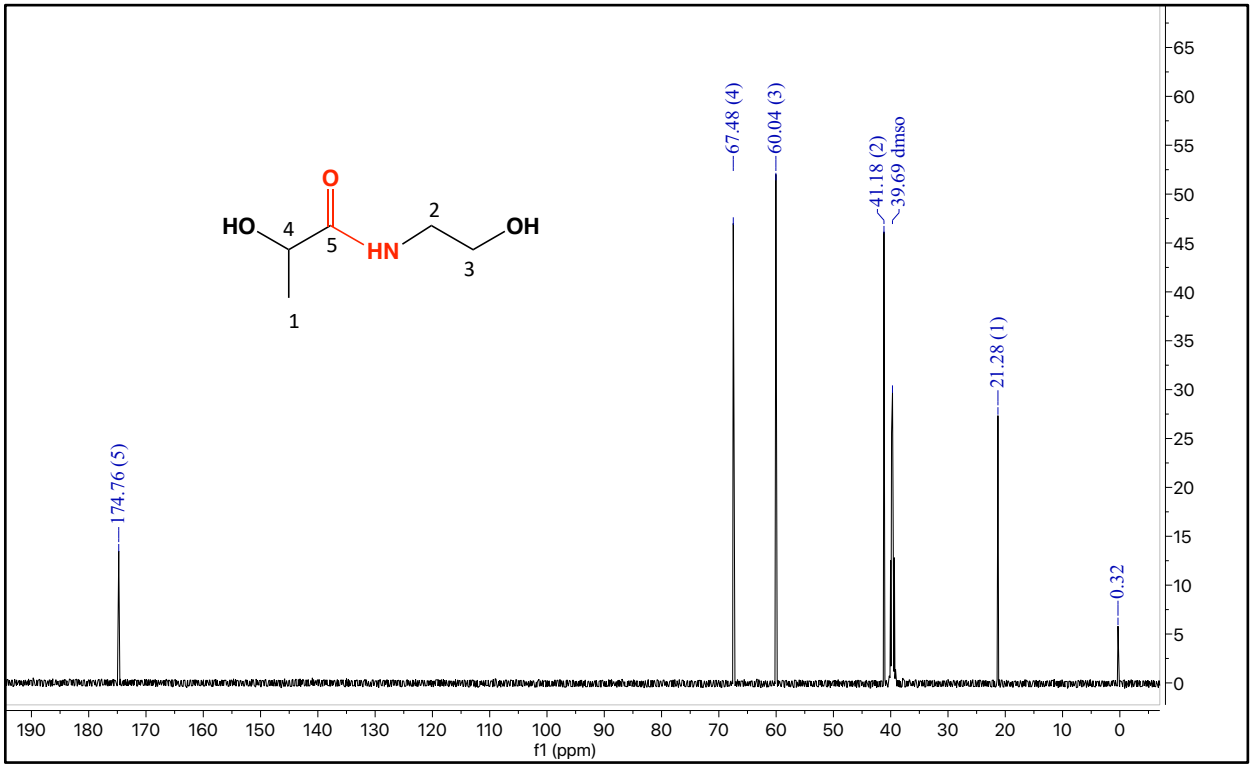


Figure 3-9: ^{13}C NMR spectrum of MLE-818

^{1}H NMR spectrum of MLE-818 is shown in Figure 3-10. The peaks at 4.7 ppm (5, triplet) correspond to primary hydroxyl proton whereas peaks at 5.5 ppm (6, doublet) correspond to secondary hydroxyl proton of MLE-818. The peak at 1.19 ppm (1, doublet) corresponds to methyl protons (CH_3) whereas peaks at 3.13 ppm (2, multiple) and 3.39 ppm (3, multiple) correspond to

methylene protons (CH_2) of MLE-818. The peak at 3.94 ppm (4, multiple) corresponds to methine protons (CH). The peak at 7.6 ppm (7, triplet) corresponds to proton attached to the nitrogen atom (NH). These NMR spectra were very identical to the predicted NMR spectra for the given structure and hence the reaction chemistry shown in Figure 3-3 is confirmed.

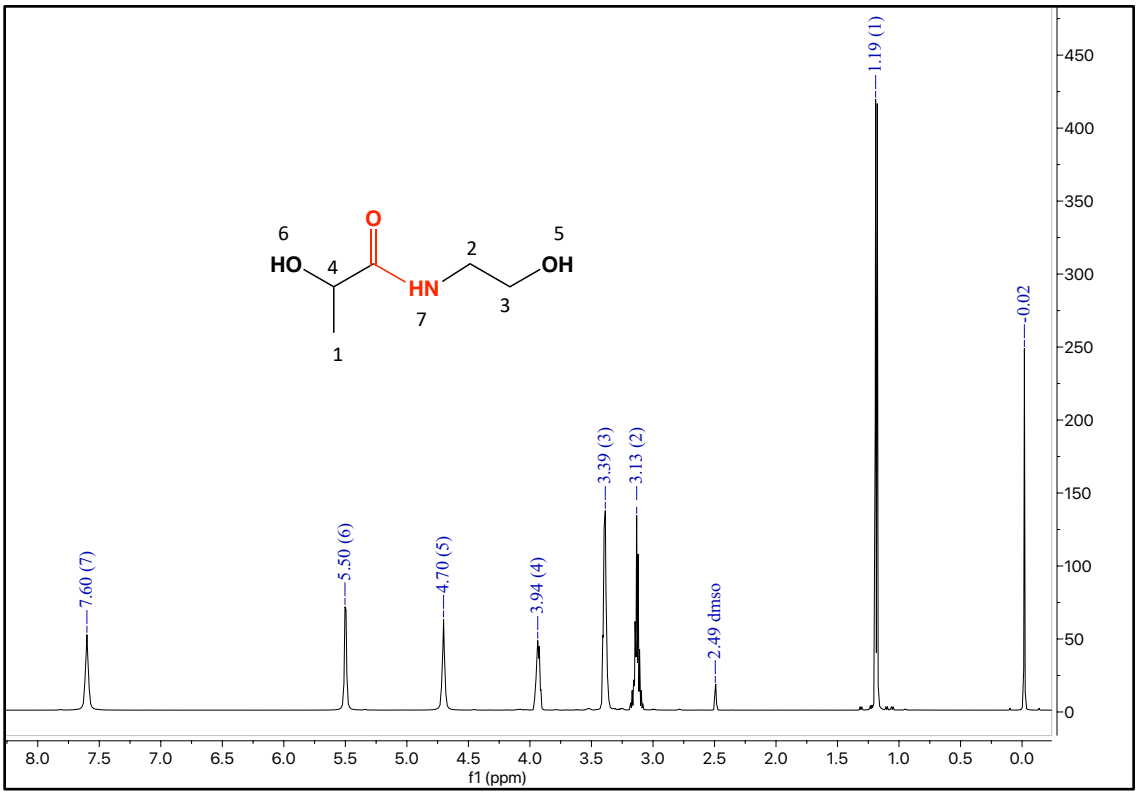


Figure 3-10: ^{1}H NMR spectrum of MLE-818

^{13}C NMR spectrum of MLE-529 is shown in Figure 3-11. The peak at 60 ppm (4) corresponds to the primary hydroxyl carbon of the diol [83, 84] whereas the peak at 66.37 (5) ppm corresponds to secondary hydroxyl carbon [84]. The peak at 20.68 ppm (2) and 21.68 ppm (1) corresponds to methyl (CH_3) carbon. The peak at 174.95 ppm (7) and 175.12 ppm (8) corresponds to carbonyl (C=O) carbon. The peak at 67.67 ppm corresponds to methine (CH) carbon (6) and the peak at 41.38 ppm (3) corresponds to methylene (CH_2) carbon in the diol. The small peaks observed in the NMR spectrum could be due to the minor product (Figure 3-2) or lactic acid.

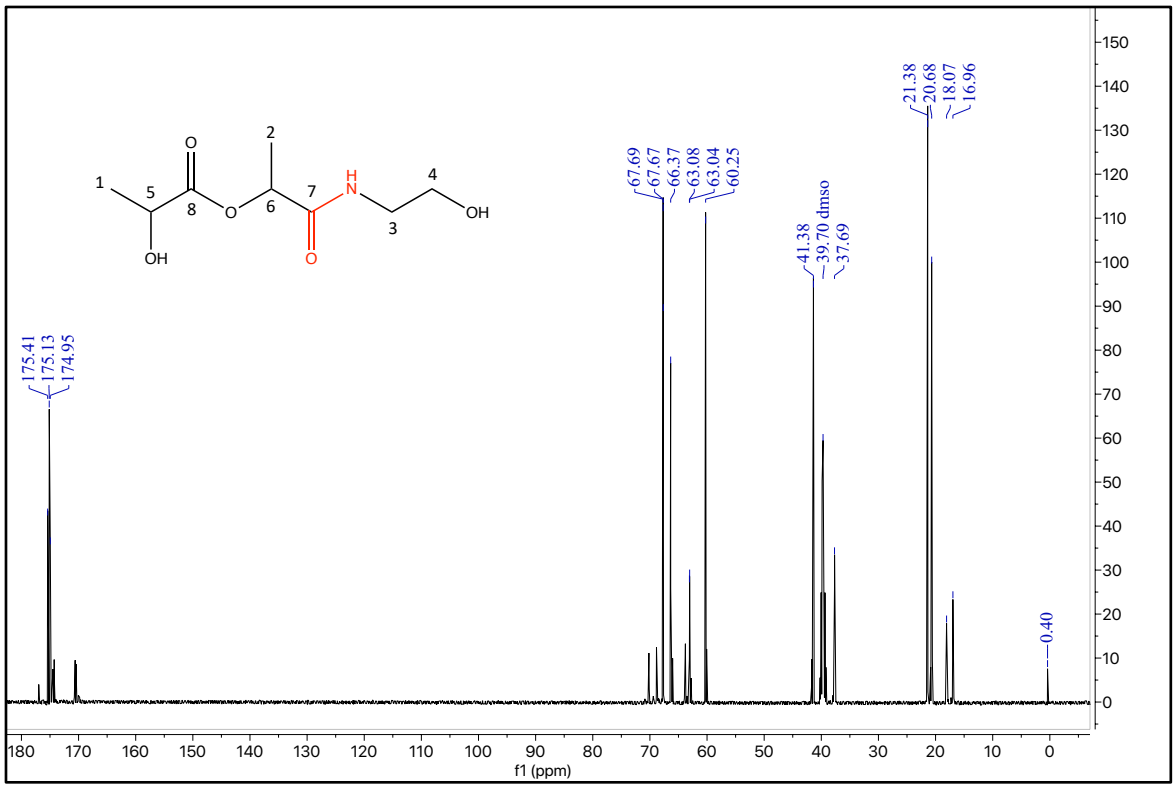


Figure 3-11: ^{13}C NMR spectrum of MLE-529

^{13}C NMR spectrum of MLPEG-7-202 is shown in Figure 3-12. The peak at 60 ppm (3) corresponds to the primary hydroxyl carbon of the diol [83, 84] whereas the peak at 66.26 ppm (6) corresponds carbon attached to secondary hydroxyl group [84]. The peak at 17.08 ppm (2) and 20.75 ppm (1) corresponds to methyl (CH_3) carbon. The peak at 170.72 ppm (12) and 174.48 ppm (11) corresponds to carbonyl (C=O) carbon. The large and sharp peak at 70.24 ppm corresponds to methylene (CH_2) carbon (7,8) present in the repeat unit of PEG. Also, the peak at 72.80 ppm corresponds to methylene (9) carbon (CH_2) adjacent to the primary hydroxyl carbon. Both of these peaks (70.24 ppm and 72.80 ppm) were observed in the ^{13}C NMR spectrum of PEG-400. The peak at 70.28 ppm which is merged with the large peak at 70.24 ppm could be due to the methine (CH) carbon (10) present in the diol. The other peaks at 64.54 ppm, 68.53 ppm, and 68.83 ppm could be coming from other carbon atoms (4, 5) in PEG. The small peaks observed in the NMR spectrum

could be due to the minor product (Figure 3-4) or lactic acid.

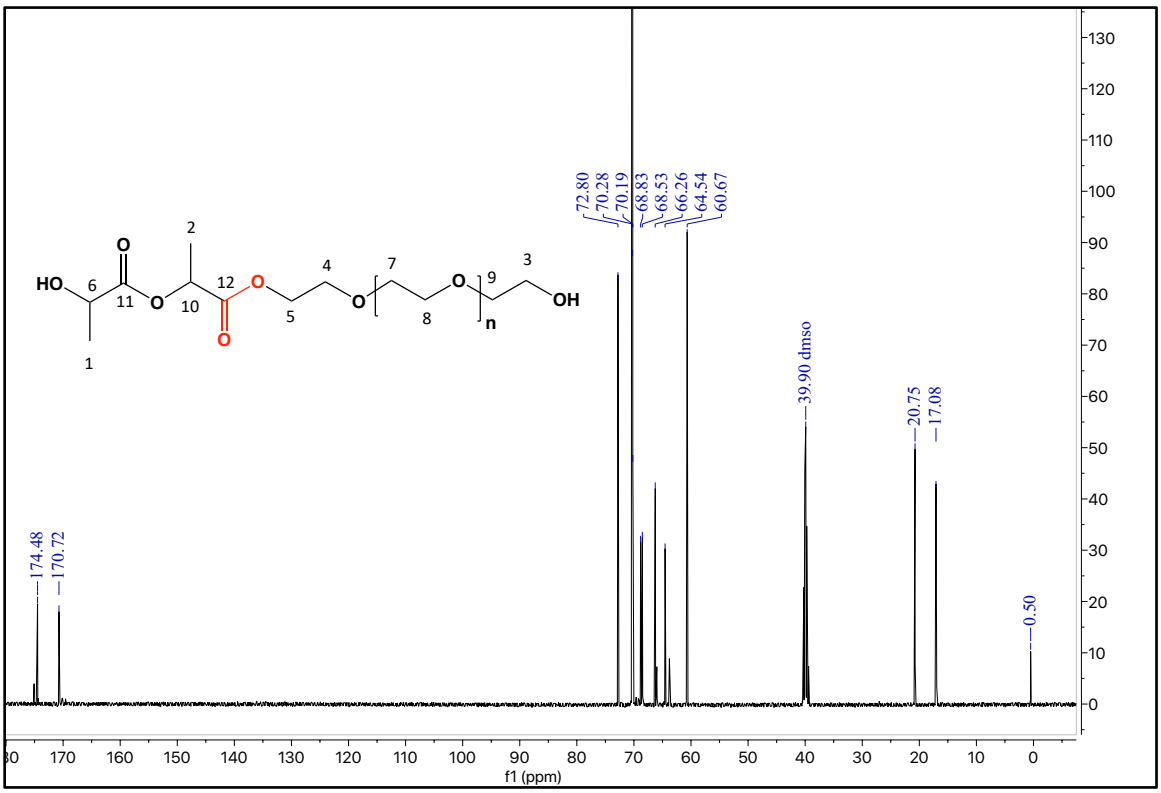


Figure 3-12: ^{13}C NMR spectrum of MLPEG-7-202

3.3.6 Thermogravimetric analysis (TGA)

Thermogravimetric analysis and derivative thermogravimetric graphs of meso-lactide and meso-lactide based diols are shown in Figure 3-13 and Figure 3-14, respectively. Meso-lactide degrades around 159ºC, MLE-529 degrades around 243ºC, and MLE-818 degrades around 268ºC. Meso-lactide has two ester linkages, MLE-529 has one ester and one amide linkage, and MLE-818 has only amide linkages. Thus, the increase in the degradation temperature of diols could be due to the increase in the number of amide linkages as they are thermally more stable than esters linkages [103]. Also, the degradation temperature of MLPEG diols is higher than PEG-400 due to the higher molecular weight of MLPEG diols and the presence of both ester and ether linkages. MLE-529 and MLE-818 diols degrade over a short range of temperature could be due to the small molecular

weight distribution. Whereas PEG-400 and MLPEG diols degrade over a wide range of temperature probably due to the large molecular weight distribution.

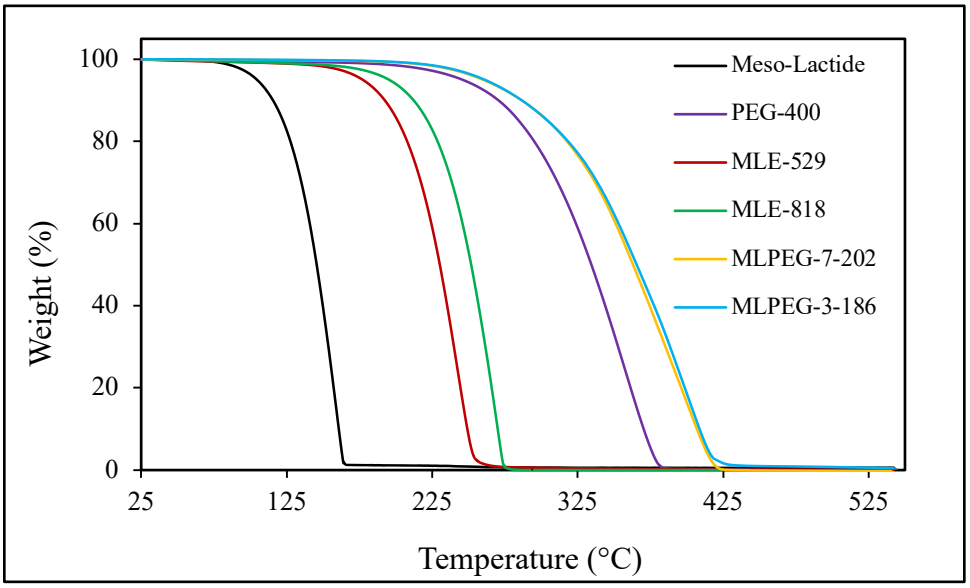


Figure 3-13: Thermogravimetric analysis of meso-lactide, PEG-400, MLE-529, MLE-818, MLPEG-7-202, and MLPEG-3-186

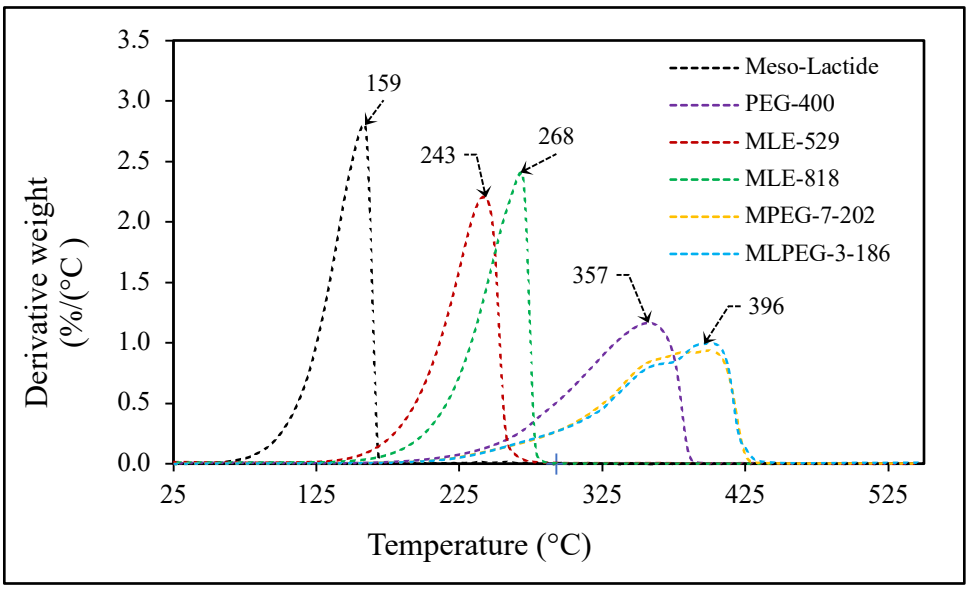


Figure 3-14: Derivative thermogravimetric graphs of meso-lactide, PEG-400, MLE-529, MLE-818, MLPEG-7-202, and MLPEG-3-186

Thermogravimetric analysis of dimer acid, PEG 400, DAMLPEG, and DAPEG polyols are shown in Figure 3-15 and Figure 3-16.

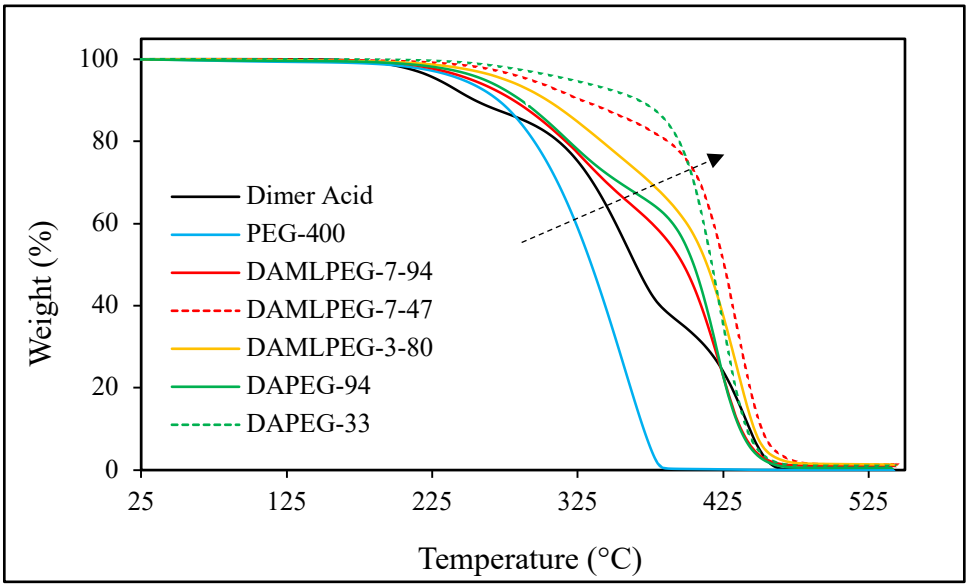


Figure 3-15: Thermogravimetric analysis of dimer acid, PEG-400, DAMLPEG-7-94, DAMLPEG-7-47, DAMLPEG-3-80, DAPEG-94, and DAPEG-33

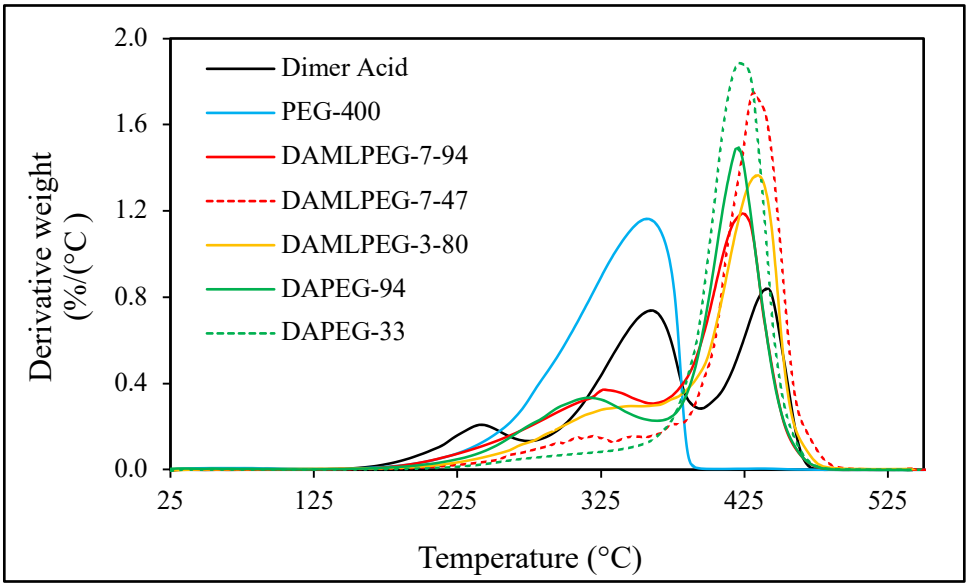


Figure 3-16: Derivative thermogravimetric graphs of dimer acid, PEG-400, DAMLPEG-7-94, DAMLPEG-7-47, DAMLPEG-3-80, DAPEG-94, and DAPEG-33

Dimer acid has three distinct degradation temperatures i.e. 241°C, 338°C, and 440°C. The polyols synthesized with a 1:2 molar ratio (DAMLPEG-7-94, DAMLPEG-3-80, and DAPEG-94) degrade in two stages 225 - 370°C and 370 - 480°C as shown in Figure 3-16. The two degradation stages could be due to the different chain length molecules. The TGA graphs of polyols (DAPEG-33 and DAMLPEG-7-47) synthesized with 1:1 molar ratio showed a single degradation stage around 422°C which could be due to the uniform chain length of all molecules.

3.4 CONCLUSION

In this work, a series of biobased diols from meso-lactide were successfully synthesized using simple reaction chemistries. Ring-opening of meso-lactide with primary amines were faster than primary hydroxyl groups. Also, the ring-opening reaction of meso-lactide with amines was exothermic while the ring-opening reaction of meso-lactide with hydroxyl group was endothermic. For flexible polyurethane foam application, the hydroxyl value of meso-lactide diols was reduced using polycondensation chemistry. Different reactant ratios produced polyols with different molecular weight and hydroxyl value. These polyols have 50 - 70% renewable carbon content, as dimer acid and meso-lactide were biobased while ethanolamine and PEG-400 were petroleum-based. However, biobased PEG-400 is commercially available which will increase the renewable carbon content to 100%. The material cost for these polyols is around 0.6 - 0.8 $/lb and its synthesis process is two-step and one-pot synthesis approach. Thus, these polyols can compete with commercially available polyols with suitable applications in polyurethanes like coatings or foams. The presence of long carbon chain in the polyol will provide flexibility in the final polymer. These polyols can also be used as a plasticizer for stiff polymers like polylactide (PLA).

Polyols were synthesized by using meso-lactide as a starting material but instead, PLA waste (cutlery or bags) can be recycled back to lactide and used as a starting material for polyols. This

will reduce the raw material cost. Also, dimer acids derived from soybean were used for polycondensation chemistry, but any long-chain dimers or trimers can be used.

4 RIGID POLYURETHANE FOAMS DERIVED FROM SOYMEAL AND LACTIDE POLYOLS

4.1 INTRODUCTION

Polyurethanes are the most versatile polymers having a variety of applications in foams, coatings, adhesive, sealants, and elastomers. Polyurethane foams (PUF) are widely used and are preferred over other foams (e.g. expanded polystyrene (EPS), extruded polystyrene (XPS), and polyethylene foam) due to their good thermal insulation properties, easy installation, and relatively low cost [25, 26]. They have various applications in building & construction, electronics, automotive, packaging materials, and cushioning industries. PUF with varying densities can be used over a wide range of temperatures [104]. The demand for PUF has been constantly on the rise. Polyol and isocyanate are the two major components used in polyurethane synthesis. Conventionally, petroleum feedstocks were used to make polyols and isocyanates, but of late, bio-based feedstocks are being used in combination with petroleum feedstocks. Recently, many companies are incorporating renewable biomass carbon in their products (e.g. Ford Motor Company's polyurethanes, Covestro's 100% biobased polyurethane) in order to reduce the product's carbon footprint and environmental impacts. Literature reports the synthesis of polyols and PUF using different biomass resources such as cardanol (obtained from cashew nutshell liquid) [41, 42], cellulose [44], and algae oil [45]. However, most of these commercially available biobased polyols are derived either from plant oils e.g. soybean oil [11] or from saccharides e.g. sucrose. At present, soybean oil is commercially used in food, in the synthesis of polyols, in production of biodiesel [10, 52], and in other industrial products. The co-product soymeal is primarily used in animal feed and human nutrition [9, 53], and a small amount is used by the chemical industry [7]. Similarly, distillers dried grains with solubles (DDGS) is a byproduct of ethanol manufacturing which is also available

in large volume. These products can be used in value-added industrial products like polyol and polyurethane foams.

Furthermore, fermentation of corn-starch gives lactic acid which is used as a starting material in polylactide (PLA) manufacturing. Lactide contains two monomers of lactic acid, and it is an intermediate product of PLA synthesis. Due to the presence of asymmetric carbon atom in lactic acid, lactide has three isomers i.e. L-lactide, D-lactide, meso-lactide. Meso-lactide content in PLA is maintained around 7.5% as it negatively affects the properties of PLA above that [23]. Thus, meso-lactide is continuously removed during PLA synthesis. PLA is commonly used in cutlery, bags, and other short life span products. This PLA waste can be recycled back to lactide and reused either for PLA synthesis or for the development of new products [24].

In previous work, polyols from soymeal and lactide have been synthesized. The presence of primary hydroxyl group (higher reactivity) and amide linkages (better thermal stability) in polyols make them an attractive material for the synthesis of polyurethane foams. The use of simple chemistry, one-pot synthesis approach, and inexpensive raw materials make the commercialization of polyols viable from a price perspective. After obtaining the new biobased polyols it was necessary to check the performance properties of polyurethane foams made out it.

In this chapter, we report the use of new biobased polyols in rigid polyurethane foams (PUF) for its application as an insulation material. The formulation for rigid PUF will be optimized, and PUF with biobased polyol content 20% and 50% will be synthesized. The mechanical properties, thermal properties, and morphology of biobased PUF will be compared with the PUF made from commercial petroleum-based polyol. The thermal conductivity, aging study, and water absorption study are very important for the insulation application. Thus, it will be performed on biobased PUF for its application in building and construction material.

4.2 EXPERIMENTAL

4.2.1 Materials and chemicals

Soymeal polyol with a hydroxyl value of 560 mg of KOH/g was synthesized previously. Lactide polyol with a hydroxyl value of 529 mg of KOH/g and acid value 6 mg of KOH/g was also synthesized previously. The Jeffol-SG-360 with hydroxyl value 360 mg of KOH/g is a commercially available sucrose-glycerine based polyol, and Rubinate M is a polymeric methylene diphenyl diisocyanate (pMDI). Both were received from Huntsman Corporation (Texas, USA). Catalysts Dabco® DC-193 (silicone-based surfactant), Polycat® 77 (tertiary amine), and Dabco® 33LV (33% triethylene diamine, $C_6H_{12}N_2$ and 67% dipropylene glycol, $C_6H_{14}O_3$) were received from Air Products and Chemicals, Inc. (Pennsylvania, USA). The Niax-A1 catalyst (70% bis(2-dimethylaminoethyl) ether, $C_8H_{20}N_2O$ and 30% dipropylene glycol, $C_6H_{14}O_3$) was received from Momentive Performance Materials (New York, USA).

4.2.2 Polyol synthesis

The synthesis procedure for both the polyols is described here briefly.

4.2.2.1 Synthesis of soymeal-based polyol

The soymeal and ethanolamine (1:3) were reacted in a round-bottom flask and nitrogen gas was purged initially for 15 - 20 minutes. The reaction was conducted for 2 hours at a temperature of 100 - 105ºC. The intermediate products obtained were referred to as amine derivatives which were converted to soymeal polyol by reacting it with propylene carbonate at 70ºC.

4.2.2.2 Synthesis of lactide polyol

Meso-lactide was reacted with ethanolamine in a molar ratio 1:1 at 20ºC in a round-bottom flask and nitrogen gas was purged initially for 15 - 20 minutes. The temperature of the reaction was raised to 150ºC to ensure completion of ring-opening reaction.

4.2.3 Free rise study of polyurethane foams

The free rise study of PUF was performed as per ASTM standard D7487-13. A side B (20 grams) which contains polyols, gelling catalyst (Dabco® 33 LV), silicone surfactant (Dabco® DC 193), blowing catalyst (Niax A-1), catalyst (Polycat® 77), and blowing agent (water) were homogeneously mixed using a stirrer at high rpm for few minutes in the following proportion:

Polyol blend	100 g
Dabco® DC193	2.5 g
Dabco® 33LV	1.8 g
Niax-A1	0.5 g
Polycat®77	1.0 g
Water	6.0 g

Rubinate M isocyanate was side A (35 - 40 grams) and the amount required for all formulations was calculated using isocyanate index 105. Side A was added to side B and the mixture was thoroughly blended for a few seconds (mix time). The characteristic times (cream, top of the cup, string gel, rise, and tack free) for each PUF were recorded. The PUF formulation for 50% biobased polyol content given in Table 4-1 was used for miscibility study. In a plastic cup, all contents of side B was mixed for 3 - 4 minutes and poured into a glass jar. The pictures were taken on the same day, next day, and after two weeks to study miscibility.

4.2.4 Box foam and its characterization

A mold of dimensions 13 cm X 18 cm X 37 cm was used to make a box foam. A mold release was applied inside the box and the box was kept in the oven for 10 minutes at 65°C. Meanwhile, all ingredients of side B was measured in the proportion mentioned earlier and mixed for 2 - 3 minutes. Side A was added to side B and mixed for 12 s. The mixture was immediately poured inside the

preheated box and lid was closed. After 10 - 15 min, the foam was removed from the box and kept at room temperature. After seven days of foam manufacturing, the foam was cut to measure its properties. The outer skin of the box foam was removed by cutting 1 cm from all sides. ASTM 1622-14 and ASTM 1621-16 standards were used to determine density, and compressive strength of the foam samples of dimension 6 cm X 6 cm X 3.5 cm, respectively. The compressive strength of foams was tested in the direction perpendicular to the rise direction of foams with a speed of 3.4 mm/min and it was measured at a deformation of 13% or yield point, whichever occurs first.

Degradation temperature of samples was obtained by thermogravimetric analysis (TGA). TGA measurements were conducted under nitrogen flow unless and until specified using a TGA Q50 (TA Instruments, Delaware, USA). In this analysis, a sample (10 - 15 mg) was taken in an aluminum pan and heated up to 550 - 600°C at a rate of 10°C/min. The weight loss (%) of a sample as a function of temperature (°C) was obtained from this analysis. The derivative thermogram (%/°C) was used to identify the degradation temperatures.

Cell morphologies of all foams were studied in parallel and perpendicular to the rise direction of foams using a JEOL 6610LV (tungsten hairpin emitter) Scanning Electron Microscope (SEM) (JEOL Ltd., Tokyo, Japan). The samples were mounted on aluminum stubs using high vacuum carbon tabs (SPI Supplies, Pennsylvania, USA). Samples were coated with platinum (Pt) approximate thickness 8 mm in a Quorum Technologies/Electron Microscopy Sciences Q150T turbo pumped sputter coater (Quorum Technologies, Laughton, East Sussex, England BN8 6BN) purged with argon gas.

An aging test of PUF was performed in accordance with the ASTM 2126-15 standard. It was performed at 25°C and 70°C and at ambient humidity. Foam dust was removed using a brush before all measurements. A water absorption test was performed based on ASTM D 2842-12

standard. The foam samples were completely immersed in water in a container at room temperature. Before each reading, the water on the surface of a foam sample was removed using tissue paper. The foam samples of dimension 130 X 110 X 20 mm (4 samples each) were used for the aging and water absorption study. The thermal conductivity data was provided by METER Group (Washington, USA) (formerly Decagon Devices Inc. lab). It was measured using a transient plane source method in accordance with ISO 22007 standard at temperature 22°C.

4.3 RESULT AND DISCUSSION

Jeffol-SG-360 is a commercially available polyol. It is synthesized using sucrose or glycerine as an initiator and using propylene oxide or ethylene oxide to build molecular weight. In this study, Jeffol-SG-360 was used as a control to compare properties of biobased foams produced from soymeal polyol and lactide polyol. Rubinate M which is a standard polymeric methylene diphenyl diisocyanate (pMDI) was chosen for polyurethane foam synthesis. Its vapor pressure at room temperature is significantly lower than the vapor pressure of toluene diisocyanate (TDI) [105]. All polyurethane foams were synthesized inside the fume hood and left there for 24 hours for evaporation of any residual gases. DC 193 is standard silicone surfactant used for polyurethane foams which also provides fire-retardant properties. Polycat 77 catalyst is a tertiary amine that provides a balanced influence on the polyol-isocyanate and isocyanate-water reactions in polyurethane foams. Dabco 33-LV catalyst is a tertiary amine which has a strong influence on the polyol-isocyanate reaction. Niax A1 catalyst also balances polyol-isocyanate and water-isocyanate reactions.

4.3.1 Free rise study of PUF

All PUF formulations made with soymeal polyol and lactide polyol are given in Table 4-1 and their free rise profiles are shown in Figure 4-1 and Figure 4-2 which were obtained using a cup

test. Various characteristic times such as cream time, top of the cup time, string gel time, end of the rise time, and tack free time was measured to study the effect of biobased polyol addition on polyurethane foam production. Each time is related to different stages of foam production. At cream time, the viscosity of polyol-isocyanate mixture increases and foam starts rising. At top of the cup time, the foam reaches top of the cup. At string gel time, polyurethane network starts building. At rise time, the foam stops rising. At tack free time, the foam is no longer sticky. It was observed that at end of rise all foams were tack free. It was also observed that the rise time of foam increases as content of biobased polyol increases except for SPF 20% and LPF 20%, where rise time decreased as compared to the control foam.

Table 4-1: Formulations of soymeal and lactide polyols with Jeffol-SG-360

Material	**Biobased Polyol Content**				
	0%	**20%**	**50%**	**80%**	**100%**
Side B (parts)					
Jeffol-SG-360	100	80	50	20	0
Soymeal Polyol (SP) Or Lactide Polyol (LP)	0	20	50	80	100
Dabco DC 193	2.5	2.5	2.5	2.5	2.5
33 LV	1.8	1.8	1.8	1.8	1.8
Niax-A1	0.5	0.5	0.5	0.5	0.5
Polycat 77	1	1	1	1	1
Water	6	6	6	6	6
Side A (parts)					
Rubinate M (Soymeal Polyol)	191	201	217	233	243
Rubinate M (Lactide Polyol)	191	199	212	226	234
ISO Index	105	105	105	105	105

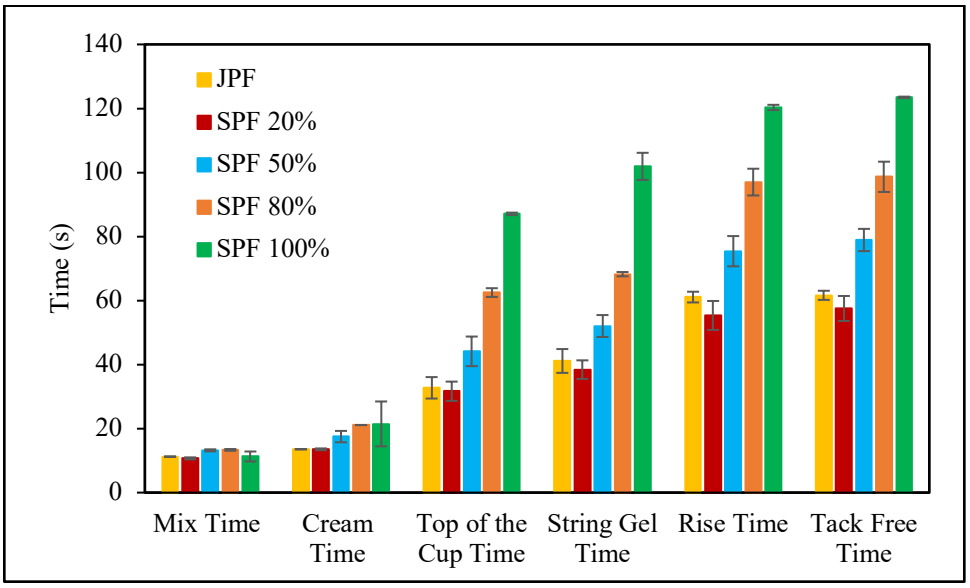


Figure 4-1: Free rise profiles of JPF (0% SP), SPF 20% (20% SP), SPF 50% (50% SP), SPF 80% (80% SP), and SPF 100% (100% SP)

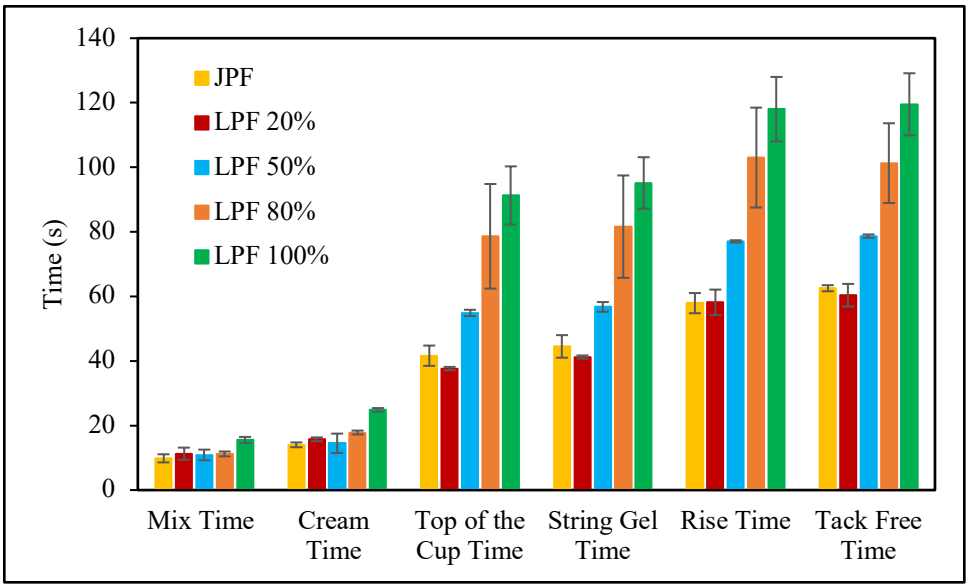


Figure 4-2: Free rise profiles of JPF (0% LP), LPF 20% (20% LP), LPF 50% (50% LP), LPF 80% (80% LP), and LPF 100% (100% LP)

The increase in the characteristic time for rest of the formulations could be due to the higher hydroxyl value of SP (570 mg of KOH/g) and LP (529 mg of KOH/g) compared to the Jeffol (360 mg of KOH/g). Thus, with an increase in biobased polyol content, the amount of isocyanate

required for foam also increased. As the same amount of catalyst was added to all formulations, its concentration (amount per polyol-isocyanate reaction) decreased with an increase in the hydroxyl value. Thus, the increase in characteristic times with an increase in the biobased content could be due to the decrease in the reaction rate of polyol-isocyanate reaction.

4.3.2 Thermogravimetric analysis of PUF

The thermogravimetric analysis (TGA) graphs of all polyols and polyurethane foams are shown in Figure 4-3. In the TGA graphs of the soymeal and Jeffol polyol, the two degradation stages observed which could be due to the low and high molecular weight segments. In the TGA graph of lactide polyol single degradation stage was observed indicating uniform molecular weight. In the TGA graphs of the foams, three degradation stages were observed i.e. stage I (75°C - 300°C), stage II (300°C - 400°C), and stage III (>400°C) [74].

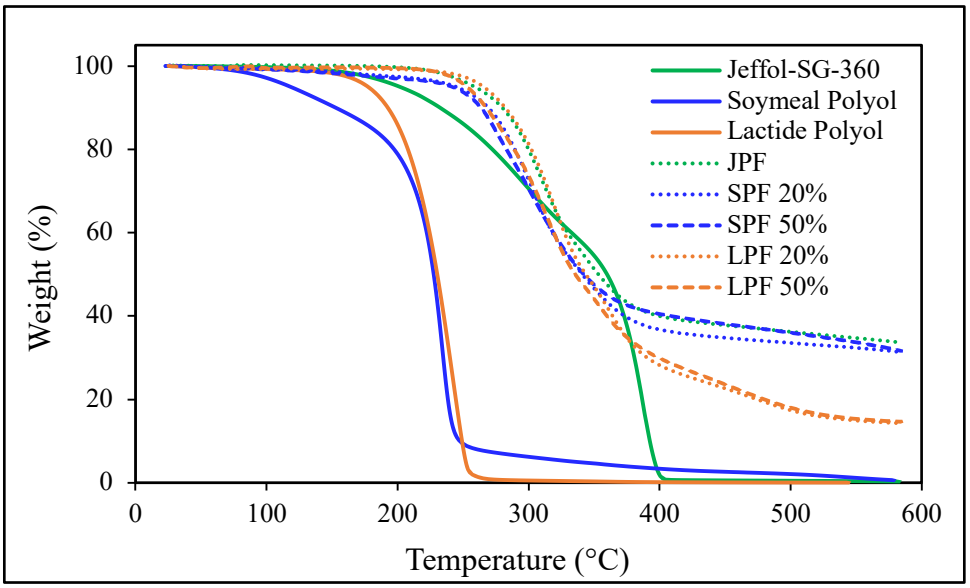


Figure 4-3: TGA graphs of Jeffol-SG-360, soymeal polyol, lactide polyol, JPF, SPF (20%, 50%), and LPF (20%, 50%)

The first stage corresponds to the degradation of less stable groups such as biuret or urethane [44]. The second stage corresponds to the degradation of soft segments of the polyol chain, and the third

stage corresponds to the further degradation of fragments produced in the second stage [78, 79]. The temperature corresponding to 5% mass loss for all foams was above 200°C as reported in Table 4-2.

Table 4-2: Thermal degradation analysis of polyurethane foams

	$T_{5\%}$ (°C)	$T_{10\%}$ (°C)	$T_{50\%}$ (°C)	$T_{1(max)}$ (°C)	$T_{2(max)}$ (°C)
Jeffol-SG-360 Polyol	201	232	360	298	389
Soymeal Polyol	118	153	228	234	-
Lactide Polyol	180	220	245	259	-
JPF (control)	277	291	346	311	342
SPF 20%	268	284	347	303	337
SPF 50%	259	273	347	269	314
LPF 20%	266	282	342	295	336
LPF 50%	257	270	337	293	333

4.3.3 Density, compressive strength, and thermal conductivity of PUF

The density of rigid PUF should be greater than 30 kg/m^3 to maintain a certain amount of strength for commercial applications [55]. The density of foam depends on the amount of CO_2 produced, which further depends on the amount of water added. Also, properties of foam are strongly dependent on its density. Hence, foam densities should be similar to compare their properties. As the density of a foam increases, its compressive strength also increases [41] (as shown in Table 4-3). The soymeal polyol contains water (1 - 2%) because of which the density of SPF decreases with an increase in the amount of soymeal polyol. Most of the commercially produced PUF are used as an insulating material. Considering this as a viable application for our foams, the thermal conductivity of all synthesized foams was determined. The heat is transferred through a PUF via gas conduction, solid conduction, convection, and radiation [106-108]. The thermal conductivity of foam depends on its density, cell size, closed-cell content, and trapped gases inside closed cells

[107, 109]. The gas composition inside the cell is a controlling factor in low density foams [110], as it is a major component. As the cell size of a foam decreases, its thermal conductivity also decreases [106, 111]. If a rigid foam contains some open cells, then carbon dioxide gas trapped inside the foam gets subsequently replaced by air through diffusion mechanism [112]. As the thermal conductivity of air (24.9 mW/m·K) is higher than carbon dioxide gas (15.3 mW/m·K) [106], the thermal conductivity of foam increases with an increase in the open cell content [112]. The thermal conductivities of rigid PUF having a density of ~40 kg/m^3 were found in a range of 24 - 35 mW/m·K [106, 109, 112]. The thermal conductivities of PUF are given in Table 4-3. The thermal conductivity of JPF 2 was found to be slightly lower than JPF 1 which could be due to the higher density and smaller cell size of JPF 2. The thermal conductivities of SPF foams were lower compared to the control foam (JPF). The decrease in the thermal conductivity of SPF with an addition of the soymeal polyol could be due to the increase in the closed-cell content or the presence of polysaccharides. Lactide polyol foams (LPF) have thermal conductivity close to the control foams.

Table 4-3: Properties of polyurethane rigid foams

	Density (kg/m^3)	**Compressive Strength (kPa)**	**Cell Size (µm) $\parallel^{el}$**	**Cell Size (µm) $\perp^{er}$**	**Thermal Conductivity (mW/m·K)**
JPF 1	39.15 $\pm$ 0.51	218.82 $\pm$ 21.59	336 $\pm$ 31	333 $\pm$ 28	32.72
JPF 2	42.42 $\pm$ 0.36	305.84 $\pm$ 21.61	323 $\pm$ 26	308 $\pm$ 17	32.41
SPF-20%	41.69 $\pm$ 0.82	257.08 $\pm$ 15.08	280 $\pm$ 27	302 $\pm$ 19	32.01
SPF-50%	40.97 $\pm$ 2.04	203.43 $\pm$ 38.94	386 $\pm$ 27	337 $\pm$ 24	31.95
LPF-20%	38.86 $\pm$ 1.60	270.10 $\pm$ 21.29	359 $\pm$ 41	303 $\pm$ 33	32.85
LPF-50%	42.39 $\pm$ 1.74	283.45 $\pm$ 20.61	312 $\pm$ 33	294 $\pm$ 30	32.51

4.3.4 Scanning Electron Microscopy (SEM) images of PUF

The SEM was used to study the foam morphology. The SEM images of JPF 2, SPF 20%, and SPF

50% foams, in parallel ($\|^{el}$) and in perpendicular ($\perp^{er}$) to the rise direction of foams are shown in Figure 4-4. The SEM images of JPF 1, LPF 20%, and LPF 50% foams, in parallel ($\|^{el}$) and in perpendicular ($\perp^{er}$) to the rise direction of foams are shown in Figure 4-5. The SEM images of all foams showed closed cell structure which is important for insulation applications. The smaller average cell size of SPF 20% ($\|^{el}$) compared to the JPF 2 ($\|^{el}$) (Table 4-3) could be due to the higher viscosity of the soymeal polyol. The higher viscosity can affect the pulling of cells against gravity during rising, thus leading to smaller average cell size [41]. An increase in water content produces more CO_2 due to which the average cell size increases [44], and a higher rise time provides cells sufficient time to grow. Thus, the average cell size of SPF 50% ($\|^{el}$) was greater than the JPF 2, as water content and rise time of SPF 50% was higher compared to the JPF 2.

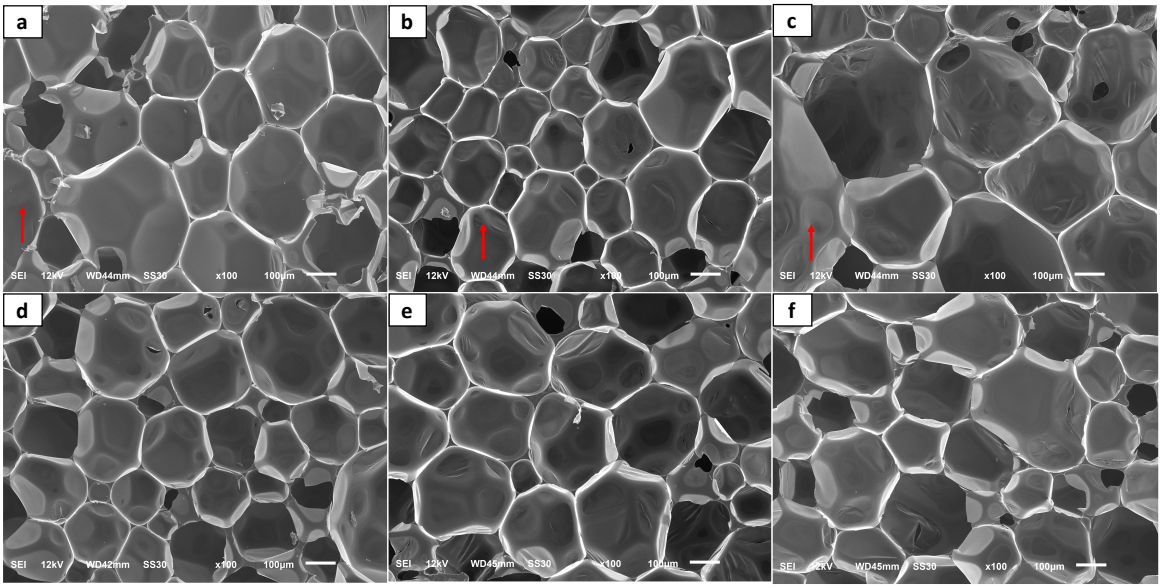


Figure 4-4: SEM images of (a) JPF 2 (b) SPF 20% (c) SPF 50% foams parallel to the rise direction; SEM images of (d) JPF 2 (e) SPF 20% (f) SPF 50% foams perpendicular to the rise direction (rise direction is shown with an arrow for a, b, c; rise direction is perpendicular to the plane of paper for d, e, f)

As cell size of a foam increases, its compressive strength and density both decreases [41]. Thus,

the compressive strength of SPF 20% and SPF 50% was lower compared to the JPF 2. The cell size of foams in perpendicular to the rise direction did not change a lot with the addition of soymeal polyol. The smaller average cell size of LPF 50% ($\|^{el}$) compared to the JPF 1 ($\|^{el}$) and LPF 20% ($\|^{el}$) could be due to the higher density of LPF 50% foam (Table 4-3). The cell size of control foam (JPF 1) was comparatively higher than the cell size of LPF 20% and LPF 50% foams in perpendicular direction. Lactide polyol foams showed higher compressive strength compared to soymeal polyol foams and control foams. This could be due to the smaller average cell size of lactide foams.

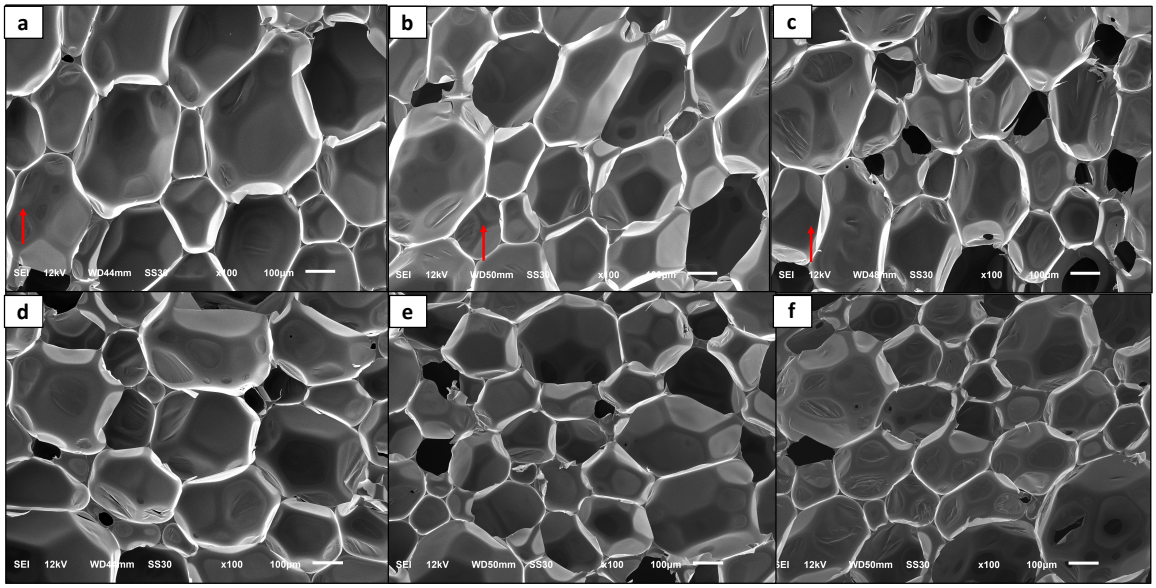


Figure 4-5: SEM images of (a) JPF 1 (b) LPF 20% (c) LPF 50% foams parallel to the rise direction; SEM images of (d) JPF 1 (e) LPF 20% (f) LPF 50% of foams perpendicular to the rise direction (rise direction is shown with an arrow for a, b, c; rise direction is perpendicular to the plane of paper for d, e, f)

4.3.5 Aging and water absorption tests of PUF

The rigid PUF are used in structural applications and other foamed-in-place insulation applications [113] where pre-conditioning of foams is not possible. Hence, it is important to evaluate the

dimensional stability of foams over a certain period of time at different conditions before its installation. The aging study of rigid PUF was conducted to find their mass loss and shrinkage or expansion over time. The aging and water absorption studies were performed on control foams (JPF 1 and JPF 2), soymeal polyol foams (SPF 20% and SPF 50%), and lactide polyol foams (LPF 20% and LPF 50%). A new set of foams were synthesized for aging and water absorption study. The densities of JPF 1, JPF 2, SPF 20, SPF 50, LPF 20, and LPF 50 foams were 38 kg/m^3, 34 kg/m^3, 35 kg/m^3, 32 kg/m^3, 35 kg/m^3, and 33 kg/m^3 respectively as given in Figure 4-6. The aging study was performed at ambient humidity and under two different temperatures i.e. 25°C and 70°C [107].

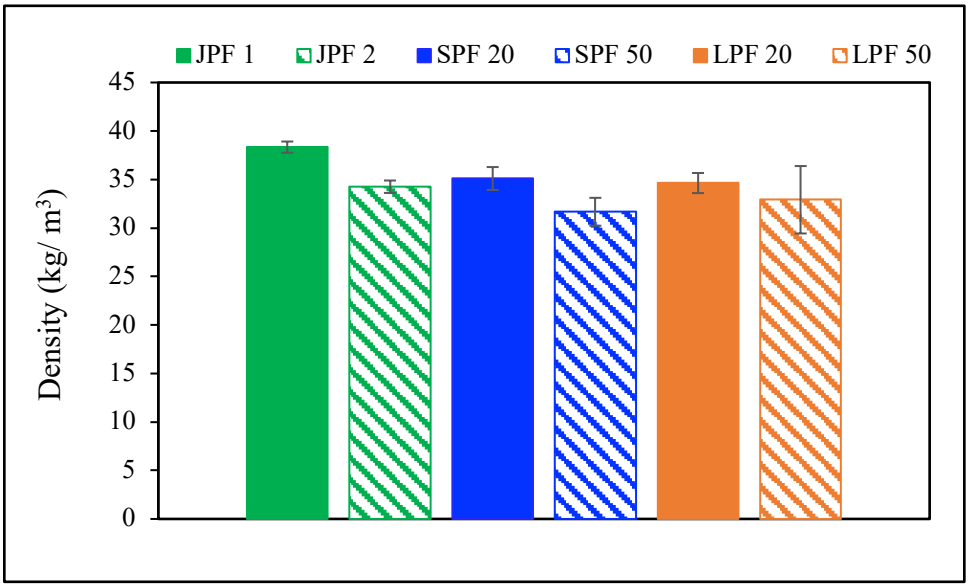


Figure 4-6: Density of control foams (JPF 1, JPF 2), soymeal polyol foams (SPF 20, SPF 50), and lactide polyol foams (LPF 20, LPF 50)

The mass loss and change in the volume of all foam samples were recorded every week. It was observed that the percent mass loss increased with an increase in time and temperature as shown in Figure 4-7 and Figure 4-8. At 25°C, all samples showed a more or less same mass loss. Samples with higher density (JPF 1, SPF 20, LPF 20) showed a higher mass loss compared to others. At

70°C, the SPF 20 and SPF 50 showed higher mass loss as compared to other foams. The mass loss for all samples at 25°C and 70°C was less than 3% over the three weeks period.

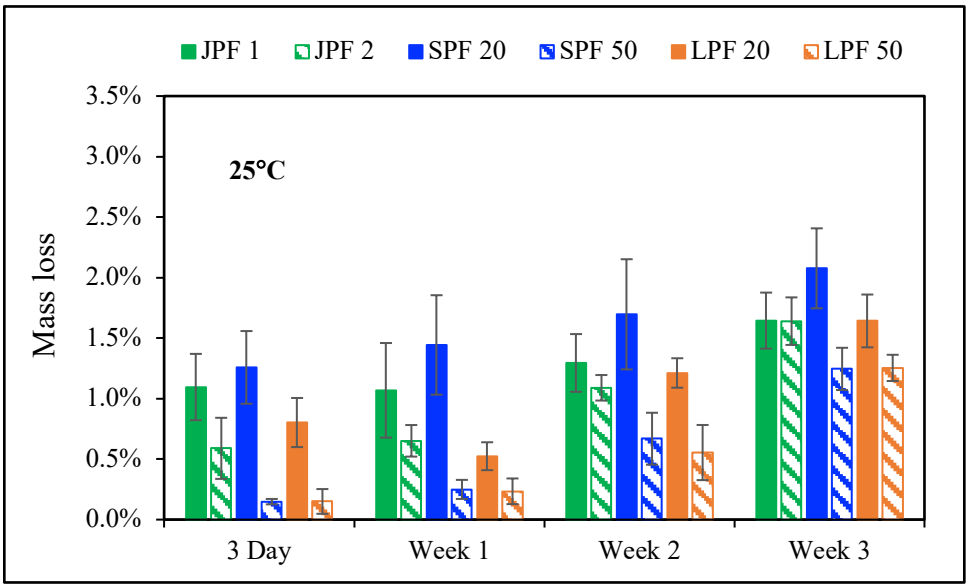


Figure 4-7: Mass loss (%) of PUF over 3 weeks at 25°C

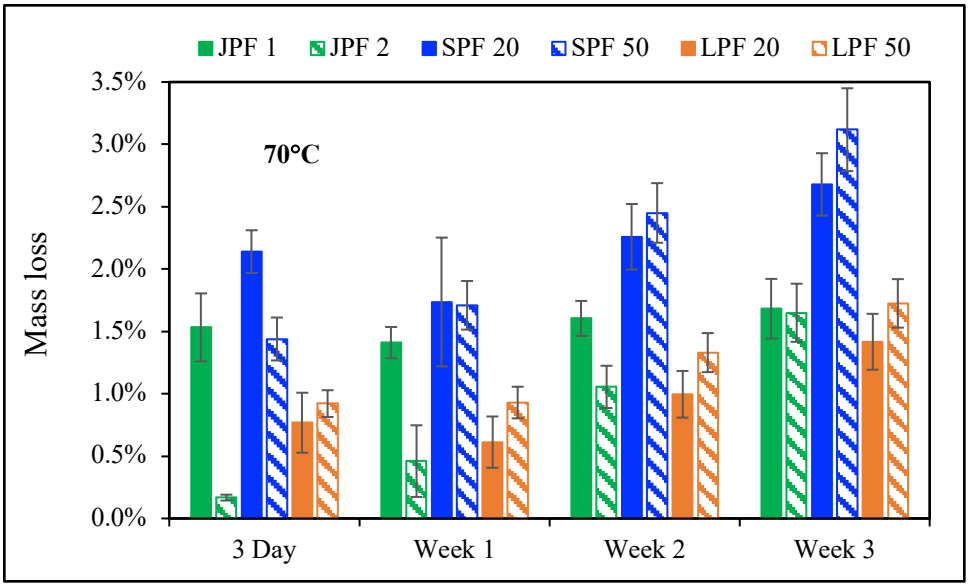


Figure 4-8: Mass loss (%) of PUF over 3 weeks at 70°C

The percent change in the volume of foam samples was recorded in order to check their dimensional stability. The volume of foam samples did not change in the first week as shown in

Figure 4-9 and Figure 4-10. The 1 - 4% change or decrease in the volume of foams after two weeks could be due to the mass loss. As no drastic change in mass or volume of foams was observed, it was concluded that the foams were dimensionally stable.

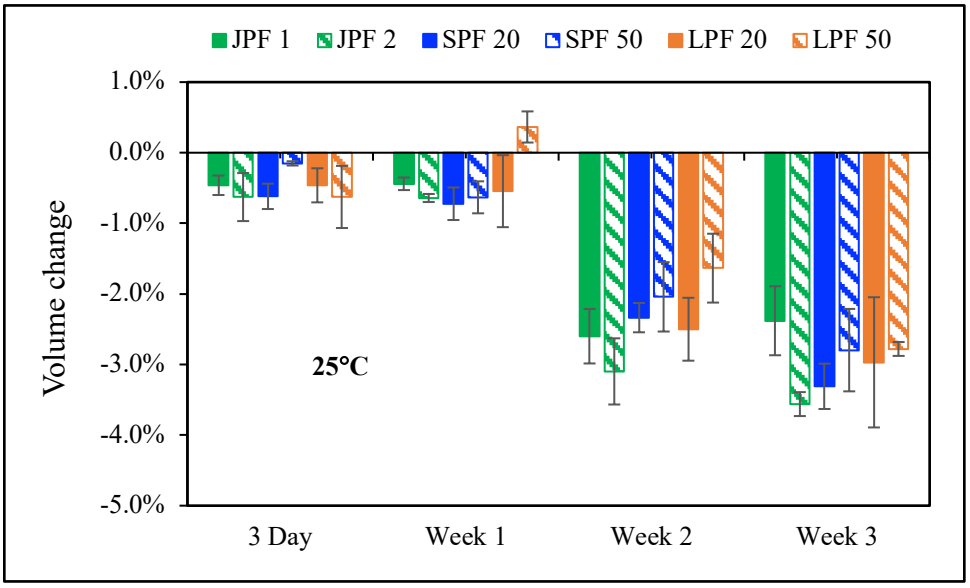


Figure 4-9: Dimensional stability of PUF over 3 weeks at 25°C

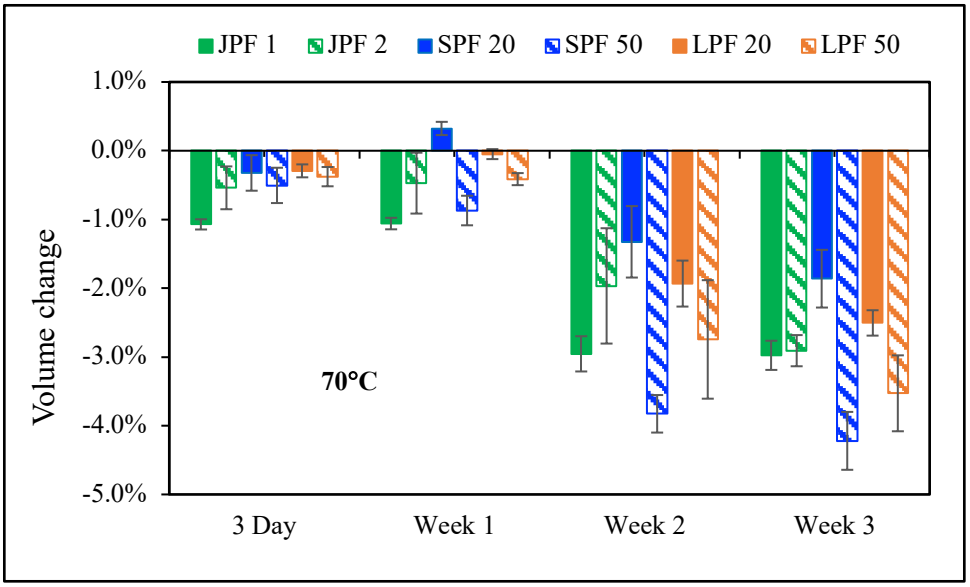


Figure 4-10: Dimensional stability of PUF over 3 weeks at 70°C

The water absorption test was performed on a similar set of samples and the results obtained are

shown in Figure 4-11. The water absorbed by the volume of a foam increased with time. Theoretically, foams with higher density will have an average smaller cell size which will limit permeation of water into the foam. Thus, the JPF 1 absorbed lesser water than JPF 2. Foams containing 20% of biobased polyol absorbed more water than foams containing 50% of biobased polyol in spite of having higher density. The water absorbed by the volume of all foams was less than 4 - 5% over a period of three weeks.

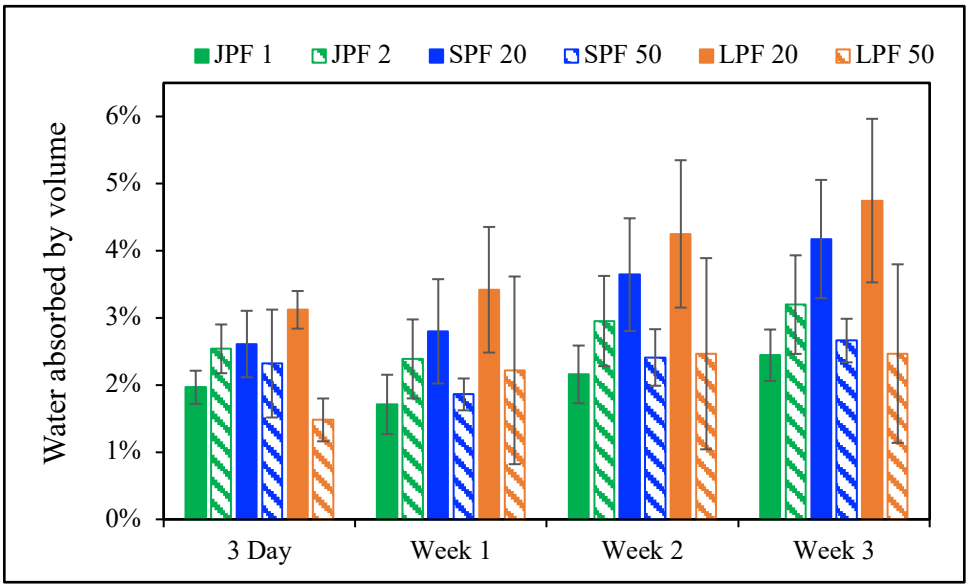


Figure 4-11: Water absorption test of PUF at room temperature

4.3.6 Comparison of biobased and petroleum-based rigid PUF

The comparison of 50% biobased and petroleum-based rigid PUF is given in Table 4-4. The compressive strength of 50% LPF is comparable with the compressive strength of control foam. Whereas, compressive strength is lower for 50% SPF as compared to the control foam. The compressive strength is directly proportional to the density of PUF. Thus, it can be increased or decreased depending on the application. The thermal conductivities of 50% biobased polyurethane foams are very close to the control foam. The aging study and water absorption study of 50% biobased PUF are comparable with that of control foam. All foams showed closed cells which is

very important for the heat insulation application. Also, lactide polyol was completely miscible with Jeffol-SG-360, and soymeal polyol was partially miscible Jeffol-SG-360 as shown in Figure 4-12. The raw material costs for these polyols were around 0.6 - 0.7 $/lb and one-pot synthesis process was used. As properties of 50% biobased PUF were comparable with properties of control foam, the use of these biobased PUF can provide the advantage of reduced carbon footprint without compromising performance or cost of PUF.

Table 4-4: Comparison of biobased and petroleum-based rigid PUF

Property	**JPF (Control)**	**50% SPF**	**50% LPF**
Density (kg/m^3)	42.4	41.0	42.4
Compressive strength (kPa)	305	205	283
Thermal conductivity at 22°C (mW/m·K)	32.41	31.95	32.51
Water absorbed by volume of foam over 2 weeks (%)	3.2	2.4	2.5
Mass loss at 70°C over two weeks (%)	1.1	2.4	1.3
Cell type (Closed/ Open)	Closed	Closed	Closed
Miscibility with Jeffol-SG-360	-	Partial	Complete

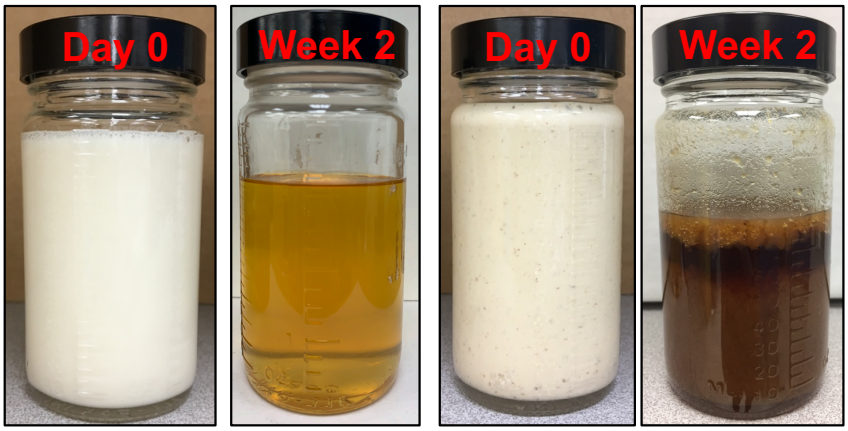


Figure 4-12: Miscibility study of lactide polyol (left, Day 0 and Week 2) and soymeal polyol (right, Day 0 and Week 2) with Jeffol-SG-360

4.4 CONCLUSION

This study mainly focuses on evaluating the performance properties of PUF synthesized from inexpensive raw material and agriculture residue. The soymeal polyol and lactide polyol contained amide linkages which are less prone to degradation by hydrolysis or UV-radiation The soymeal polyol foams (SPF) showed compressive strength slightly lower than the control foam whereas lactide polyol foam (LPF) showed compressive strength close to the control PUF. The thermal conductivity of all rigid polyurethane foams was very similar. The scanning electron microscopy images of SPF and LPF showed closed cell structure which was very important for heat insulation application. The aging study on PUF showed that change in mass and change in dimensions over a period of three weeks were negligible. Also, water absorption by PUF over a period of three weeks was less than 5%. Thus, it can be concluded that rigid PUF synthesized from biobased polyols showed properties comparable to the properties of PUF made from commercially available polyols. Also, the raw material cost of these biobased polyols was less than 0.7 $/lb which makes the commercialization of polyols viable. These polyols can be used in rigid PUF which can be used as an insulating material for applications in building & construction, electrical appliances, and automotive industries.

4.5 ACKNOWLEDGMENTS

The authors thank Zeeland Farm Services, Inc. for providing the soymeal sample. The authors acknowledge Bryan Wacker from Meter Group (formerly Decagon Devices, Inc.) for determining the thermal conductivities of foam samples. The authors also acknowledge Huntsman Corporation (Texas, USA), Air Products and Chemicals, Inc. (Pennsylvania, USA), and Momentive Performance Materials (New York, USA) for providing materials for foam formulations.

5 BIOBASED FLEXIBLE POLYURETHANE FOAMS FOR AUTOMOTIVE APPLICATIONS

5.1 INTRODUCTION

Polyurethane is a most versatile polymeric material used in coatings, adhesive, sealants, elastomers, and foams. Rigid and flexible polyurethane foam being the major market of polyurethanes [27]. The rigid polyurethane foams are widely used in insulating materials (refrigerator, panels for wall and roof), automotive components (door panel, interior body), and construction material. Whereas flexible polyurethane foams are used as a packaging material, cushioning material (mattresses and furniture in a home, car seats in automotive), and sometimes in insulating material. The global market for polyurethane is continuously growing. Polyurethane foam market was valued at 50 billion dollars in 2017 and is expected to increase in the near future [114]. Polyol and isocyanate are two major components present in polyurethane foams. Conventionally, polyol and isocyanate were synthesized from crude oil or petroleum products. But in recent years biobased aliphatic isocyanates, as well as biobased polyols, were commercially used in polyurethane synthesis [11, 115, 116]. Currently, most of the commercially available biobased polyols are synthesized by epoxidation of soybean oil followed by ring-opening [11] e.g. BiOH® and Agrol® from Cargill, SOVERMOL® from BASF [11]. Several other routes such as hydroformylation, ozonolysis, transesterification were also used for polyol synthesis from soybean oil [39]. Apart from soybean oil other triglycerides such as castor oil [39], palm oil [117], rapeseed oil [118], sunflower oil, and linseed oil [119] were also used for biobased polyol and polyurethane foam synthesis. Nowadays, new biobased sources such as cashew nutshell liquid [42] and lignin [120] are being used for biobased polyol synthesis.

The vegetable oils have a triglyceride structure which can be converted to fatty acids and fatty acid

methyl esters by hydrolysis and transesterification with water and alcohol, respectively [39]. The unsaturated fatty acids (oleic acid, linoleic acid, linolenic acid) or fatty acid methyl esters contain double bonds which can be modified to obtain polyols or other derivatives [11]. The dimerization of a conjugated linoleic acid with another linoleic acid by a Diels-Alder reaction produces a cyclohexane adduct [11]. The oleic acid can also be dimerized by using a clay catalyst through protonation of the double bond which attacks the double bond present on another molecule [11]. These dimerized products of fatty acids are called as "dimer acids". Several companies like Croda and Oleon produces different grades of dimer acids from soybean oil. These dimer acids contain long carbon chains. The incorporation of dimer acids in a polymer will provide value addition of increased flexibility and renewable carbon content.

In previous literature, a few studies have been reported on the use of dimer acids in thermoplastic synthesis [116], polyester polyol, and polyurethane foam synthesis [121]. In our previous work, polyols were synthesized from polycondensation of dimer acids and biobased diols. The use of different diols and molar ratios (dimer acid: diol) produced a series of biobased polyols with varying hydroxyl value from about 35 to about 100 mg of KOH/g suitable for their application in polyurethane foams.

In this study, a series of biobased polyols produced from dimer acids will be used in flexible polyurethane foam synthesis. As flexible polyurethane foams have application in automotive and cushioning, the properties of produced flexible PUF will be tested accordingly. The polyurethane foams will be produced with the increasing concentration of biobased polyol with maximum biobased polyol content up to 50%. The effect of different catalysts concentration on PUF, and optimization of catalysts concentration for biobased PUF will be discussed. The mechanical properties, thermal properties, and morphology of biobased PUF will be compared with the PUF

made from commercial petroleum-based polyol and commercial biobased polyol. The miscibility of biobased and petroleum-based polyol will also be evaluated. The effect of different hydroxyl value on characteristic times and properties of foams will be discussed.

5.2 EXPERIMENTAL

5.2.1 Materials and chemicals

Flexible polyurethane foams were synthesized using six different biobased polyols. The properties were compared with commercially available petroleum-based polyol. The isocyanate (Rubinate 7304) was kindly provided by Huntsman Corporation (Texas, USA). It is a mixture of monomeric and polymeric methylene diphenyl diisocyanate (MDI). The commercial petroleum-based polyether polyol Voranol™ 4701 was supplied by The Dow Chemical Company (Michigan, USA). Agrol Prime™ A-56 was supplied by Biobased Technologies® LLC (Arkansas, USA). It is a commercial soybean oil-based polyol. The Cargill Incorporated acquired Biobased Technologies in 2017 and renamed the polyol as BiOH® 7050. All other polyols DAMLPEG-7-94, DAMLPEG-7-47, DAPEG-94, DAPEG-33, and DAMLPEG-3-80 were synthesized from dimer acid using polycondensation chemistry. DAMLPEG polyols having primary as well as secondary hydroxyl groups were obtained by reacting dimer acid with diols derived from meso-lactide (MLPEG-3 or MLPEG-7). DAPEG polyols having primary hydroxyl group were obtained by reacting dimer acid with polyethylene glycol (PEG-400). The properties of all polyols are given in Table 5-1.

A silicone-based surfactant, Tegostab B4690 was supplied by Evonik (Virginia, USA). A cell-opener, Lumulse POE (26) GLYC was supplied by Lambent Corporation (Illinois, USA). The Niax-A1 (70% bis(2-dimethylaminoethyl) ether, $C_8H_{20}N_2O$ and 30% dipropylene glycol, $C_6H_{14}O_3$) and Niax A300 were received from Momentive Performance Materials (New York, USA). A crosslinking agent, diethanolamine was purchased from Sigma-Aldrich (Wisconsin,

USA).

Table 5-1: Physical properties of polyols

Compound	Hydroxyl Value (mg of KOH/g)	Acid Value (mg of KOH/g)	MW* (g/mol)	Functionality	Viscosity @ 25ºC (cPs)	Renewable Carbon Content (%)
Voranol 4701	34	-	4950	3	888	-
Agrol Prime-A-56	56	< 2	2000	2	5090	75
DAMLPEG-7-94	94 $\pm$ 9	1 $\pm$ 0	1194	~2	2980	57
DAMLPEG-7-47	47 $\pm$ 4	3 $\pm$ 0	2387	~2	5850	70
DAPEG-94	94 $\pm$ 5	2 $\pm$ 0	1194	~2	1022	50
DAPEG-33	33 $\pm$ 3	1 $\pm$ 0	3400	~2	7130	67
DAMLPEG-3-80	80 $\pm$ 5	2 $\pm$ 0	1400	~2	1968	57

*molecular weight calculated based on functionality

5.2.2 Free rise study of PUF

The free rise study of PUF was performed as per ASTM standard D7487-13. The side B (60 grams) which contains polyols, crosslinking catalyst (diethanolamine), silicone surfactant (Tegostab B4690), blowing catalyst (Niax A-1 and Niax A300), cell opener (Lumulse POE (26) GLYC), and blowing agent (water) in the proportion given in Table 5-2. Rubinate 7304 isocyanate was side A (26-30 grams). The parts of Rubinate 7304 for all formulations were calculated using isocyanate index 100. All formulations are given in Table 5-2.

For free rise study, side B was homogeneously mixed using a laboratory hand-mixer at high rpm for a few minutes and side A was added. The mixture was thoroughly blended for a few seconds (mix time). The characteristic times (cream, top of the cup, string gel, rise, and tack free) for each PUF were recorded.

Table 5-2: Formulation used for flexible polyurethane foams

Material	Biobased Polyol Content					
	0%	10%	20%	30%	40%	50%
Side B (parts)						
Voranol 4701	100	90	80	70	60	50
Biobased Polyol	0	10	20	30	40	50
Lumulse POE (26) GLYC	1.20	1.20	1.20	1.20	1.20	1.20
Tegostab B4690	0.70	0.70	0.70	0.70	0.70	0.70
Diethanolamine	1.50	1.50	1.50	1.50	1.50	1.50
Niax A-300	0.60	0.60	0.60	0.60	0.60	0.60
Niax A-1	0.40	0.40	0.40	0.40	0.40	0.40
Water	2.80	2.80	2.80	2.80	2.80	2.80
Side A- Rubinate 7304 (parts)						
DAMLPEG-7-94	51	52	54	55	56	58
DAMLPEG-7-47	51	51	51	52	52	52
DAPEG-94	51	52	54	55	56	58
DAPEG-33	51	51	51	51	51	51
DAMLPEG-3-80	51	52	53	54	55	56
Agrol Prime A-56	51	52	52	53	53	54
ISO Index	100	100	100	100	100	100

5.2.3 Box foam and its characterization

A mold of dimensions 30 cm X 30 cm X 6 cm was used to make a box foam. A mold release Chem-Trend PU-11331 was applied inside the mold which was maintained at 65°C. Meanwhile, all ingredients of side B was measured in the proportion mentioned earlier and mixed for 2 - 3 minutes. Side A was added to side B and mixed for 12 s. The mixture was immediately poured inside the mold and the lid was closed. After 6 min, the foam was removed from the box and kept in an oven at 65°C for 30 minutes. After seven days of foam manufacturing, the foam was cut to measure its properties. The outer skin of the box foam was removed by cutting 1 cm from all sides using a band saw. The foam was cut into small blocks 25 mm X 50 mm X 50 mm for wet

compression set, compression, and apparent density testing. A foam sheet of thickness 10 mm and 12.5 mm was used for die-cutting tear and tensile samples respectively. A USM Hytronic Model B press was used to die cut tear and tensile samples.

ASTM 3574-08 (Test A) was used for apparent density, ASTM 3574-08 (Test L) was used for wet compression set, ASTM 3574-08 (Test C) was used for compression force deflection, ASTM 3574-08 (Test E) was used for tensile testing, and ASTM D 624 (Die C) was used for tear strength. An Instron model 5565 with a 500 N load cell was used to measure mechanical properties of the foam. The compressive strength of foams was tested in the direction perpendicular to the rise direction of foam with a speed of 50 mm/min. The tensile and tear samples were testing in the direction perpendicular to the rise direction of foam with a speed of 500 mm/min.

Cell morphologies of all foams were studied in perpendicular to the rise direction of foam using a JEOL 6610LV (tungsten hairpin emitter) Scanning Electron Microscope (JEOL Ltd., Tokyo, Japan). The polyurethane sample was immersed in liquid nitrogen for a minute and a thin section was cut using a double-edged razor blade. The samples were mounted on aluminum stubs using high vacuum carbon tabs (SPI Supplies, Pennsylvania, USA). Samples were coated with gold (~30 nm thickness) in an Emscope Sputter Coater model SC 500 (Ashford, Kent, England) purged with argon gas.

Degradation temperature of samples was obtained by thermogravimetric analysis (TGA). TGA measurements were conducted under nitrogen flow unless and until specified using a TGA Q50 (TA Instruments, Delaware, USA). In this analysis, a sample (10 - 15 mg) was taken in an aluminum pan and heated up to 550 - 600°C at the rate of 10°C /min. The weight loss (%) of a sample as a function of temperature (°C) was obtained from this analysis. The derivative thermogram (%/°C) was used to identify degradation temperatures. The PUF formulation for 50%

biobased polyol content given in Table 5-2 was used for miscibility study. In a plastic cup, all contents of side B was mixed for 3 - 4 minutes and poured into a glass jar. The pictures were taken on the same day, next day, and after two weeks to study miscibility.

5.3 RESULT AND DISCUSSION

For flexible polyurethane foam synthesis, the acid value of polyols should be lower than 2 - 3 mg of KOH/g, as polyol with higher acid value produces foam with dark yellow color and irregular internal structure. Thus, the biobased polyols with an acid value less than 2 mg of KOH/g were used for making flexible polyurethane foams. The formulation given in Table 5-2 was optimized by changing catalysts concentration one at a time for a foam containing 30% biobased polyol. If strings were observed on the edges of a foam (Figure 5-1 a), it was probably due to the high concentration of crosslinking agent which was reduced for the next formulation. Increase in the surfactant concentration helped to reduce uneven cell size distribution of a foam (shown in Figure 5-1 (b)) and produced a foam with uniform cellular structure (Figure 5-1 c). It was also observed that increasing cell opener concentration, increased the resiliency of foam along with the uniform cell distribution (Figure 5-1 d).

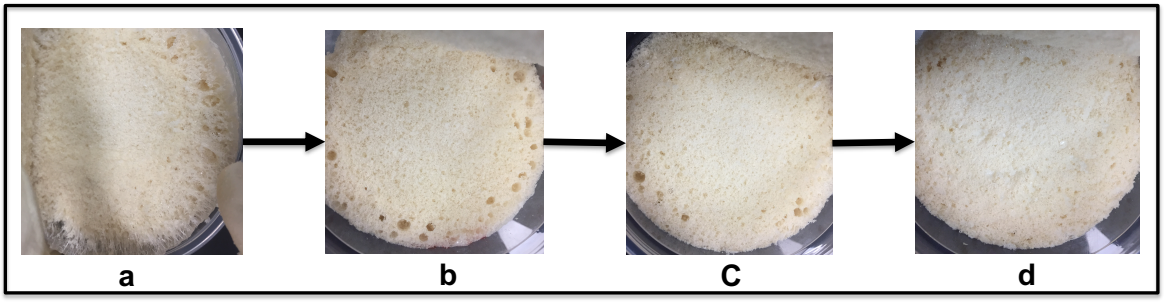


Figure 5-1: Effect of change in concentration of different catalysts on flexible foams

Another issue with the flexible polyurethane foam is shrinkage. The flexible polyurethane foams mostly have open cells. The isocyanate-water reaction generates heat and carbon dioxide gas. When the foam starts cooling, the carbon dioxide gas inside foam cells starts contracting [122].

The gas inside the open cells gets replaced by the surrounding air and hence foams containing open cells are stable. Whereas, the gas trapped inside the unopened cells can't get replaced by the surrounding air due to closed cell structure. Thus, if the foam has a lot of unopened cells, it collapses after a few minutes as shown in Figure 5-2 (right side). The foam synthesized using exactly the same formulation does not collapse if it is mechanically crushed after 15 - 20 minutes of foam manufacturing as shown in Figure 5-2 (left side). The mechanical crushing opens up closed cells and avoids further shrinking of a foam. Thus, a slight mechanical force was applied to each box foam to avoid its shrinking which is a common industrial practice.



Figure 5-2: Effect of unopened cells on flexible foams

5.3.1 Free rise study of PUF

All PUF formulations for biobased polyols are given in Table 5-2. The mix time, cream time, top of the cup time, string gel time, rise time, and tack free time for each formulation was measured. The mix time represents mixing of polyol (side B) and isocyanate (side A) components. At cream time, the viscosity of polyol-isocyanate mixture increases and foam starts rising. At top of the cup time, the foam reaches the top of the cup. At string gel time, polyurethane network starts building. At rise time, the foam stops rising. At tack free time, the foam is no longer sticky. The mix time and cream time for all formulations were 12 s and 15 - 18 s respectively. The difference was observed in top of the cup time, string gel time, and rise time. The tack free time for all PUF was

higher than 3 - 4 minutes. These characteristic times are given in Table 5-3.

Table 5-3: Characteristic time (top of the cup, string gel time, rise time) for all free rise profiles

Polyol	**Top of the cup time(s) String gel time (s) Rise time (s)**				
	0%	**10%**	**20%**	**30%**	**40%**
DAMLPEG-7-94	34 45 73	34 43 73	33 44 71	35 46 78	36 48 85
DAMLPEG-7-47	33 39 66	30 39 66	39 48 78	40 48 80	40 49 85
DAPEG-94	35 45 73	43 60 100	60 80 152	67 88 183	77 110 202
DAPEG-38	32 41 76	30 41 78	33 41 80	38 48 84	38 49 84
DAMLPEG-3-80	30 36 61	27 35 59	37 48 64	34 50 88	38 55 102
Agrol Prime A-56	34 45 70	34 45 72	33 45 71	35 47 74	34 47 75

The characteristic times increases slightly with increasing biobased polyol content. The increase in the characteristic time for the rest of the formulations could be due to the higher hydroxyl value of biobased polyol compared to the control polyol. Thus, with an increase in biobased polyol content, the amount of isocyanate required for foam also increased. As the same amount of catalyst was added to all formulations, its concentration (amount per polyol-isocyanate reaction) decreased with an increase in the hydroxyl value. Thus, the increase in characteristic times with an increase in the biobased content could be due to the decrease in the reaction rate of polyol-isocyanate reaction.

5.3.2 Thermogravimetric analysis of PUF

The thermogravimetric analysis (TGA) graphs of PUF containing 20% of biobased polyol content are shown in Figure 5-3, and 40% of biobased polyol content are shown in Figure 5-4. In the TGA graphs of the foams, three degradation stages were observed i.e. stage I (75°C - 300°C), stage II (250°C - 350°C), and stage III (>350°C).

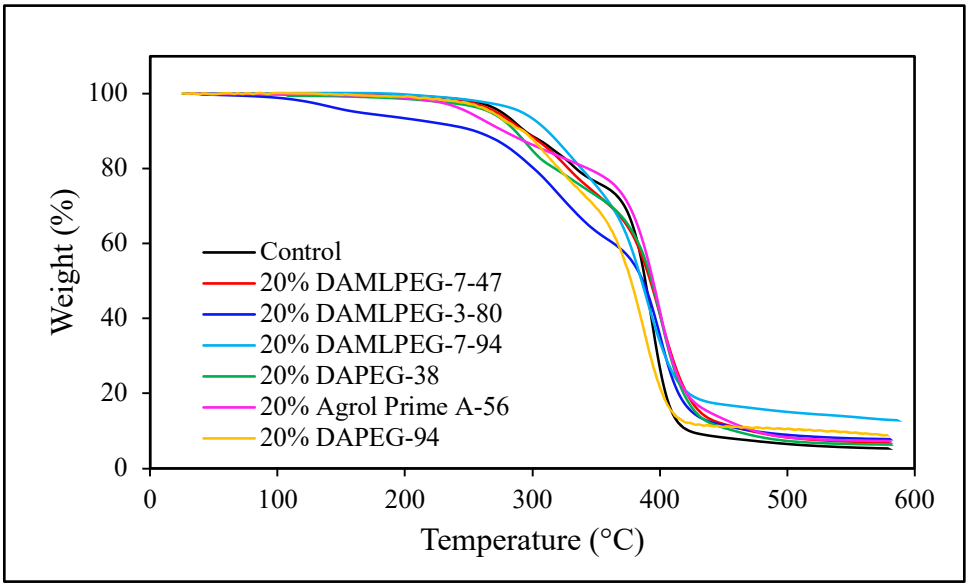


Figure 5-3: TGA graphs of flexible PUF containing 20% of biobased polyol

The first stage corresponds to the degradation of less stable groups such as biuret or urethane [44]. The second stage corresponds to the degradation of soft segments of the polyol chain, and the third stage corresponds to the further degradation of fragments produced in the second stage [78, 79]. The temperatures for 5% and 10% mass loss increased with increasing biobased polyol content, except for Agrol Prime A-56 and DAMLPEG-3-80 polyols as given in Table 5-4. The increase in temperatures indicates the presence of more stable groups on polyol side. The temperatures for 50% mass loss increased with increasing biobased polyol content. This could be due to the presence of long carbon chains and ester linkages in biobased polyols.

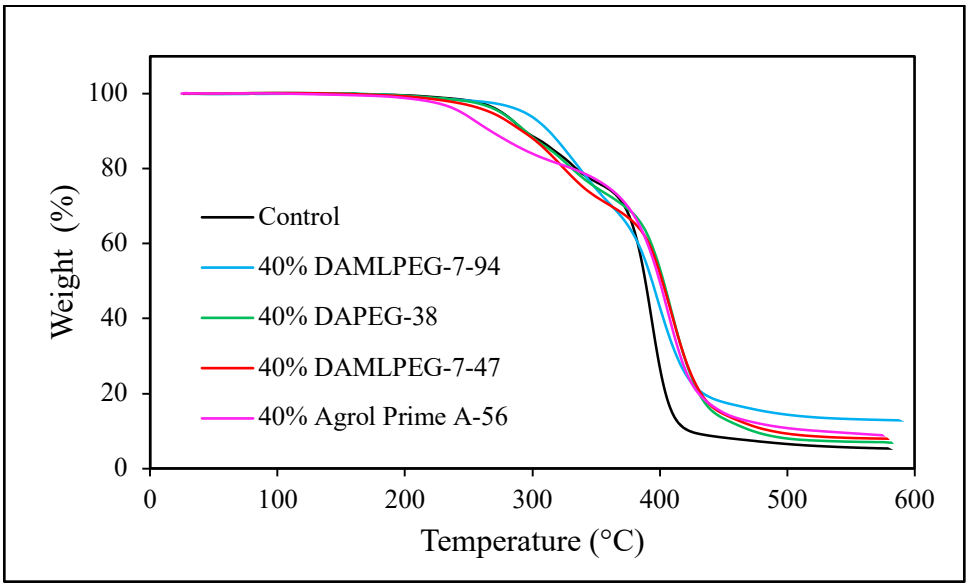


Figure 5-4: TGA graphs of flexible PUF containing 40% of biobased polyol

Table 5-4: Temperatures for 5%, 10%, and 50% mass loss, and residual weight of PUF

Polyol	Biobased Polyol Content (%)	5% Mass Loss (°C)	10% Mass Loss (°C)	50%Mass Loss (°C)	Residual Mass (%)
DAMLPEG-3-80	0	276	294	388	5
	20	164	255	386	8
DAMLPEG-7-94	0	283	305	374	13
	20	293	314	387	12
	40	296	315	396	13
DAPEG-94	0	266	285	369	6
	20	265	288	379	6
DAPEG-38	0	276	294	388	5
	20	267	286	394	6
	40	275	294	402	7
DAMLPEG-7-47	0	276	294	388	5
	20	272	293	392	7
	40	267	292	401	8
Agrol Prime A-56	0	265	283	367	8
	20	249	276	395	7
	40	244	266	401	7

5.3.3 Density of PUF

The density of flexible PUF used in car cushions and backs is in the range of 20 - 95 kg/m^3 to maintain a certain amount of strength for commercial applications [123]. The density of foam depends on the amount of CO_2 produced, which further depends on the amount of water added. Also, properties of foam are strongly dependent on its density. Hence, foam densities should be similar to compare their properties. The densities of biobased polyurethane foams are shown in Figure 5-5.

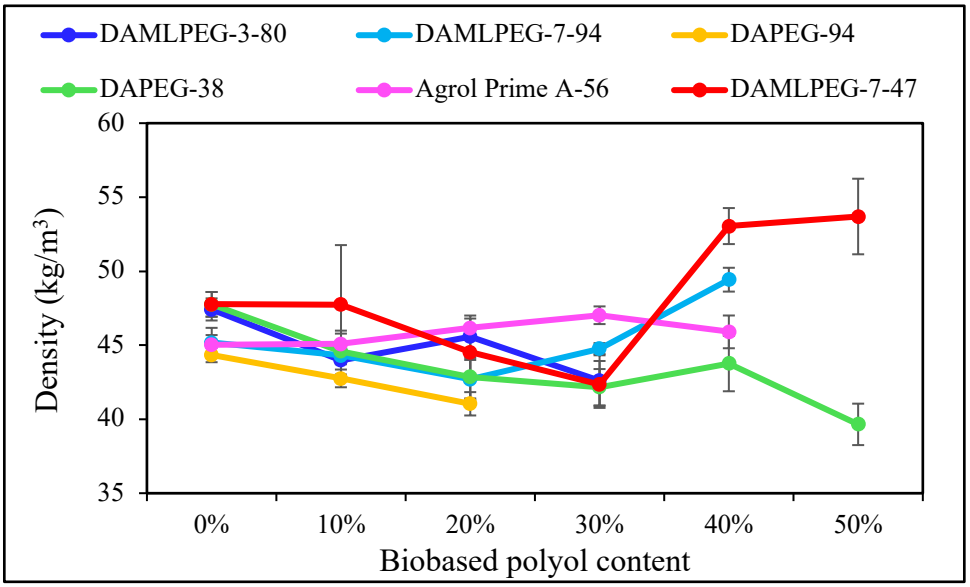


Figure 5-5: Densities of flexible polyurethane foams

The density of a foam containing biobased polyol (except for Agrol Prime A-56) decreased slightly with an increase in the biobased content. A significant decrease in the density of foams containing 20% and 30% of DAMLPEG-7-47 and DAPEG-38 polyol was observed which might have an effect on the mechanical properties of foams. Whereas the density of foams containing 40% or more of DAMLPEG-7-47 and DAMLPEG-7-94 polyol increased significantly. It is very difficult to control the density of molded polyurethane foams as it completely depends on the amount of material poured inside the mold.

5.3.4 Scanning Electron Microscopy (SEM) images of PUF

The scanning electron microscopy images of 0%, 20%, and 40% biobased flexible PUF are shown in Figure 5-6, Figure 5-7, and Figure 5-8. These images were taken perpendicular to the rise direction of foam. The SEM images of all PUF showed a majority of open-cell structure. A very few cells showed closed-cell window. The cell size of 40% DAMLPEG-7-94 foam was comparatively smaller than the cell size of 0% DAMLPEG-7-94 foam as given in Table 5-5. With the addition of Agrol Prime-A-56, the cell size slightly decreased for 40% foam. It can be seen that 0% and 20% of DAMLPEG-7-94 foams and Agrol Prime A-56 foams have a lot more closed windows of cells as compared to their 40% formulation. These results were also observed with 40% DAMLPEG-7-47 and DAPEG-38 foams.

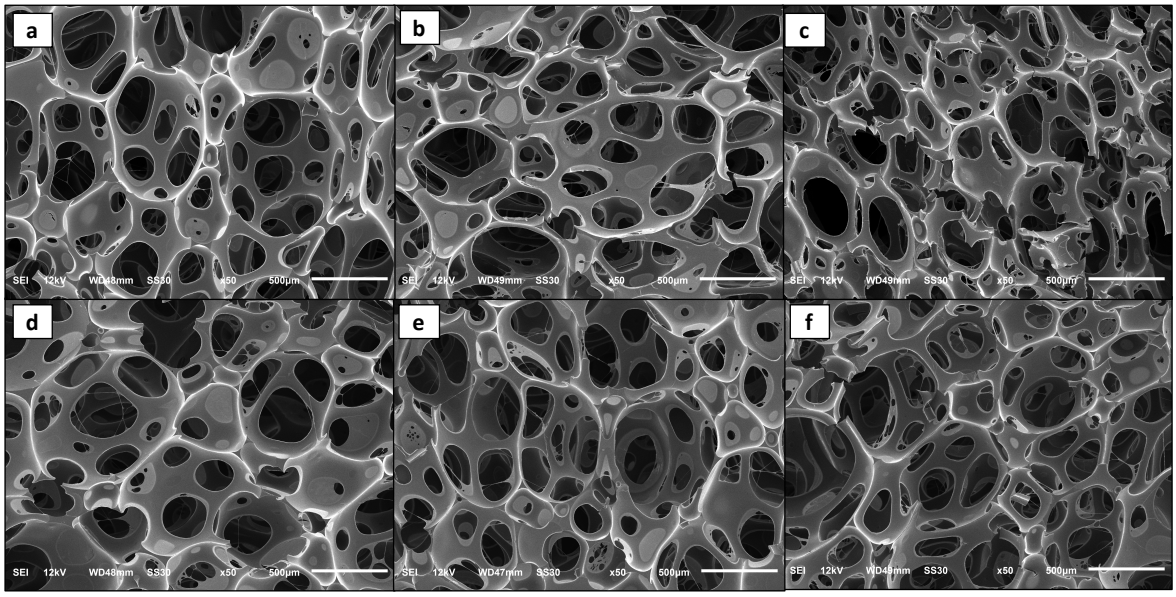


Figure 5-6: SEM images of (a) 0% (b) 20% (c) 40% of DAMLPEG-7-94, (d) 0% (e) 20% (f) 40% of Agrol Prime A-56

The cell size did not change much with the addition of DAPEG-38 and DAMLPEG-7-47 polyols as given in Table 5-5. The PUF made from DAPEG-94 and DAMLPEG-3-80 showed open cell structure as shown in Figure 5-8. The foams containing 40% DAPEG-94 and DAMLPEG-3-80

polyols were not possible to manufacture as these foams collapsed after making them. This could be due to the high percentage of closed cells compared to open cells. But the 20% DAPEG-94 and 20% DAMLPEG-3-80 foams did not collapse or shrink.

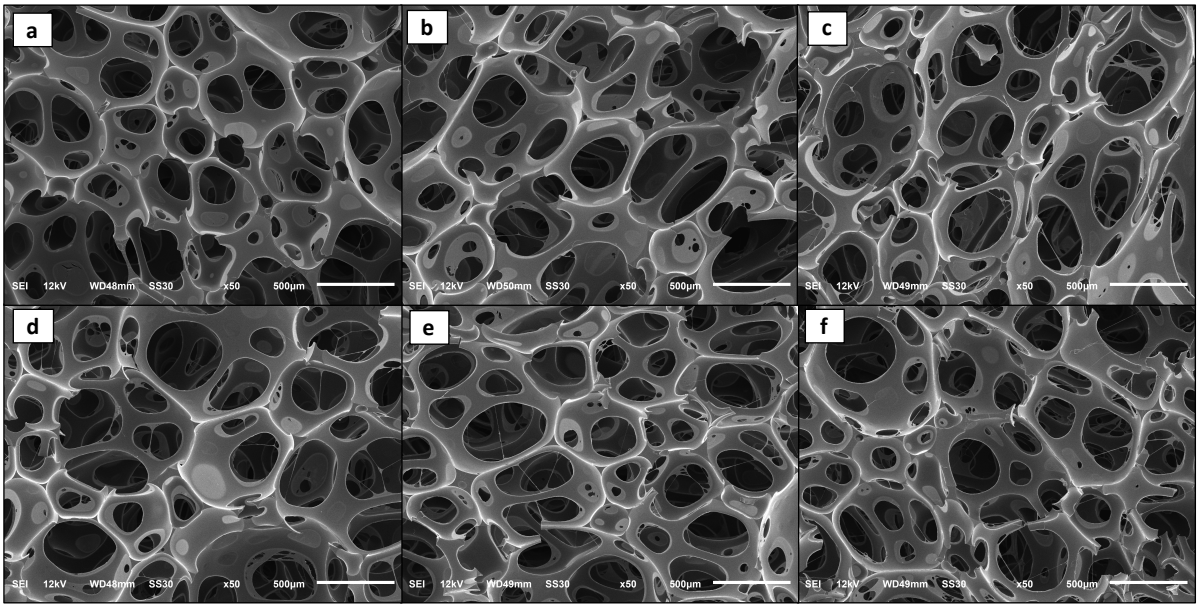


Figure 5-7: SEM images of (a) 0% (b) 20% (c) 40% of DAPEG-38, (d) 0% (e) 20% (f) 40% of DAMLPEG-7-47

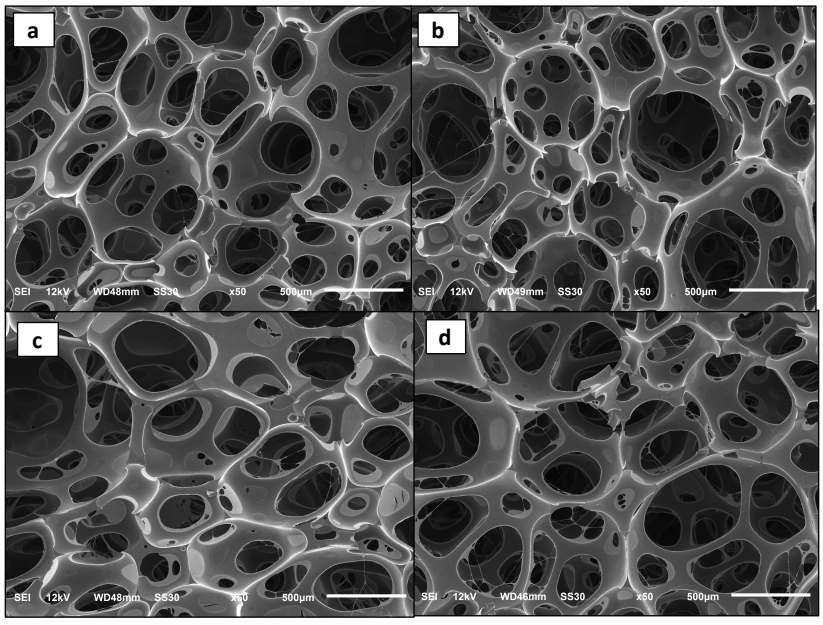


Figure 5-8: SEM images of (a) 0% (b) 20% of DAPEG-94, (c) 0% (d) 20% of DAMLPEG-3-80

Table 5-5: Cell size of biobased PUF

Polyol	Polyol Content (%)	Cell size (μm)	Polyol	Polyol Content (%)	Cell size (μm)
DAMLPEG-7-94	0	672 ± 71	Agrol Prime A-56	0	646 ± 93
	20	596 ± 50		20	654 ± 65
	40	496 ± 40		40	575 ± 49
DAMLPEG-7-47	0	626 ± 79	DAPEG-38	0	617 ± 80
	20	625 ± 75		20	619 ± 54
	40	656 ± 49		40	584 ± 62
DAMLPEG-3-80	0	588 ± 85	DAPEG-94	0	623 ± 49
	20	604 ± 88		20	596 ± 69

5.3.5 Wet compression set of PUF

For automotive applications, such as seat cushioning, armrest, headrest the compression set is very important. Compression set measures the ability of the foam to recover after being exposed to heat and compressive stress. In previous literature, the compression set was measured by compressing a foam to 50% of its original height and heating it in an oven at 70°C [124]. The compression set values were less than 10 - 15% [124] for foams containing 40% biobased polyol content. As some of the applications where foams are exposed to high temperature along with the humidity, just compression set values based on dry heat aging were not adequate. Thus, the wet compression set was performed on flexible PUF samples instead of compression set. The foams were compressed between two parallel plates with 50% of the deflection and kept in a chamber maintained at 50°C and 95% humidity. After 22 hours, the compressive stress on the foams was removed and final height was measured after 2 hours. The wet compression set represents the ability of the foam to go back to its original shape after being exposed to the wet heat aging. Lower values of wet compression set indicate a better probability of foams going back to the original shape. For general applications of flexible PUF in automotive, this value should be less than 40%. The wet

compression set values for biobased polyurethane foams are given in Figure 5-9. The wet compression set increased above 40% for the foams containing 20% of DAMLPEG-7-94 and DAPEG-94 polyol, and 30% of DAMLPEG-3-80 polyol.

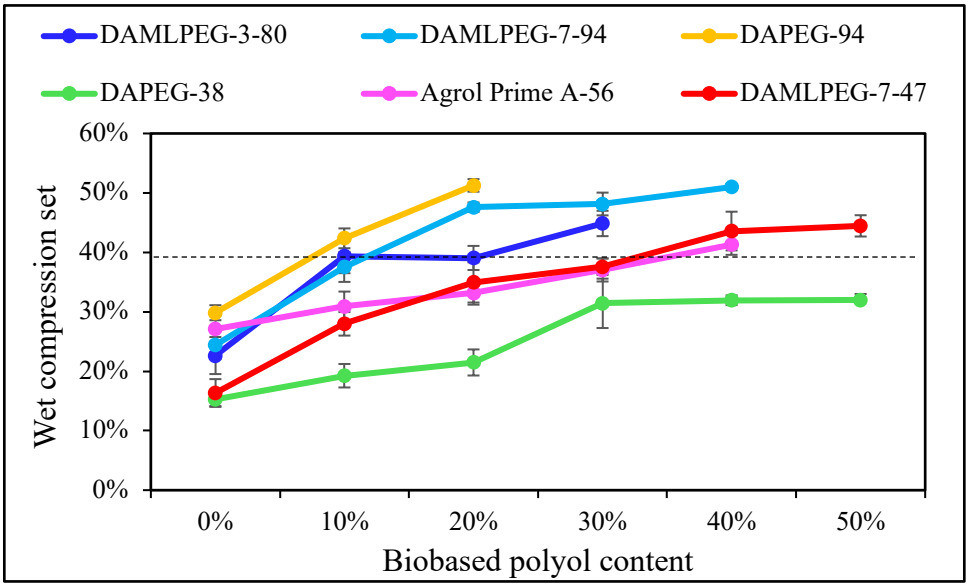


Figure 5-9: Wet compression set values of biobased PUF

The initial assumption for higher compression set values for these foams was the presence of ester linkages in the polyol which are susceptible to the moisture absorption. But the wet compression set for foams containing 30% of DAMLPEG-7-47 and Agrol Prime A-56 polyols, and 40% of DAPEG-38 polyol was lower than 40%. This indicates that the increase in the wet compression set could be due to the higher hydroxyl value of a polyol, and not because of the presence of ester groups. Increase in the hydroxyl value increases the number of urethane linkages which increases the rigidity and reduces the resiliency of a foam. Thus, the foam containing 50% of a biobased polyol having a hydroxyl value of 38 mg of KOH/g has wet compression set around 32%.

5.3.6 Tensile properties of PUF

The tensile properties of foam were measured to compare the strength of foam under tension. The tensile stress at maximum load (kPa), Young's modulus (kPa), and elongation at maximum load

(mm) were measured for all samples. The tensile strength for all biobased PUF slightly increased with increasing biobased polyol content as shown in Figure 5-10. But the tensile strength for foams containing 20% and 30% of DAPEG-38 polyol decreased significantly compared to the control foam. This could be due to the lower density values of 20 - 30% biobased PUF (42 - 43 kg/m^3) compared to the control foam (48 kg/m^3). The tensile strength of DAMLPEG-7-47 and DAMLPEG-7-94 remains constant with increasing biobased polyol content. As PUF containing 20 - 30% DAMLPEG-7-47 have lower densities, the tensile strength of these PUF was comparatively better than control the PUF.

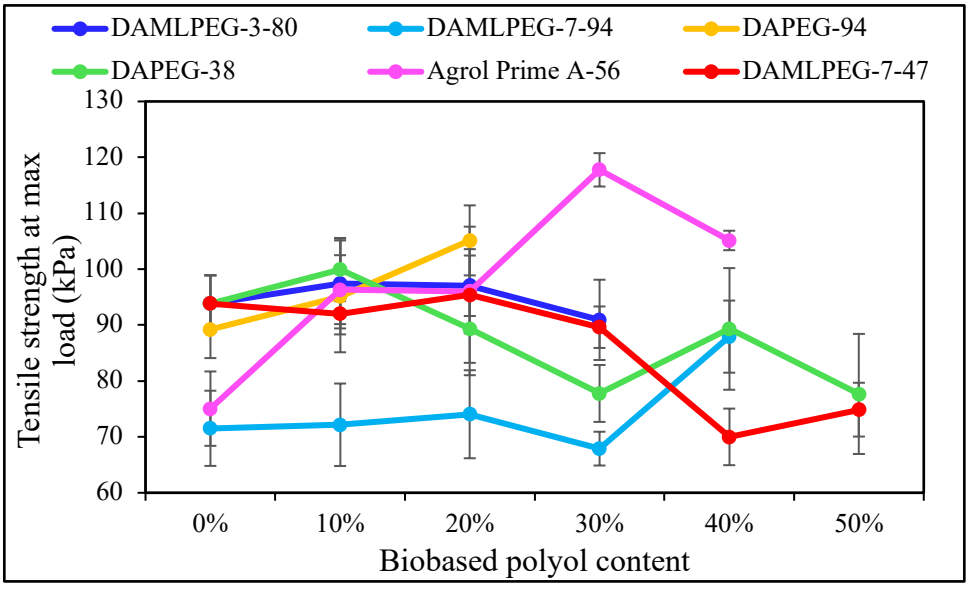


Figure 5-10: Tensile strength at maximum load of biobased PUF

The minimum tensile strength for headrest application is 90 kPa and for seat cushion application is 130 kPa [124] for a foam having 45 kg/m^3 density. Thus, the current biobased formulation is suitable for headrest application. However, the tensile strength of foams strongly depends on the cross-linking density and it increases with an increase in the isocyanate index [118]. Thus, it is possible to increase the tensile strength by increasing the isocyanate index. The Young's modulus measures the resistance of a material to elastic deformation under tension or load. The higher

Young's modulus value indicates higher stress is required to stretch the material compared to the stress required to stretch a material having lower Young's modulus to the same extent. The Young's modulus was measured in the region of 0 - 10 mm extension and shown in Figure 5-11 for biobased PUF. The Young's modulus for foams containing DAMLPEG-7-47, DAMLPEG-3-80, DAPEG-94, and Agrol Prime A-56 polyols increases with increasing polyol content up to 30%. However, Young's modulus slightly increased for the foam containing 40% of DAPEG-38, and slightly decreased for 10 - 30% of DAMLPEG-7-94 foams.

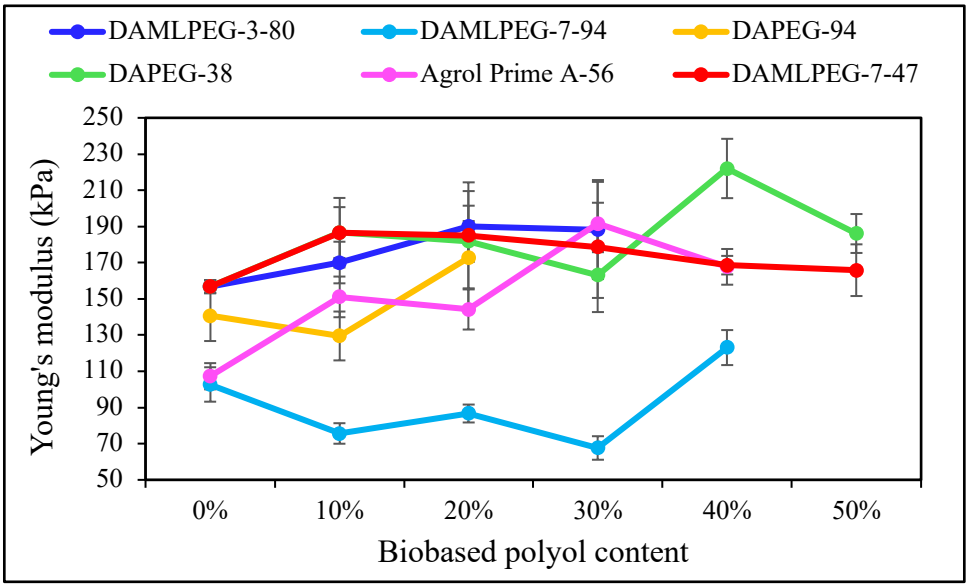


Figure 5-11: Young's modulus of biobased PUF

The elongation at maximum load is shown in Figure 5-12 for all samples. It was observed that elongation at maximum load increases with increasing DAMLPEG-7-47, DAMLPEG-3-80, DAMLPEG-7-94, DAPEG-94, and Agrol Prime A-56 polyol content in PUF. It was observed that elongation at maximum load does not change with addition of DAPEG-38 polyol. The minimum elongation required for headrest application is 80 mm and for seat cushion application is 105 mm [124] for a foam having 45 kg/m^3 density. Thus, all biobased PUF can be used for headrest application. Some of the PUF containing 20 - 40% of biobased polyol can be used for seat cushion

application.

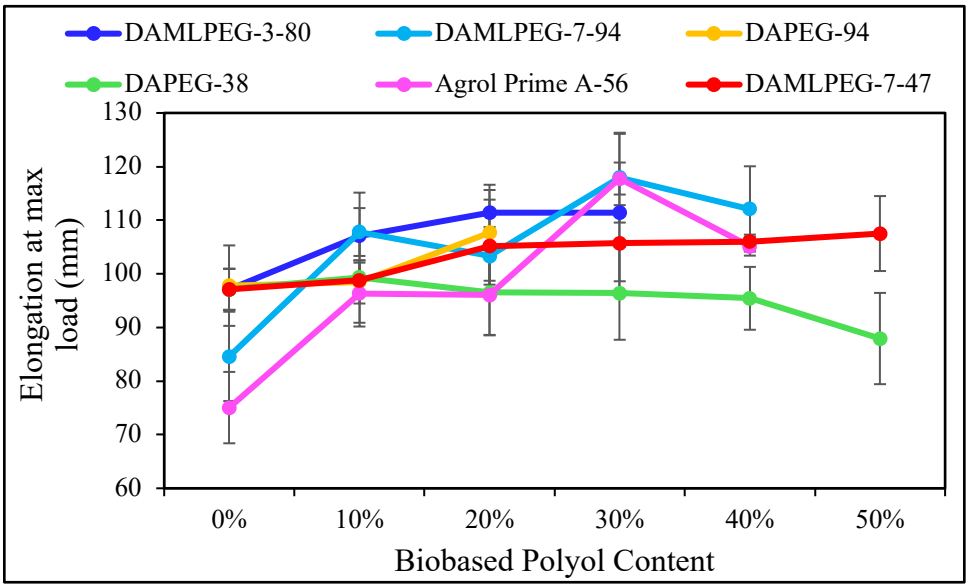


Figure 5-12: Elongation at maximum load of biobased PUF

5.3.7 Tear resistance of PUF

The tear resistance values of biobased PUF are shown in Figure 5-13. The tear resistance measures the ability of the foam to resist the growth of any cut under tension.

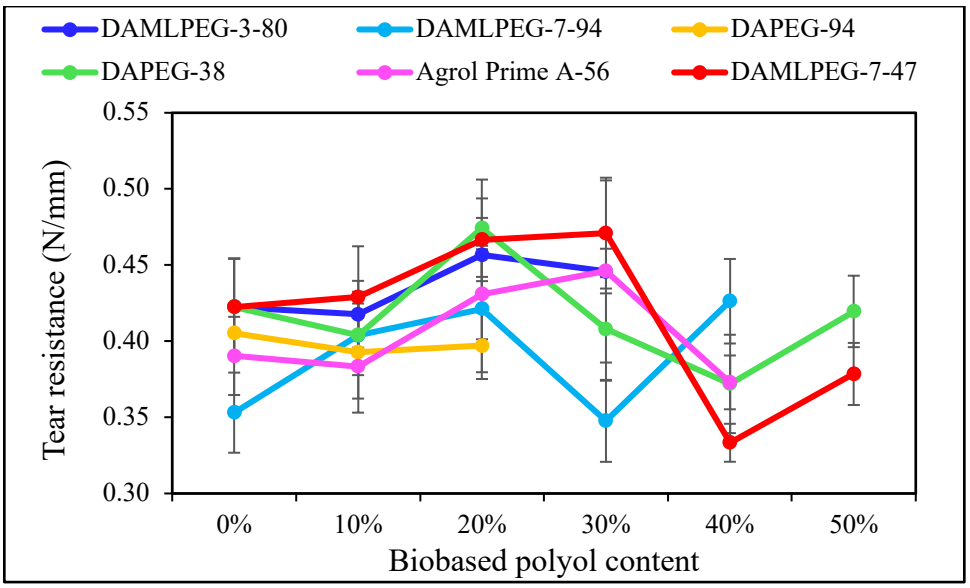


Figure 5-13: Tear resistance of biobased PUF

All PUF containing 10 - 30% of biobased polyol content showed tear resistance equal to or greater

than 0.4 N/mm. The tear resistance of a foam (density 45 kg/m^3) for use in the interior automotive application should be at least 0.2 N/mm [124]. All biobased PUF have tear resistance higher than 0.2 N/mm.

5.3.8 Compressive properties of PUF

The compressive moduli for all biobased PUF samples are shown in Figure 5-14. The compressive properties of biobased PUF were measured in order to evaluate its behaviour under compressive load. The compression modulus measures the stiffness of a foam.

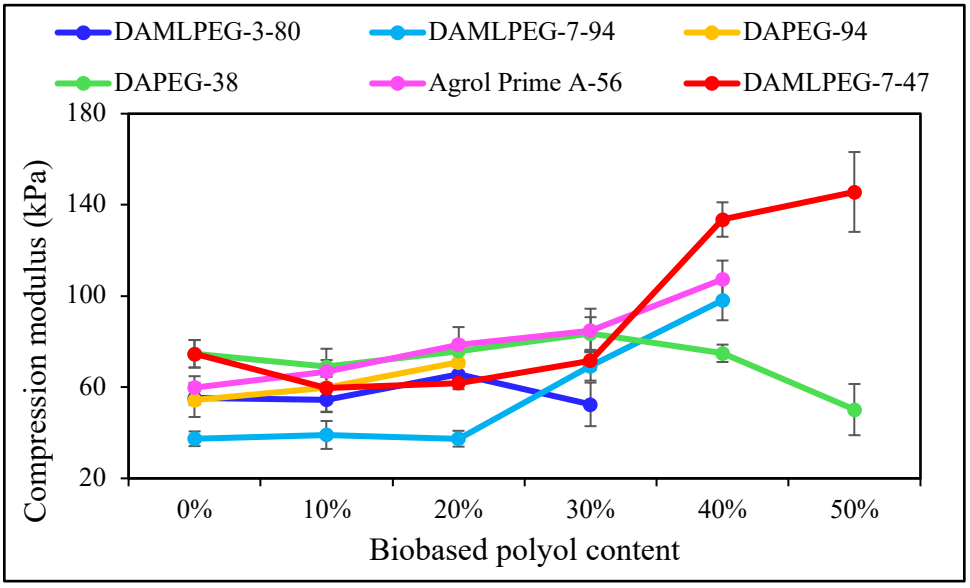


Figure 5-14: Compression modulus of biobased PUF

Higher compressive modulus value indicates higher compressive stress is required to deform the foam sample compared to a foam sample having lower compressive modulus. The modulus slightly increases with increasing biobased polyol content in PUF. The drastic increase in the compressive moduli of PUF containing 40% and 50% of DAMLPEG-7-47 polyol could be due to the higher density of PUF.

The compressive stress values required to deform a foam sample to 25%, 50%, and 65% deflection of its original height are shown in Figure 5-15, Figure 5-16, and Figure 5-17. The compressive

stress for PUF containing DAMLPEG-7-94, DAMLPEG-7-47, and DAPEG-38 polyols remains constant up to 20 - 30% of polyol content and increases after that.

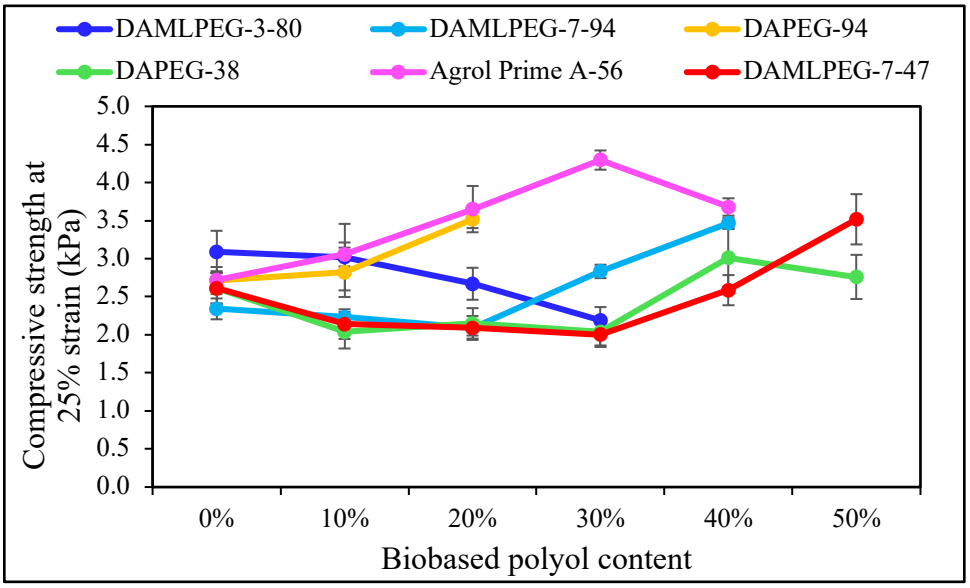


Figure 5-15: Compressive strength at 25% strain of biobased PUF

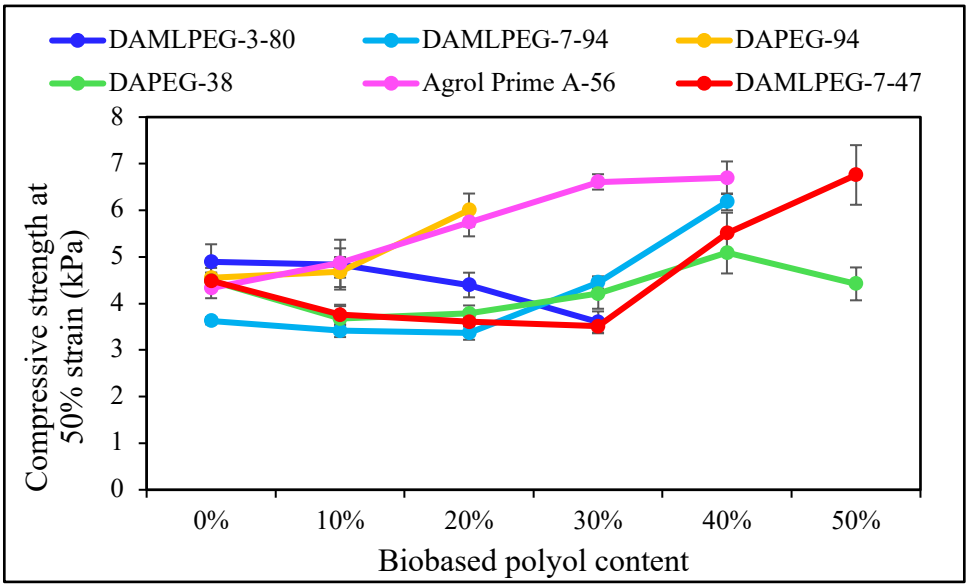


Figure 5-16: Compressive strength at 50% strain of biobased PUF

The compressive stress is directly related to the foam density which means compressive stress decreases with the decrease in foam density. However, the PUF containing 20 - 30% of

DAMLPEG-7-47 and DAPEG-38 polyol have the same compressive stress as that of control foam in spite of having lower densities. Thus, the compressive properties of DAMLPEG-7-47 and DAPEG-38 are better than that of the control foam. The compressive stress increased with the addition of Agrol Prime A-56, DAMLPEG-7-94, and DAPEG-94 polyols.

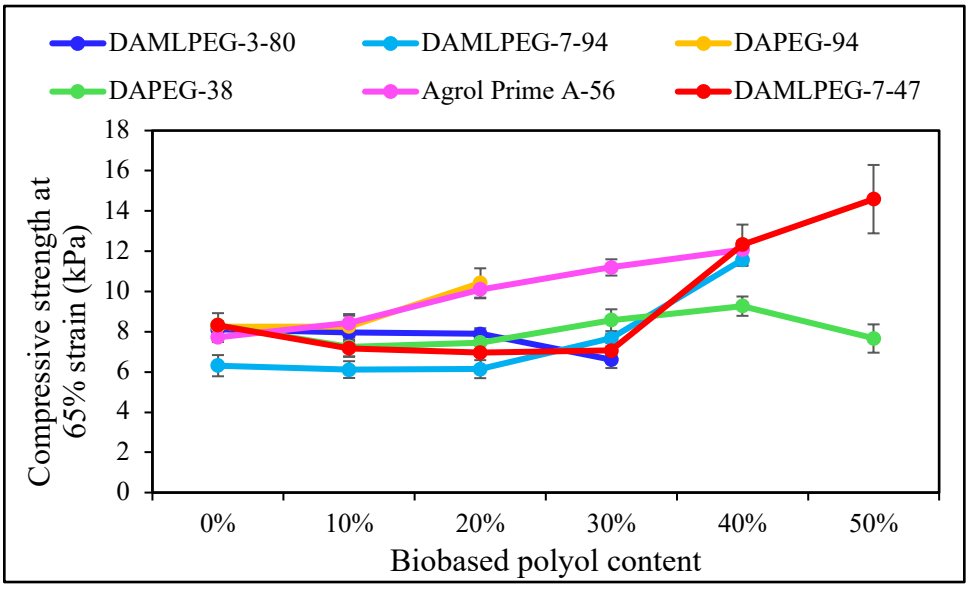


Figure 5-17: Compressive strength at 65% strain of biobased PUF

The sag factor is another measurement of the cushioning quality of foams. Higher values indicate higher resistance to "bottoming out". The foam used for cushioning application should have certain sag factor so that the support used under the foam is not felt [123]. The sag factor is a ratio of compressive stress at different strains. The ratio of compressive stress at 50% deflection to compressive stress at 25% deflection is shown in Figure 5-18. The ratio of compressive stress at 65% deflection to compressive stress at 25% deflection is shown in Figure 5-19. The sag factor either remains constant or increases slightly with increasing biobased polyol content in PUF. The sag factor for 50%/25% ratio increases from 1.6 to 1.8 and the sag factor for 65%/25% ratio increases from 2.5 to 3.5 with increasing biobased polyol content.

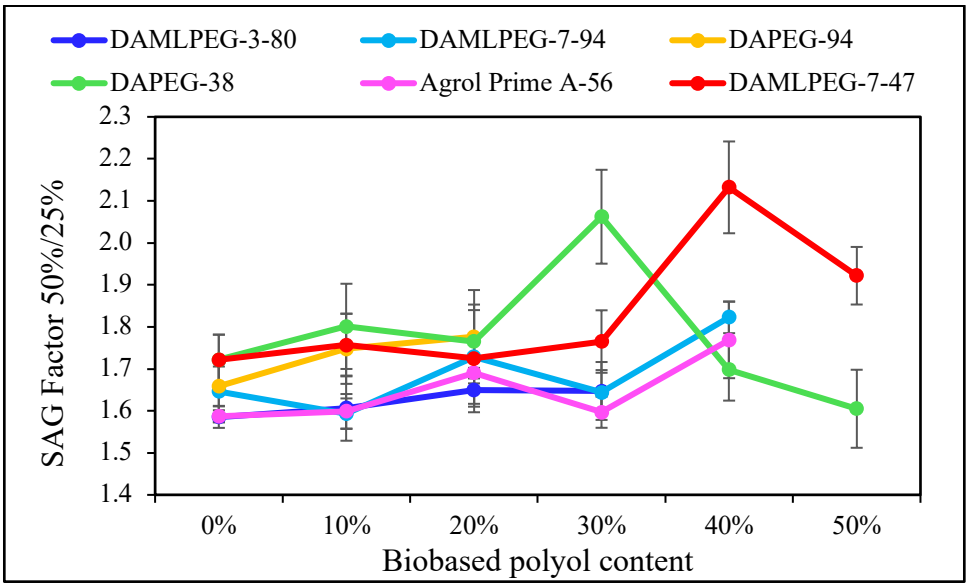


Figure 5-18: Sag factor 50%/25% of biobased PUF

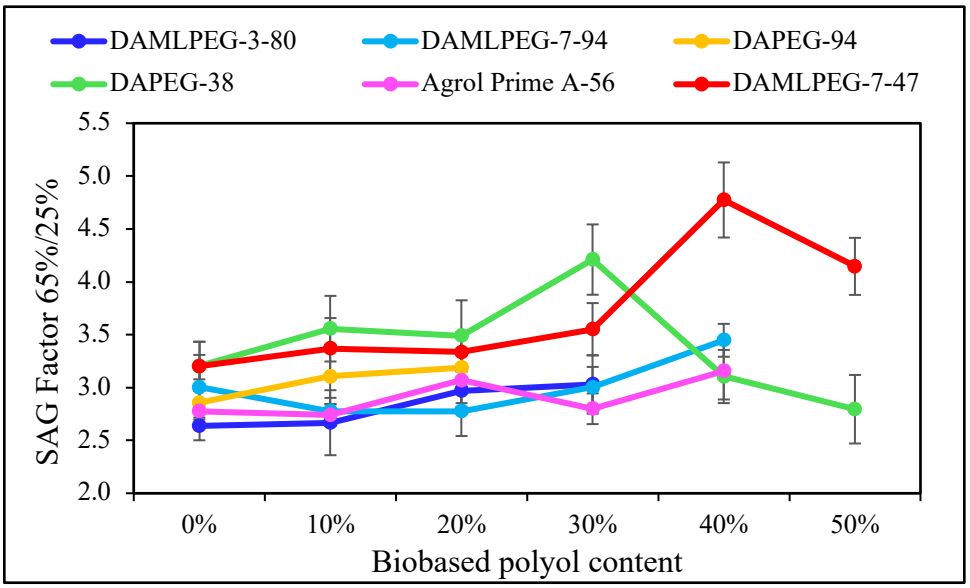


Figure 5-19: Sag factor 65%/25% of biobased PUF

5.3.9 Miscibility study and comparison of different biobased PUF

The polyols DAMLPEG-7-94, DAMLPEG-7-47, DAMLPEG-3-80 were completely miscible with Voranol 4701. No phase separation was observed after two weeks as shown in Figure 5-20 (a, b, c). It was observed that DAMLPEG-7-94 polyol was completely miscible with Voranol 4701

without the addition of any catalysts. A very thin layer was observed at the bottom of the jar containing DAPEG-94 polyol with Voranol 4701 Figure 5-20 (d). The phase separation was clearly observed (Figure 5-20 (e)) in DAPEG-38 polyol which could be due to the huge viscosity difference between DAPEG-38 and Voranol 4701. The mixture of Agrol Prime A-56 and Voranol 4701 showed some phase separation after 2 weeks (Figure 5-20 (f)).

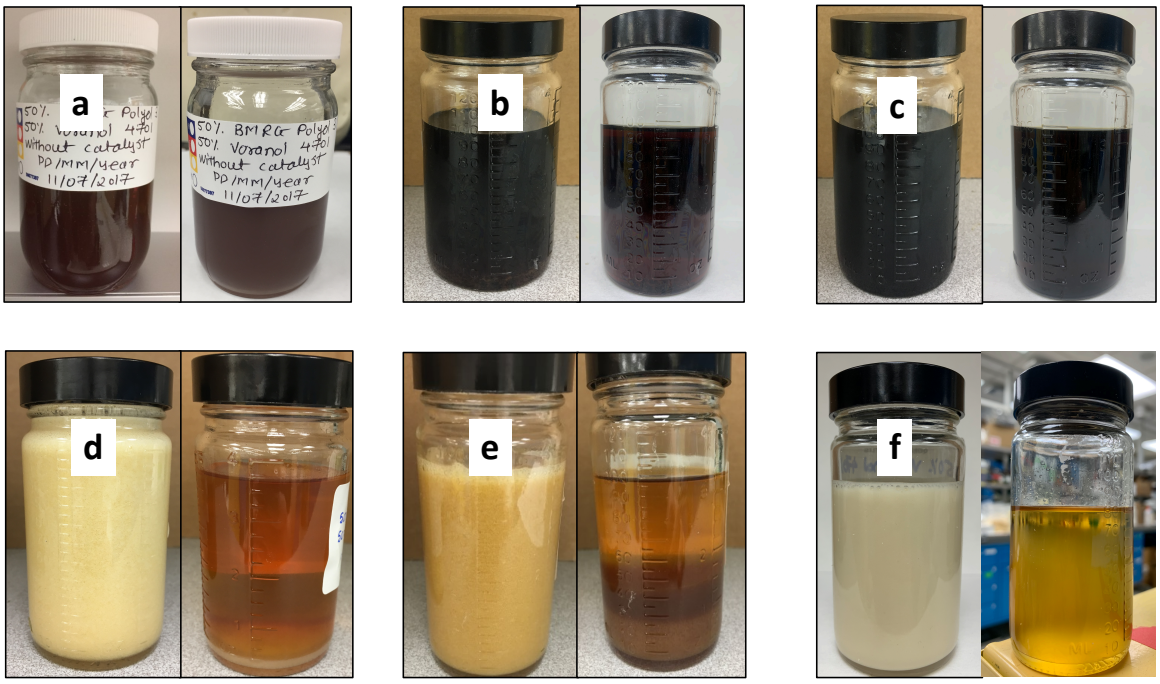


Figure 5-20: Miscibility study of biobased polyols (a) DAMLPEG-7-94, (b) DAMLPEG-3-80, (c) DAMLPEG-7-47, (d) DAPEG-94, (e) DAPEG-38, (f) Agrol Prime A-56, with Voranol 4701

The comparison of different biobased PUF containing 30% of biobased polyol is given in Table 5-6. The mechanical properties of 30% DAPEG-38 and 30% DAMLPEG-7-47 PUF were better than the control PUF at a lower density. The thermal stability of 30% DAPEG-38 and 30% DAMLPEG-7-47 PUF was better than the thermal stability of PUF synthesized from commercially available biobased polyol (Agrol Prime A-56). The DAMLEPG-7-47 polyol was completely miscible with Voranol 4701 polyol. Thus, it can be used with commercially available petroleum-based polyols to improve performance properties of polyurethanes and to increase renewable

carbon content in PUF.

Table 5-6: Comparison of different biobased PUF containing 30% biobased polyol with petroleum-based PUF

Property	Voranol 4701 (Control)	30% Agrol Prime A-56	30% DAPEG-38	30% DAMLPEG-7-47
Density (kg/m^3)	45	47	42	42
Compressive strength at 25% strain (kPa)	2.6	4.3	2	2
Compressive strength at 65% strain (kPa)	7.7	11.2	8.6	7
Sag factor 65%/25%	2.8	2.8	4.2	3.5
Tear resistance (N/mm)	0.39	0.45	0.41	0.47
Tensile strength (kPa)	75	118	77	90
Elongation (mm)	75	117	96	105
Temperature at 10% mass loss (ºC)	283	269	290	290
Wet compression set (%)	27	38	31	38
Miscibility with Voranol 4701	-	Partial	Partial	Complete

5.4 CONCLUSION

Biobased polyols derived from dimer acids and lactide were successfully used in the synthesis of flexible PUF. The formulation for biobased PUF was optimized by changing catalysts concentration. The free rise profile of polyols with lower hydroxyl value did not show any difference compared to the control PUF. The thermal degradation behaviour of biobased PUF was better than PUF made from the commercially available biobased and petroleum-based polyols. The biobased flexible PUF was tested for application in car seats, headrest, and engine cover in the automotive industry. The SEM images of all PUF showed an open cell structure which is required for cushioning application. The wet compression set which is very important for car seating application improved with the decrease in the hydroxyl value of a polyol. PUF containing

50% DAPEG-38 and 40% DAMLPEG-7-47 polyols passed the wet compression set test. The tensile properties of PUF increased with increasing biobased polyol content. The tensile stress slightly decreased for foams containing 30 - 40% DAPEG-38 polyol. The tear resistance for all biobased PUF increased with increase in the biobased polyol content. The tear resistance of foams made with DAMLPEG-7-47 and DAPEG-38 polyols was higher than the tear resistance of foams made with Agrol Prime A-56 polyol. A slight increase in compressive properties was observed with increase in the biobased polyol content. In the end, the miscibility study showed that polyols (DAMLPEG) containing lactide component were completely miscible with petroleum-based polyol i.e. Voranol 4701. This miscibility is very important in order to obtain a foam having uniform properties after blending different polyols. Thus, the biobased PUF containing 30% biobased polyol content and having performance properties better than the commercially available petroleum-based and biobased polyols were successfully synthesized.

5.5 ACKNOWLEDGMENTS

The authors are very grateful to Dr. Deborah Mielewski and Dr. Alper Kiziltas at Ford Motor Company, Dearborn, MI for providing support through Ford-MSU Alliance funding and the facility for polyurethane foams testing. The authors also acknowledge Huntsman Corporation (Texas, USA), Evonik (Virginia, USA), Lambent Corporation (Illinois, USA), The Dow Chemical Company (Michigan, USA), and Momentive Performance Materials (New York, USA) for providing materials required for foam formulations.

6 PLASTICIZATION OF POLYLACTIDE WITH BIOBASED POLYOLS VIA REACTIVE BLENDING

6.1 INTRODUCTION

The demand for single-use plastics has increased tremendously in the past few years. This plastic waste ends up in landfill where it takes many years to decompose, and leaks pollutants in soil and water. The plastic waste in the ocean is also a problem. Since million tons of plastic debris floating around in oceans has an adverse effect on health and safety of marine life [125]. The most concerning part is microplastics ingested by marine life. As humans are part of a food chain the microplastics entering in the human body could be harmful. Incineration of plastic waste is also not a solution as it generates gases which could be toxic, and it could contribute to the global warming potential. The only viable option to reduce the accumulation of plastic waste is recycling and use of biodegradable plastics. Some polymers are biobased and biodegradable e.g. polyhydroxyalkanoates (PHA) and polylactide (PLA). Some polymers are derived from petrochemical products, but they are biodegradable e.g. polycaprolactone (PCL), polybutylene adipate terephthalate (PBAT).

Polylactide (PLA) is derived from lactic acid. The lactic acid is produced by fermentation of starch. NatureWorks LLC (Minnesota, USA) is the largest producer of PLA and their plant is located in Nebraska, USA with a capacity of producing 140 kt/year. PLA is commercially available at a price of ~1 $/lb. This has definitely increased the use of PLA in short life span product applications e.g. cutlery, bags, packaging material. Poor mechanical properties such as low toughness and high glass transition temperature limit the application of PLA as an engineering plastic. PLA has a lower impact strength and elongation at break as compared to the polyethylene terephthalate (PET) and polypropylene (PP) [126]. Also, the presence of ester linkages in PLA makes it susceptible to

hydrolytic degradation. In order to overcome these disadvantages of PLA, a lot of research is being done on the modification of PLA via blending [127] and reactive extrusion [128].

PLA is modified by the addition of plasticizers [129-131] and toughing agents [132] to improve its mechanical properties. The flexibility of PLA has also been increased by blending it with polycaprolactone (PCL) and polybutylene adipate terephthalate (PBAT) [127]. Some of the commonly used plasticizers include citrate esters and polyethylene glycol [127, 133]. In recent years, epoxidized natural oils such as sunflower oil [134], soybean oil [135], and palm oil [136] have been used as a plasticizer for PLA. Oligomeric lactic acid (OLA) has a similar chemical structure as that of PLA which makes it a better candidate for plasticizing PLA. Lactide monomer is an excellent plasticizer for PLA but it migrates towards surface eventually affecting the properties of the polymer [127]. To avoid leaching out of small molecules like PEG they were grafted on PLA [137]. Transesterification of PLA with natural oils [138] and 1,4-butanediol [139] was also studied for the improvement of mechanical properties of PLA. Increase in the demand of biobased products has led to the development of biobased building blocks such as diols, dimer acids, epoxy derived from natural oils, lactide, and cashew nutshell liquid (CNSL). These building blocks contain reactive sites such as epoxy, acids, alcohol, and double bonds which could be used for the development of a variety of additives for bioplastics. In our previous work, dimer acids from soybean oil and lactide from lactic acid were used in the synthesis of biobased polyol. The dimer acid has a long carbon chain which can give flexibility to the stiff polymer such as PLA. Lactide based diol can provide better compatibility with PLA.

Thus, in this study polyols derived from lactide and dimer acids will be used as a plasticizer for PLA at different concentrations. The transesterification of polyols with PLA will be done via reactive extrusion. The thermal properties of modified PLA such as glass transition temperature,

crystallization temperature, and crystallinity will be studied. The effect of reactive blending of PLA and polyol on mechanical properties such as tensile modulus, elongation at break, and impact strength will be evaluated. The morphology of tensile and impact fractured surfaces will be studied to evaluate the mechanism of fracture. Finally, the melt crystallization kinetics of all modified resins will be studied using Avrami analysis.

6.2 EXPERIMENTAL

6.2.1 Materials and chemicals

Ingeo™ biopolymer 3001D is a commercially available semi-crystalline grade of polylactide (PLA) with D-lactide content 1.4% and number average molecular weight around 90,000 – 100,000 g/mol. It was purchased from NatureWorks LLC (Minnesota, USA). The transesterification catalyst, tin (II)-ethylhexanoate or $Sn(Oct)_2$, was purchased from Sigma-Aldrich (Wisconsin, USA). All polyols MLE-529, DAMLPEG-7-81, and DAPEG-94 were synthesized from dimer acid using polycondensation chemistry. Dimer acid (Radiacid 0955, MW = 575 g/mol, f = 2.02) was purchased from Oleon (Ertvelde, Belgium). DAMLPEG polyol having primary as well as secondary hydroxyl groups were obtained by reacting dimer acid with diols derived from meso-lactide (MLPEG-7-202). DAPEG polyols having primary hydroxyl group were obtained by reacting dimer acid with polyethylene glycol (PEG-400). The properties of all polyols are given in Table 6-1.

Table 6-1: Properties of biobased polyols

Compound	Hydroxyl Value (mg of KOH/g)	Acid Value (mg of KOH/g)	MW (g/mol)	Functionality	Viscosity @ 25°C (cPs)
Dimer Acid	-	188 ± 3	575	2.02	4950
MLE-529	529 ± 4	5.8 ± 1.2	212	~2	30000
DAMLPEG-7-81	81 ± 5	2 ± 0	1385	~2	2190
DAPEG-94	94 ± 5	1.5 ± 0	1194	~2	1022

6.2.2 Synthesis via Reactive extrusion

The polyols were incorporated into the PLA matrix using transesterification chemistry via reactive extrusion. Polylactide quickly absorbs moisture from the atmosphere. Thus, it was dried at 55°C for 12 hours before the reactive extrusion. The modified PLA was synthesized using 10% and 15% (w/w) of polyols with 0.1% (w/w) of a transesterification catalyst. All raw materials i.e. polyol, transesterification catalyst (Tin (II)-ethylhexanoate), and PLA were weighed out separately and premixed in an aluminum tray. The PLA pellets coated with polyol and catalyst were fed into the hopper of a century ZSK-30 (Michigan, USA) co-rotating twin-screw extruder. The extruder has a screw diameter of 30 mm and a L/D ratio of 42 with a screw configuration as shown in Figure 6-1.

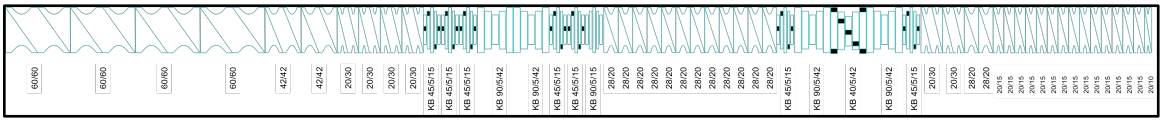


Figure 6-1: Screw configuration of twin-screw extruder from feed-die

The temperature profile used on the extruder going from the feed section to die was as follows: 140/160/170/180/180/180/170/160/155/145 for MLE-529 polyol, and 140/160/170/180/180/180/175/170/160/150 for dimer acid, DAPEG-94 polyol, and DAMLPEG-7-81 polyol. These temperatures were selected based on processing temperatures of 3001D.

The screw speed and throughput were 100 rpm and 130 g/min. The extrudate in the form of the strand was directly quenched by passing through a cold-water bath. The strand was pelletized using a pelletizer. The new polymer was dried in an oven for 48 hours to get rid of moisture and packed in sealed bags.

6.2.3 Characterization of modified PLA

The Attenuated Total Reflection-Fourier Transform Infrared (ATR-FTIR) spectra were acquired

on a FT-IR (Shimadzu Co., Tokyo, Japan, IRAffinity-1) equipped with a single reflection ATR system (PIKE Technologies, Wisconsin, USA, MIRacle ATR). The ATR-FTIR was used with resolution 4 cm^{-1}, Happ-Genzel apodization function and 64 scans were conducted on samples.

The degradation temperature of samples was obtained by thermogravimetric analysis (TGA). TGA measurements were conducted under nitrogen flow using a TGA Q50 (TA Instruments, Delaware, USA). In this analysis, a sample (10 - 15 mg) was taken in an aluminum pan and heated to 600°C with a heating rate of 10°C /min. The weight loss (%) of a sample as a function of temperature (°C) was obtained from this analysis. The derivative thermogram (DTG) (%/°C) was used to identify the degradation temperatures. Also, the thermal transitions of the samples were obtained by using a differential scanning calorimeter (DSC). The sample was heated to 200°C in DSC Q20 (TA Instruments, Delaware, USA) with the heating rate of 10°C/ min to remove any thermal and stress history. The sample was then cooled back to 20°C and heated again to 200°C with the heating rate of 10°C/ min. The transitions appearing on the second heating cycle was recorded for analysis. The crystallinity of samples was calculated using Equation 6-1. Enthalpy of melting (ΔH_m) and enthalpy of cold crystallization (ΔH_{cc}) was recorded from DSC in J/g. The enthalpy of melting for 100% crystalline PLA was obtained from the literature.

Equation 6-1:

$$\text{Crystallinity (\%)} = \frac{\Delta H_m - \Delta H_{cc}}{\Delta H_m \; of \; 100\% \; crystalline \; PLA \;\; \times \;\; Percent \; PLA} \text{ x } 100$$

The molecular weight distribution of the modified PLA resins was obtained by using the gel permeation chromatography (GPC) technique. A Waters GPC (Massachusetts, USA) equipped with a Waters 1515 isocratic HPLC pump, a Waters 717+ autosampler, Waters Styragel columns, and a Waters 2414 refractive index detector were used for the study. Tetrahydrofuran (THF) was

used as a mobile phase with a flow rate of 1 ml/min. The detector and columns were maintained at 35°C throughout the runs. The samples (three samples per resin) were dissolved in THF at a concentration of 2 mg/ml and filtered using a PTFE syringe filter into vials which were then loaded on the autosampler plate. A runtime of 50 minutes was used per sample. Polystyrene calibration standards were used as references for the final molecular weight calculations.

The unreacted polyol was separated out from a modified resin using a Soxhlet extractor. Methanol (CH_3OH) was chosen as a solvent for extraction as PLA was insoluble and polyols were soluble in methanol. Approximately 2.5 grams of the modified PLA pellets were kept inside a dried cellulosic thimble which was placed inside the Soxhlet extractor. The setup was made of a round bottom flask placed at the bottom for the solvent reservoir, an apparatus having a siphon in the middle to hold a thimble, and a condenser at the top to condense solvent vapors. The methanol was heated in the glass round bottom flask to its boiling point. The methanol vapors pass through the siphon apparatus and got condensed by the condenser into the thimble containing the sample. When the solvent reaches a certain level, the siphon carries the liquid methanol into the round bottom flask. The extraction was carried out over a period of 48 hours. In this manner, the methanol was passed through the modified PLA sample several times to ensure complete removal of unreacted polyol. The thimble was dried in an oven at 60°C for 24 hours. The weight loss by samples was recorded by subtracting the final weight of the sample plus thimble from the original weight of sample plus thimble. As initial polyol content in the modified PLA sample was known (10% and 15%), the percent of polyol reacted with PLA was calculated using the following Equation 6-2. The Soxhlet extractions were performed in triplicates.

Equation 6-2:

$$\text{Extent of reaction (\%)} = \frac{(\text{Polyol content x Weight of sample}) - \text{Weight loss}}{\text{Polyol content x Weight of sample}} \text{ x } 100$$

Injection-molded tensile test bars were prepared using a table-top DSM micro-injection molding machine. The neat PLA pellets were fed into the co-rotating twin-screw DSM Micro 15 cc compounder (DSM Research B. V., The Netherlands) at a temperature of 200°C and 100 rpm. The modified PLA resins were fed at a slightly lower temperature around 180°C. After attaining a constant level of torque which ensures proper mixing, the polymer melt was transferred to a DACA Micro injector (DACA Instruments, USA) with a barrel temperature of 200°C for neat PLA and 180°C for modified PLA resins. The melt was then injected into a mold which was maintained at a temperature of 55°C for neat PLA and 40°C for modified PLA. The injection pressure of 10 bar was used and the sample was held for 10 - 15 seconds inside the mold to cool down before it was removed. The tensile, as well as impact samples, were molded using the DSM.

The DSC of injection-molded samples showed cold crystallization peak (crystallization peak on heating cycle). In order to check the effect of crystallinity on mechanical properties of neat PLA and modified resins, a thermal annealing step was introduced. The injection molded tensile and impact samples were placed on an aluminum sheet. All samples were placed inside a uniformly heated oven at 90°C for an hour. The samples were removed from the oven and allowed to cool down slowly to room temperature. The samples were tested after 24 hours.

The tensile testing was performed using an Instron model 5565-P6021 (Instron, Massachusetts, USA) mechanical testing fixture setup with a 5 kN load cell. The testing was carried out in accordance with the ASTM D882-12 standard test method for tensile properties of thin plastic sheeting. The rate of grip separation was set at 12.5 mm/min which was as per the ASTM D882-12 specifications and six replicates were used per sample.

The notched Izod impact properties were studied using a Ray-Ran RR-IMT (Warwickshire, UK) pendulum impact tester equipped with a Techni-Test software. The testing was performed in

accordance with the ASTM D256 - 10 (2018) standard test method for determining the Izod pendulum impact resistance of plastics. The samples with a dimension 64 mm (length) X 12.7 mm (width) X 4 mm (thickness) were notched using a Tinius Olsen Model 22-05-03 Motorized Specimen Notcher (Pennsylvania, USA). The notch marked was 2.54 mm deep and six replicates were used per sample.

All tensile and impact surfaces were examined in a JEOL 6610LV (tungsten hairpin emitter) Scanning Electron Microscope (JEOL Ltd., Tokyo, Japan). Samples were mounted on aluminum stubs using epoxy glue, System Three Quick Cure 5 (System Three Resins, Inc., Washington, USA). Samples were coated with gold (~30 nm thickness) in an Emscope Sputter Coater model SC 500 (Ashford, Kent, England) purged with argon gas.

Dynamic mechanical analysis (DMA) was carried out on the samples using an RSA-G2 Solids Analyzer (TA Instruments, Delaware, USA) to evaluate the storage modulus, loss modulus, and tan δ as a function of temperature. The injection-molded samples with dimension 50 mm X 12.7 mm X 4 mm was used for DMA analysis. The testing was carried out using the three-point bending mode. The samples were heated from 25 - 150°C at a constant heating rate of 3°C/min and frequency of 1 Hz.

The melt crystallization kinetics of samples were evaluated using the DSC. The isothermal melt crystallization behavior was studied using the following procedure: the samples (~10 mg) were heated from room temperature up to 200°C at a heating rate of 10°C/min, where they were held isothermally for 5 minutes to remove previous thermal and stress history. The samples were then cooled down to one of the four different isothermal temperatures (90°C, 100°C, 110°C, and 120°C) at a rate of 20°C/min. The samples were held at that temperature for a sufficient amount of time until the entire crystallization process was complete.

6.2.4 Effect of lower concentrations of polyols on performance properties of PLA

The 10% DAPEG and 10% DAMLPEG resins were added to neat PLA in the concentration of 10% and 50% in order to synthesize modified PLA samples containing 1% and 5% of polyol. These different formulations were fed into the co-rotating twin-screw DSM at a temperature of 200°C with screw speed 100 rpm. The polymer melt was transferred to a DACA Micro injector with a barrel temperature of 200°C for modified PLA resins. The melt was then injected into a mold which was maintained at a temperature of 55°C and the injection pressure of 10 bar was used. The sample was held for 10 - 15 seconds inside the mold to cool down before it was removed. The tensile, as well as impact samples, were molded using the DSM.

6.3 RESULTS AND DISCUSSION

6.3.1 Transesterification chemistry

The structure of polyols used for transesterification is shown in Figure 6-2. The MLE-529 polyol has a low molecular weight (212 g/mol) and some residual lactic acid. The DAMLPEG-7-81 and DAPEG-94 polyols were comparatively higher molecular weight (1200 - 1300 g/mol) polyols with low acid value. The MLE-529 polyol contains an amide and ester linkage. DAMLPEG-7-81 and DAPEG-94 polyols contain ester as well as ether linkages. DAMLPEG-7-81 polyol has more ester linkages compared to the DAPEG-94 polyol. The schematic of transesterification chemistry is shown in Figure 6-3. The hydroxyl group of polyol attacks ester groups of polylactide (PLA) and forms a new ester linkage as shown in Figure 6-3. The transesterification catalyst, Tin (II) ethylhexanoate ($Sn(Oct)_2$) accelerates this process. Tin (II) ethylhexanoate is more commonly used as a catalyst for ring-opening polymerization of lactide and lactones [140] and transesterification reactions [141]. The modified PLA resins obtained from MLE-529 polyol were labelled as 10% MLE (10% of polyol MLE-529, 0.1% of catalyst, 89.9% of 3001D) and 15% MLE (15% of polyol

MLE-529, 0.1% of catalyst, 84.9% of 3001D). In a similar manner, modified PLA resins obtained from DAPEG-94 polyol were labelled as 10% DAPEG and 15% DAPEG, and those obtained from DAMLPEG-7-81 polyol were labelled as 10% DAMLPEG and 15% DAMLPEG. The modified PLA obtained from dimer acid was labelled as 10% Dimer acid.

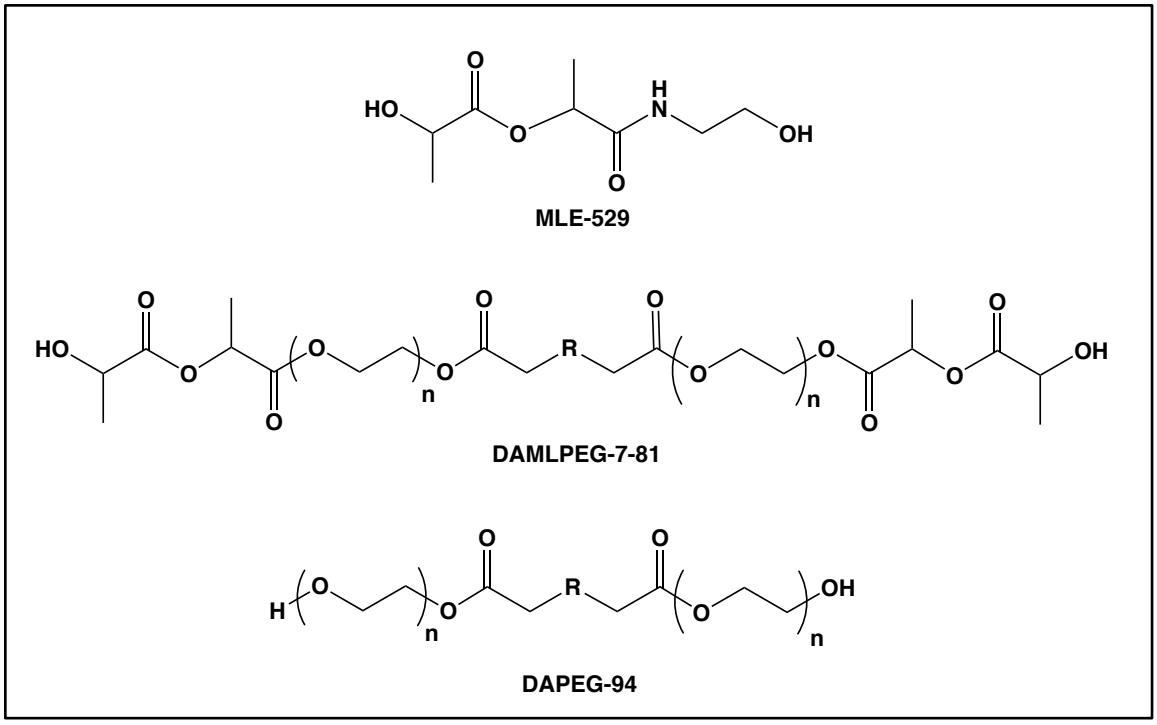


Figure 6-2: Structures of different polyols used in transesterification reaction

Presence of lactic acid in MLE-529 polyol might act as a catalyst and breakdown PLA chains thereby reducing the molecular weight of 10% MLE and 15% MLE resins. The DAPEG-94 polyol has primary hydroxyl groups which could possibly react with acid groups of PLA chains acting as a chain extender. The DAMLPEG-7-81 polyol also has primary as well as secondary hydroxyl groups which could also react with acid groups of PLA chains. The extent of reaction was calculated by Soxhlet extraction.

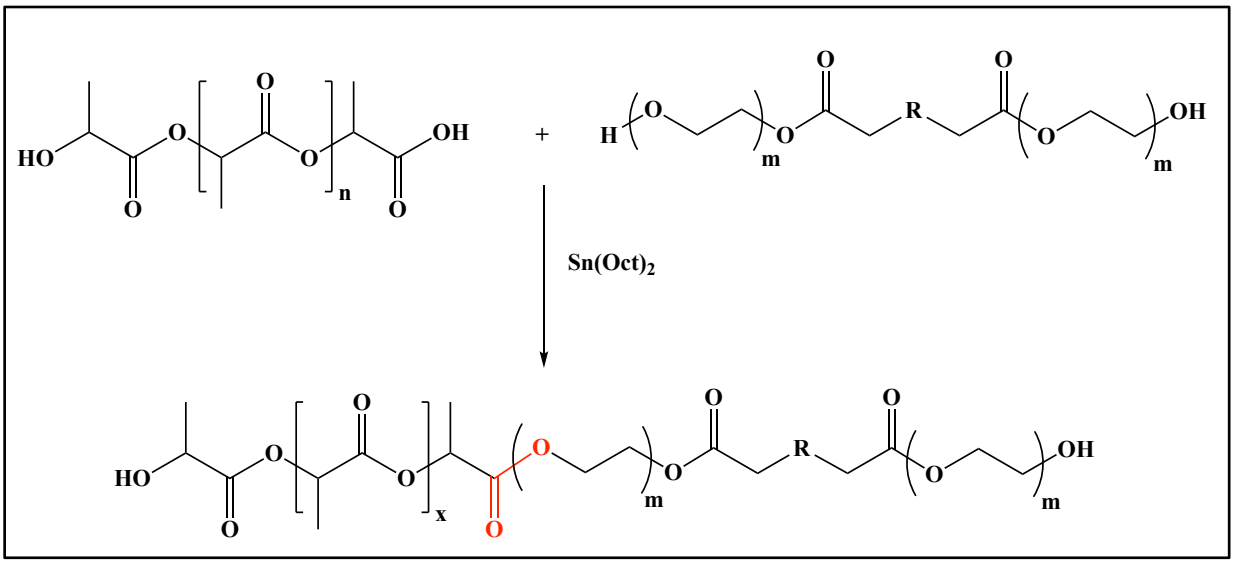


Figure 6-3: Transesterification reaction between PLA and DAPEG-94

6.3.2 Soxhlet extraction

The amount of polyol reacted with PLA was calculated by using the Soxhlet extraction. All polyols were soluble in methanol. Thus, methanol can easily extract unreacted polyols from modified resins. It was found that the extent of grafting of MLE-529 polyol was only 20% for 10% MLE resin and 40% for 15% MLE resin. The extent of grafting of DAMLPEG-7-81 and DAPEG-94 polyols was around 45 - 47% for 10% and 15% of DAMLPEG and DAPEG resins. This concludes that the modified PLA resins have some unreacted polyol which will act as a plasticizer.

6.3.3 Gel Permeation Chromatography (GPC)

The molecular weight distribution of neat PLA, extruded PLA, and modified PLA pellets are given in Table 6-2. The extruded PLA was obtained by processing neat PLA at the same conditions in the extruder. The number average (M_n) and weight average molecular weight (M_w) of extruded PLA were lower compared to the neat PLA. The decrease in molecular weights is due to the chain scission of PLA at high temperature and shear in the extruder. The molecular weights of 10% MLE and 15% MLE resins have decreased substantially compared to the other resins. This could be due

to the presence of lactic acid which attacked ester linkages of PLA and reduced its chain length. However, the addition of DAPEG-94 and DAMLPEG-7-81 polyols has a negligible effect on molecular weights of modified resins compared to the extruded PLA. The slight decrease in the molecular weights was observed with the addition of 15% of DAMLPEG-7-81 polyol. The polydispersity index which is essentially a ratio of weight average molecular weight (M_w) to number average molecular weight (M_n) was around 1.55 - 1.60 for all samples.

Table 6-2: Molecular weight distribution of neat PLA, extruded PLA, and modified PLA resins

Sample	**M_n (g/mol)**	**M_w (g/mol)**	**PDI**
Neat PLA	95344 ± 1126	153248 ± 2191	1.61 ± 0.01
Extruded PLA	85018 ± 1146	137254 ± 3478	1.61 ± 0.06
10% MLE	58032 ± 3802	89967 ± 8218	1.55 ± 0.04
15% MLE	57765 ± 517	88767 ± 1451	1.56 ± 0.05
10% DAPEG	84963 ± 2409	136225 ± 2317	1.60 ± 0.02
15% DAPEG	83772 ± 6007	131623 ± 8492	1.57 ± 0.01
10% DAMLPEG	87378 ± 2100	137216 ± 3241	1.57 ± 0.01
15% DAMLPEG	73438 ± 1513	112073 ± 2775	1.53 ± 0.03

6.3.4 Thermal properties of modified PLA resins

The thermogravimetric analysis (TGA) and derivative thermogravimetric (DTG) graphs of modified PLA resins containing 10% and 15% of biobased polyols are shown in Figure 6-4 and Figure 6-5. In the TGA graphs of 10% and 15% of MLE resins, two degradation stages were observed i.e. stage I (75°C - 280°C), stage II (280°C - 330°C). The first stage could be due to the degradation of unreacted polyol whereas the second stage corresponds to the degradation of the reactive blend of PLA and MLE-529 polyol. Similarly, in the TGA graphs of 10% and 15% of DAPEG and DAMLPEG resins, two degradation stages were observed i.e. stage I (250°C - 340°C), stage II (340°C - 450°C). The first stage corresponds to the degradation of the reactive blend of PLA and polyol whereas the second stage corresponds to the degradation of unreacted

polyol and high molecular weight segments. The TGA of modified PLA resins after removal of unreacted polyol showed two degradation stages and the peak degradation temperature shifted towards the higher temperature (increased by 10 - 20°C).

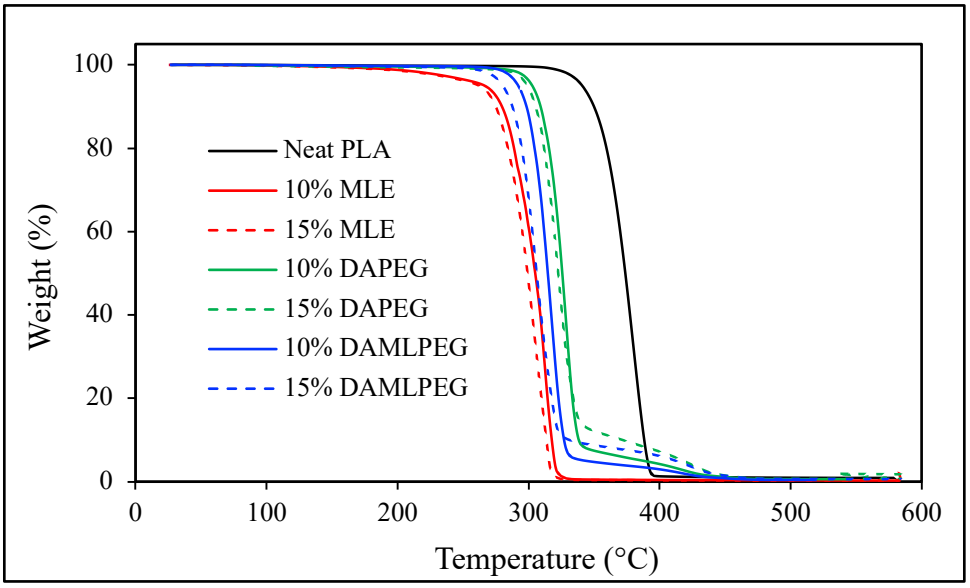


Figure 6-4: Thermogravimetric (TGA) graphs of modified PLA resins

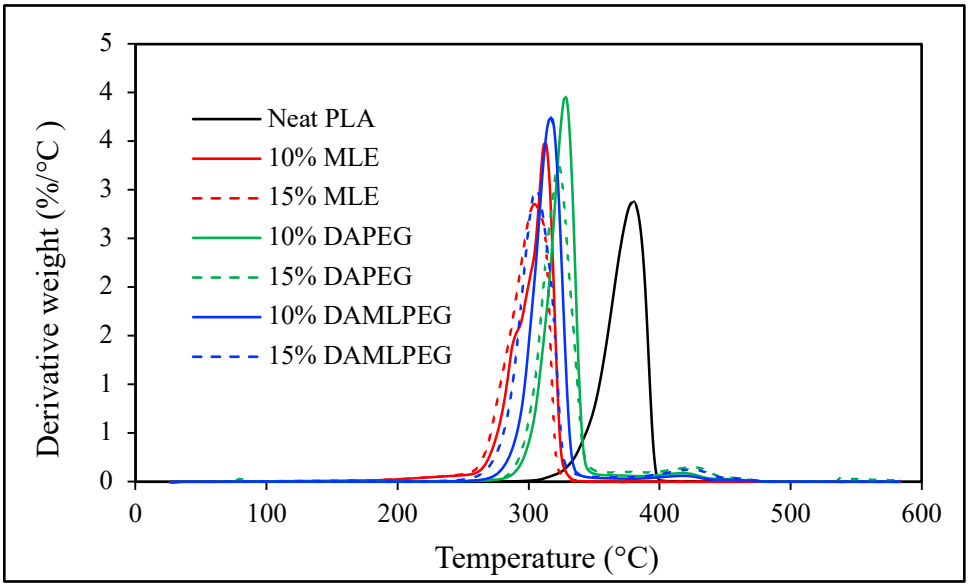


Figure 6-5: Derivative thermogravimetric (DTG) graphs of modified PLA resins

Also, the degradation temperature of modified PLA resins containing 10% of polyol was slightly

higher than the resins containing 15% of a polyol as shown in Figure 6-5. Thus, it can be confirmed that the addition of polyol decreases the degradation temperature of PLA.

The glass transition temperature T_g (°C), crystallization temperature T_{cc} (°C), melting temperature T_m (°C), enthalpy of crystallization (J/g), enthalpy of melting (J/g), and crystallinity (%) data of modified PLA pellets are given in Table 6-3. The percent crystallinity of each sample was calculated based on the enthalpy of melting of 100% crystalline PLA, equal to 93 J/g [130]. It was observed that the glass transition temperature T_g of all modified PLA samples decreased with the addition of polyols. The small molecules dispersed in the PLA matrix increases the free volume. This provides enhanced chain mobility of PLA thereby decreasing its glass transition temperature (T_g) [129-131]. The glass transition temperature (T_g) of modified PLA samples containing DAPEG-94 and DAMLPEG-7-81 polyols decreased linearly with the increase in the polyol content. The decrease in the crystallization temperature (T_{cc}) was also due to the increase in the chain mobility of PLA with addition of polyol [131]. The increase in crystallinity [142] and a decrease in the crystallization temperature with the addition of plasticizer was reported previously for PLA [131].

Table 6-3: Thermal transition and crystallinity of modified PLA resins - non-annealed

	T_g (°C)	**T_{cc} (°C)**	**T_m (°C)**	**ΔH_{cc} (J/g)**	**ΔH_m (J/g)**	**Crystallinity (%)**
Neat 3001D	64.4	143.4	171.8	6.3	8.8	2.7
10% MLE	52.2	108.7	163.5	33.5	41.2	9.2
15% MLE	52.0	108.9	162.4	33.3	40.3	9.0
10% DAPEG	51.5	95.3	168.2	27.8	45.2	22.0
15% DAPEG	45.8	88.3	167.0	20.9	44.5	29.8
10% DAMLPEG	51.6	95.4	168.6	20.6	46.1	30.4
15% DAMLPEG	46.4	86.7	167.7	9.5	42.9	42.2
10% Dimer Acid	61.9	115.3	171.7	29.5	34.0	5.3

The crystallinity of 10% DAMLPEG and 15% DAMLPEG samples increased to 30% and 42%, respectively. Similar behavior was observed for 10% DAPEG and 15% DAPEG samples. Previous studies showed an increase in the crystallinity of PLA up to 25% with the addition of 10 - 20% PEG [137, 143]. Thus, it can be concluded that the DAPEG-94 and DAMLPEG-7-81 polyols were acting as a plasticizer as well as nucleating agents for PLA. The addition of MLE-529 decreased the glass transition temperature T_g of modified PLA and increased its crystallinity slightly. But the addition of dimer acid had a negligible effect on the glass transition temperature (T_g) and the crystallinity of modified PLA. Thus, the effect of addition dimer acid on mechanical properties were not studied. The DSC thermograms of the second heating cycle of injection-molded test bars of modified PLA resins are shown in Figure 6-6. A slight decrease in the crystallization temperature of neat PLA was observed due to the processing.

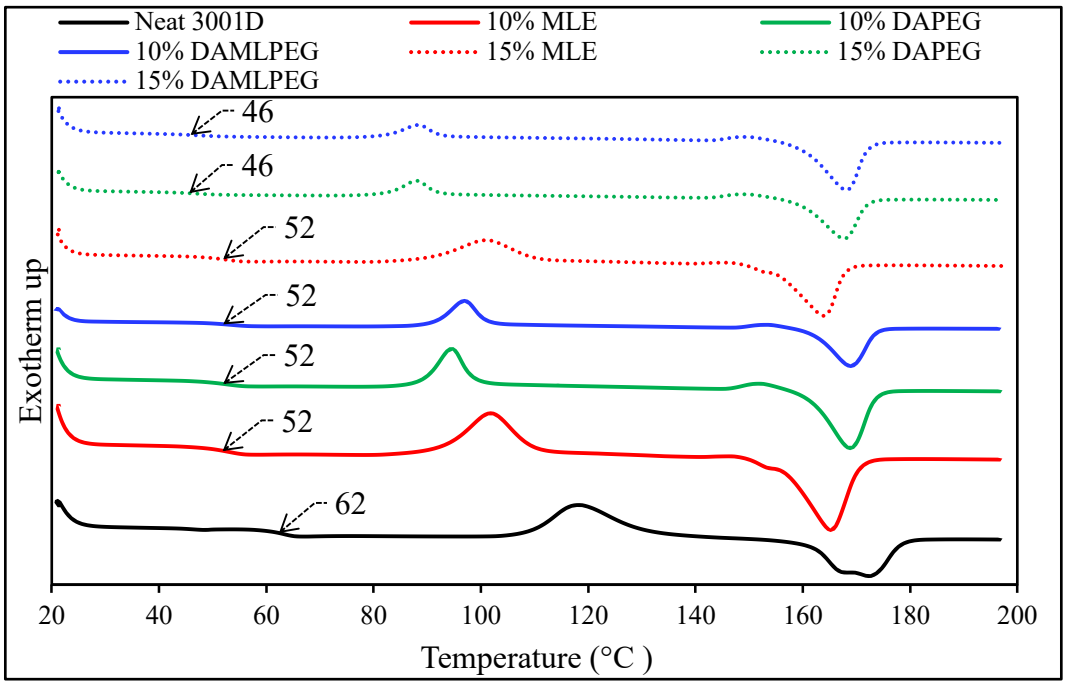


Figure 6-6: DSC thermograms of modified PLA test bars – non-annealed

Thermal transitions for rest of the samples remained unchanged after processing as shown in Table 6-4. But a slight increase in the percent crystallinity for all samples was observed after injection

molding. This could be due to additional processing effect on modified PLA. The crystallinity of PLA increased with increasing concentration of polyol.

Table 6-4: Thermal transitions and crystallinity of modified PLA test bars - non-annealed

	T_g (°C)	T_{cc} (°C)	T_m (°C)	ΔH_{cc} (J/g)	ΔH_m (J/g)	Crystallinity (%)
Neat 3001D	63.3	119.1	172.6	34.7	38.0	3.5
10% MLE	52.6	101.8	165.3	31.1	44.4	16.5
15% MLE	52.6	101.2	163.9	29.3	45.3	20.3
10% DAPEG	52.5	102.9	168.8	23.5	47.1	28.2
15% DAPEG	47.2	88.0	167.7	12.9	45.3	41.0
10% DAMLPEG	53.8	97.0	168.9	24.5	44.4	23.8
15% DAMLPEG	46.8	88.3	168.1	9.7	45.3	45.0

The DSC thermograms of the first heating cycle of annealed injection-molded test bars of modified PLA are shown in Figure 6-7. The glass transition temperature T_g (°C), melting temperature T_m (°C), enthalpy of melting (J/g), and crystallinity (%) data of annealed modified PLA test bars are given in Table 6-5. The annealing was performed at 90°C which is above the glass transition temperature of PLA for an hour. At this temperature, the mobility of polymer chains in the amorphous region increases and they rearrange themselves in a crystalline structure thereby decreasing the free energy of the system [144]. Holding a semi-crystalline PLA above its glass transition temperature for an hour gives enough time for complete crystallization. Hence, the annealing process increases the overall crystallinity of the polymer. In previous literature, increased in the crystallinity was observed after annealing [145, 146] for PLA. It can be seen from Figure 6-7 that the cold crystallization peak is completely removed from DSC thermograms of all samples. A slight increase in the glass transition temperature and the melting temperature was observed in annealed samples [146]. This could be a result of increased crystallinity of overall polymer as shown in Table 6-5. After annealing, the crystallinity of modified PLA increased to

50% compared to the neat PLA which is around 40%. The increase in the crystallinity of annealed test bars could increase the performance properties of modified PLA resins.

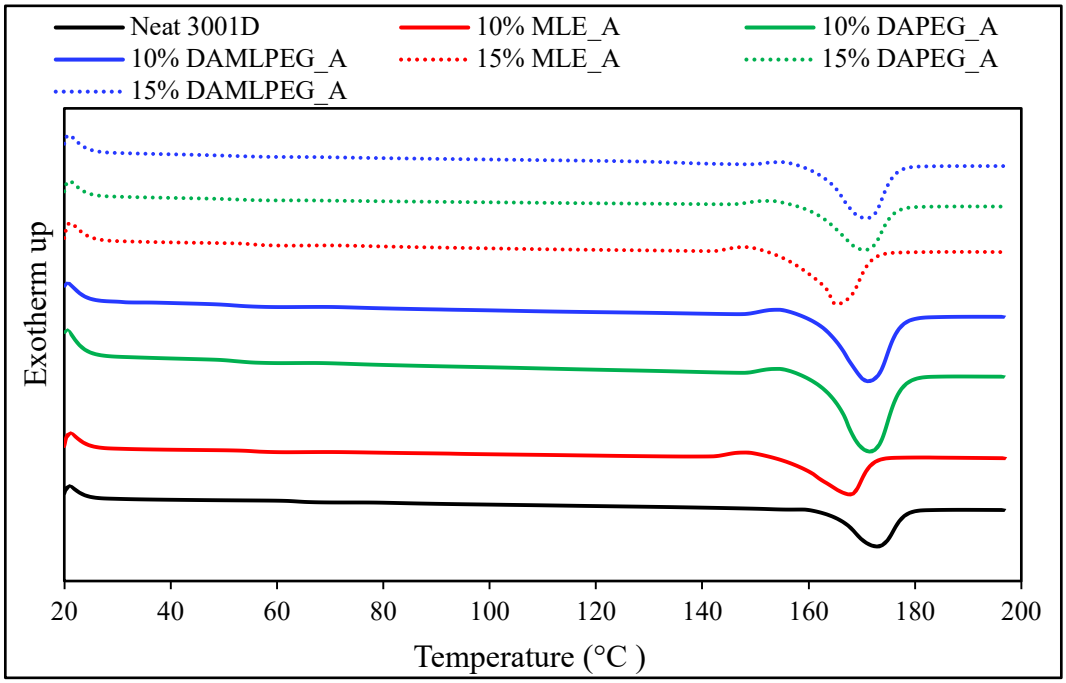


Figure 6-7: DSC thermograms of modified PLA test bars – annealed

Table 6-5: Thermal transitions and crystallinity of modified PLA test bars - annealed

	T_g (°C)	T_m (°C)	ΔH_{cc} (J/g)	ΔH_m (J/g)	Crystallinity (%)
Neat 3001D_A	63.9	173.6	0	36.3	39.0
10% MLE_A	55.4	167.7	0	44.4	53.0
15% MLE_A	55.7	165.3	0	42.4	53.6
10% DAPEG_A	51.5	171.4	0	42.3	50.5
15% DAPEG_A	52.0	170.4	0	38.8	49.1
10% DAMLPEG_A	51.5	171.1	0	42.6	50.9
15% DAMLPEG_A	51.7	170.7	0	39.9	50.5

6.3.5 Mechanical properties of modified PLA resins

The stress-strain of modified PLA resins are shown in Figure 6-8 and Figure 6-9. Increase in the elongation to break confirms the plasticization of PLA with the addition of DAPEG-94 and

DAMLPEG-7-81 polyols.

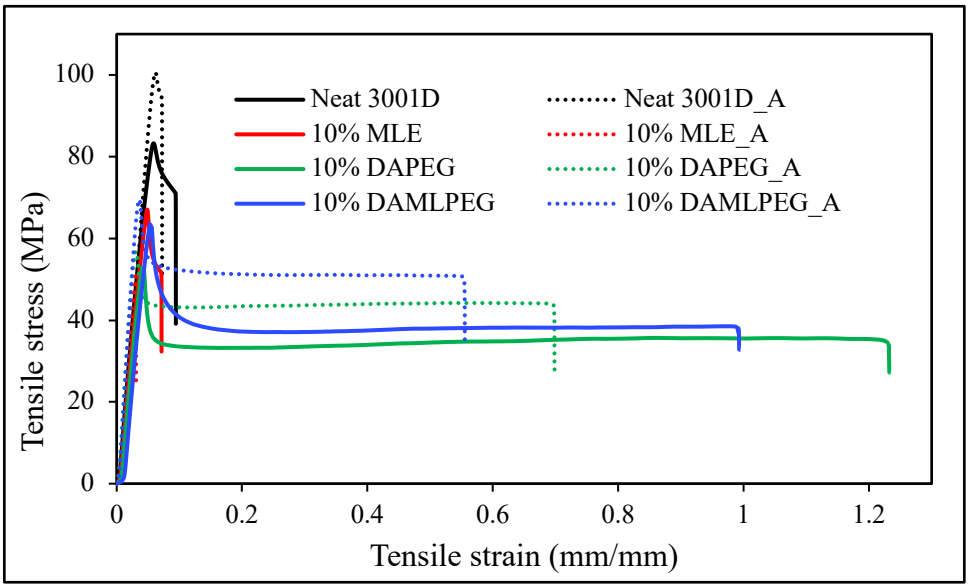


Figure 6-8: Stress-strain graph of modified PLA containing 10% of polyols

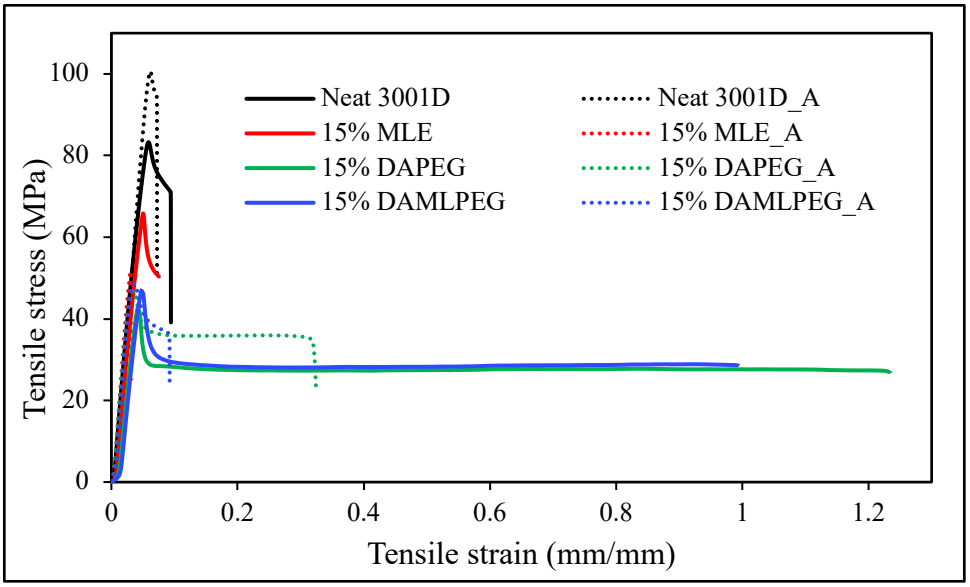


Figure 6-9: Stress-strain graph of modified PLA containing 15% of polyols

The elongation to break increased to 100 - 120% with the addition of 10% of DAPEG-94 and DAMLPEG-7-81 polyols. The strain at break increased slightly with increasing concentration of polyol to 15%. Similar results were observed with the addition of 10 - 12% of PEG-400 and PEG-

1500 but modulus and tensile stress at break both were decreased by 50 - 70% [147].

The tensile moduli of non-annealed samples decreased slightly with addition of polyols as shown in Figure 6-10. Further decrease in the moduli was observed with an increase in the amount of DAPEG-94 and DAMLPEG-7-81 polyols. However, tensile moduli increased after the annealing step. This is due to the increase in crystallinity of the polymer. The tensile moduli of annealed samples of 10% DAPEG and 10% DAMLPEG were 9% and 13% higher than the tensile modulus of neat PLA.

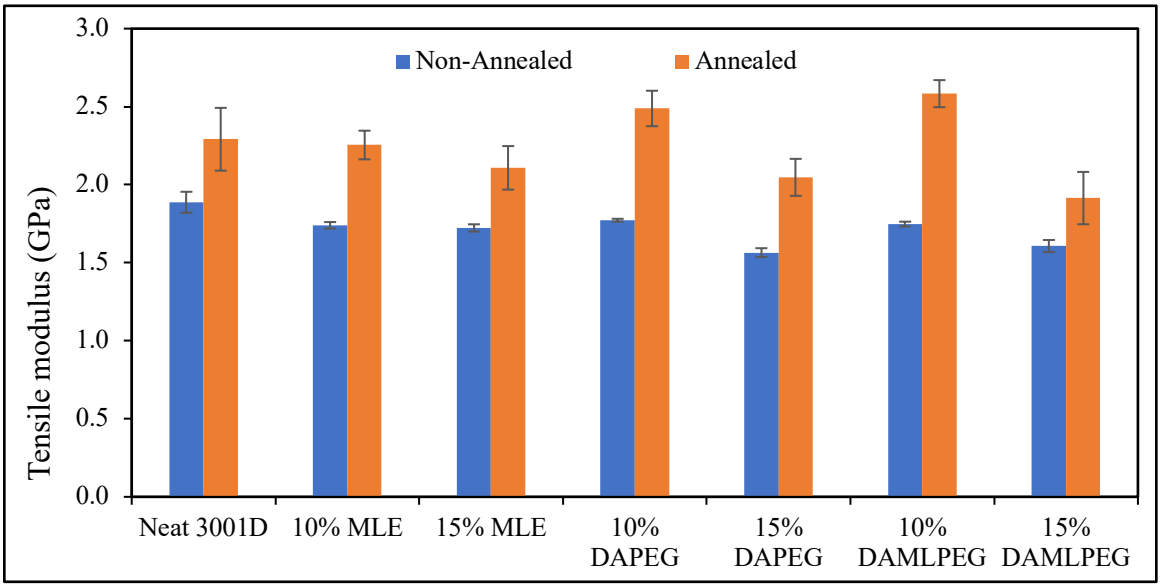


Figure 6-10: Tensile moduli of modified PLA resins

As polyols were acting as a plasticizer for PLA it will have an effect on tensile strength. The tensile stress at yield decreased with the addition of polyols as shown in Figure 6-11. The tensile stress at yield was decreased by 22% with the addition of 10% and 15% of MLE-529 polyol. The tensile stress at yield was decreased by 35% and 23% with the addition of 10% of DAPEG-94 and DAMLPEG-7-81 polyol, respectively. The tensile stress at yield increased slightly after annealing modified PLA resins except for 10% MLE and 15% MLE resins. Effect of the addition of plasticizer was clearly seen in the elongation at break data as shown in Figure 6-12. The strain at

the break increased extensively with the addition of DAPEG-94 and DAMLPEG-7-81 polyols. However, the strain at break did not increase with addition of MLE-529 polyol.

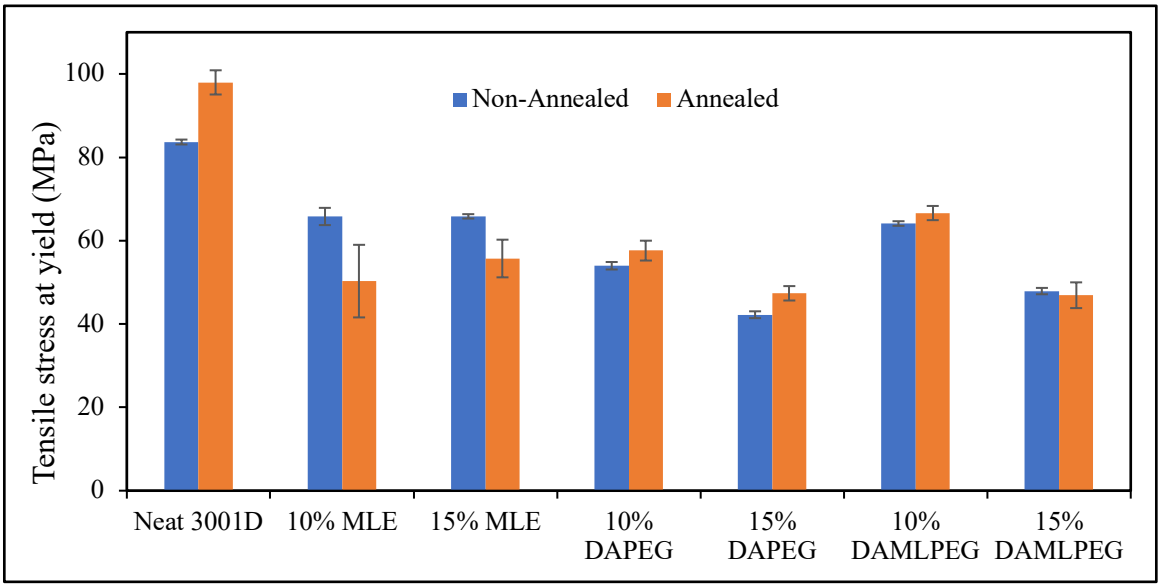


Figure 6-11: Tensile stress at yield of modified PLA resins

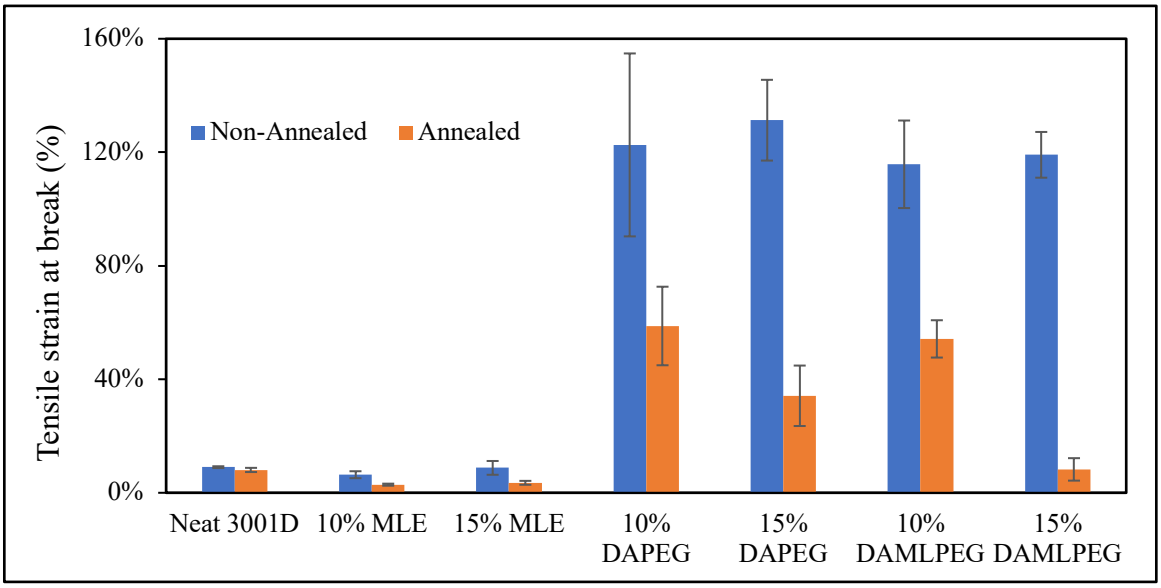


Figure 6-12: Tensile strain at break of modified PLA resins

The increase in the strain at break for 10% DAPEG, 15% DAPEG, 10% DAMLPEG, and 15% DAMLPEG resins could be due the presence of long carbon chains as well as polyether linkages

in respective polyols. Thus, it can be confirmed that DAPEG-94 and DAMLPEG-7-81 polyols act as a plasticizer for PLA. Whereas, MLE-529 does not act a plasticizer for PLA.

The strain at break for annealed samples decreased after annealing which could be due to the increase in the crystallinity or formation of larger modifier domains. In previous literature, the coalescence of modifier domains in the amorphous region after annealing is reported [148]. The coalescence could form larger modifier domains which might be affecting the tensile toughness. However, the strain at break for annealed modified PLA is still higher than annealed neat PLA. This could be due to "brittle to ductile" transition of the amorphous region of PLA [148].

The effect of the addition of polyols on the impact strength of PLA is shown in Figure 6-13. The impact strength increased slightly with the addition of DAPEG-94 and DAMLPEG-7-81 polyols. But it remained almost unchanged with the addition of MLE-529 polyol. After annealing the samples, the impact strength was increased by 175% and 300% for 10% DAPEG and 15% DAPEG resins, respectively, as compared to the impact strength of neat PLA.

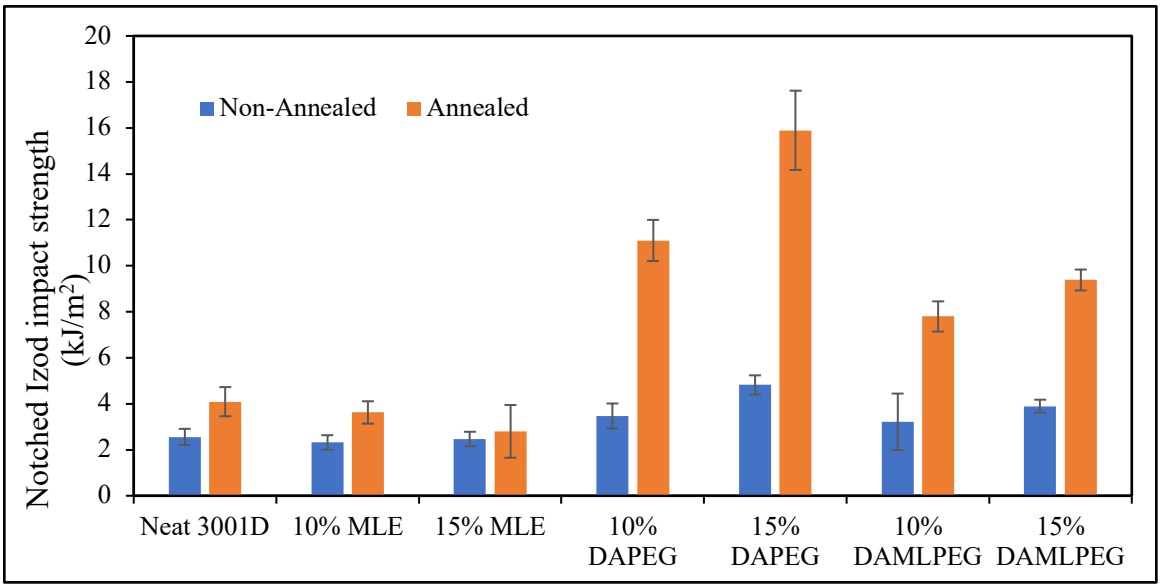


Figure 6-13: Notched Izod impact strength of modified PLA resins

Also, the impact strength of annealed 10% DAMLPEG and 15% DAMLPEG resins was increased

by 48% and 134%, respectively, as compared to the impact strength of neat PLA. All annealed samples of 10% DAPEG had a hinge break. Some of the annealed samples of 10% DAMLPEG and 15% DAPEG had a hinge break. The increase in the impact strength of PLA concludes that DAPEG-94 and DAMLPEG-7-81 polyols were acting as a toughing agent for PLA. Similar increase in impact properties was observed for annealed PLA samples with addition of polycarbonate [149] and increase in the annealing time [148]. The increase in impact strength of modified PLA after annealing could be due to the increase in the crystallinity which increases the ability to sustain the local stress [149], or the formation of larger spherulite [150], or increase in the modifier domain size via coalescence [148].

6.3.6 Scanning Electron Microscopy (SEM) images

The SEM images were taken on the fractured surface in order to better understand the behavior of tensile and impact fracture. The SEM images of tensile fractured samples are given in Figure 6-14 and Figure 6-15.

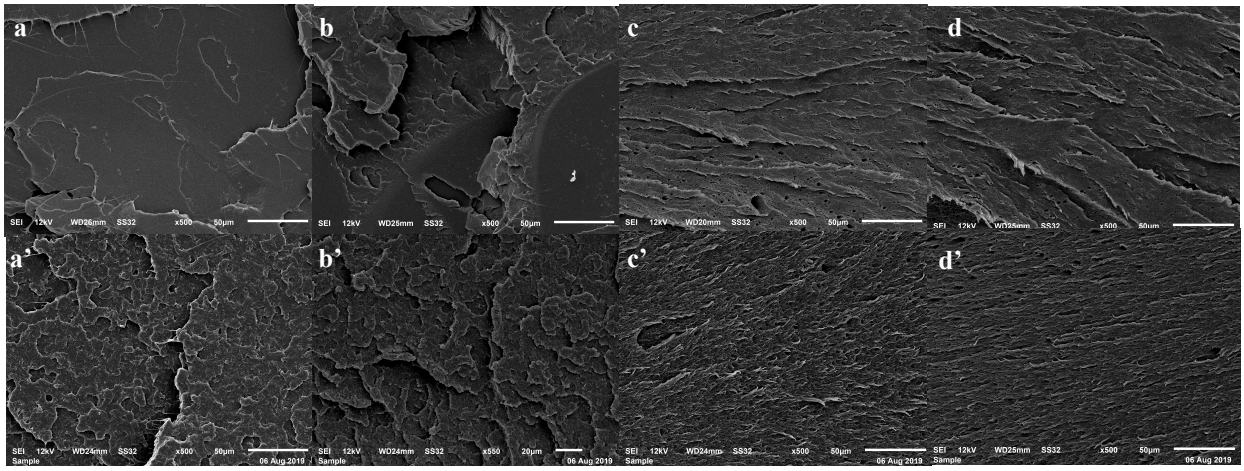


Figure 6-14: SEM images of tensile fractured surfaces of (a) Neat 3001D (a') Neat 3001D_A (b) 10% MLE (b') 10% MLE_A (c) 10% DAPEG (c') 10% DAPEG_A (d) 10% DAMLPEG (d') 10% DAMLPEG_A

The SEM images of neat PLA, 10% MLE, and 15% MLE samples showed a smooth surface

indicating a brittle fracture. Whereas, modified PLA containing DAPEG and DAMLPEG polyols showed rough surface indicating a ductile fracture. The annealing process increases the surface roughness for all samples indicating a ductile fracture.

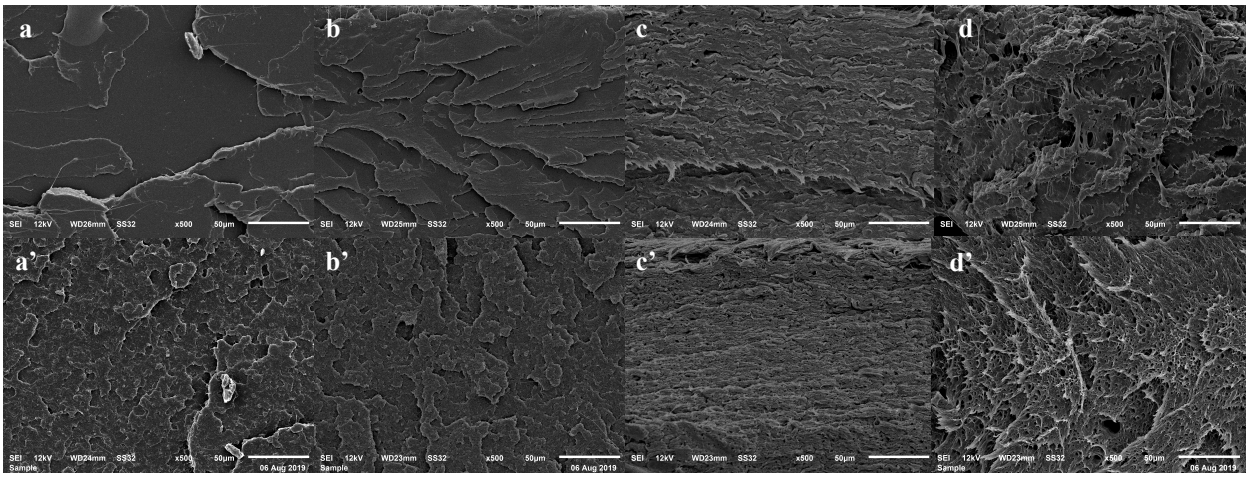


Figure 6-15: SEM images of tensile fractured surfaces of (a) Neat 3001D (a') Neat 3001D_A (b) 15% MLE (b') 15% MLE_A (c) 15% DAPEG (c') 15% DAPEG_A (d) 15% DAMLPEG (d') 15% DAMLPEG_A

The SEM images of the impact fractured surface are shown in Figure 6-16 and Figure 6-17. The neat PLA, 10% MLE, and 15% MLE samples showed a smooth surface indicating less energy dissipation during the impact fracture [151]. The SEM images of some non-annealed samples revealed mackerel pattern on the fractured surface showing the propagation of a crack in the sample [152]. This indicates the non-annealed samples have low impact toughness. The surface roughness increased for modified PLA containing DAPEG and DAMLPEG polyols. This indicates higher energy dissipation during the impact. The annealed samples showed a rougher fractured surface compared to non-annealed samples. Thus, the impact strength of annealed samples was higher compared to non-annealed samples. The increase in impact toughness could be due to the coalescence of modifier domains in the amorphous region after annealing, which absorbed the impact energy thereby increasing the impact strength of modified PLA.

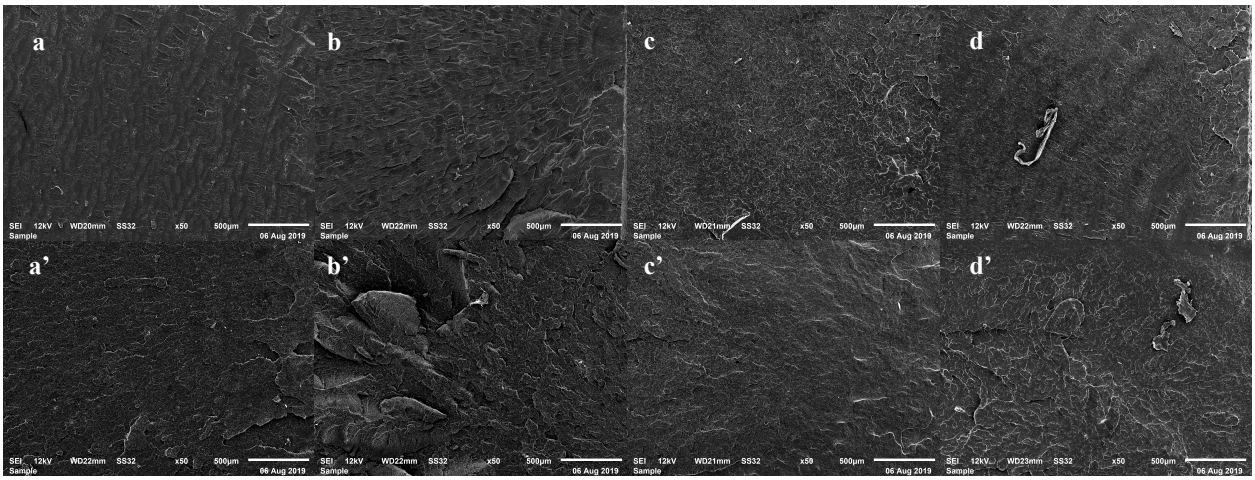


Figure 6-16: SEM images of impact fractured surfaces of (a) Neat 3001D (a') Neat 3001D_A (b) 10% MLE (b') 10% MLE_A (c) 10% DAPEG (c') 10% DAPEG_A (d) 10% DAMLPEG (d') 10% DAMLPEG_A

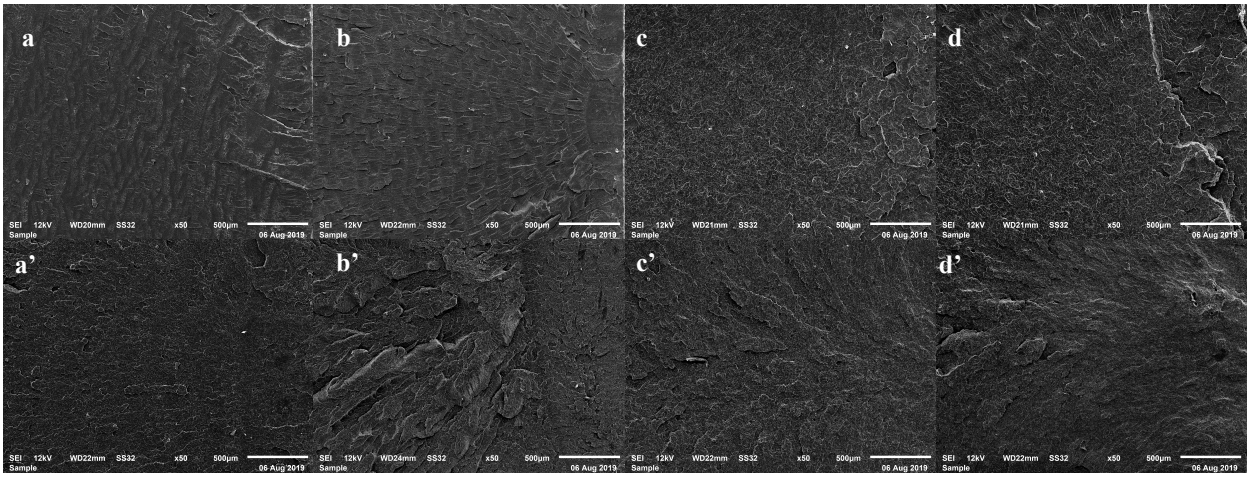


Figure 6-17: SEM images of impact fractured surfaces of (a) Neat 3001D (a') Neat 3001D_A (b) 15% MLE (b') 15% MLE_A (c) 15% DAPEG (c') 15% DAPEG_A (d) 15% DAMLPEG (d') 15% DAMLPEG_A

6.3.7 Dynamic Mechanical Analysis (DMA)

DMA is widely used to study the viscoelastic behaviour of a material. The storage modulus accounts for elastic component whereas loss modulus accounts for viscous component of the material. The storage moduli of modified PLA injection molded samples are shown in Figure 6-18.

The storage modulus for neat PLA decreased around 56°C which is near its glass transition temperature. This decrease is attributed to softening of polymer matrix due to increase in the chain mobility above the glass transition temperature [153]. The storage moduli of all modified PLA injection molded samples decreased around their glass transition temperature which is around 46 - 52°C. After annealing, the increase in the storage moduli was observed for all samples which is due to the increase in the crystallinity. Also, the sharp decrease in the storage moduli shifted to the higher temperature after annealing.

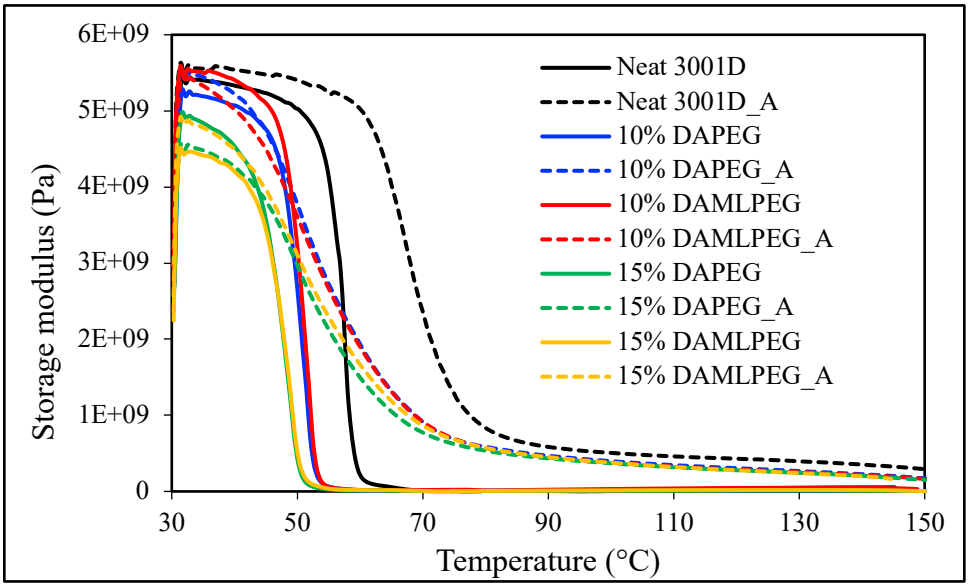


Figure 6-18: Storage modulus of modified PLA injection molded samples

The loss moduli of all injection molded samples are shown in Figure 6-19. The peak of loss modulus curve indicates a sharp decrease in the storage modulus. This also represents the upper temperature limit (Heat deflection temperature, HDT) at which material can be used. HDT for samples increased after annealing. However, the HDT of modified PLA samples were 10°C lower than HDT of neat PLA. Tan δ curves of injection molded samples are shown in Figure 6-20. Tan δ is the ratio of loss modulus to the elastic modulus. The area under Tan δ curves indicates the material's damping ability, which is the material's ability to absorb dissipated energy [150]. The

decrease in the area under Tan δ curves after annealing indicates a decrease in the damping ability of samples with an increase in the crystallinity [150].

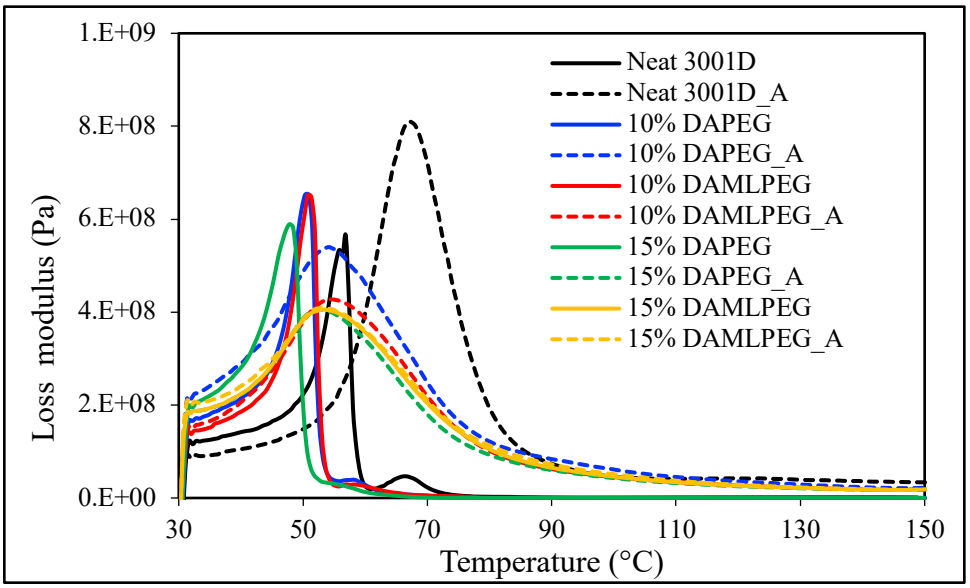


Figure 6-19: Loss modulus of modified PLA injection molded samples

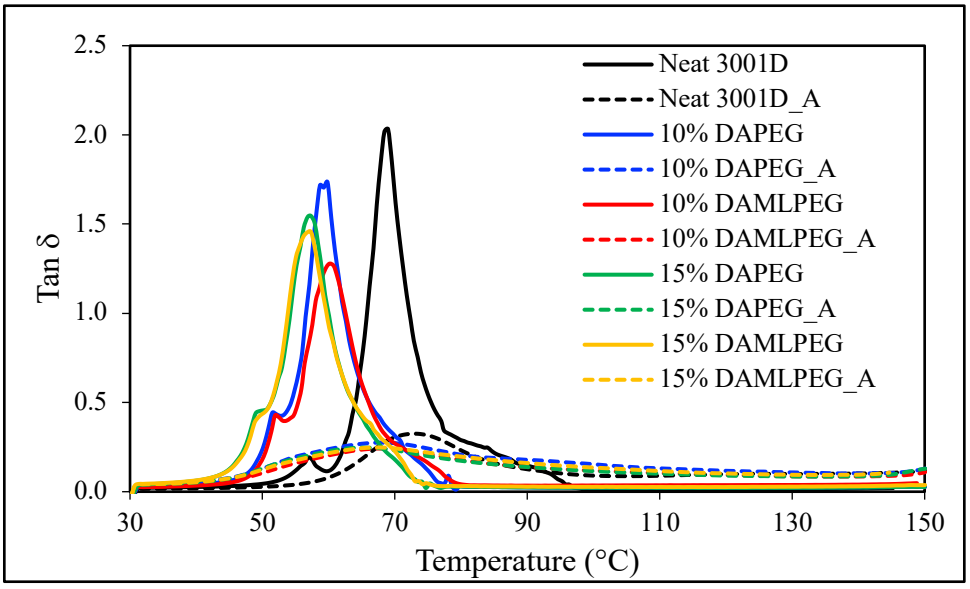


Figure 6-20: Tan δ curves of modified PLA injection molded samples

6.3.8 Melt crystallization kinetics

PLA is a slow crystallizing polymer and its heat deflection temperature can be increased with increasing its crystallinity [154]. To increase the crystallinity of PLA, nucleating agents such as talc is added [154]. The crystallinity of modified PLA resins was comparatively higher than the crystallinity of neat PLA as shown in Table 6-4. It could be possible that the polyol molecule was acting as a nucleating site thereby increasing the crystallinity of PLA. Thus, the effect of the addition of polyols on melt crystallization kinetics of PLA was studied. All injection-molded samples were held at desired temperature i.e. 90°C, 100°C, 110°C, and 120°C until the complete crystallization was achieved. The DSC graphs of isothermal melt crystallization of all samples are shown in Figure 6-21. It was observed that the total crystallization time was significantly decreased (<10 minutes) with the addition of polyol compared to neat PLA (20 - 30 min) at 90 - 110°C.

A similar reduction in total crystallization time was observed with addition nucleating agent e.g. talc [154], plasticizer e.g. PEG [155] or combination of both e.g. talc plus PEG [156]. However, at 120°C the total crystallization time increased which was also reported in previous studies [157]. In order to better understand the melt crystallization behavior, the kinetics of isothermal melt crystallization was analyzed by Avrami equation [154] as follows:

Equation 6-3:

$$X(t) = 1 - exp(-kt^n) \quad \text{or}$$

$$ln\left[-ln\left(1 - X(t)\right)\right] = n \ln t + \ln k$$

Where X(t) is fractional crystallinity at time t, k is crystallization kinetic constant for nucleation and growth rate, and n is the Avrami constant with a value indicating the mechanism of nucleation and the growth dimension. Initially, the plots of fractional crystallinity vs time were plotted as shown in Figure 6-22.

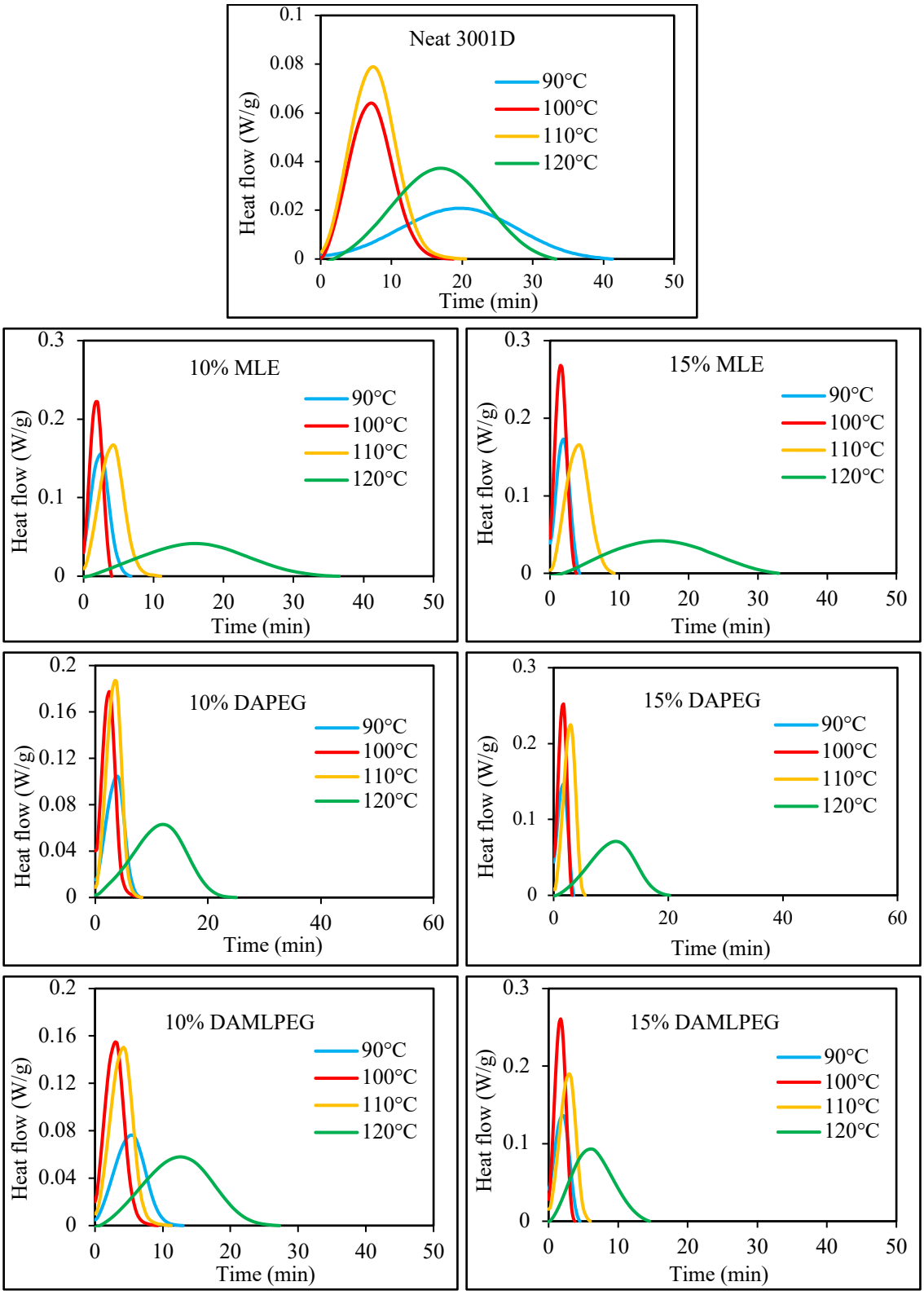


Figure 6-21: DSC graphs of isothermal melt crystallization of modified PLA samples at different isothermal temperatures

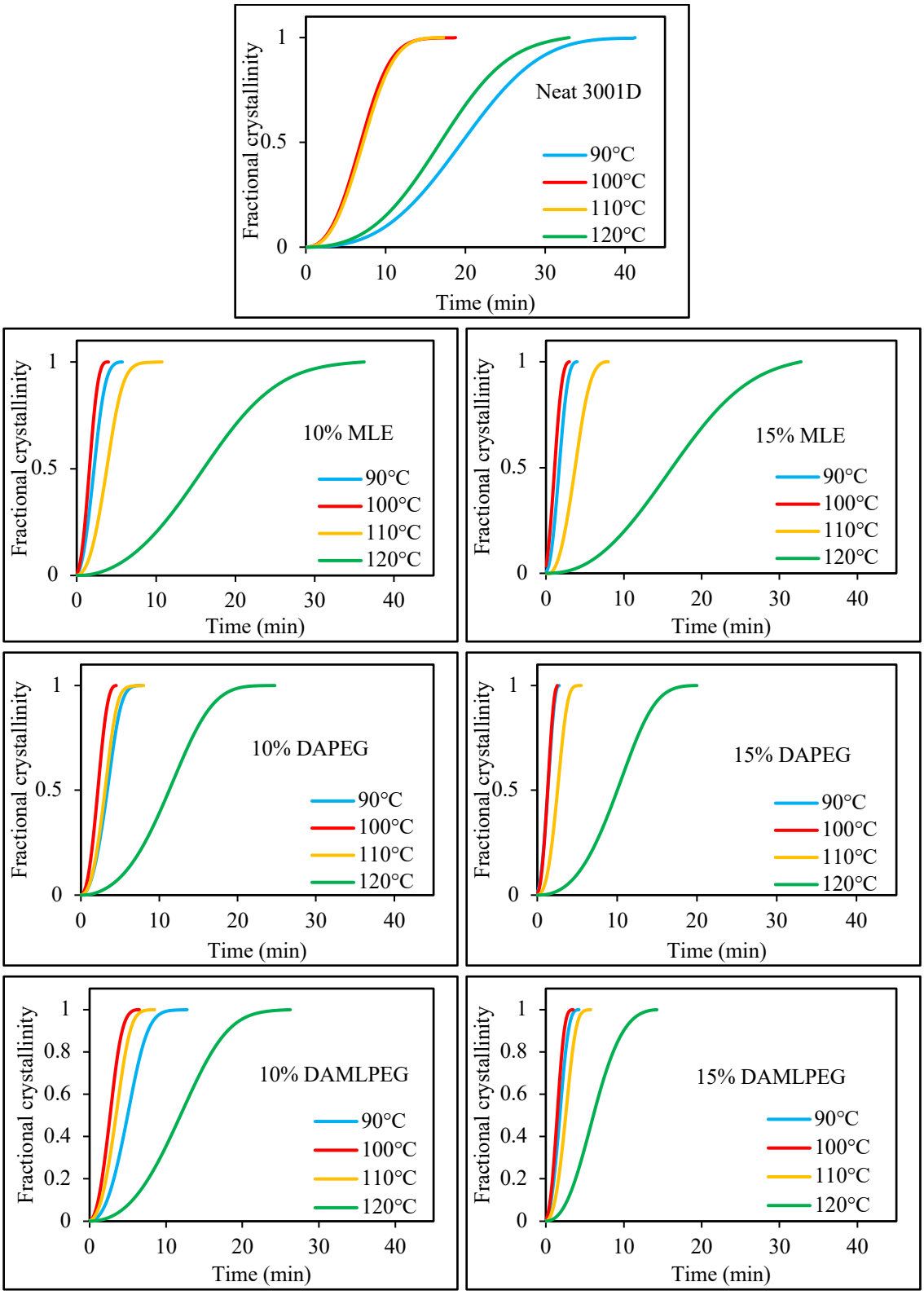


Figure 6-22: Change in fractional crystallinity of modified PLA samples with time at different isothermal temperatures

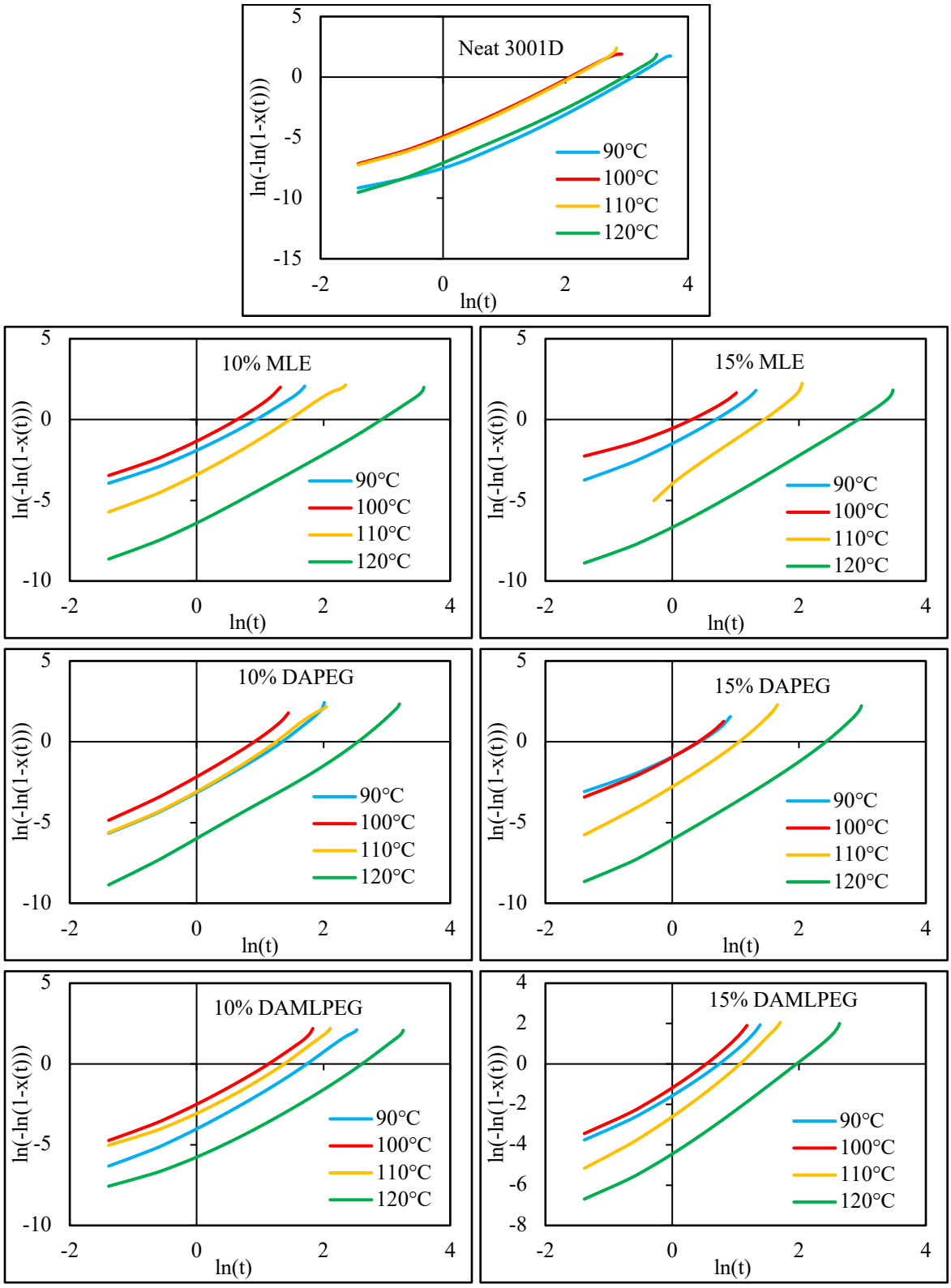


Figure 6-23: Avrami double-log plots for the melt crystallization kinetics of samples at different isothermal temperatures

The half time for crystallization corresponds to the time when the fractional crystallinity is 0.5. The half time ($t_{1/2}$) for all samples at different isothermal temperatures was calculated and is reported in Table 6-6. It was observed that $t_{1/2}$ reduces to 1 min for 15% MLE, 1.25 min for 15% DAPEG, and 1.5 min for 15% DAMLPEG resins at 100°C isothermal temperature.

Table 6-6: Isothermal melt crystallization half times and Avrami constants for modified PLA

Sample	Temperature (°C)	n	$t_{1/2}$ (min)	ln k	k
Neat 3001D	90°C	2.55	19.5	-7.8906	3.74E-04
	100°C	2.36	7	-4.8604	7.75E-03
	110°C	2.44	7.25	-5.0532	6.39E-03
	120°C	2.50	16.75	-7.3612	6.35E-04
10% MLE	90°C	2.00	2.25	-1.7391	1.76E-01
	100°C	2.04	1.5	-1.1238	3.25E-01
	110°C	2.29	3.75	-3.2872	3.74E-02
	120°C	2.27	16	-6.5621	1.41E-03
15% MLE	90°C	2.08	1.75	-1.2957	2.74E-01
	100°C	1.60	1	-0.3745	6.88E-01
	110°C	2.50	3.75	-3.8489	2.13E-02
	120°C	2.32	16.25	-6.7691	1.15E-03
10% DAPEG	90°C	2.40	3.25	-3.0614	4.68E-02
	100°C	2.35	2.25	-2.0204	1.33E-01
	110°C	2.45	3	-2.9365	5.31E-02
	120°C	2.52	11.25	-6.2707	1.89E-03
15% DAPEG	90°C	1.56	1.25	-1.2201	2.95E-01
	100°C	2.11	1.25	-0.7732	4.62E-01
	110°C	2.67	2.5	-6.2159	2.00E-03
	120°C	2.61	10	-6.2159	2.00E-03
10% DAMLPEG	90°C	2.34	5	-3.9711	1.89E-02
	100°C	2.20	2.75	-2.34	9.63E-02
	110°C	1.97	3.5	-2.8188	5.97E-02
	120°C	1.95	13.75	-6.5959	1.37E-03
15% DAMLPEG	90°C	2.08	1.75	-1.371	2.54E-01
	100°C	2.32	1.5	-1.1002	3.33E-01
	110°C	2.42	2.5	-2.4339	8.77E-02
	120°C	2.27	6	-4.3974	1.23E-02

In previous literature, the decrease in the $t_{1/2}$ of semi-crystalline PLA to 1-1.5 min was reported

with addition of 1% of talc with 5% of PEG or 1% of talc with 5% of acetyl triethyl citrate (ATC) [156]. However, in our system, the decrease in the half-time for crystallization was observed without adding any nucleating agents.

The Avrami analysis as shown in Figure 6-23 and Table 6-6 confirmed two-dimensional crystal growth as n was around 2-2.5 [154]. Thus, it can be concluded that polyols were acting as a nucleating agent. The k values as shown in Table 6-6 were high for modified PLA resins containing 15% of polyols indicating faster nucleation and crystal growth at those conditions.

6.3.9 Effect of lower concentrations of polyols on performance properties of PLA

The addition of 10% of DAMLPEG and DAPEG polyols showed an increase in the mechanical as well as thermal properties. Thus, the effect of their lower concentration of polyols on mechanical properties of PLA was studied. The 10% DAMLPEG resin was added to neat PLA in a concentration of 10% and 50%. The samples obtained contain 1% and 5% of polyol and were labelled as 10% DAMLPEG-1% and 10% DAMLPEG-5%, respectively. Similarly, samples obtained from 10% DAPEG resin were labelled as 10% DAPEG-1% and 10% DAPEG-5%. Since, the addition of MLE-529 polyol did not improve the properties of PLA at a concentration of 10 - 15%, its lower concentrations in PLA were not studied.

6.3.9.1 Gel Permeation Chromatography (GPC)

The molecular weight distribution of neat PLA, and modified PLA containing 1 - 5% of polyols are given in Table 6-7. The injection-molded test bars were used as a sample for molecular weight measurements. The number average (M_n) and weight average molecular weight (M_w) of neat PLA and modified PLA were very close. No significant decrease in the molecular weight was observed for samples containing 1 - 5% of polyol. The polydispersity index was around 1.6 - 1.7 for all samples.

Table 6-7: Molecular weight distribution of neat PLA, and modified PLA containing 1% and 5% of polyols

Sample	M_n (g/mol)	M_w (g/mol)	PDI
Neat 3001D	91563 ± 4803	157383 ± 2322	1.72 ± 0.06
10% DAMLPEG-1%	95347 ± 2197	152598 ± 1094	1.71 ± 0.04
10% DAMLPEG-5%	92071 ± 4309	152518 ± 2676	1.66 ± 0.07
10% DAPEG-1%	92713 ± 2635	155389 ± 1225	1.68 ± 0.04
10% DAPEG-5%	90422 ± 5597	144460 ± 2519	1.60 ± 0.07

6.3.9.2 Thermal properties

The TGA graphs of neat PLA and modified PLA test bars are shown in Figure 6-24. The degradation temperature of neat PLA decreases with an increase in the concentration of polyols.

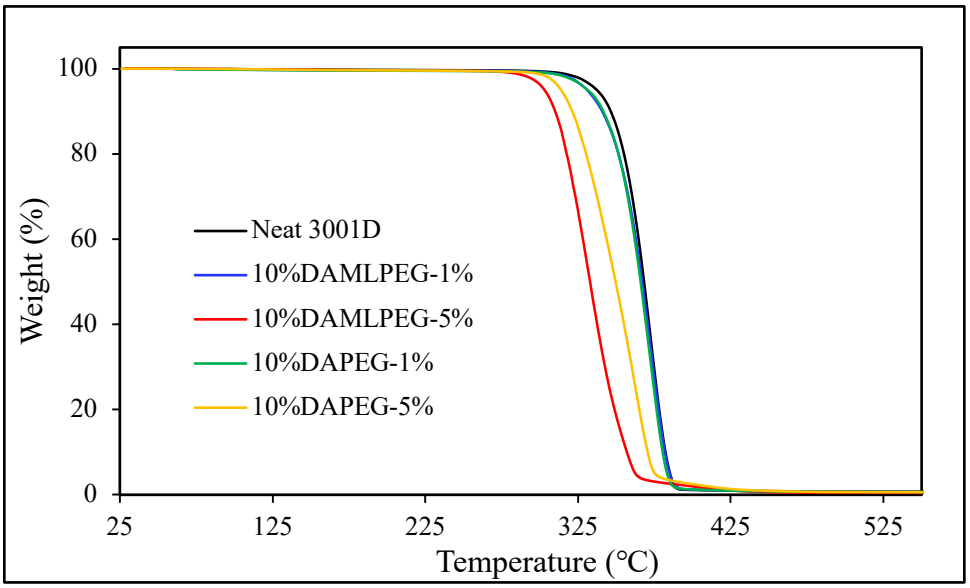


Figure 6-24: TGA graphs of modified PLA test bars containing 1% and 5% of polyols

The DSC thermograms of neat PLA and other modified PLA test bars are given in Figure 6-25. The addition of 1% of polyol reduced the glass transition temperature and crystallinity of PLA slightly as shown in Table 6-8. The modified PLA containing 5% of polyol reduced the glass transition temperature by 6 - 7°C and increased the crystallinity of PLA to 12 - 15%. Increase in

the crystallization temperature was observed with the addition of 1% of polyol compared to the neat PLA. However, the crystallization temperature decreased with the addition of 5% of polyol compared to neat PLA.

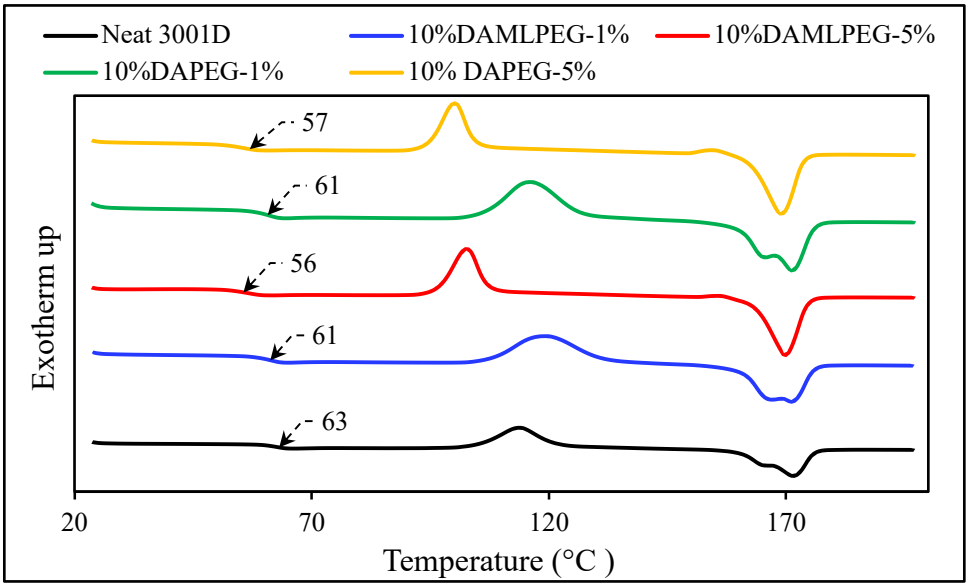


Figure 6-25: DSC thermograms of modified PLA test bars containing 1% and 5% of polyols

Table 6-8: Thermal transition and crystallinity of modified PLA test bars containing 1% and 5% of polyols

	T_g (°C)	T_{cc} (°C)	T_m (°C)	ΔH_{cc} (J/g)	ΔH_m (J/g)	Crystallinity (%)
Neat 3001D	63.4	113.7	171.6	27.5	34	6.9
10% DAMLPEG-1%	61.5	119.6	171.2	39	40.9	2
10% DAMLPEG-5%	56.5	102.7	169.8	29	40.1	12.5
10% DAPEG-1%	61.1	115.9	171.4	28.9	33.2	4.6
10% DAPEG-5%	57.0	110.1	169	28.9	43	15.8

The DSC thermograms of annealed test bars of neat PLA and modified PLA containing 1% and 5% of polyols are shown in Figure 6-26. The analysis is given in Table 6-9. The annealing process increases the crystallinity of PLA which might improve its mechanical properties. The annealed test bars of neat and modified PLA showed crystallinity of 50%.

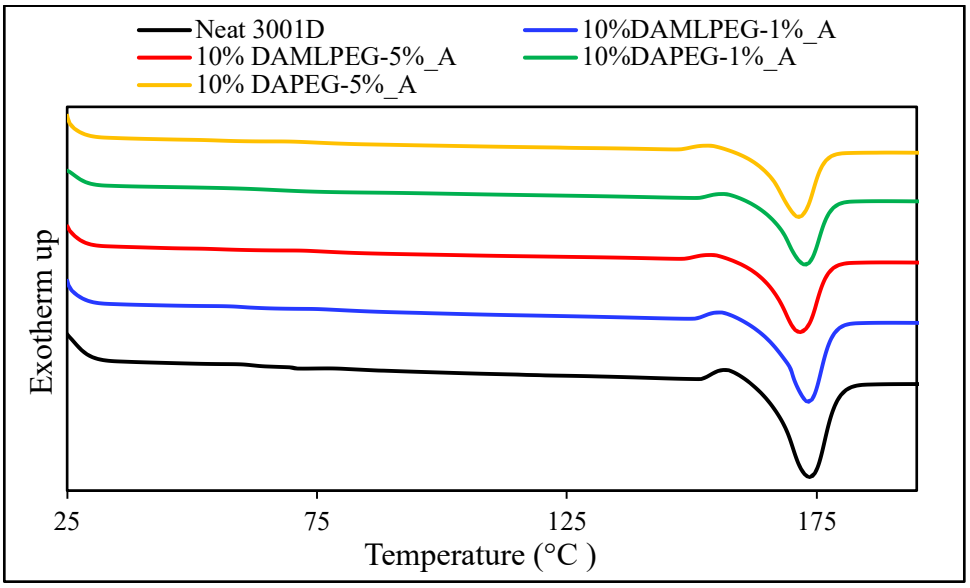


Figure 6-26: DSC thermograms of modified PLA test bars containing 1% and 5% of polyols – Annealed

Table 6-9: Thermal transition and crystallinity of modified PLA test bars containing 1% and 5% of polyols - Annealed

	T_g (°C)	T_m (°C)	ΔH_{cc} (J/g)	ΔH_m (J/g)	Crystallinity (%)
Neat 3001D	61.7	173.5	0	49.4	52.7
10% DAMLPEG-1%	59.6	173.3	0	50.0	53.9
10% DAMLPEG-5%	56.0	171.6	0	47.1	52.9
10% DAPEG-1%	67.0	172.7	0	44.0	47.4
10% DAPEG-5%	55.0	171.3	0	48.0	53.9

6.3.9.3 Mechanical properties

The stress-strain curves of modified PLA samples containing 1% and 5% of polyols are shown in Figure 6-27. The addition of 1% of DAMLPEG and DAPEG polyols had a negligible effect on tensile properties. Addition of 5% of DAMLPEG and DAPEG polyols showed increased strain without significantly reducing the tensile stress at yield. The strain at break increases after annealing which is unusual as compared to the previous results where strain decreased after

annealing.

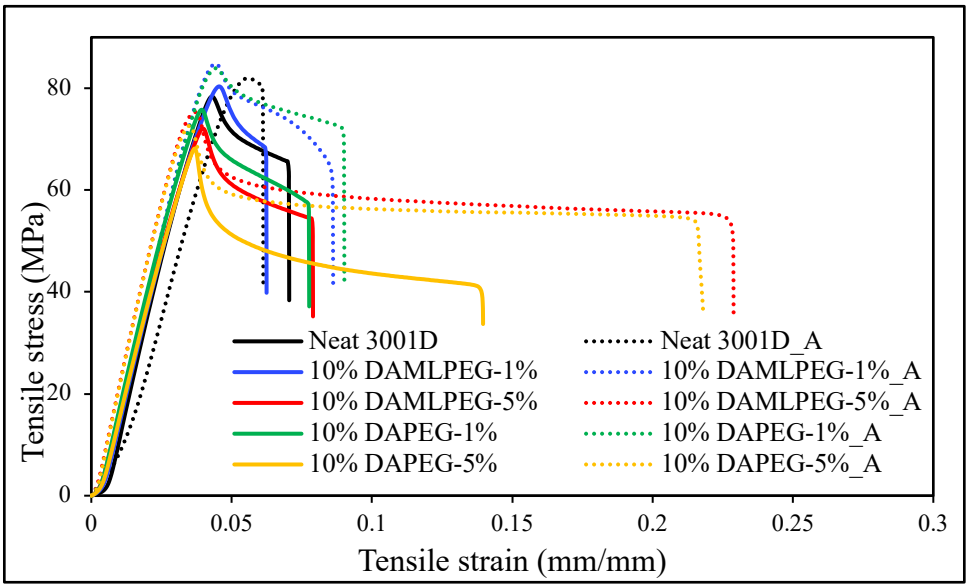


Figure 6-27: Stress-strain curves of modified PLA containing 1% and 5% of polyols

The tensile modulus and tensile stress at yield of modified PLA samples containing 1% and 5% of DAPEG and DAMLPEG polyols are shown in Figure 6-28 and Figure 6-29.

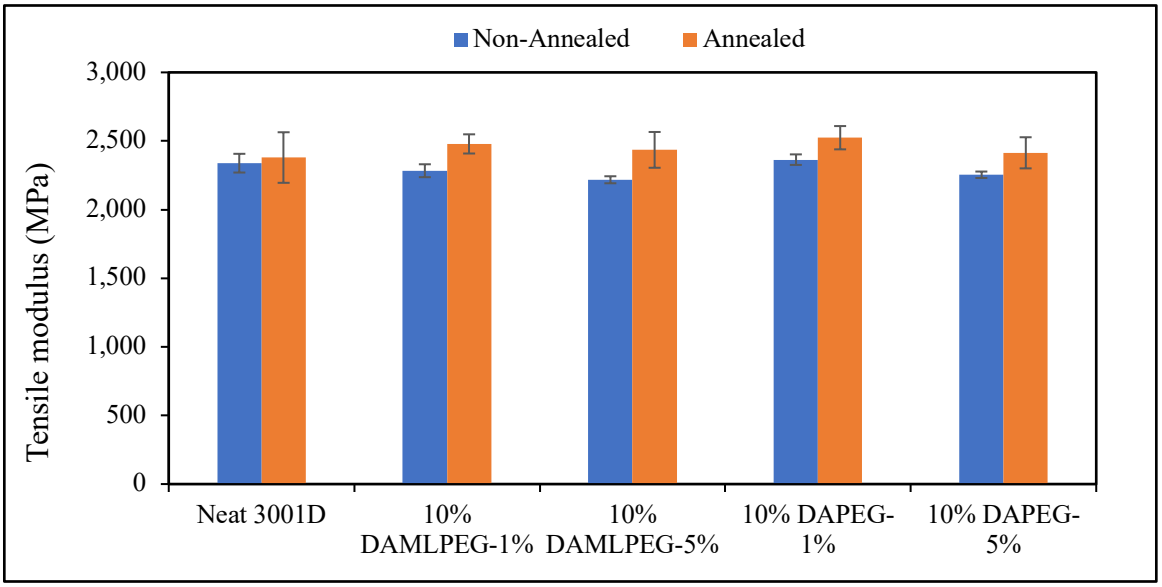


Figure 6-28: Modulus of modified PLA samples containing 1% and 5% of polyols

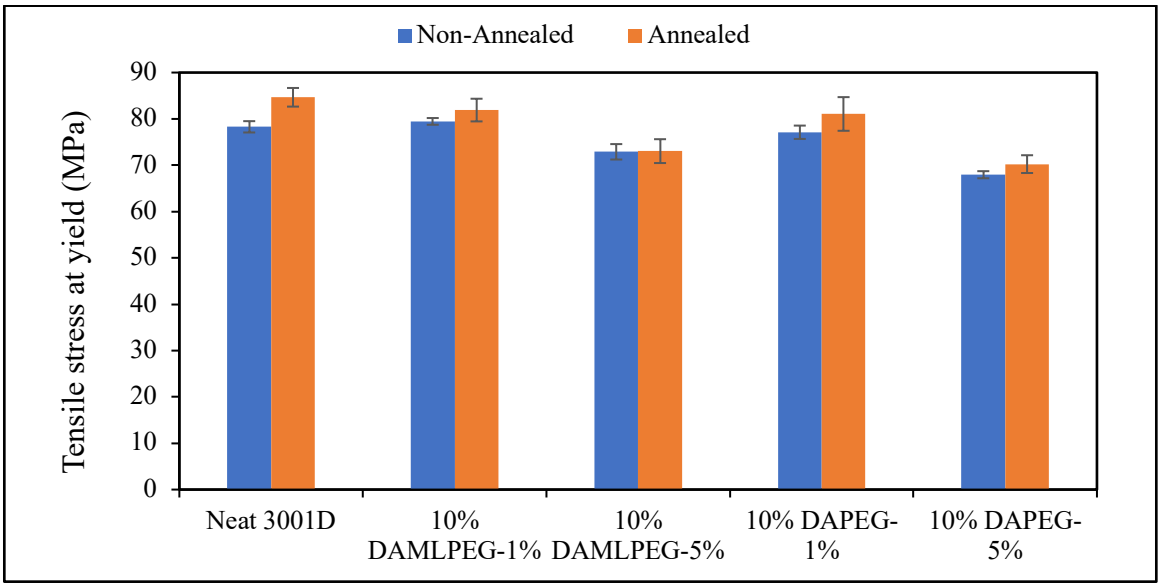


Figure 6-29: Tensile stress at yield of modified PLA containing 1% and 5% of polyol

The tensile modulus, as well as tensile stress at yield, remains unchanged with the addition of 1% of polyols. However, modulus and tensile stress at yield decreased slightly with the addition of 5% of polyols. The tensile strain remains unaffected with the addition of 1% of polyols as shown in Figure 6-30. Tensile strain increased to 15% from 5% with the addition of 5% of DAPEG polyol. However, after annealing the tensile strain increased to 25% and 20% with the addition of 5% of DAMLPEG and DAPEG polyols, respectively. The impact strength of modified PLA samples remained unaffected after addition of 1% and 5% of polyols as shown in Figure 6-31. The impact properties of modified PLA samples containing 5% of polyol slightly improved after annealing as compared neat PLA. It can be seen from Figure 6-13 and Figure 6-31 that impact strength of non-annealed samples was slightly increased after increasing the concentration of DAPEG or DAMLPEG polyols from 1% (2.5 kJ/m^2) to 15% (4 - 5 kJ/m^2). But the impact strength of annealed samples increased significantly with increasing concentration of DAPEG or DAMLPEG polyols from 1% (4 - 5 kJ/m^2) to 15% (10 - 16 kJ/m^2). The increase in the impact strength after annealing could be due to the increase in the modifier domain size with increasing concentration of polyols.

These modifier domains could be acting as a toughening agent in the amorphous region thereby increasing the impact strength.

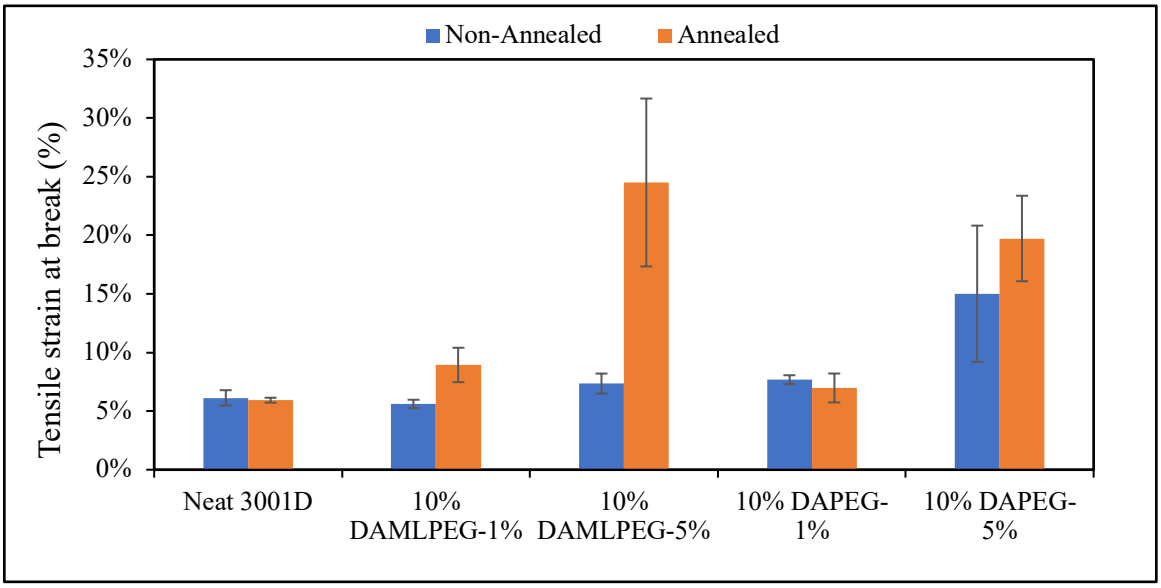


Figure 6-30: Tensile strain at break of modified PLA samples containing 1% and 5% of polyols

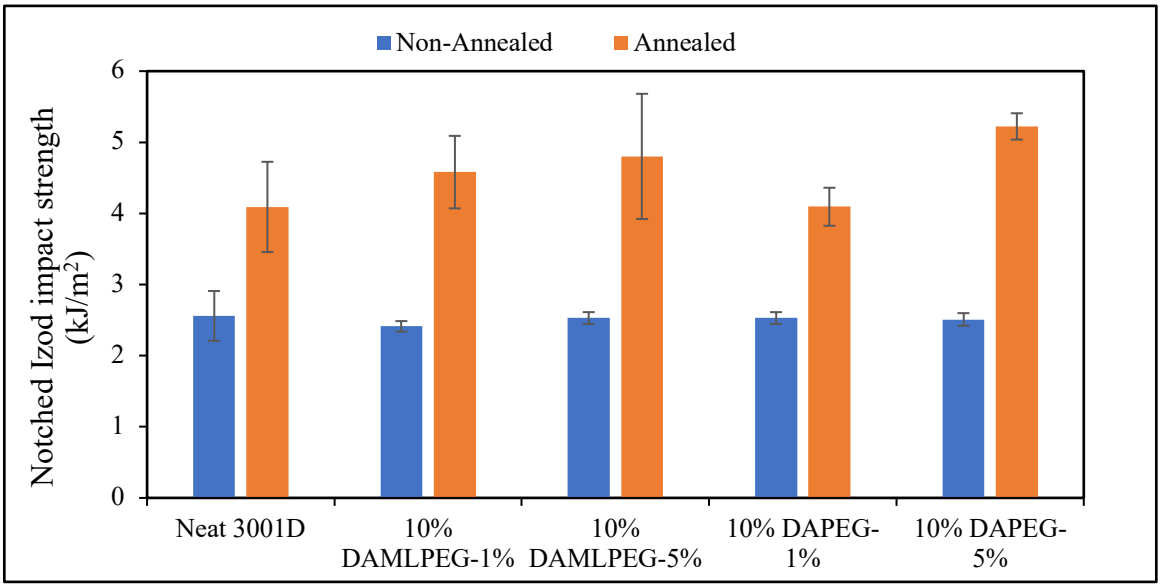


Figure 6-31: Notched Izod impact strength of modified PLA samples containing 1% and 5% of polyols

6.3.9.4 Scanning Electron Microscopy (SEM) images

The SEM images of tensile fractured samples are shown in Figure 6-32. The SEM images of non-annealed neat PLA and modified PLA tensile fractured samples showed brittle fracture as it has a smooth surface. After annealing, the neat PLA sample showed some rough surface. However, the 10% DAMLPEG-5%_A and 10% DAPEG-5%_A samples showed rough surface indicating a ductile fracture. During annealing, the crystallization of PLA would push the other components from its position [148]. This induces the phase migration and coalescence of modifier domains in the amorphous region causing “brittle to ductile” transition [148].

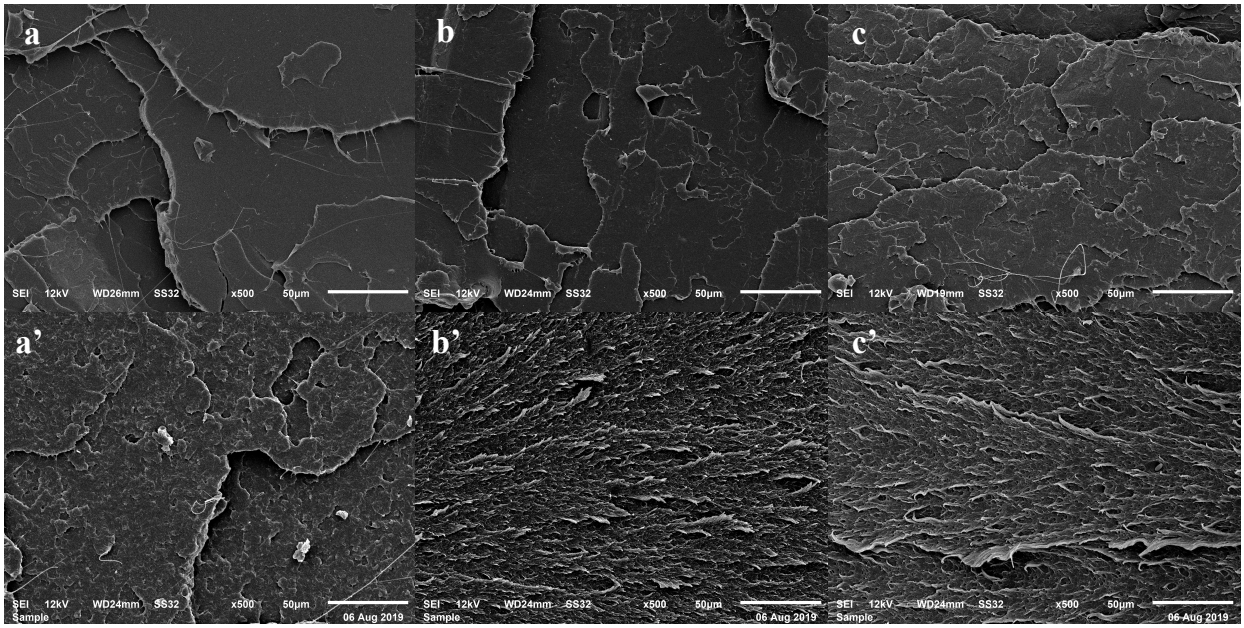


Figure 6-32: SEM images of tensile fractured surfaces of (a) Neat 3001D (a’) Neat 3001D_A (b) 10% DAMLPEG-5% (b’) 10% DAMLPEG-5%_A (c) 10% DAPEG-5% (c’) 10% DAPEG-5%_A

The SEM images of the impact fractured samples are shown in Figure 6-33. All non-annealed samples showed smooth surface and mackerel pattern on the fractured surfaces indicating low impact strength. However, the surface roughness increased after annealing which can be correlated

to the increase in impact strength after annealing.

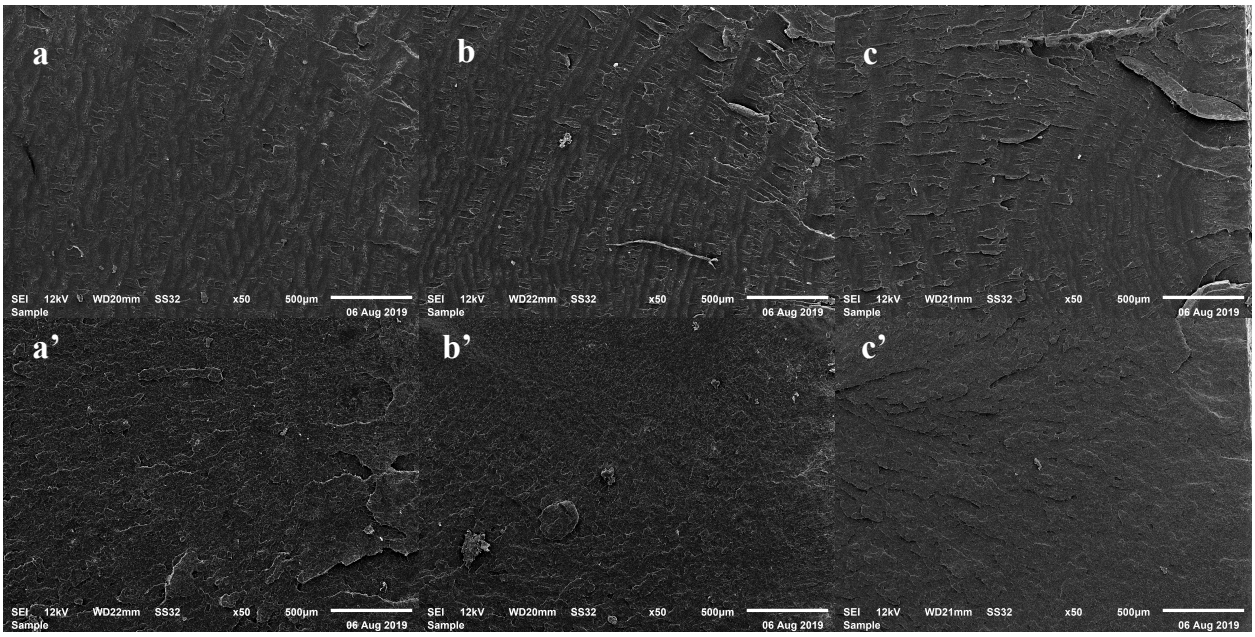


Figure 6-33: SEM images of impact fractured surfaces of (a) Neat 3001D (a') Neat 3001D_A (b) 10% DAMLPEG-5% (b') 10% DAMLPEG-5%_A (c) 10% DAPEG-5% (c') 10% DAPEG-5%_A

6.3.9.5 Dynamic Mechanical Analysis (DMA)

The storage moduli of modified injection-molded samples containing 1% and 5% of polyols are given in Figure 6-34. The storage moduli of all samples decreased around their glass transition temperature which is around 52 - 56°C. After annealing, the increase in the storage moduli was observed for all samples which is due to the increase in the crystallinity. The loss moduli of injection-molded samples containing 1% and 5% of polyols are shown in Figure 6-35. The peak of loss moduli curves shifts towards lower temperature with an increase in the concentration of polyols. Addition of 1% of polyol decreases the peak temperature by 2°C and addition of 5% of polyol decreases the peak temperature by 6°C. This peak temperature for modified PLA samples increased after annealing but it was lower than that of neat PLA.

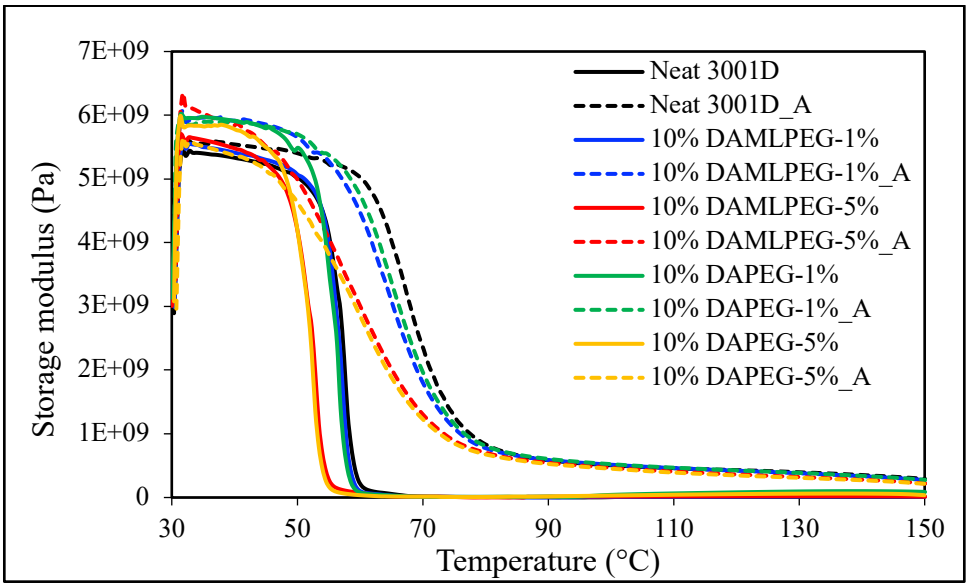


Figure 6-34: Storage modulus of modified PLA injection molded samples containing 1% and 5% of polyols

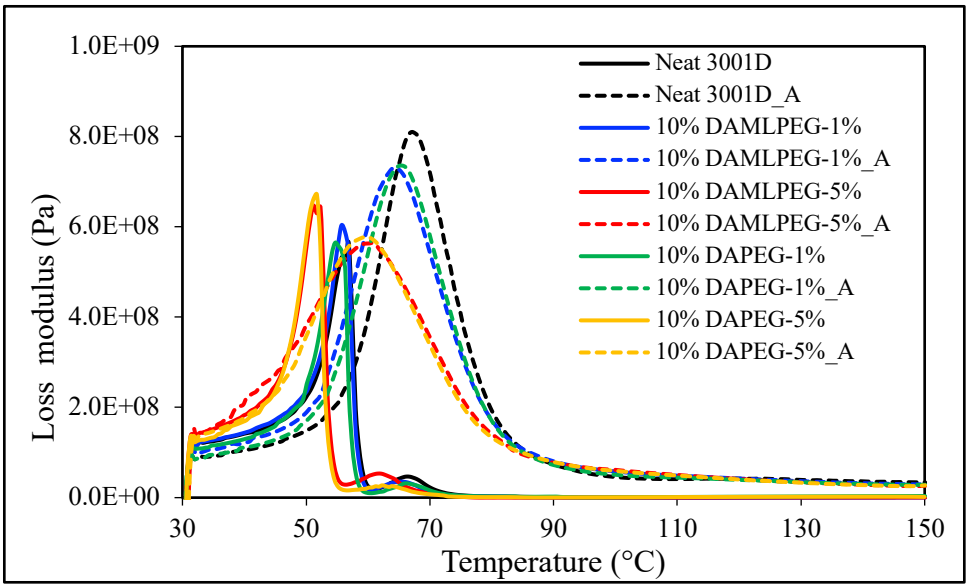


Figure 6-35: Loss modulus of modified PLA injection molded samples containing 1% and 5% of polyols

The Tan δ curves for injection molded samples are shown in Figure 6-36. The Tan δ curves for all samples showed one small peak which is close to the glass transition temperature of samples. The

area under Tan δ curves decreased after annealing due to the decrease in damping ability with an increase in the crystallinity.

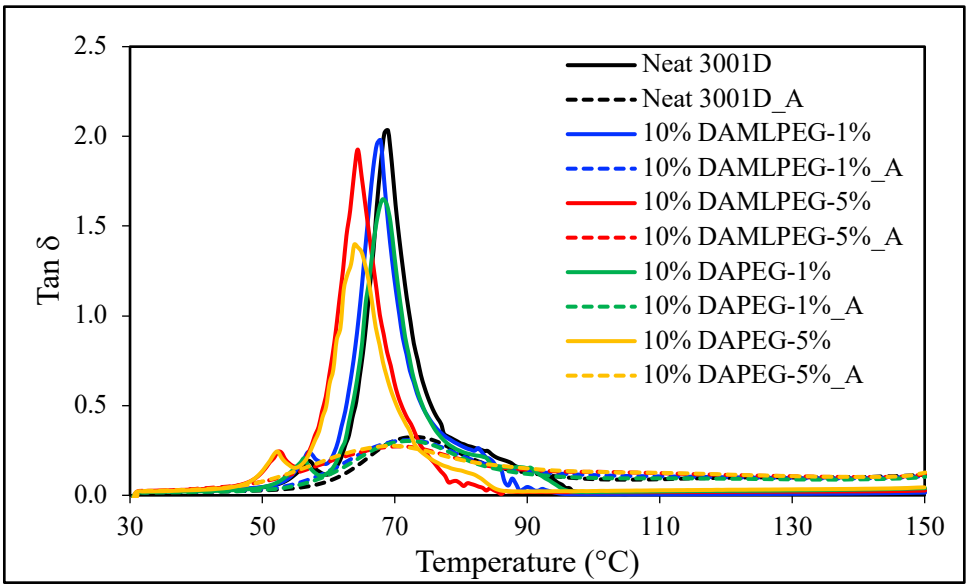


Figure 6-36: Tan δ of modified PLA injection molded samples containing 1% and 5% of polyols

6.4 CONCLUSION

The addition of biobased polyols into the PLA matrix showed plasticization as well as nucleation effect. The reactive blending of DAPEG-94 and DAMLPEG-7-81 polyols with PLA showed improvement in the thermal properties. The decrease in the glass transition temperature was observed with increasing concentration of DAPEG-94 and DAMLPEG-7-81 polyols. The addition of 15% of polyols decreased the glass transition temperature to 46 - 47°C. The crystallinity decreased slightly with the addition of 1% of polyols and increased with increasing weight percent of polyol from 5 - 15%. The crystallinity of modified PLA containing 15% of polyols were around 50%. The addition of MLE-529 polyol did not show a significant effect on thermal properties.

The improvement in the mechanical properties was observed with the addition of DAPEG-94 and DAMLPEG-7-81 polyols. The addition of 1% of polyol did not change the mechanical properties of PLA significantly. However, a decrease in the tensile moduli and tensile stress at yield was

observed with increasing concentration of polyols from 5 to 15%. As these polyols were acting as a plasticizer, a decrease in tensile strength at yield was expected. The elongation at break increased slightly with the addition of 1 - 5% of polyol, but it was increased to 120% with the addition of 10 - 15% of DAPEG-94 and DAMLPEG-7-81 polyols. The impact strength of modified PLA resins increased slightly with increasing concentration of polyols from 1 to 15%.

The thermal annealing of these samples showed an interesting trend in the performance properties. The elongation at break decreased after annealing from 120% to 55% for 10% DAPEG and 10% DAMLPEG resins. But elongation at break increased from about 10 - 15% to about 25% after annealing of modified PLA samples containing 5% of DAMLPEG or DAPEG polyols. The annealing process increased the tensile moduli and tensile stress at yield. The impact strength of annealed modified PLA samples showed a significant improvement with increasing polyol concentration from 5% to 15%. This could be due to the increase in the crystallinity and formation of larger modifier domains via coalescence after annealing. The increase in the polyol concentration could be increasing the size of modifier domains thereby improving the impact strength as modifier domains sustain the local stress. The tensile strain at break increased after annealing for modifier PLA containing 5% of polyol. This could be due to the coalescence of modifier in the amorphous region causing “brittle to ductile” transition. However, a decrease in the tensile strain was observed after annealing with increasing concentration of polyol to 10 - 15%. This could be due to the formation of larger modifier domains in the amorphous region affecting the tensile toughness. Thus, the increase in tensile strain after annealing was observed only up to 5% of polyol concentration. However, the tensile strain after annealing for modified PLA containing 10 - 15% of polyol was still higher than that of neat PLA.

The melt crystallization kinetics studied using Avrami analysis showed 2-dimensional growth of

crystals for all samples. Also, it was observed that polyols were acting as a nucleation site decreasing the total crystallization time. The SEM images of the tensile fractured samples showed a smooth surface for neat PLA indicating a brittle fracture. Whereas, SEM images of the tensile fractured samples containing 10 - 15% of polyol showed a rougher surface indicating a ductile fracture. The surface roughness increased after annealing indicating a ductile fracture after annealing. The SEM images of the impact fractured surfaces showed a “mackerel pattern” on non-annealed samples. However, the surface roughness increased after annealing indicating higher energy to break and a ductile fracture. The peak of loss moduli shifted to a lower temperature with increasing the concentration of polyols. Thus, the dimer acid-based polyols act as a nucleating agents, plasticizers, and impact modifiers for PLA.

7 SUMMARY AND FUTURE WORK

This work was focused on the engineering of value-added industrial products from co-products of biorefineries and bioplastics industries. As polyurethane has a variety of uses and polyol being one of its major components, our research was mainly targeted on the synthesis of biobased polyols. This study highlights the use of simple reaction chemistries, one-pot synthesis process, and inexpensive raw materials for cost-effective biobased polyols production. The raw materials were used without any purification and the overall synthesis process does not generate any waste. To demonstrate the feasibility of these biobased polyols in polyurethane foams, the performance properties of biobased polyurethane foams were evaluated against commercial polyurethane foams.

In the second chapter, the composition of soymeal was determined by separating soluble carbohydrates using the ethanol-water solution. Proteins and carbohydrates degrade over a wide range of temperatures which were obtained from previous literature. After obtaining the peak degradation temperatures for proteins and carbohydrates, the deconvolution of DTG graphs of soluble carbohydrates and ethanol washed soymeal was done. This combined technique can be applied to any other protein-carbohydrate residues to determine the composition of components. If the degradation temperatures of the two components are very close it is very difficult to find their exact composition. This technique can give approximate compositions of each component. The composition of soymeal was studied because its protein content may vary based on the species or location where it is grown. The polyol from soymeal was synthesized by adopting a two-step process: transamidation followed by ring-opening reaction with carbonates. In the transamidation step, the soymeal was converted to amine derivatives containing a majority of hydroxylamine. In the subsequent ring-opening step, amine derivatives were converted to the soymeal polyol which

was majorly comprised of primary hydroxyl groups. The insoluble soymeal content in the soymeal polyol was less than 2% which confirmed that all constituents of soymeal were taking part in the reaction except probably insoluble carbohydrates. Also, it was found that the primary amino groups were breaking peptide linkages of proteins and the resultant product was soluble in the reaction mixture. The soymeal polyol itself has amide linkages, as well as urethane linkages, which are less prone to degradation by hydrolysis or UV-radiation. The commercially available polyols contain ether or ester linkages. The hydroxyl value of the polyol can be reduced by using long chain amino-alcohol or diamines like biobased hexamethylene diamine (HMDA). Also, other protein carbohydrate residues like DDGS and algae residue can be used instead of soymeal. The material cost of soymeal polyol is ~0.6 - 0.7 $/lb which could be a driving force for its commercialization.

In the third chapter, a side product of the PLA manufacturing process, meso-lactide, was used for the synthesis of biobased building blocks. The diols were synthesized using ring-opening of meso-lactide with primary amines and hydroxyl groups. The ring-opening reaction of meso-lactide with amines was exothermic and faster, while with hydroxyl group it was endothermic and slower. The diols containing amide linkages could be used in the synthesis of a new biobased polyester-amide polymer and polyurethanes. The hydroxyl value of these polyols was quite high for flexible polyurethane foam application. The polycondensation chemistry was used to reduce the hydroxyl value by reacting diols with biobased dimer acids. Two different reactant ratios produced polyols with different molecular weight and hydroxyl value. These polyols currently have 50 - 70% renewable carbon content since dimer acid and meso-lactide were biobased but ethanolamine and PEG-400 were petroleum-based. However, biobased PEG-400 is commercially available which will increase the renewable carbon content to 100%. The material cost for these polyols is around

0.6 - 0.8 $/lb and the synthesis procedure is simple. Thus, these polyols can compete with commercially available polyols with suitable applications in polyurethanes like coatings or foam. The presence of long carbon chain in the polyol might give enough flexibility in the final polymer. These polyols can also be used as a plasticizer for stiff polymers like polylactide (PLA). PLA waste (cutlery or bags) can be recycled back to lactide and used as a starting material for the synthesis of polyols. PLA waste can also be converted to diols by reacting it with amino-alcohols. This will lower the raw material cost and also reduce the carbon footprint. Also, dimer acids derived from soybean were used for polycondensation chemistry, but any long-chain dimer or trimer acids can be used.

The fourth chapter mainly focuses on demonstrating the use of biobased polyols synthesized from lactide and soymeal in rigid polyurethane foams. The soymeal and lactide polyol have amide linkages which might give additional thermal stability to the PUF produced from them. The soymeal polyol foams (SPF) and lactide polyol foams (LPF) showed compressive strength close to the control PUF. The thermal conductivity of PUF which is very important for heat insulation application did not change with the addition of biobased polyols. The scanning electron microscopy images of SPF and LPF showed closed-cell structure indicating better insulation. The aging study on PUF showed a negligible change in mass and dimensions. Also, water absorption by PUF over a period of three weeks was less than 4 - 5%. Thus, it can be concluded that rigid PUF synthesized from biobased polyols showed properties comparable to the properties of PUF made from commercially available polyols. This concluded that the SPF and LPF foams can be used as an insulating material in building & construction, in electrical appliances, and in automotive industries.

The work in chapter five was again focused on demonstrating the use of biobased polyols with low

hydroxyl value for flexible polyurethane foam application. In the beginning, the formulation for biobased PUF was optimized by changing catalysts concentration. This was a very important and critical step in flexible polyurethane foam synthesis. The thermal degradation behaviour of all biobased PUF was better than commercial biobased PUF and petroleum-based PUF. A slight increase in the degradation temperature was observed with increasing biobased polyol content. The mechanical properties of biobased PUF synthesized were evaluated against properties of petroleum-based PUF and commercial biobased PUF. The SEM images of all flexible PUF showed an open cell structure which is required for cushioning application. The wet compression set was very important in terms of car seating application. The wet compression set decreased with the decrease in the hydroxyl value of a polyol. The PUF containing 50% of our biobased polyol passed the wet compression set test but PUF made from 40% of commercially available biobased polyol did not pass the wet compression set test. The tensile properties of PUF increased with increasing the biobased polyol content. The tear resistance for all biobased PUF increased with increase in the biobased polyol content. The tear resistance of foams made with our biobased polyols was higher than foams made with commercially available biobased polyol. A slight increase in the compressive properties was observed with increase in the biobased polyol content. In the end, miscibility study showed that polyols containing lactide component were completely miscible with petroleum-based Voranol 4701 even after 2 years. Whereas, commercial biobased polyol showed a slight phase separation within the first two weeks. Thus, dimer acid and meso-lactide based polyols showed better thermal and mechanical properties than control PUF.

In the last chapter, the concept behind the application of the polyol was completely different from the previous chapters by focusing on identifying alternate applications of these biobased polyols apart from PUF. The dimer acid-based polyols and lactide polyols were used as a plasticizer for a

stiff polymer i.e. PLA. The addition of biobased polyols into the PLA matrix showed plasticization as well as nucleation effect. The reactive blending of dimer acid-based polyols with PLA using extrusion process showed an improvement in the thermal properties as well as mechanical properties. The decrease in the glass transition temperature and increase in the crystallinity were observed with increasing the concentration of dimer acid-based polyols. The addition of lactide polyol did not show a significant effect on thermal properties. A decrease in the tensile moduli and tensile stress at yield was observed with increasing concentration of polyols from 5 to 15%. As these polyols were acting as a plasticizer, a decrease in tensile strength at yield was expected. The elongation at break increased slightly with the addition of 1 - 5% of polyol, but it was increased to 120% with the addition of 10 - 15% of dimer acid-based polyols. The impact strength of modified PLA resins increased slightly with increasing concentration of polyols from 1 to 15%. The thermal annealing was introduced to study effect of increased crystallinity on performance properties of modified PLA. The annealing of tensile and impact samples showed an interesting trend in the properties. The elongation at break decreased after annealing for modified PLA samples containing 10 - 15% of dimer acid-based polyols. But elongation at break increased after annealing for modified PLA samples containing 5% of dimer acid-based polyols. The impact strength of annealed modified PLA samples showed a significant improvement with increasing polyol concentration from 5% to 15%. This could be due to the increase in the crystallinity and formation of larger modifier domains via coalescence after annealing. The increase in the polyol concentration could be increasing the size of modifier domains thereby improving the impact strength. The increase in the tensile strain at the break after annealing for modifier PLA containing 5% of polyols could be due to the coalescence of modifier in the amorphous region causing “brittle to ductile” transition. However, the decrease in the tensile strain after annealing with an increasing

concentration of polyol to 10 - 15% could be due to the formation of larger modifier domains in the amorphous region thereby reducing the plasticization effect. Thus, the tensile strain after annealing can be improved only up to the certain concentration of polyol or certain particle size of modifier domain. However, the tensile strain after annealing for modified PLA samples containing 10 - 15% of polyols was still higher than neat PLA. The melt crystallization kinetics using Avrami analysis showed 2-dimensional growth of crystals for all samples. Also, it was observed that polyols were acting as a nucleation site decreasing the total crystallization time. The SEM images of the tensile fractured samples showed a smooth surface for neat PLA indicating a brittle fracture. Whereas, SEM images of the tensile fractured samples containing 10 - 15% of polyol showed a rougher surface indicating a ductile fracture. The surface roughness increased after annealing indicating a ductile fracture after annealing. The SEM images of the impact fractured surfaces showed a “mackerel pattern” on non-annealed samples. However, the surface roughness increased after annealing indicating higher energy to break and a ductile fracture. The heat deflection temperature shifted to a lower temperature with increasing the concentration of polyols. These dimer acid-based polyols can be used as plasticizers and impact modifiers for PLA. These modified PLA resins can be used in PLA film which might improve tensile and dart properties neat PLA films.

To conclude the entire work, a series of cost-effective, scalable, diverse applications-oriented, and most importantly biobased, polyols were synthesized using inexpensive bioresources that have a potential for commercialization.

APPENDIX

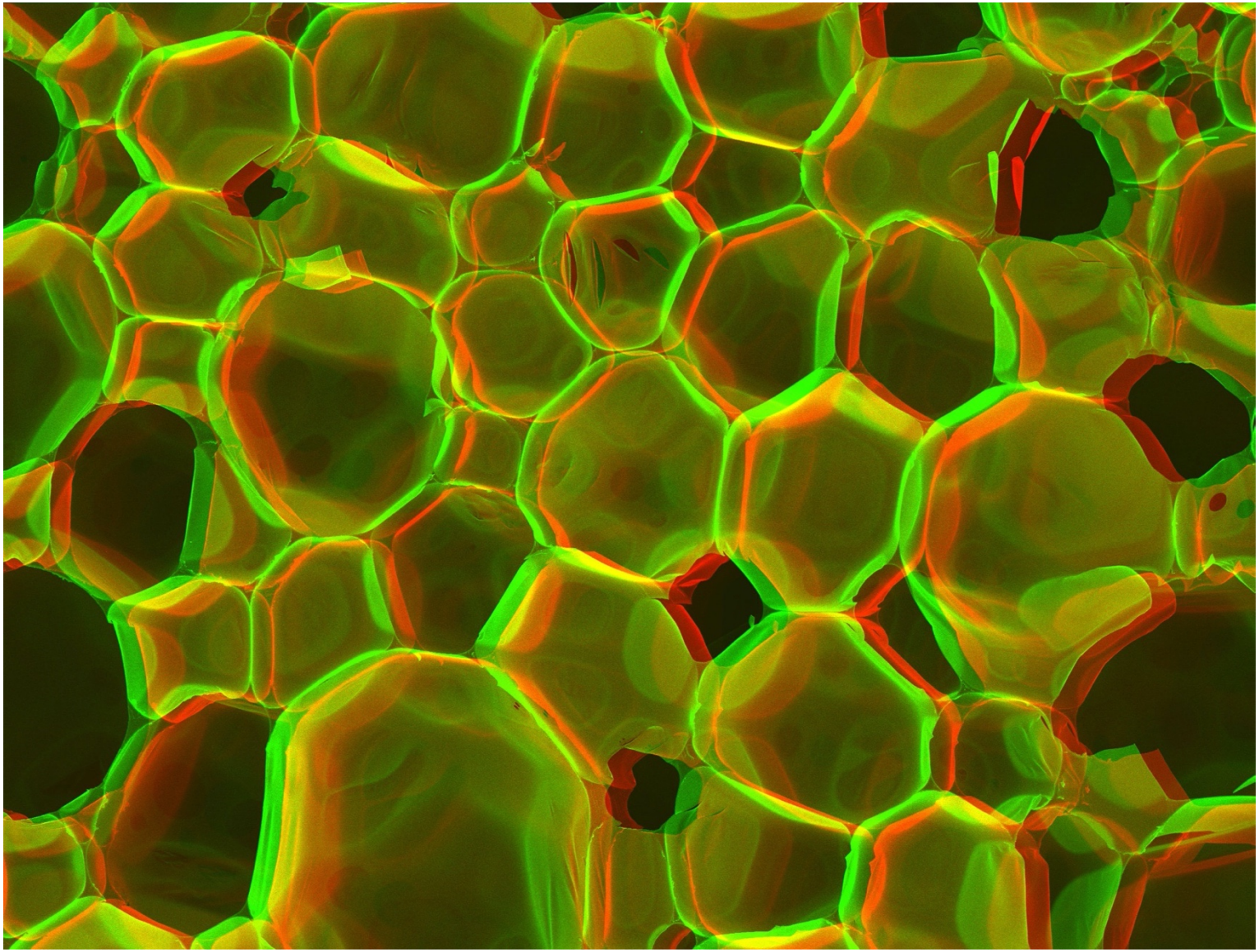


Figure A.1: 3D image of rigid closed cell polyurethane foam

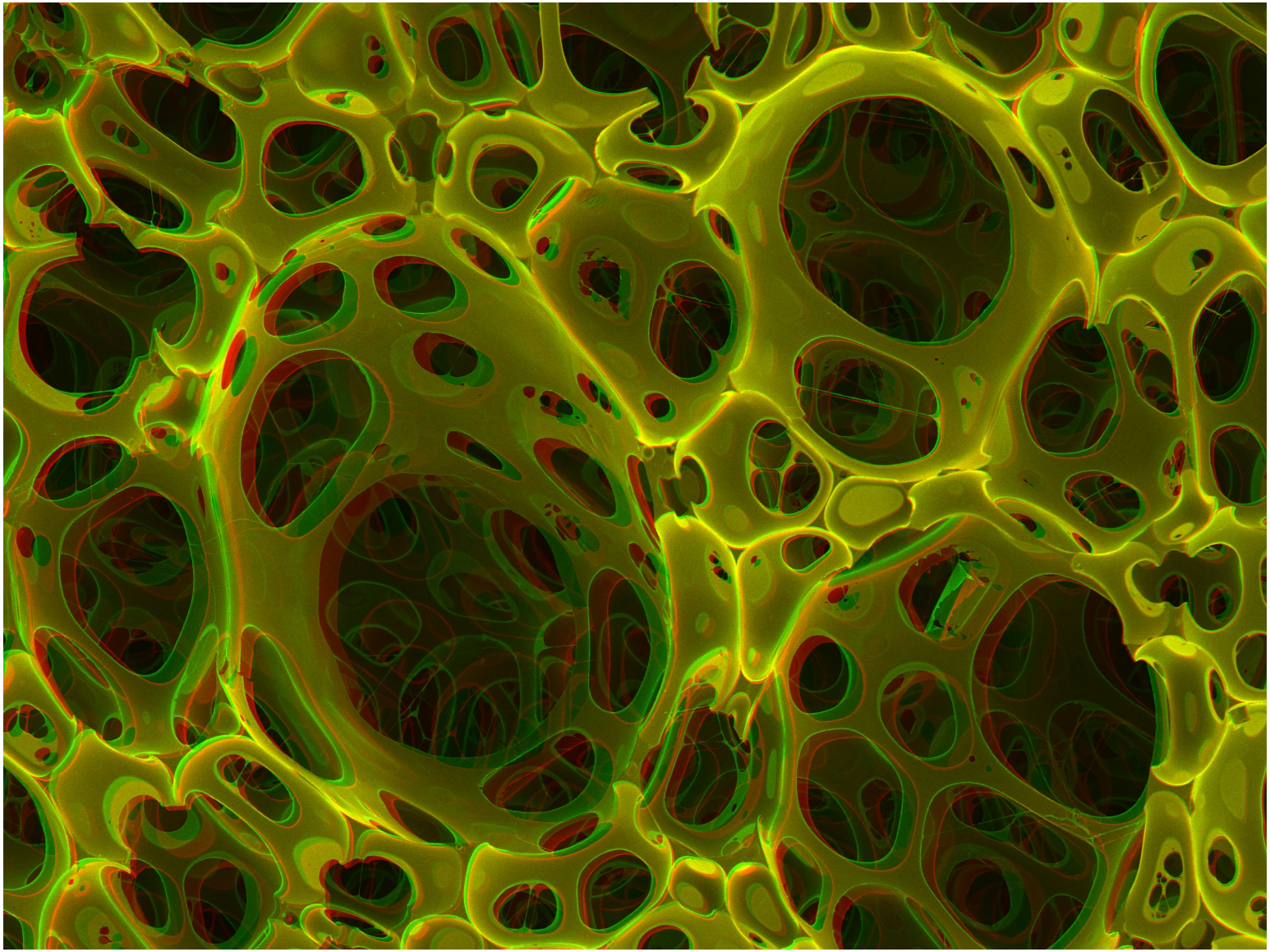


Figure A.2: 3D image of flexible open cell polyurethane foam

BIBLIOGRAPHY

BIBLIOGRAPHY

1. *United States Department of Agriculture*. [cited 2019 June]; Available from: https://www.dm.usda.gov/procurement/programs/biobased/awarenessbrochure_may2006.pdf.

2. *Bioplastic Feedstock Alliance*. [cited 2019 June]; Available from: https://bioplasticfeedstockalliance.org/.

3. *Crops*. August 20, 2019 [cited 2019 November, 17th]; Available from: https://www.ers.usda.gov/topics/crops/.

4. Cheng, M.-H., *Sustainability analysis of soybean refinery: soybean oil extraction process.* 2017.

5. Langhauser, L.H., *Corn refining process*. 2008, Google Patents.

6. Chalasani, S.R.K., *Efficient Green Synthetic Routes to Bio-based Polyurethanes from Soymeal*. 2014: Michigan State University. Packaging.

7. Graiver, D., K. Farminer, and R. Narayan, *Soybean-Based Polyols and Silanols.* Soy-Based Chemicals and Materials, RP Brentin, ed.(Washington, DC: American Chemical Society), 2014: p. 137-166.

8. *Oil Crops Sector at a Glance*. 2019 August 20, 2019 [cited 2019 November, 17th]; Available from: https://www.ers.usda.gov/topics/crops/soybeans-oil-crops/oil-crops-sector-at-a-glance/.

9. Kumar, R., et al., *Adhesives and plastics based on soy protein products.* Industrial crops and products, 2002. **16**(3): p. 155-172.

10. Liu, X., et al., *Transesterification of soybean oil to biodiesel using CaO as a solid base catalyst.* Fuel, 2008. **87**(2): p. 216-221.

11. Desroches, M., et al., *From vegetable oils to polyurethanes: synthetic routes to polyols and main industrial products.* Polymer Reviews, 2012. **52**(1): p. 38-79.

12. *Composition of Soy*. 2019 [cited 2019 June]; Available from: http://www.wishh.org/soy-resources/about-soy/soystats-publication/.

13. Cromwell, G., et al., *Variability among sources and laboratories in nutrient analyses of corn and soybean meal.* Journal of animal science, 1999. **77**(12): p. 3262-3273.

14. Morr, C., *Recalculated nitrogen conversion factors for several soybean protein products.* Journal of Food Science, 1982. **47**(5): p. 1751-1752.

15. Choct, M., et al., *Soy oligosaccharides and soluble non-starch polysaccharides: a review*

of digestion, nutritive and anti-nutritive effects in pigs and poultry. Asian-Australasian Journal of Animal Sciences, 2010. **23**(10): p. 1386-1398.

16. List, G., et al., *Hydrogenation of soybean oil triglycerides: Effect of pressure on selectivity.* Journal of the American Oil Chemists' Society, 2000. **77**(3): p. 311-314.

17. Paschke, R., L. Peterson, and D. Wheeler, *Dimer acid structures. The thermal dimer of methyl 10-trans, 12-trans, linoleate.* Journal of the American Oil Chemists' Society, 1964. **41**(11): p. 723-727.

18. Çavuş, S. and M.A. Gürkaynak, *Influence of monofunctional reactants on the physical properties of dimer acid-based polyamides.* Polymers for advanced technologies, 2006. **17**(1): p. 30-36.

19. *Fatty acids, C-18 Unsaturated, Dimers*. [cited 2019 June]; Available from: https://echa.europa.eu/registration-dossier/-/registered-dossier/16133.

20. Garlotta, D., *A literature review of poly (lactic acid).* Journal of Polymers and the Environment, 2001. **9**(2): p. 63-84.

21. Witzke, D.R., *Introduction to properties, engineering, and prospects of polylactide polymers.* 1999.

22. Auras, R., B. Harte, and S. Selke, *An overview of polylactides as packaging materials.* Macromolecular bioscience, 2004. **4**(9): p. 835-864.

23. Schneider, J.S., *Design of biobased and biodegradable-compostable engineered plastics based on poly (lactide)*. 2016: Michigan State University.

24. Narayan, R., W.-M. Wu, and C.S. Criddle, *Lactide Production from Thermal Depolymerization of PLA with applications to Production of PLA or other bioproducts*. 2013, Google Patents.

25. *Foam Insulation Comparison*. November, 2017 [cited 2019 June]; Available from: https://kpsglobal.com/blog/foam-insulation-comparison/.

26. *Polyurethane Insulation*. [cited 2019 June]; Available from: http://www.huntsman.com/polyurethanes/a/Products/Insulation.

27. Abraham, T.W., *Advances in the Use of BiOH® Polyols in Polyurethanes*, in *Biobased Monomers, Polymers, and Materials*. 2012, ACS Publications. p. 165-181.

28. *Polyurethane (Flexible Foam, Rigid Foam, Coatings, Adhesives, Sealants, and Elastomers) Market for Furniture, Building & Construction, Electronics, Automotive, Footwear, Packaging, Other Applications - Global Industry Perspective, Comprehensive Analysis, Size, Share, Growth, Segment, Trends and Forecast, 2014 - 2020*. 2016 [cited 2019 June]; Available from: https://www.marketresearchstore.com/report/polyurethane-market-z47737.

29. Barman, S., et al., *A copper based catalyst for poly-urethane synthesis from discarded motherboard.* RSC Advances, 2016. **6**(79): p. 75749-75756.

30. *Open cell vs Closed cell Foam*. [cited 2019 June]; Available from: https://www.thesleepjudge.com/open-cell-vs-closed-cell-foam/.

31. Chian, K. and L. Gan, *Development of a rigid polyurethane foam from palm oil.* Journal of Applied Polymer Science, 1998. **68**(3): p. 509-515.

32. Bello, A., et al., *Assessment and control of exposures to polymeric methylene diphenyl diisocyanate (pMDI) in spray polyurethane foam applicators.* International journal of hygiene and environmental health, 2019.

33. Zhang, S., et al., *Water-blown Castor oil-based polyurethane foams with soy protein as a reactive reinforcing filler.* Journal of Polymers and the Environment, 2018. **26**(1): p. 15-22.

34. Shrestha, M.L. and M. Ionescu, *Aliphatic–Aromatic Polyols by Thiol–Ene Reactions.* Journal of Polymers and the Environment, 2018. **26**(6): p. 2257-2267.

35. Lligadas, G., et al., *Plant oils as platform chemicals for polyurethane synthesis: current state-of-the-art.* Biomacromolecules, 2010. **11**(11): p. 2825-2835.

36. Campanella, A., L. Bonnaillie, and R. Wool, *Polyurethane foams from soyoil-based polyols.* Journal of Applied Polymer Science, 2009. **112**(4): p. 2567-2578.

37. Wang, C.S., et al., *Polyurethane networks from different soy-based polyols by the ring opening of epoxidized soybean oil with methanol, glycol, and 1, 2-propanediol.* Journal of applied polymer science, 2009. **114**(1): p. 125-131.

38. Tran, P., D. Graiver, and R. Narayan, *Ozone-mediated polyol synthesis from soybean oil.* Journal of the American Oil Chemists' Society, 2005. **82**(9): p. 653-659.

39. Li, Y., X. Luo, and S. Hu, *Introduction to Bio-based Polyols and Polyurethanes*, in *Bio-based Polyols and Polyurethanes*. 2015, Springer. p. 1-13.

40. Petrović, Z.S., *Polyurethanes from vegetable oils.* Polymer Reviews, 2008. **48**(1): p. 109-155.

41. Suresh, K.I., *Rigid polyurethane foams from cardanol: synthesis, structural characterization, and evaluation of polyol and foam properties.* ACS Sustainable Chemistry & Engineering, 2012. **1**(2): p. 232-242.

42. Ionescu, M., et al., *Polyols and rigid polyurethane foams from cashew nut shell liquid.* Journal of Polymers and the Environment, 2012. **20**(3): p. 647-658.

43. Li, X., et al., *Synthesis and application of a novel bio-based polyol for preparation of polyurethane foams.* New Journal of Chemistry, 2014. **38**(8): p. 3874-3878.

44. Kosmela, P., et al., *Biopolyols obtained via crude glycerol-based liquefaction of cellulose: their structural, rheological and thermal characterization.* Cellulose, 2016. **23**(5): p. 2929-2942.

45. Pawar, M.S., et al., *Synthesis and characterization of rigid polyurethane foams from algae oil using biobased chain extenders.* Polymer Bulletin, 2016. **73**(3): p. 727-741.

46. Petrović, Z.S., et al., *Polyester polyols and polyurethanes from ricinoleic acid.* Journal of Applied Polymer Science, 2008. **108**(2): p. 1184-1190.

47. Guo, A., Y. Cho, and Z.S. Petrović, *Structure and properties of halogenated and nonhalogenated soy-based polyols.* Journal of Polymer Science Part A: Polymer Chemistry, 2000. **38**(21): p. 3900-3910.

48. Guo, Y., et al., *Hydrolysis of epoxidized soybean oil in the presence of phosphoric acid.* Journal of the American Oil Chemists' Society, 2007. **84**(10): p. 929-935.

49. Petrović, Z.S., et al., *Polyurethane networks from polyols obtained by hydroformylation of soybean oil.* Polymer International, 2008. **57**(2): p. 275-281.

50. Cromwell, D., *Soybean Meal–An Exceptional Protein Source*. 2008.

51. Diebel, W., et al., *Material property characterization of co-products from biofuel industries: Potential uses in value-added biocomposites.* Biomass and bioenergy, 2012. **37**: p. 88-96.

52. Kumar, S., et al., *Polyurethanes preparation using proteins obtained from microalgae.* Journal of materials science, 2014. **49**(22): p. 7824-7833.

53. Pettersson, D. and K. Pontoppidan, *Soybean meal and the potential for upgrading its feeding value by enzyme supplementation*, in *Soybean-bio-active compounds*. 2013, IntechOpen.

54. Mekonnen, T., M. Misra, and A.K. Mohanty, *Fermented soymeals and their reactive blends with poly (butylene adipate-co-terephthalate) in engineering biodegradable cast films for sustainable packaging.* ACS Sustainable Chemistry & Engineering, 2016. **4**(3): p. 782-793.

55. Mu, Y., et al., *Rigid polyurethane foams based on activated soybean meal.* Journal of Applied Polymer Science, 2012. **124**(5): p. 4331-4338.

56. Qin, Z., et al., *Glycidyl methacrylate grafted onto enzyme-treated soybean meal adhesive with improved wet shear strength.* BioResources, 2013. **8**(4): p. 5369-5379.

57. Carrier, M., et al., *Thermogravimetric analysis as a new method to determine the lignocellulosic composition of biomass.* Biomass and Bioenergy, 2011. **35**(1): p. 298-307.

58. Narayan, R., D. Graiver, and E. Hablot, *Polyols from protein biomass*. 2015, Google

Patents.

59. Narayan, R., et al., *Polyols from biomass and polymeric products produced therefrom*. 2016, Google Patents.

60. Habtie, T., S. Adrnassu, and K. Asres, *Effects of processing methods on some phytochemicals present in the seeds of Lupinus albus L. grown in Ethiopia.* Ethiopian Pharmaceutical Journal, 2009. **27**(2).

61. Cozzani, V., et al., *A new method to determine the composition of biomass by thermogravimetric analysis.* The Canadian Journal of Chemical Engineering, 1997. **75**(1): p. 127-133.

62. Cegla, G. and K. Bell, *High pressure liquid chromatography for the analysis of soluble carbohydrates in defatted oilseed flours.* Journal of the American Oil Chemists' Society, 1977. **54**(4): p. 150-152.

63. Johansen, H.N., V. Glitsø, and K.E. Bach Knudsen, *Influence of extraction solvent and temperature on the quantitative determination of oligosaccharides from plant materials by high-performance liquid chromatography.* Journal of Agricultural and Food Chemistry, 1996. **44**(6): p. 1470-1474.

64. Shukla, V., *Quantitative determination of oligosaccharides in defatted soybean products by high speed liquid chromatography.* Lipid/Fett, 1987. **89**(2): p. 75-79.

65. Raemy, A. and T. Schweizer, *Thermal behaviour of carbohydrates studied by heat flow calorimetry.* Journal of Thermal Analysis and Calorimetry, 1983. **28**(1): p. 95-108.

66. Räisänen, U., et al., *Formation of the main degradation compounds from arabinose, xylose, mannose and arabinitol during pyrolysis.* Journal of thermal analysis and calorimetry, 2003. **72**(2): p. 481-488.

67. Alvarez, V. and A. Vázquez, *Thermal degradation of cellulose derivatives/starch blends and sisal fibre biocomposites.* Polymer degradation and stability, 2004. **84**(1): p. 13-21.

68. Wojdyr, M., *Fityk: a general-purpose peak fitting program.* Journal of Applied Crystallography, 2010. **43**(5-1): p. 1126-1128.

69. Pretsch, E., et al., *Structure determination of organic compounds*. 2000: Springer.

70. Jones, D.B., *Factors for converting percentages of nitrogen in foods and feeds into percentages of proteins.* 1931.

71. Mariotti, F., D. Tomé, and P.P. Mirand, *Converting nitrogen into protein—beyond 6.25 and Jones' factors.* Critical reviews in food science and nutrition, 2008. **48**(2): p. 177-184.

72. Morr, C., *Nitrogen conversion factors for several soybean protein products.* Journal of Food Science, 1981. **46**(5): p. 1362-1363.

73. Mosse, J., *Nitrogen-to-protein conversion factor for ten cereals and six legumes or oilseeds. A reappraisal of its definition and determination. Variation according to species and to seed protein content.* Journal of Agricultural and Food Chemistry, 1990. **38**(1): p. 18-24.

74. Bhoyate, S., et al., *Highly flame-retardant polyurethane foam based on reactive phosphorus polyol and limonene-based polyol.* Journal of Applied Polymer Science, 2018. **135**(21): p. 46224.

75. *Price of propylene carbonate and ethylene carbonate*. [cited 2019 May]; Available from: https://www.alibaba.com/.

76. Webster, D.C., *Cyclic carbonate functional polymers and their applications.* Progress in Organic Coatings, 2003. **47**(1): p. 77-86.

77. Harry-O'Kuru, R., et al., *Synthesis and characteristics of polyhydroxy triglycerides from milkweed oil.* Industrial crops and products, 2002. **15**(1): p. 51-58.

78. Feng, Y., et al., *A Solvent-Free and Scalable Method To Prepare Soybean-Oil-Based Polyols by Thiol–Ene Photo-Click Reaction and Biobased Polyurethanes Therefrom.* ACS Sustainable Chemistry & Engineering, 2017. **5**(8): p. 7365-7373.

79. Ji, D., et al., *Synthesis of soy-polyols using a continuous microflow system and preparation of soy-based polyurethane rigid foams.* ACS Sustainable Chemistry & Engineering, 2015. **3**(6): p. 1197-1204.

80. Tomita, H., F. Sanda, and T. Endo, *Structural analysis of polyhydroxyurethane obtained by polyaddition of bifunctional five-membered cyclic carbonate and diamine based on the model reaction.* Journal of Polymer Science Part A: Polymer Chemistry, 2001. **39**(6): p. 851-859.

81. Baizer, M., J. Clark, and E. Smith, *Reaction of 4-methyldioxolone-2with aqueous ethylamine.* The Journal of Organic Chemistry, 1957. **22**(12): p. 1706-1707.

82. Steblyanko, A., et al., *Addition of five-membered cyclic carbonate with amine and its application to polymer synthesis.* Journal of Polymer Science Part A: Polymer Chemistry, 2000. **38**(13): p. 2375-2380.

83. Bürgel, T. and M. Fedtke, *Reactions of cyclic carbonates with amines: Model studies for curing process.* Polymer Bulletin, 1991. **27**(2): p. 171-177.

84. Lebas, C. and P. Turley, *Primary hydroxyl content in polyols-evaluation of two nuclear magnetic resonance (NMR) methods.* Journal of cellular plastics, 1984. **20**(3): p. 194-199.

85. Elbers, N., et al., *Synthesis of novel biobased polyol via thiol-ene chemistry for rigid polyurethane foams.* , 5, 1, 2017. **5**(1): p. 74-83.

86. Jambeck, J.R., et al., *Plastic waste inputs from land into the ocean.* Science, 2015.

347(6223): p. 768-771.

87. Harmsen, P.F., M.M. Hackmann, and H.L. Bos, *Green building blocks for bio-based plastics.* Biofuels, Bioproducts and Biorefining, 2014. **8**(3): p. 306-324.

88. Jaillet, F., et al., *New biobased epoxy materials from cardanol.* European Journal of Lipid Science and Technology, 2014. **116**(1): p. 63-73.

89. Heidbreder, A., et al., *Oleochemical products as building blocks for polymers.* Lipid/Fett, 1999. **101**(11): p. 418-424.

90. Laurichesse, S., C. Huillet, and L. Avérous, *Original polyols based on organosolv lignin and fatty acids: new bio-based building blocks for segmented polyurethane synthesis.* Green Chemistry, 2014. **16**(8): p. 3958-3970.

91. Caillol, S., *Cardanol: A promising building block for biobased polymers and additives.* Current opinion in green and sustainable chemistry, 2018. **14**: p. 26-32.

92. Hablot, E., et al., *Dimer acid-based thermoplastic bio-polyamides: reaction kinetics, properties and structure.* Polymer, 2010. **51**(25): p. 5895-5902.

93. Izadi-Vasafi, H., et al., *A novel biodegradable polyurethane based on hydroxylated polylactic acid and tung oil mixtures. I. Synthesis, physicochemical and biodegradability characterization.* Fibers and Polymers, 2016. **17**(3): p. 311-323.

94. Owen, S., et al., *Biodegradation of poly-D, L-lactic acid polyurethanes.* Journal of Macromolecular Science, Part A: Pure and Applied Chemistry, 1995. **32**(4): p. 843-850.

95. Chen, S.H., et al., *Synthesis of poly (lactic acid)-based polyurethanes.* Polymer International, 2013. **62**(8): p. 1159-1168.

96. Wu, D. and M. Hakkarainen, *Recycling PLA to multifunctional oligomeric compatibilizers for PLA/starch composites.* European Polymer Journal, 2015. **64**: p. 126-137.

97. Cheng, S., et al., *Radiation curable coating compositions comprising a lactide reaction product*. 2010, Google Patents.

98. Kulfan, J.L. and D.R. Fenn, *Coating compositions comprising the reaction product of a biomass derived polyol and a lactide*. 2010, Google Patents.

99. Kamber, N.E., et al., *Organocatalytic ring-opening polymerization.* Chemical reviews, 2007. **107**(12): p. 5813-5840.

100. Coulembier, O., et al., *A distinctive organocatalytic approach to complex macromolecular architectures.* Angewandte Chemie International Edition, 2007. **46**(25): p. 4719-4721.

101. Alba, A., et al., *Direct ring-opening of lactide with amines: application to the organo-catalyzed preparation of amide end-capped PLA and to the removal of residual lactide*

from PLA samples. Polymer Chemistry, 2015. **6**(6): p. 989-997.

102. *Biobased ethylene glycol*. [cited 2019 June]; Available from: https://www.indiaglycols.com/divisions/ethylene_glycols.htm.

103. Van Bennekom, A., P. Willemsen, and R. Gaymans, *Amide-modified poly (butylene terepthalate): thermal stability.* Polymer, 1996. **37**(24): p. 5447-5459.

104. Demharter, A., *Polyurethane rigid foam, a proven thermal insulating material for applications between+ 130 C and− 196 C.* Cryogenics, 1998. **38**(1): p. 113-117.

105. Allport, D.C., D.S. Gilbert, and S. Outterside, *MDI and TDI: safety, health and the environment: a source book and practical guide*. 2003: John Wiley & Sons.

106. Tan, S., et al., *Rigid polyurethane foams from a soybean oil-based polyol.* Polymer, 2011. **52**(13): p. 2840-2846.

107. Paruzel, A., et al., *Rigid polyurethane foam fabrication using medium chain glycerides of coconut oil and plastics from end-of-life vehicles.* ACS Sustainable Chemistry & Engineering, 2017. **5**(7): p. 6237-6246.

108. Tseng, C.-j., M. Yamaguchi, and T. Ohmori, *Thermal conductivity of polyurethane foams from room temperature to 20 K.* Cryogenics, 1997. **37**(6): p. 305-312.

109. Hakim, A.A., et al., *Preparation and characterization of rigid polyurethane foam prepared from sugar-cane bagasse polyol.* Materials Chemistry and Physics, 2011. **129**(1-2): p. 301-307.

110. Tao, W.-H., et al., *Measurement and prediction of thermal conductivity of open cell rigid polyurethane foam.* Journal of cellular Plastics, 2001. **37**(4): p. 310-332.

111. Widya, T. and C.W. Macosko, *Nanoclay-modified rigid polyurethane foam.* Journal of Macromolecular Science, Part B: Physics, 2005. **44**(6): p. 897-908.

112. Zhang, C. and M.R. Kessler, *Bio-based polyurethane foam made from compatible blends of vegetable-oil-based polyol and petroleum-based polyol.* ACS Sustainable Chemistry & Engineering, 2015. **3**(4): p. 743-749.

113. Chang, L.C., Y. Xue, and F.H. Hsieh, *Comparative study of physical properties of water-blown rigid polyurethane foams extended with commercial soy flours.* Journal of applied polymer science, 2001. **80**(1): p. 10-19.

114. Report, M.R. *Polyurethane Foam Market by Type (Flexible, Rigid, Spray Foam), End User (Bedding & Furniture, Building & Construction, Electronics, Automotive, Footwear, Packaging), and Region (Asia Pacific, Europe, North America)*. 2018 [cited 2019 June 20th]; Available from: https://www.marketsandmarkets.com/Market-Reports/polyurethane-foams-market-1251.html?gclid=CjwKCAjwuqfoBRAEEiwAZErCspK-AqTZv9bn9CKgPMq3scaELc-

lCJnES_YoekRwiFmhrvYe14poaBoCTXoQAvD_BwE.

115. Guzman, D.D. *100% bio-based Polyurethane in the market*. 2015 [cited 2019 June 20th]; Available from: https://greenchemicalsblog.com/2015/04/27/100-bio-based-polyurethane-in-the-market/.

116. Bueno-Ferrer, C., et al., *Structure and morphology of new bio-based thermoplastic polyurethanes obtained from dimeric fatty acids.* Macromolecular Materials and Engineering, 2012. **297**(8): p. 777-784.

117. Pawlik, H. and A. Prociak, *Influence of palm oil-based polyol on the properties of flexible polyurethane foams.* Journal of Polymers and the Environment, 2012. **20**(2): p. 438-445.

118. Rojek, P. and A. Prociak, *Effect of different rapeseed-oil-based polyols on mechanical properties of flexible polyurethane foams.* Journal of Applied Polymer Science, 2012. **125**(4): p. 2936-2945.

119. Zlatanić, A., et al., *Effect of structure on properties of polyols and polyurethanes based on different vegetable oils.* Journal of Polymer Science Part B: Polymer Physics, 2004. **42**(5): p. 809-819.

120. Bernardini, J., et al., *Flexible polyurethane foams green production employing lignin or oxypropylated lignin.* European Polymer Journal, 2015. **64**: p. 147-156.

121. Liu, X., et al., *Preparation and properties of waterborne polyurethanes with natural dimer fatty acids based polyester polyol as soft segment.* Progress in Organic Coatings, 2011. **72**(4): p. 612-620.

122. Polymers, N. *Firm-Grade Flexible Open-Cell Foam*. 2019 [cited 2019 June 20th]; Available from: http://www.northstarpolymers.com/NorthstarPolymers/Foam/FlexibleFoam/FFM-1_Firm_Flexible_Foam.htm.

123. DeBolt, M., et al., *Flexible polyurethane foams formulated with polyols derived from waste carbon dioxide.* Journal of Applied Polymer Science, 2016. **133**(45).

124. Flanigan, C., D. Mielewski, and C. Perry, *Automotive grade, flexible polyurethane foam and method for making the same*. 2005, Google Patents.

125. Cho, R. *What Happens to all That Plastic?* 2012 [cited 2019 June 25th]; Available from: https://blogs.ei.columbia.edu/2012/01/31/what-happens-to-all-that-plastic/.

126. Kfoury, G., et al., *Recent advances in high performance poly (lactide): from "green" plasticization to super-tough materials via (reactive) compounding.* Frontiers in chemistry, 2013. **1**: p. 32.

127. Anderson, K.S., K.M. Schreck, and M.A. Hillmyer, *Toughening polylactide.* Polymer Reviews, 2008. **48**(1): p. 85-108.

128. Narayan, R. *Using reactive extrusion to manufacture greener products-from laboratory fundamentals to commercial scale*. in *ABSTRACTS OF PAPERS OF THE AMERICAN CHEMICAL SOCIETY*. 2017. AMER CHEMICAL SOC 1155 16TH ST, NW, WASHINGTON, DC 20036 USA.

129. Jacobsen, S. and H.-G. Fritz, *Plasticizing polylactide—the effect of different plasticizers on the mechanical properties.* Polymer Engineering & Science, 1999. **39**(7): p. 1303-1310.

130. Ljungberg, N. and B. Wesslen, *The effects of plasticizers on the dynamic mechanical and thermal properties of poly (lactic acid).* Journal of Applied Polymer Science, 2002. **86**(5): p. 1227-1234.

131. Martin, O. and L. Averous, *Poly (lactic acid): plasticization and properties of biodegradable multiphase systems.* Polymer, 2001. **42**(14): p. 6209-6219.

132. Liu, H. and J. Zhang, *Research progress in toughening modification of poly (lactic acid).* Journal of polymer science part B: Polymer Physics, 2011. **49**(15): p. 1051-1083.

133. Pillin, I., N. Montrelay, and Y. Grohens, *Thermo-mechanical characterization of plasticized PLA: Is the miscibility the only significant factor?* Polymer, 2006. **47**(13): p. 4676-4682.

134. Prempeh, N., et al., *Plasticizing effects of epoxidized sun flower oil on biodegradable polylactide films: a comparative study.* Polymer Science Series A, 2014. **56**(6): p. 856-863.

135. Xu, Y., M. You, and J. Qu, *Melt rheology of poly (lactic acid) plasticized by epoxidized soybean oil.* Wuhan University Journal of Natural Sciences, 2009. **14**(4): p. 349-354.

136. Al-Mulla, E.A.J., et al., *Epoxidized palm oil plasticized polylactic acid/fatty nitrogen compound modified clay nanocomposites: preparation and characterization.* Polymers and Polymer Composites, 2010. **18**(8): p. 451-460.

137. Hassouna, F., et al., *New approach on the development of plasticized polylactide (PLA): Grafting of poly (ethylene glycol)(PEG) via reactive extrusion.* European Polymer Journal, 2011. **47**(11): p. 2134-2144.

138. Kenion, G.B., et al., *Transesterification of polylactic acid with natural oils*. 2019, Google Patents.

139. Mei, T., et al., *Synthesis, characterization, and biocompatibility of alternating block polyurethanes based on PLA and PEG.* Journal of Biomedical Materials Research Part A, 2014. **102**(9): p. 3243-3254.

140. Dong, C.-M., et al., *Synthesis of star-shaped poly (ε-caprolactone)-b-poly (dl-lactic acid-alt-glycolic acid) with multifunctional initiator and stannous octoate catalyst.* Macromolecules, 2001. **34**(14): p. 4691-4696.

141. Casas, A., et al., *Tin compounds as Lewis acid catalysts for esterification and*

transesterification of acid vegetable oils. Fuel processing technology, 2013. **106**: p. 321-325.

142. Murariu, M., et al., *Polylactide (PLA) designed with desired end-use properties: 1. PLA compositions with low molecular weight ester-like plasticizers and related performances.* Polymers for Advanced Technologies, 2008. **19**(6): p. 636-646.

143. Parak, A., et al., *Functionalizing bioinks for 3D bioprinting applications.* Drug discovery today, 2018.

144. Abhari, R.E., et al., *Effect of annealing on the mechanical properties and the degradation of electrospun polydioxanone filaments.* Journal of the mechanical behavior of biomedical materials, 2017. **67**: p. 127-134.

145. Takayama, T., M. Todo, and H. Tsuji, *Effect of annealing on the mechanical properties of PLA/PCL and PLA/PCL/LTI polymer blends.* Journal of the mechanical behavior of biomedical materials, 2011. **4**(3): p. 255-260.

146. Park, S.-D., M. Todo, and K. Arakawa, *Effect of annealing on the fracture toughness of poly (lactic acid).* Journal of materials Science, 2004. **39**(3): p. 1113-1116.

147. Baiardo, M., et al., *Thermal and mechanical properties of plasticized poly (L-lactic acid).* Journal of Applied Polymer Science, 2003. **90**(7): p. 1731-1738.

148. Wu, M., et al., *Simultaneous the thermodynamics favorable compatibility and morphology to achieve excellent comprehensive mechanics in PLA/OBC blend.* Polymer, 2014. **55**(24): p. 6409-6417.

149. Lin, L., et al., *Super toughened and high heat-resistant poly (lactic acid)(PLA)-based blends by enhancing interfacial bonding and PLA phase crystallization.* Industrial & Engineering Chemistry Research, 2015. **54**(21): p. 5643-5655.

150. Srithep, Y., P. Nealey, and L.S. Turng, *Effects of annealing time and temperature on the crystallinity and heat resistance behavior of injection-molded poly (lactic acid).* Polymer Engineering & Science, 2013. **53**(3): p. 580-588.

151. Yang, G., et al., *Toughening of poly (L-lactic acid) by annealing: the effect of crystal morphologies and modifications.* Journal of Macromolecular Science, Part B, 2012. **51**(1): p. 184-196.

152. Nascimento, L., et al., *Effect of the recycling and annealing on the mechanical and fracture properties of poly (lactic acid).* Journal of Polymers and the Environment, 2010. **18**(4): p. 654-660.

153. Sahoo, S., M. Misra, and A.K. Mohanty, *Enhanced properties of lignin-based biodegradable polymer composites using injection moulding process.* Composites Part A: Applied Science and Manufacturing, 2011. **42**(11): p. 1710-1718.

154. Nofar, M., et al., *Crystallization kinetics of linear and long-chain-branched polylactide.* Industrial & engineering chemistry research, 2011. **50**(24): p. 13789-13798.

155. Mohapatra, A.K., S. Mohanty, and S.K. Nayak, *Properties and characterization of biodegradable poly (lactic acid)(PLA)/poly (ethylene glycol)(PEG) and PLA/PEG/organoclay: A study of crystallization kinetics, rheology, and compostability.* Journal of Thermoplastic Composite Materials, 2016. **29**(4): p. 443-463.

156. Li, H. and M.A. Huneault, *Effect of nucleation and plasticization on the crystallization of poly (lactic acid).* Polymer, 2007. **48**(23): p. 6855-6866.

157. Xiao, H., et al., *Kinetics and crystal structure of isothermal crystallization of poly (lactic acid) plasticized with triphenyl phosphate.* Journal of applied polymer science, 2010. **117**(5): p. 2980-2992.